UNIVERSITAT DE
BARCELONA

Regulatory subunits controlling
the Kv1.3 channelosome

Silvia Cassinelli

Regulatory subunits controlling the Kv1.3 channelosome

Silvia Cassinelli

Barcelona, 2023

Regulatory subunits controlling the K$_v$1.3 channelosome

Dissertation presented by Silvia Cassinelli, to qualify for the Doctorate degree by the Universitat de Barcelona (UB).

This doctoral thesis was performed under the direction of Professor Antonio Felipe Campo, in the Molecular Physiology Laboratory in the Department of Biochemistry and Molecular Biomedicine, Faculty of Biology, Institute of Biomedicine (IBUB), Universitat de Barcelona

Antonio Felipe Campo

PhD Thesis director

Silvia Cassinelli

PhD candidate

PhD Thesis

Department of Biochemistry and Molecular Biomedicine

Faculty of Biology, Universitat de Barcelona

Doctoral program in Biomedicine

Barcelona, 2023

Ciò che non abbiamo osato,
abbiamo certamente perduto.
Oscar Wilde

A Simone,
non so come avrei fatto se
non fossi nato prima tu.
Grazie di cuore.

Acknowledgments

Acknowledgments

A *Jorge*, por haber compartido conmigo muchas, pero muchas, lágrimas y sonrisas durante este doctorado. Por haber entrado en mi estimado club de compañeros de piso y haberte convertido en un gran amigo. Gracias por poder contar contigo, te quiero mi amor.

Gracias a *Paul*, por todas las experiencias que ya podemos ir contando. Por esta bellísima amistad que ha nacido y por supuesto, por invitarme a mis primeras Fallas de Valencia y habérmelo hecho pasar taaaan bien. ¡Te quiero HoMMMMBBBBBRe! A *Néstor*, por todo el apoyo en Groningen, por toda tu sensibilidad, empatía y respeto hacia los demás. Gracias por haber sido mi amigo desde el primer momento, te quiero mi guapo. Gracias a *Alba, Fernando, David, Federica*, por el apoyo y todos los momentos bonitos y divertidos que me habéis regalado, os quiero chicos. Grazie *Riccardo* per essere stato un buon amico, in piu di un occasione, ti voglio bene bellezzz.

A *Xavi*, gracias por todo el apoyo durante la finalización de este doctorado y en la escritura de esta tesis. Pero sobretodo, gracias por todos estos años, por cada cuidado y cada fiesta juntos. Y sobretodo gracias por haberme permitido conocer *Kora y Lee*…Gracias a mis pequeñas bolas <3 por ser tan maravillosos y por haberme regalado paz durante muchas tormentas, ¡os quiero a los tres! A *Cristina*, gracias por haber entrado a ser parte de mis amigos y GRACIAS por permitirme entregar este manuscrito de una forma digna! Te quiero bonita!

Grazie a Christian per i mesi di convivenza bellissimi, compreso il lockdown, e per esserci sempre nel momento del bisogno! ti voglio bene Marione.

Mymi, gracias por todo lo que hemos vivido y lo que nos falta. Por cada risa sin fin, por no haberme abandonado nunca a pesar de todo lo que me he perdido o en que he faltado. Por aceptarme tal como soy y por haber estado sin dudar, cada vez que lo haya necesitado. Te quiero mucho belleza, eres familia.

Fiammi, grazie di cuore per ogni singolo giorno da quando ti conosco ad oggi amica mia. Non so chi devo ringraziare per aver cliccato CONTATTA su "Idealista" quel giorno, ma gli devo un favore enorme. Ti voglio bene tesoro, sei casa e famiglia per me.

A mi Dech, grazie per ogni anno condiviso amico mio, per esserci sempre stato, nonostante la distanza e le vite diverse. Ti voglio proprio bene Dear.

A *Pancho, Michele, Dario, Luana* e a TUTTO il *CazzeggioTime*, che non posso citare per intero causa estrema estensione. Grazie ragazzi, per tutto il sostegno ricevuto, per essere al mio fianco da veramente troppi anni, per organizzare ancora cene, viaggi, pomeriggi e momenti tutti insieme, di quelli che racconteremo ai futuri noi. Siamo proprio belli. Vi voglio bene.

Alla *zia Candi e zio Nicola*, per esserci sempre e avermi accompagnato fin dal principio di questo lungo percorso, senza essersi mai persi l'occasione di festeggiare con me un traguardo raggiunto, nazionale o internazionale! Vi voglio tanto bene. Grazie a tutta la mia famiglia.

Grazie *Matti*, per avermi spronata a partire cinque anni fa sostenendomi in tutte le mie scelte, comprese quelle proprio complicate.

Stefi, grazie per essere passata in questi anni da "La fidanzata di Simo" ad amica, compagna e famiglia non solo per lui, ma anche per me. Sono felice che tu sia parte del mio futuro, spero di essere una cognata e una zia all'altezza. Ti voglio bene cognatina.

Simo… a parte le adolescenziali, normali, strillate dell'infanzia, non riesco a ricordare momenti della mia vita in cui tu non me l'abbia semplificata. Modificherei tante cose nella mia vita, col senno di poi, ma non cambierei proprio NIENTE di tutto quello che ho vissuto e costruito con te. Grazie di tutto Nene. Ti voglio bene.

A *Mamma e Papá*… bueno, come ve lo dico senza essere ripetitiva rispetto alle due tesi precedenti? Ci provo. Ovviamente, vi devo ringraziare per il sostegno morale ed economico ricevuto, cominciando dall'asilo fino a questo lungo e sudato dottorato. Niente di tutto questo sarebbe stato possibile senza voi due. Gratitudine onerosa a parte, GRAZIE soprattutto per avermi cresciuta con valori buoni e altruisti, per avermi mostrato quando stavo sbagliando e insegnato come chiedere scusa, per avermi obbligata ad imparare e ad informarmi prima di parlare, nonostante vi abbia dato del filo da torcere. Grazie per avermi dato l'educazione necessaria per potermi muovere nel mondo, a casa mia o al di fuori, nel mio paese o all'estero, con gli amici di sempre o con persone appena conosciute. Senza di voi non avrei potuto mettere un piede fuori di casa. Infinitamente grazie, per ogni singolo giorno. Vi voglio tanto bene.

Abstract

Abstract

The Kv1.3 voltage-dependent potassium channel plays a crucial role in the immune response participating in various cellular functions like proliferation, activation, and apoptosis. The aberrant expression of this channel is associated with autoimmune diseases, highlighting the need for precise regulation in leukocyte physiology.

Kvβ proteins, the first identified modulators of Kv channels, have been extensively studied in their regulation of α-subunit kinetics and traffic. However, limited information is available regarding their own biology. Despite their cytosolic distribution, Kvβ subunits show spatial localization near plasma membrane-Kv channels for an effective immune response. Our study focused on the structural elements influencing Kvβ distribution. We discovered that Kvβ peptides could target the cell surface independently of Kv channels. Additionally, Kvβ2.1, but not Kvβ1.1, targeted lipid raft microdomains via S-acylation of two C-terminal cysteines (C301/C311), concomitantly with the peptide localization at the immunological synapse. Moreover, growth factor-dependent proliferation increased the Kvβ2.1 surface targeting, whereas PKC activation disrupted lipid raft localization, but PSD95 counteracted this action. These findings elucidate the mechanisms by which Kvβ2 clusters within immunological synapses during leukocyte activation.

Kvβ peptides, interacting with Kv channels, exhibited a suggested α4/β4 conformation. While Kvβ2 and Kvβ1 can form homo- and heterotetramers with similar affinities, only Kvβ2.1 forms tetramers independently of α subunits. Thus, Kvβ oligomers stoichiometry fine-tunes hetero-oligomeric Kv channel complexes. Similar to Kvβ1.1, Kvβ1.1/Kvβ2.1 heteromers did not target lipid rafts. Therefore, because Kvβ2 is an active partner of the Kv1.3-TCR complex at the immunological synapse, an association with Kvβ1 would alter its location, impacting on immune responses. Differential regulation of Kvβs influences the traffic and architecture of Kvβ heterotetramers, modulating Kvβ-dependent physiological responses.

Regulatory KCNE subunits are expressed in the immune system and KCNE4 tightly regulates Kv1.3. KCNE4 modifies Kv1.3 currents altering kinetics and retaining the channel at the endoplasmic reticulum (ER). This function affects in turn membrane localization of the channel. Our research showed that KCNE4 can dimerize via the juxtamembrane tetraleucine carboxyl-terminal domain of KCNE4. This cluster serves as a competitive structural platform for Kv1.3, Ca^{2+}/calmodulin (CaM) and KCNE4 dyads. While KCNE4 is typically retained in the ER, the association with CaM leads to COP-II-dependent forward trafficking. Consequently, CaM plays a vital role in controlling the dimerization and membrane targeting of KCNE4, affecting the regulation of Kv1.3 and, subsequently, leukocyte physiology.

Kv1.3, localized in membrane lipid rafts, accumulates at immunological synapses during cell activation, influencing membrane potential and downstream calcium-signalling pathways. KCNE4 acts as a dominant negative regulatory subunit on Kv1.3, causing intracellular retention. Palmitoylation, a reversible post-translational modification, enhances protein hydrophobicity, facilitating membrane association, protein interactions, and subcellular trafficking. Our data demonstrated the S-acylation of KCNE4, resulting in spatial rearrangements that reduce ER distribution, which in turn affects Kv1.3 regulation. KCNE4 partially traffics to the cell surface with Kv1.3 in activated dendritic cells but alters immunological synapse targeting. This highlights the significance of KCNE4 palmitoylation in regulating protein subcellular localization and oligomeric state, subsequently affecting channel membrane expression. Given the role of Kv1.3 as an immunomodulatory target, these findings offer insights for future clinical and pharmacological studies.

Table of contents

Table of contents

List of abbreviations

List of abbreviations

Aβ	Amyloid β
ADP	Adenosine diphosphate
AMPA	α-amino-3-hydroxy-5-methyl-4-isoxazolepropionic acid
AMPK	AMP-activated protein kinase
AKR	Aldoketoreductase
APC	Antigen-presenting cells
APP	Amyloid precursor proteins
APP-1 -2	ArfGAP-putative, Pix-interacting, paxillin-interacting protein 1 -2
APT	palmitoyl protein thioesterases
ARFGAP	ADP-ribosylation factor GTPase-activating proteins
ASIC	Acid-sensing ion channels
ATP	Adenosine triphosphate
BACE1	Ancillary polypeptides include the β-secretase 1
BSA	Bovine serum albumin
CaM	Calmodulin
CaMKII	CaM Kinase II
CD44	Cluster-differentiating 44 protein
CFP	Cyan fluorescent protein
CFTR	Cystic fibrosis transmembrane conductance regulator
cGAS	Cyclic guanosine monophosphate-adenosine monophosphate synthase
CoA	Acetyl-coenzyme A
COPII	Coat protein complex II
CRAC	Ca^{2+} release-activated Ca^{2+}
Ct	Carboxy-terminal enD
DAT	Dopamine transporter
DCs	Dendritic cells
DMEM	Dulbecco's Modified Eagle's Medium
DMSO	Dimethyl sulfoxide
EDTA	Ethylene diamine tetraacetic acid
EGF	Epidermal growth factor
EGTA	Ethylene glycol-bis(β-aminoethyl ether)-N,N,N′,N′-tetraacetic acid
eNOS	Endothelial nitric oxide synthase
ER	Endoplasmic Reticulum
ERGIC	ER-Golgi intermediate compartment
ERRM	ER retention motif

EZH2	Histone-lysine N-methyltransferase enzyme
FRET	Förster Resonance Energy Transfer
GFP	Green fluorescent protein
GLUT	Glucose transporter
GPCR	G protein-coupled receptors
GRIP1	Glutamate receptor proteins 1b
HA	Hemagglutinin
HEK	Human embryo kidney
hERG	Human Ether-à-go-go
HSP	Heat shock proteins
IFN1	Type I interferone
IL2	Interleukine-2
IK	Steady state short-circuit current
IKK	IκB Kinase Complex
iNOS	Inducible nitric oxide synthase
IRF3	Interferon regulatory factor 3
KChIP	Kv channel-interacting proteins
KCNE	Potassium voltage-gated channel subfamily E
Kv	Voltage-dependent potassium channel
Kvβ	Voltage-gated potassium channels β subunits
LQTS	Long QT syndrome
LPS	Lipopolysaccharide
MAP	Mitogen-activated protein
MAGUK	Membrane-associated guanylate kinases proteins
MDA	Melanoma differentiation-associated proteins
MHC	Peptide-major histocompatibility complexes
moDCs	monocyte-derived dendritic cells
mRNA	Messenger ribonucleic acid
NAD(H)	Nicotinamide adenine dinucleotide (hydrogene)
NADP(H)	Nicotinamide adenine dinucleotide phosphate (hydrogen)
Nedd4-2	Neural precursor cell-expressed developmentally downregulated gene 4-2
NEMO	NF-kB essential modulator proteins
NF-kB	Nuclear factor-kB
NOD	Nucleotide-binding oligomerization domain
ORAI	Calcium release-activated calcium modulator
PAT	Palmitoyl Transferases

PIP2	Phosphatidylinositol 4,5-bisphosphate
PKL	Paxillin kinase linker
PKC	Protein kinase C
PBS	Phosphate-buffered saline
PBS Ø K+	Phosphate buffered saline without potassium
PM	Plasma Membrane
PSD-95	Postsynaptic density protein-95
RIG-I	Retinoic acid inducible gene-I
SDS	Sodium dodecyl sulphate
SEM	Standard error of the mean
Sig-1R	Reticulum-Resident protein-1
Slc7a5	Solute Carrier Family 7 Member 5
SMAC	Concentric supramolecular activation clusters
SNAP-25	Synaptosomal-associated protein 25
SOCE	Store operated calcium entry
STIM	Stromal interaction molecules
STING	Synthase-stimulator of interferon genes
TANK	TRAF Family Member Associated NFKB Activator
TBK1	TANK-binding kinase 1
TBS	Tris-buffered saline
TCR	T-cell receptor
TLR	Tall-like receptors
TM	Transmembrane
TRAF	Tumour necrosis factor receptor-associated factor
TREK	Two-pore-domain background potassium channel
VGIC	Voltage-gated ion channels
WGA	Wheat Germ Agglutinin
WT	Wild type
YFP	Yellow fluorescent protein
ZAPS	Zinc finger antiviral proteins
zDHHC	Zinc finger DHHC domain containing proteins
ZIP	Zinc-regulated, iron-regulated transporter-like proteins

1. Introduction

1. Introduction

1.1. Voltage-gated ion channels

Voltage-gated ion channels are integral membrane proteins that respond to electrical stimuli controlled by the voltage, along cellular membranes. Channels modulate ion fluxes playing crucial roles in electrical signalling and cell homeostasis. One of the first purified member was a K+ channel from the Shaker mutant of *Drosophila melanogaster*. Based on ion conductance, these proteins are divided into voltage-gated Na$^+$ (Nav), Ca^{2+} and K$^+$ (Kv) channels, along with the anion-selective (Cl$^-$) channels (*1*). In Eukaryotes, functional Nav and Cav are structured in a major α-subunit composed of four homologous domains, each presenting six transmembrane segments S1–S6 (*2*). However, Kv channels consist of only one domain, homologous to the four structural sections of the abovementioned α-subunits, forming tetramers. Thus, the structural four-fold symmetry found in Kv channels lacks in Nav and Cav and this is crucial for understanding channel gating and ion selectivity (*3*). The most conserved features among the three groups are the voltage sensors, harboured at the S4 domain, and the selectivity filter placed at the pore-region between the S5 and S6 segment (Figure 1). All of these channels may associate with ancillary β-subunits (*4*).

Regarding kinetics, those channels are quite different. Indeed, Nav polypeptides are crucial for the initiation of action potentials in excitable cells and Cav activate upon depolarization events and calcium entry. However, voltage-dependent potassium channels (Kv) channels are responsible for maintaining the resting-membrane potential of cells (*5*). They belong to a large family of transmembrane proteins with more than 40 members, divided into 12 subfamilies in humans. They are evolutionarily conserved and extensively expressed in multiple tissues, including excitable and non-excitable cells. A polarized cell membrane consists of a negative voltage at the inner cell and a positive voltage at the exterior. In this situation, Kv channels are in the closed state. Upon depolarization events, they rapidly open driving K$^+$ ions through passive transport following the electrochemical gradient. In this way, the cellular membrane potential returns to the resting state (*6*) (*7*). For that reason, Kv channels contribute to trigger physiological processes. In the nervous, cardiovascular and muscular systems, they contribute to the modulation of waveform and action potential responses (*8*). In non-excitable cells, such as the immune system, they controls different steps of the cells life cycle including cell volume, activation, proliferation, migration and apoptosis (*9*) (*10*) (*11*) (*12*).

Figure 1. Phylogenetic diagram of the voltage-gated ion channel superfamily. Colour code: Orange; Kv10-12 and cyclic nucleotide-dependent potassium channels. Blue; calcium and sodium channels. Green; TRP channels. Red: Inward-rectifier potassium channel (Kir), Calcium-activated potassium channels (KCa), Voltage-gated-potassium channels (Kv), Two-pore-domain potassium channels (K2P). From Alexander et al. (2019).

1.1.1. Kv1.3

Kv1.3 is the third member of the Shaker subfamily, encoded by the KCNA3 gen. Kv1.3 presents the typical six transmembrane segments, with the voltage sensor placed at the S4 domain and the pore between the S5 and S6. The channel, which responses to depolarization events, is classified as an outward delayed rectifier channel, with an action potential firing at approximately -35mV (*13*). Moreover, Kv1.3 presents a strong C-type inactivation and, because of the slow recovery, a cumulative inactivation upon membrane depolarisations (*14*). Kv1.3 is expressed in a wide range of tissues, playing key role in different physiological mechanisms such as T-lymphocytes activation in the immune system (*15*), or modulation of depolarization events triggering action potentials, in neurons (*16*). Within the sympathetic nervous system, Kv1.3 has been reported to participate in the regulation of body weight and energy homeostasis

(*17*). In skeletal muscle and adipocytes, it is crucial for glucose homeostasis, where it influences the plasma membrane inclusion of the insulin-sensitive GLUT4 (*18*) (*19*). Furthermore, in white adipose tissue, the caveolar-dependent membrane expression of Kv1.3 increases during adipogenesis (*20*). Interestingly, the channel targets to the inner mitochondrial membrane by a complex import pathway, which involve the HSP70/HSP90 cytosolic complex (*21*). Mitochondrial-Kv1.3 drastically affects the apoptotic signalling in T-Lymphocytes, by direct interaction with Bax protein (*22*). Therefore, this channel is expressed in multiple cellular membranes belonging to different organelles, where it plays multifunctional roles that are determinant for the physiology of cells.

In this scenario, Kv1.3 associates with Kv1.5, another *Shaker*-member encoded by the KCNA5 gen (*23*) (*24*). Like Kv1.3, it has been observed in both excitable and non-excitable cells, such as nervous and immune system, skeletal and smooth muscle and kidney (*25*) (*26*) (*27*). In cardiomyocytes, the Kv1.5 current contributes to the generation of the ultra-rapid activating K^+ currents (I_{kur}), which are important for action potentials repolarization (*28*). Contrary to Kv1.3, the gating mechanism of Kv1.5 presents a slow inactivation and no cumulative inactivation. However, since this channel exists in a long and short isoforms, the NH_2-terminally truncated forms (*29*) show excessive cumulative inactivation (*29*). In BV2 microglia cells, both Kv1.3 and Kv1.5 are functionally expressed at the cell membrane, but only Kv1.3 participates in the cell migration (*30*). Moreover, they co-express in leukocytes and, unlike T-lymphocytes presenting only Kv1.3, in most of the immune cells such as macrophages, dendritic cells and B-Lymphocytes. This is of physiological relevance because those channels contribute to diverse cellular processes and activate at different voltages, hence, Kv1.3/Kv1.5 complexes will generate different cell responses, depending on the ratio of each member composing the functional heteromer (*31*).

Finally, Kv1.3 interacts with several β-subunits affecting the channel functions and subcellular compartmentalization (*32*).

1.1.1.1. Secretory pathway and Turnover

Kv1.3 translocates toward the plasma membrane by following the conventional secretory pathway, as most of the transmembrane proteins. This signalling starts at the ER thanks to the ERGIC compartment,

following by the Golgi apparatus and the trans-Golgi network, until the plasma membrane (*33*). However, some channels may follow the unconventional pathway, which involves COPI (the coat proteins complex I) vesicles but bypass the Golgi apparatus, reaching the endosomal system preceding the membrane inclusion. An example following an unconventional pathway is the cystic fibrosis transmembrane conductance regulator (*34*). Furthermore, the KCNE1-Kv7.1 complexes co-assemble at the ER-plasma membrane junction in order to reach the plasma membrane, while in the case of Kv4 / KChIP system, the channel bypass COPII and Golgi by using COPI vesicles (*35*). The conventional pathway is triggered by COPII, which is composed of the GTPase Sar1 and heteromeric systems involving Sec23-Sec24 and Sec13-Sec3 (*36*). In this context, di-acidic (DXE) or di-hydrophobic motifs (LL or YY) are the canonical cargo export signals. However, some Kv1 presents non-canonical motifs, such as the C-terminal HRETE, which causes the anterograde trafficking of both Kv1.2 and Kv1.4 (*37*). Considering Kv1.3, although the channel sequence includes the HRETE signal, the ER export of Kv1.3 is mostly mediated by a C-terminal YMVIEE sequence (*38*).

Concerning channel turnover, the majority of ion channels follow an ubiquitin-mediated degradation. Kv1.3 is ubiquitinated by the Nedd4-2 ubiquitin ligase member, which may be induced by the PKC-phosphorylation of the channel (*39*) (*40*). Therefore, the channel undergoes endocytosis and lysosome-degradation. In this context, Kv1.3 localizes at lipid raft microdomains, thanks to the association with PSD-95. The PKC-dependent endocytosis is a mechanism regulating the Kv1.3 surface expression, but the interaction with PSD-95 prevents this modulation (*41*).

1.1.1.2. Kv1.3 regulation

Kv1.3 is regulated by a multitude of physiological processes. Post-translational phosphorylation either by PKA and PKC Serine/Threonine kinases suppresses Kv1.3 currents in both *Xenopus* oocytes and Jurkat-T cells. Interestingly, in human T-lymphocytes the effects of those enzymes are the opposite (*42*) (*43*). Moreover, the epidermal growth factor (*44*) receptor activation also reduces Kv1.3 current (*44*). Furthermore, another important regulation of Kv1.3 involves the Ca^{2+} signalling, which via both Calmodulin and CAMKII, decreases

the channel currents (*45*). However, the association with CaM is under investigation.

1.1.1.2.1. Kvβs Ancillary subunits

Kvβs, which are cytosolic peptides, were the first ancillary Kv proteins identified. They were purified in association with Kv channels by using α-dendrotoxin. Thus, Kvβ1 and Kvβ2 polypeptides were identified sharing partial sequences configuring the mammalian Kvβ family (*46*), which is composed of three genes encoding for Kvβ1, β2, β3 families. Each one presents different splicing variants: Kvβ1.1, 1.2 and 1.3 for the first family, whereas only two splicing variant were observed for Kvβ2 and one for Kvβ3 (*47*) (*48*). These ancillary proteins mainly regulate both the gating and the subcellular trafficking of Kv channels. The interaction with α-subunits takes place between the C-terminus of Kvβs and the N-terminus of the regulated channel, which an up to a four-fold symmetry (*49*). The specificity of that binding is via a conserved region in Kv members named as the Tetramerization-1 domain (T1), which contacts four loops of the tetrameric β-subunit. Particularly, in the rKv1.1 member the position of the interaction domain is located between M70 and Y80 residues, of the T1 (*50*) (*51*).

The members of this family share 70% of similarity. Indeed, protein sequences alignments revealed that the most diversity is given by the variable N-terminal domain, while the conserved Core region, which is constituted of approximately 330 aa, allowed researchers to classify the Kvβ peptides within the Aldoketoreductase-6 (*52*) group (*52*) (*53*). The crystal structure of Kvβ2 shares the typical AKR architecture, with each subunit consisting of a TIM barrel: α8β8 arrangement (*54*). AKRs act in association with nicotinamide adenine dinucleotides (*55*) as hydride transfer cofactors and are susceptible to the cellular redox state, predominant in most of the metabolic pathways (*55*). In this scenario, Kvβ proteins have been reported to strictly bind pyridine nucleotides, with a ~10-fold greater affinity for NADP(H) compared to NAD(H) cofactors. The Kvβ2 crystal showed that the association with the cofactor takes place at the C-terminus and this is probably a general feature between Kvβ members. However, the affinity of Kvβ2 for the cofactor is higher than the Kvβ1.3, thus, this parameter may vary within the same protein family (*56*). Moreover, Kvβ2 catalyse the reduction of a wide range of aldehydes and ketones, showing higher catalytic efficiencies for aromatic aldehydes (*57*) (*58*).

1.1.1.2.1.1. Kvβ1

This family presents three isoforms Kvβ1.1, β1.2, β1.3, with similar structures. Kvβ1s are wide expressed in rat brain, but also in immune system cells (*59*). The main feature of Kvβ1 peptides is the presence of a ball-and-chain domain at the NH2-terminus, which confers rapid inactivation to Kv1 channels (*60*). The Kvβ1.1 member is encoded by KCNAB1 gene and mainly found in nervous and cardiovascular systems. In neurons, knockout studies on mice highlighted reduced K^+ channels inactivation and increased neuronal excitability (*61*) (*62*). In cardiac cells, deletions of the protein lead to cardiac death. Moreover, different genomic studies associate the KCNAB1 gene with human hypertension (*63*). In T-lymphocytes, Kvβ1.1 increases the expression upon IL2 treatment, thus suggesting a certain role also in non-excitable cells (*64*). As aldoketoreductase, the subunit modulate redox sensitivity of cells and in turn, the regulation of Kv channels (*65*). In *Xenopus* oocytes, Kvβ1.1 causes the inactivation of Kv1.1 channel and confers rapid N-type inactivation to Kv1.5. By contrast, Kvβ3.1 association with Kv1.5 impairs the typical N-terminal inactivation (*66*) (*53*). Kvβ1.1 accelerates the time constant activation of Kv1.4 without affecting the channel voltage dependence (*67*). Kvβ1.2 regulates the Kv1.2 channel, which also interacts with the neutral amino acid transporter Slc7a5. The Kv1.2/Kvβ/Slc7a5 complex displays rapid inactivation time constants and this regulation can be altered by the intervention of other Kvβ, such as Kvβ2 (*68*). In general, Kvβ1.2 is able to regulate the amplitude of the endogenous Kv currents in HEK293 cells, as well as the rate of inactivation of *Shakers*. Interestingly, Kvβ1.2 modulates the redox and oxygen sensitivity of the Kv4.2, but not of *Shakers* currents (*69*). Regarding Kvβ1.3, the peptide alters the electrophysiological properties of Kv1.5 triggering rapid but partial inactivation (*70*). At the proximal N-terminus, an arginine residue has been identified, which is a binding site for intracellular PIP2. This association would prevent the N-type inactivation mediated by Kvβ1.3 (*71*).

1.1.1.2.1.2. Kvβ2

Two members belong to the Kvβ2 family, Kvβ2.1 and Kvβ2.2. The unique difference between these two proteins consists in 14 aa placed at the N-terminal

domain. For that region, most of the time is hard to distinguish the tissue proteins expression (*72*). Kvβ2.1 is the abundant member in brain, but it was also found in the immune system and skeletal muscle cells, where knockout of KCNAB2 gene leads to reduction of the skeletal muscle size.

As already mentioned, Kvβ2.1 is an AKR6 reducing preferentially aldehydes than ketones. This catalysis is NADPH-dependent respecting the typical steps of enzymatic reactions (*73*). Thus, showing an increment in the reduction rate upon major substrate concentrations, distinct pH dependences and saturated initial velocity at high substrate concentrations. An important feature that allowed the AKR classification is the fact that, by mutating the T90 to F90, the association with NADPH cofactor is impaired and this is respected in other AKR enzymes, since this residue is implied in the catalysis (*74*). Interestingly, the enzymatic activity of the subunit was observed also for lipid peroxidation products, like 1-palmitoyl, 2-oxovaleroyl, phosphatidyl and other compounds generated during fatty acids oxidation in the plasma membrane. Because Kvβ2 is in close proximity to the cell surface, the peptide catalysis may detoxify the peroxidation products protecting Kv channels. On the other hand, this mechanism could potentially modulate Kv kinetics under oxidative stress conditions (*75*).

Considering the regulation of Kv channels, the subunit is mostly described as a chaperone-like protein modulating the channels surface (*76*). However, the peptide may alter the electrophysiological properties of the channels without affecting the membrane trafficking, as in the case of the two-pore-domain potassium channels TREK1. Here, Kvβ2.1 increases the channel currents by almost 3-fold, in a concentration-dependent manner, with no effect on TREK1 surface expression (*77*) (*78*). The Kv1.2 channel presents slow inactivation and direct interacts with the endoplasmic Sig-1R that, upon ligand-activation, inhibits the channel's current. Evidences show that Kv1.1/Kv1.2/Kvβ2.1 is the most abundant complex in brain. Thus, co-expression of Kvβ2 and Kv1.2 in HEK293 cells mitigates effects of Sig-1R on Kv1.2 conductance but not the gating, probably due to competitive interaction within the macromolecular system (*79*) (*80*) (*81*).

Kvβ2.1 involves tertiary protein-protein interactions during PKC-ζ / Kv1 assembly, acting as a physical link between the other two proteins, thanks to the action of ZIP1 and ZIP2 peptides. Moreover,

Kvβ2.1 can also bind PSD95, which is known to cluster with many Kv channels at the excitatory synapses (*82*) (*83*). All these findings indicate that Kvβ2.1 modulatory peptide influences both the membrane expression and the biophysical properties of Kv channels. The association with other molecular partners, which may drastically affect α-subunits functions, further expands this regulation.

1.1.1.2.1.3. Kvβ3

As mentioned above for Kvβ1, the N-type inactivation of Kv channels may be coupled to the oxidoreductase activity of both Kvβ1.1 and Kvβ3.1. However, the inactivation of Kv1.5 by Kvβ3 N-terminus is compromised (*66*). The most abundant activity of Kvβ3 is related to Kv4 channels, especially for Kv4.3 during cardiovascular activities. Here, Kvβ3.1 along with KchIP2 accessory peptide, gives rise to unique phenotype of the channel, expressing diverse currents respect to the typical cardiac transient outward potassium currents (I_{to}). More particularly, KChIP2 normally slows the current decay rate and increases the recovery from inactivation of Kv4.3 and those effects are lost in the presence of Kvβ3.1 (*84*) (*85*). In *Xenopus* oocytes, the association between Kvβ3.1 and Pannexin1 protein directly affects the regulation of Panx1 channels, linking up the complex formation to the redox signalling (*86*).

1.1.1.2.2. KCNE modulatory proteins

KCNE gene family encodes for five single spanning transmembrane proteins. Unlike Kvβs, each KCNE is encoded by one specific gene and no splicing isoforms are known (*53*). Those peptides are expressed in various human tissues, including cardiac and immune systems (*87*) (*88*). Although they are very small peptides, not forming functional channels themselves, they associate with numerous K^+ channels drastically affecting their kinetics (*89*). Small changes in the activation motifs of KCNEs may lead to different functional consequences on the same α-subunit, as in the case of the Kv7.1 potassium channel, where a single amino acid mutation generates KCNE1-like kinetics or KNCE3-like activation (*90*). Moreover, these channels differentially target lipid rafts upon association with KCNEs, thus, the subunits affect also the subcellular targeting of conducting proteins (*91*). In leukocytes, KCNEs gene expression depends on cell proliferation and activation, and this can influence the conformation of macromolecular complexes (*92*). Mutations of KCNEs are associated with different

genetic diseases such as hereditary Long Q-T syndrome and familial periodic paralysis, arousing interest in pharmacological studies (*93*) (*94*) (*95*).

1.1.1.2.2.1. KCNE1

KCNE1 is the first KCNE-encoded protein described. KCNE1 contains around 130 amino acids and is expressed in different tissues including heart, ear, colon, uterus and lymphocytes (*96*). KCNE1 association with Kv7.1 recapitulates the cardiac slow delayed-rectifier current IKs (*97*). Moreover, KCNE1 increases hERG (*12*) current density. Indeed, the heteromer KCNQ1/KCNE1 is one of the primary sources controlling the duration of ventricular action potentials by repolarizing currents, and this corresponds to the QT interval in the electrocardiogram (*98*). For that reason, mutations of the macromolecular complex lead to the LQT syndrome development, where the QT interval is extended by prolonging the ventricular action potential's duration. Therefore, the KCNQ1/KCNE1 channel is considered a potential target for LQTS treatments (*99*) (*100*) (*101*). In this context, the heteromer undergoes endocytosis by the activation of PKC, reducing in turn the IKs (*102*). Furthermore, the KCNQ1/KCNE1 internalization may be regulated by the AMPK kinase, which mediates the Nedd4.2-dependent ubiquitinylation and consequent decrease of IKs (*103*). Thus, the channel turnover is under pharmacological investigation. Evidences show that in LQTS patients, presenting the polymorphism D85N, the Ca^{2+} channel blocker Verapamil can rescues the IKs by suppressing the ubiquitination of KCNE1 D85N (*104*). Alterations in KCNE1 gene expression has been associated also to Jervell and Lange-Nielsen-2 Syndromes (166). With respect to other Kv channels, KCNE1 can also modulate the gating of Kv2.1, Kv3.1, Kv3.2, and Kv4.3 channels (*105*) (*106*) (*107*), as well as it suppresses Kv1.4, Kv3.3, and Kv3.4 currents by intracellular retention (*108*).

1.1.1.2.2.2. KCNE2

KCNE2 mRNA has been mostly detected in heart, smooth and skeletal muscle, epithelia, and brain, as well as in cone photoreceptors and road bipolar cells, bone marrow and pancreas (*109*) (*110*) (*111*). The protein mostly affects cardiac Kv channels, but also some L-type Ca(2+) channels, such as Cav1.2, which is responsible for the cardiac L-type Ca^{2+} currents. Cav1.2 physically interacts with KCNE2, which modulates ion currents by regulation of the channel's

N-terminal inhibitory [NTI] module (*112*). KCNE2 strongly suppresses Kv1.4 and Kv3.4 currents by confining N-type α-subunits intracellularly (*113*). Moreover, association of the peptide with KCNQ1 drastically decreases the lipid rafts targeting of the channel (*114*). KCNE2 regulates hERG, Kv4.2 and Kv2.1 depending on the species (*115*). Evidence show that KCNE2 deletion in mice, leads to a switched trafficking polarity for Kv7.1 and Kv1.3, in the choroid plexus epithelium. Instead, Kv1.5 member requires KCNE2 association to localize the intercalated disks of murine ventricular myocytes (*116*). Pathologies involving KCNE2 alterations are mostly related to the cardiac tissue, where, some findings reported that KCNE2-deficient mice exhibit a higher risk for cardiovascular events, since the absence of KCNE2 gene would provide efficient substrates for the development of sudden cardiac death (*117*). However, posterior studies showed how, surprisingly, KCNE2-knockout was cardioprotective, during acute post-ischaemic period, reducing the infarct size and protecting cardiac functions (*118*). Moreover, KCNE2 associates with LQT6 syndrome and gastric cancer (*119*) (*120*).

1.1.1.2.2.3. KCNE3

KCNE3, like other KCNE subunits, is widely expressed in human tissues, associating with several Kv α subunits. High relative levels of *KCNE3* transcripts have been found in kidney, prostate, leukocytes, liver, ovary, placenta and spleen, while, minimal expression where observed in heart, colon, as well as in skeletal muscle and brain (*121*). Functionally, KCNE3 can modulate different Kv channels. Thus, KCNE3 regulates Kv2.1 homotetramers and Kv12.1 channels (*122*). Kv4.3 currents are strongly reduced in the presence of the subunit, which alters channel's activation, inactivation and recovery (*123*). KCNE3 can modulate Kv7.1 kinetics maintaining the channel constitutively active, bypassing the membrane depolarization for opening (*124*). Beside the importance of both the channel and the subunit during cardiac events, KCNE3 can be altered in atrial fibrillation, where its gene deletion increases Kv1.5 currents in atrial cardiomyocytes (*125*). Augmented KCNE3 expression has been found in ventricular tachycardia cycles leading to healed myocardial infarction scar (*126*). Furthermore, the subunit contributes to the LQTS reducing the long QT interval. In both of the cases, the alteration of KCNE3 results in impaired Kv7.1 function, leading to the

abovementioned pathological conditions (*127*). Deletion of KCNE3 gene have been also associated to the impairment of the skeletal muscle contractility and electrical properties of myoblasts (*128*), as well as to Brugada syndrome and ulcerative colitis (*129*) (*130*).

1.1.1.2.2.4. KCNE4

KCNE4 is the largest member of the protein family, approximately of 20KDa and presenting the most variable and disordered C-terminus. KCNE4 is promiscuously expressed in several tissues including heart, skeletal muscle, uterus and kidney, and less distribute also in blood cells, placenta, lungs, liver, and brain (*131*) (*132*). KCNE4 mostly acts as a dominant negative modulatory protein on numerous K^+ channels. In Big calcium-activated potassium (BK) channels reduces $K_{Ca}1.1$ currents by two mechanisms; upon KCNE4 association, the voltage-dependence of activation is shifted to more depolarizing voltages in a calcium-dependent manner. Moreover, the channel degradation is enhanced in the presence of the subunit, with a consistent decrease in the half-life of the protein, resulting in a lower membrane expression (*131*) (*133*). KCNE4 inhibits Kv1.1 currents and, with minor effects, can modulate Kv2.1 kinetics (*134*) (*122*). In Kv4.3, the subunit impairs the function of Kv4.3-KChIP2b complexes and accelerates channel's inactivation, whereas, it may strongly inhibit Kv4.2, independently to KChIP peptides (*135*) (*136*). Similarly, KCNE4 may inhibit Kv7.1 currents without affecting activation kinetics (*137*). Furthermore, KCNE4 can suppress the channel activity by interacting with Calmodulin, through a specific juxtamembrane tetraleucin motif, placed at the KCNE4 C-terminus (*138*). In the case of Kv1.3, KCNE4 affects both kinetics and current density, mediating a strong intracellular retention that traps the complex at the ER, during early stages of the secretory pathway (*139*). In addition, both the channel and the subunit have been found highly expressed in immune cells, such as macrophages and dendritic cells, where proliferation, activation, and apoptosis, along with the spatial organization of Kv1.3 at the immunological synapse, are modulated by KCNE4 (*140*).

1.1.1.2.2.5. KCNE5

KCNE5 mRNA has been detected in human heart, brain, thymus, testes, spleen, ovaries, and placenta (*121*). KCNE5 mainly regulates Kv7.1 activity, and altered expression of those complexes was found in preeclamptic placentas (*141*). Mutations in KCNE5 associate to atrial fibrillation and, distinct polymorphisms in KCNE5 have been linked to altered cardiac electrical properties (*142*). For example, the 97T polymorphism of the KCNE5 gene associates with myoblasts atrial fibrillation (*143*), while, the rs697829 polymorphism leads to survival in patients with acute coronary syndrome (*144*). Conforming to the HPA (www.proteinatlas.org) platform, KCNE5 expression was also found in Brugada syndrome and urothelial and testis cancers (176) (177).

1.1.2. Kv1.3 channelosome in the immune system

Kv1.3 is abundantly expressed in T-lymphocytes playing crucial roles during activation, directly contributing to the cellular immune response (*145*).

Upon APC-antigen presentation, T-cells proliferation is initiated by a strong Ca^{2+} influx, which may originate from both intracellular stores, mainly harboured at the ER, and from the extracellular space through specific Ca^{2+} channels placed at the plasma membrane. CRACs channels control the store operated calcium entry (SOCE) and are encoded by ORAI1 gene. Two membrane proteins residing at the ER, STIM 1 and 2, mediate activation of CRACs (*146*). When ER-Ca^{2+} stores are depleted, STIM undergoes conformational rearrangements that expose the structural domains necessary for STIM1 and STIM2 oligomerization and consequent plasma membrane trafficking. At the cell surface, the oligomer form platforms recruiting ORAI1. Thus, STIM1 deletion impairs SOCE (*147*). The increment of membrane positive charges due to Ca^{2+} influx generates a depolarization event that is detected by Kv1.3, which becomes active and repolarizes the membrane by K^+ exit. In this way, the channel provides the driving force required for calcium signalling, crucial during T-cells maturation (*148*). The K^+ efflux is supported also by the KCa3.1 channel, which activation does not depend on voltage, but rather from the Ca^{2+} binding mediated by calmodulin, in permanent association with the channel's C terminus (*149*). Hence, Kv1.3 is recruited to lipid rafts and redistributed within immunological synapses (IS) during immune responses (*150*) (*151*). PSD95 proteins ensure those mechanisms (*41*) (*152*), while, KCNE4 and Kv1.5 counteract that association (*153*). A recent work from *Capera et al*. demonstrated how Kv1.3 fills the distal SMAC of the immune interface in activated CD4$^+$ T cells, in order to favour Ca^{2+} signalling and cells activation. Later on, the Kv1.3 aggregations transfer to the centric SMAC for

internalization and release, through extracellular vesicles (*154*).

Considering the relevance of Kv1.3 in the immune environment, alterations of channel functions associate with a plethora of immunological disorders. Overexpression of the channel is detected in chronic obstructive pulmonary disease (*155*), cystic fibrosis, liver and renal disease (*156*) (*157*), psoriasis (*158*), lupus erythematosus (*159*), rheumatoid arthritis, as well as in multiple sclerosis (*160*), Alzheimer's disease and different human cancers (*161*) (*162*).

In this context, most of the modulatory subunits triggering the Kv1.3-related cell signalling, are expressed in the immune system and involved in pathological events. Kvβ1 is linked to cardiac hypertrophy in mice (*63*) and epilepsy (*163*). Kvβ2 associates with Brugada syndrome (*164*), monosomy 1p36 and epilepsy (*165*) (*166*), as well as with autoimmune encephalomyelitis (*167*) and glioma (*168*). Between KCNEs, altered KCNE4 is related to cardiac arrhythmogenesis and is directly associated with colon adenocarcinoma (*131*) (*169*). Moreover, elevated KCNE4 mRNA levels have been found in head and neck squamous cell-carcinoma and lymph node metastatic melanoma, as well as in acute lymphoblastic leukaemia and allergic rhinitis (*170*) (*171*) (*172*) (*173*). A part from their individual pathogenesis, those modulatory proteins regulates Kv1.3 during immune signalling, in some cases, with drastic effects on the channel activity. Unlike Kvβs, KCNE4 impairs the Kv1.3 lipid rafts targeting and dramatically affects the physiology of Jurkat T-lymphocytes, reducing cells proliferation (*153*).

Taking all of this in mind, the Kv1.3 channelosome might be considered a source of multiple, potential drug targets, in the channel-related immunomodulation therapy.

1.2. Protein Acylation

S-acylation consists of the posttranslational attachment of monosaturated and polyunsaturated lipids to amino acid residues of soluble, transmembrane and peripheral membrane proteins. The palmitic fatty acid addition can be classified in three categories, based on the residue involved. Thus, the *S*-palmitoylation is the major form of protein palmitoylation and consists of the addition of a palmitic (C16:0) fatty acid to cysteines via a thioester bond (*174*). The O-Palmitoylation is the addition of palmitic (C16:0), or palmitoleic fatty acids to serines or threonines by an oxyester bond (*175*) (*176*) (*177*).

Finally, the N-palmitoylation is the addition of a palmitic fatty acid to N-terminal glycines, lysines or cysteines. Although protein palmitoylation is a reversible process, the N-type does not fit this rule forming stable amide bonds (*178*) (*179*) (*180*). The enzymes responsible for this modification are protein Acyltransferases and Palmitoyl Transferases (zDHHC-PATs), presenting a conserved Asp-His-His-Cys motif, which is necessary for catalysis. However, although the reaction involves the amino acid cysteine, no consensus sequence governs this mechanism (*181*) (*182*). zDHHC-PATs are distributed in many cellular compartments, including the ER, Golgi apparatus and endosomes (*183*) (*184*). Thus, they increase palmitoylation heterogeneity by transporting proteins among different cellular levels, throughout subsequent cycles of acylation and deacylation (*185*).

Since the palmitoylated proteins are abundant and quite diverse, the function of this modification strongly depends on the targeted protein. In general, palmitoylation increases the hydrophobicity of protein domains, facilitating their membrane association and stabilization, as well as contributing to protein–protein interactions and subcellular trafficking among membrane organelles and within specific membrane microdomains (*186*). Palmitoyl chains act as a lipid anchor for various secreted signaling proteins, such as the membrane fusion SNAP-25 (*183*). In addition to membrane association, palmitoylation controls the patterning of SNAP25 across the endoplasmic reticulum (ER) and the trans-Golgi network. Mutations of Cys88, 90 increases this localization. In the case of Gα subunits of trimeric G proteins, palmitoylation mediates the phosphorylation-dependent internalization of the protein, ensuring the proper ER-Golgi trafficking and targeting membrane lipid rafts (LRs) (*187*) (*188*). Instead, in Ras GTPases the loss of palmitoylation sites show inhibitory effects, moving out H-RAS of LRs and thereby influencing the correct activation of the Raf-MAPK cascade (*189*).

Together these findings indicate that palmitoylation has pleiotropic effects on cell biogenesis, controlling the subcellular trafficking and fine-tuning the precise number and distribution of palmitoylated cysteine residues (Figure 2).

1.2.1. Palmitoylation of voltage-gated potassium channels

Kv channels are post-translationally modulated by a wide range of modifications, including phosphorylation, N-glycosylation, ubiquitination, redox modifications and lipidation (190). In this scenario, the majority of palmitoylated Kv channels belong to the Shaker subfamily. For instance, Kv1.1, Kv1.2 and Kv1.4 are palmitoylated by zDHHC14 in neurons (191). Specifically, Kv1.1 member is covalently palmitoylated at cysteine 243 and no other modified residues showed the same effect. In this context, C243 alone is responsible for the channel acylation and in absence of the modification, Kv1.1 inactivates at higher depolarized potentials (192). Similarly, although Kv1.5 can be palmitoylated in both the COOH and the NH2 terminus, only a C-terminal cysteine is responsible for channel thioesterification (193). Moreover, palmytoilated Kv1.5 redistributes into different intracellular compartments, skipping the protein degradation. Because the degradation rate of palmitoylated Kv1.5 channels is lower, their surface expression increases along with K+ currents generation (194). These evidences highlights palmitoylation-dependent pleiotropic roles in the regulation and biogenesis of voltage-gated ion channels.

1.2.2. Palmitoylation of macromolecular systems

In addition to the modulation of α-subunits, palmitoylation may affect the accessory proteins composing different macromolecular complexes, which in turn fine-tunes ion channel physiology. For instance, the glutamate receptor proteins 1b (GRIP1) palmitoylation is catalysed by zDHHC5/8, accelerating the recycling of AMPA receptors, thereby facilitating the synaptic vesicle trafficking in neurons (195) (196). Moreover, the zDHHC5 cycling between the plasma membrane and endosomes of dendrites, contributes to the stability of AMPA channels at the postsynaptic membrane (197). Another example is the Nav β1/2 non-pore-forming subunits associated with Nav channels. Such adhesion molecules can also modulate K+ currents and intracellular calcium signalling pathways. Navβ1 subunit undergoes palmitoylation at Cys162 (198). Addition of palmitate enhances the β1 membrane association and stabilizes the polypeptide at this compartment while reducing the clathrin-mediated endocytosis of the protein (199). In PSD-95 protein, palmitoylation at N-terminal Cys3-5 residues is necessary for a proper function during Kv1.4-clustering. The impairment of protein thioesterification dysregulates perinuclear trafficking, postsynaptic targeting and ion channel clustering activity (200). Interactions with BACE1, which acts in lipid rafts driving the amyloid precursor protein APP in the amyloidogenic direction and causing β-amyloid production. Outside the raft domains, BACE1 is preferentially cleaved by nonamyloidogenic α-secretase. Since BACE1 uses palmitoylation for this specific membrane anchoring, the modification is critical not only for polypeptide cellular localization but also for pathologic Aβ generation (201). Moreover, Kv7 channels localize to lipid rafts upon interaction with palmitoylated BACE1, leading to a new gating rearrangement (202). Further examples of palmytoilation of ancillary subunits include the KChIP members in association with Kv4 channelosomes. Kv4.3 exhibits higher current densities in the presence of palmitoylated KChIP2 concomitantly with an elevated number of channels at the cell membrane (203). Simultaneously, palmitate attachment reduces the cytoplasmic mobility of KChIP2, thereby stabilizing the polypeptide in the cytosol. However, palmitoylation also triggers KChIP2 distribution between the nucleus and plasma membrane, promoting the Kv4.3 surface trafficking (204). In summary, thioesterification of auxiliary subunits may result in double regulation. First, β-subunit homeostasis is directly affected by altering cellular localization. Second, palmytoilation affects channel function by spatial reorganization. Therefore, palmitoylation of ancillary polypeptides within macromolecular complexes, either directly or indirectly, influences the functional properties of the regulated channels.
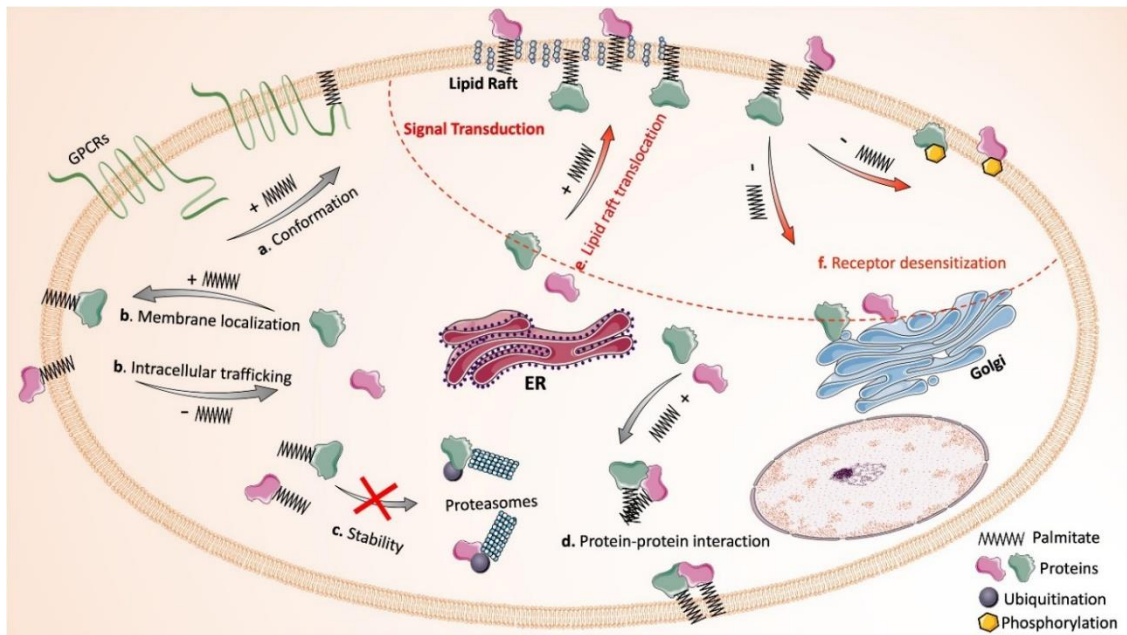
Figure 2. Dynamic regulation of protein palmitoylation. **a)** Palmitoylation altering the conformation or structure of proteins; **b)** Palmitoylation mediating intracellular trafficking and membrane stabilization of proteins; **c)** Palmitoylation stabilizing proteins by preventing misfolding and ubiquitination-dependent degradation; **d)** Palmitoylation favouring protein-protein interaction directly and indirectly. The upper right region circled by red dash line indicates how palmitoylation and de-palmitoylation cycles drastically impact signal transductions; **e)** Signalling proteins requiring palmitoylation for lipid-rafts localization; **f)** Receptor desensitization mediated by de-palmitoylation and followed by activation, promoted by the phosphorylation of receptors or the translocation of membrane signalling proteins to the cytosol. From Yang et al. (2020).

1.2.3. Immunological consequences of VGIC palmitoylation

The importance of protein palmitoylation is steadily emerging, not only for the dynamism and for regulation of a wide range of polypeptides but also in several diseases, such as cancer, Huntington's disease, LQT syndrome and mental disorders like schizophrenia, Alzheimer's disease and Parkinson's disease (205) (206). Given the multitude of cellular processes and signalling pathways in which lipidation is involved, the lipid metabolism is crucial for a correct cell homeostasis. There are different types of lipid-addition, including fatty acids. Their intracellular concentrations are highly regulated; indeed, fatty acids are elementary units for the biosynthesis of other complex lipid molecules. Palmitate is synthetized by the fatty acid synthase (207) complex, because of condensation reactions between CoA and malonylCoA. Both of the enzymes are products of glucose metabolism and Krebs cycle, therefore, the lipid biosynthesis is

directly involved in the cellular energy homeostasis. Alterations of the lipid metabolism are prevalent in many human diseases, affecting the availability of lipid donors and thereby the general proteins lipidation (208). Thus, protein lipidation is partially involved in the pathological consequences of the dysregulated lipid metabolism, such as in cancers and metabolic diseases.

Among the protein lipidations, S-palmitoylation plays an important role in the innate immune response, by acting on many immune receptors. For instance, palmitoylation of ORAI1 is modulates the calcium fluxes during immune activation (209), as well as inducing the STING clustering at the trans-Golgi membrane. This is an important starting point for the phosphorylation of the IRF3 triggered by TANK1 (210). The loss of palmitoylation causes the blockage of the type I interferon response (211). Furthermore, thioesterification is involved in the correct functioning of distinct TLRs. The

binding of TCR to MHC complexes on antigen-presenting cells (212) represents the first step of the TCR transduction pathway. This is followed by the recruitment of protein tyrosine kinase Lck to the cytoplasmic domains of CD4 and CD8 co-receptors, triggering the signalling cascade that lead to the formation of the LAT signalosome. In this context, CD4 palmitoylation at Cys394 and Cys397 regulates the clustering with TCR/PKC in lipid raft microdomains. Palmitoylation is required also for the appropriate CD8 function, increasing its association with Lck in lipid rafts. In the case of TLR2, palmitoylation of Cys609 ensures the correct surface localization and the consequent expression of the NF-kB gene. Therefore, palmitoylation connects the lipid metabolism to the immune response and host defence (213). In this scenario, the enzymes responsible for thioesterification and deacylation became attractive pharmacological targets. For example, ZDHHC5 may function as an oncoprotein by catalysing the enzyme EZH2 palmitoylation, thereby contributing to the progression of p53-mutated associated cancers, such as glioma and non-small-cell lung cancer. On the other hand, ZDHHC2 has been described as a probable tumor suppressor in different human cancers (214) (215). The ZDHHC9 protein mediates the palmitoylation of N-Ras and H-Ras and alterations of its activity are associated with X-linked mental retardation and colorectal cancer. ZDHHC21 deficiency also results in endothelial inflammation and systemic inflammatory response syndrome (216). With respect to APT1 and APT2, they are responsible for the abolishment of fatty acids addition from acylated proteins, during the lysosome degradation. The inhibition of these thioesterases blocks the Ras trafficking, impeding their oncogenic activity (217).

1.3. Protein dimerization, interplay with palmitoylation.

Dimerization is a diffuse physiological mechanism by which two interacting proteins assemble in functional homo or hereto dimers, conferring several structural and functional advantages that include improved stability and complexity, and regulation of specificity and accessibility of active sites (218). For this reason, molecular mechanisms behind this process are physiologically relevant.

Dimerization can be enhanced by introducing coiled-coil zipper sequences, which act by hydrophobic interactions between leuchine rich motifs forming homo or heterodimers (219). Between members of the ARFGAP protein family, p95-APP1 forms homo and heteroligomers with PKL/p95-APP2. Both of them contain a coiled-coil region including a leucine zipper pattern, involved in dimerization (220). One of the best example of dimerizing proteins are GPCR, characterized by seven transmembrane structures. Between them, somatostatin receptors 2-3 and 1-5 dyads result in altered functions and pharmacology (221).

Dimerization is involved in a variety of pathological conditions, for example, the mechanism is crucial for the activation of EGF receptors, which are mutated in many cancers, especially in breast and ovarian cancers, as well as in non-small cell lung cancer (222). Homodimerization is also required for the TBK1 activation, together with autophosphorylation of a serine residue. Alteration of those mechanisms have been related to amyotrophic lateral sclerosis (210).

An additional interplay is between dimerization and protein palmitoylation. The dynamism between the two modifications may controls both spatial organization and functional activity of many molecular complexes. For instance, the rearrangement of GPCRs into lipid rafts and proteins dimerization is modulated by palmitoylation (223). The human dopamine transporter regulates the dopamine intracellular concentrations in neurons forming stable oligomers at the plasma membrane. The stability of dyads involving the TM12, is modified when this transmembrane domain is palmitoylated. Therefore, palmitoylation may change the cellular predisposition generating different dimers settings (224). Palmitoylation of APP allows the peptide dimerization, hence, palmitoylated APPs dimers may undergo β-

cleavage (225). Considering the enzymes responsible for protein acylation, the oligomerization of the ZDHHC6 member is strongly affected by protein's palmitoylation (226). Dimerization of the CD44 is critical for the signal transduction that leads to tumor progression, including angiogenesis, cell migration and metastasis. Addition of palmitate molecules to cysteine chains impairs the self-recognition of CD44 (227). Moreover, palmitoylation induces the dimerization of rhodopsin, modifying its affinity for raft-like membrane domains (228).
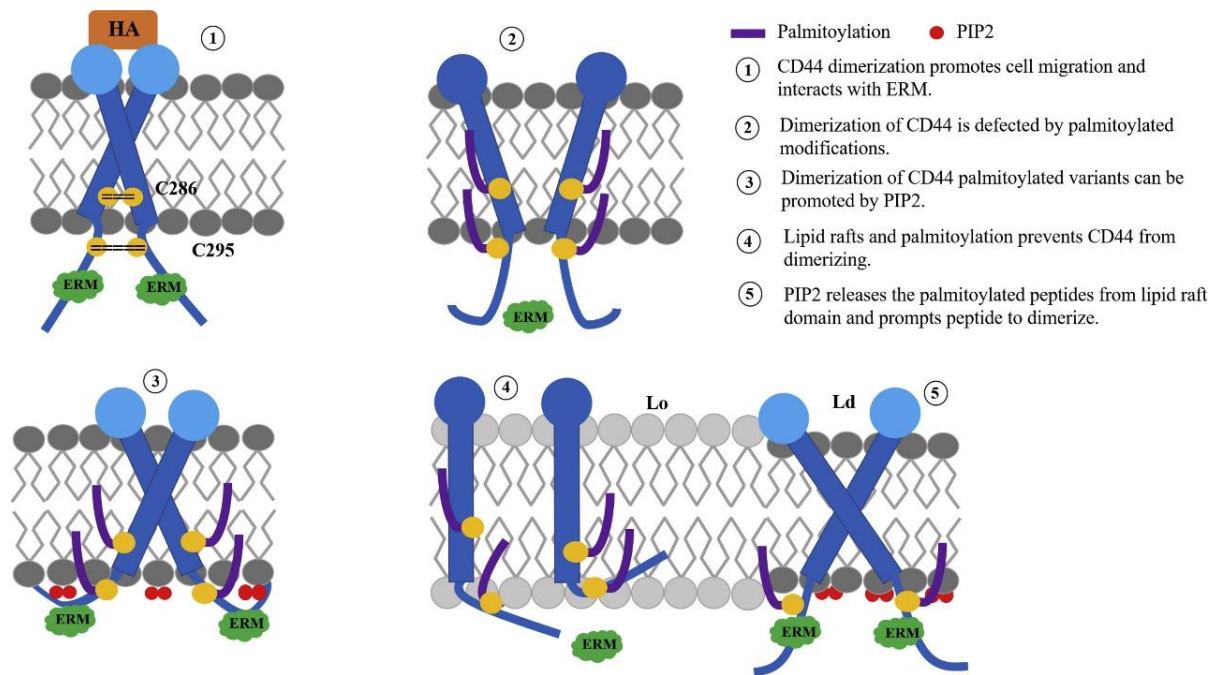
Figure 3. Palmitoylations regulating CD44 homodimerization. Dimerization and localization of CD44 is sensitive to palmitoylation and specific membrane environments. The homodimerization of the wild-type protein depends on the interaction of cysteines on the juxta-membrane domain and is favourable for hyaluronic acid (HA) binding. Insertion of palmitate molecules impairs CD44 dimerization, impeding the binding between the receptor and the cytoskeleton adaptors (ERM). Dimerization of CD44 palmitoylated variants can be promoted by PIP2 addition. The presence of PIP2 lipids allows ERM to bind to the surface of the membrane and further promotes protein association. From Ma et al. (2022).

2. Aims

2. Aims

Voltage-gated potassium (Kv) channels regulate the repolarization of excitable cells and maintain the resting potential in both excitable and non-excitable cells. Because they are ubiquitously expressed, Kv play distinct functions including the regulation of cell volume, adhesion, mobility, cell-cycle, homeostasis and apoptosis. Functional channels are generally formed by the tetramerization of four conducting α subunits association with multiple regulatory β subunits. Accessory subunits can modulate different properties of Kv channels such as traffic, electrophysiology and association with other molecular partners.

Kv1.3 is mainly expressed in the nervous and immune systems being crucial in T lymphocyte physiology. Thus, Kv1.3 participates in their activation and proliferation. Upon T cell activation, Kv1.3 contributes to the immune response by clustering at the immunological synapse regulating the calcium signalling. Several ancillary subunits, such as Kvβs and KCNEs are expressed in the immune system and participate in the Kv1.3-related immune pathways, triggering notable consequences on the leukocyte physiology. S-acylation and protein oligomerization are key modifications for the majority of immunological partners. These mechanisms are also predominant within the Kv1.3 channelosome, affecting plasma membrane expression and oligomeric state of both Kvβs and KCNE4 and in turn, the modulation of Kv1.3

The present PhD thesis aimed to elucidate the regulation of multiple modulatory proteins and their consequences on the Kv1.3 physiology. For this purpose, we analysed the homo and heteroligomerization, the S-acylation and the subcellular trafficking of Kvβs and KCNE4. Moreover, we studied the relationship between Kv1.3, KCNE4 and calmodulin in heterologous expression systems and the Kv1.3/KCNE4 complex in activated antigen presenting cells. Therefore, the specific goals of this PhD thesis were:

1. To characterize the structural elements and molecular mechanisms underlying the Kvβ2.1 clustering into immunological synapses during leukocyte activation.

2. To elucidate the stoichiometry and cellular distribution of the Kvβ oligomers.

3. To determine molecular rearrangements underlying the regulation of Kv1.3 by KCNE4.

4. To characterize the Kv1.3/KCNE4 complexes in antigen presenting cells.

3. Results

Report
of the thesis director

Dr. Antonio Felipe Campo, Full Professor at the Department of Biochemistry and Molecular Biomedicine, as director of the PhD thesis of Silvia Cassinelli, reports that in the development of her PhD project "Regulatory subunits controlling the Kv1.3 channelosome", the candidate Silvia Cassinelli has actively participated in three research articles published in peer-reviewed journals, and one additional contribution pending to be submitted:

1. **S-acylation-dependent membrane microdomain localization of the regulatory Kvβ2.1 subunit.** Sara R. Roig, Silvia Cassinelli*, María Navarro-Pérez, Mireia Pérez-Verdaguer, Irene Estadella, Jesusa Capera, Antonio Felipe. Published in Cellular and Molecular Life Sciences: 2022 April, 79(5), 230. Doi: 10.1007/s00018-022-04269-3. Impact Factor: 8. Quartile: 1. Decile: 2. Subject area and category: Biochemistry and Molecular Biology. This article belong to the first Contribution, Chapter I, of this manuscript. Silvia Cassinelli participated in the corrections proposed by the reviewers and performed all the experiments containing biochemical and confocal analyses of protein palmitoylation.

2. **Oligomerization and Spatial Distribution of Kvβ1.1 and Kvβ2.1 Regulatory Subunits.** Sara R. Roig, Silvia Cassinelli*, Andre Zeug , Evgeni Ponimaskin and Antonio Felipe. Published in Frontiers in Physiology, 2022 June, (13) 930769. Doi:10.3389/fphys.2022.930769. Impact Factor: 4. Quartile: 2. Decile: 3. Subject Area: Molecular Biology; Category: Physiology. This article belong to the second Contribution, Chapter I, of this manuscript. Silvia Cassinelli participated in the corrections proposed by the reviewers experiments containing protein extraction from native tissues.

3. **Calmodulin-dependent KCNE4 dimerization controls membrane targeting**. Sara R Roig, Laura Solé, Silvia Cassinelli, Magalí Colomer-Molera, Daniel Sastre, Clara Serrano˘Novillo, Antonio Serrano-Albarrás, M Pilar Lillo, Michael M Tamkun, Antonio Felipe. Published in Scientific Reports; 2021 July, 11(1):14046. doi: 10.1038/s41598-021-93562-5. Impact factor: 4.997. Quartile: 1. Decile: 3. Subject area and category: Multidisciplinary science. This article belong to the third Contribution, Chapter II, of this manuscript. Silvia Cassinelli participated in the corrections proposed by the reviewers and contributed to the realization of figures containing co-immunoprecipitation studies. This article has been used also in the PhD dissertation titled "Molecular determinants of the Kv1.3/KCNE4 interaction" performed by doctor Daniel Sastre Martínez at the Molecular Physiology laboratory, in the University of Barcelona, Department of Biochemistry and Molecular Biomedicine, under the supervision of Professor Antonio Felipe Campo.

4. **Palmitoylation regulates the architecture and cellular targeting of KCNE4**. Silvia Cassinelli, Carla Viñola-Renart, Alexine. De Wit, María Navarro-Pérez, Jesusa Capera, Geert Van Den Bogaart, Antonio Felipe. This article belong to the fourth Contribution, Chapter III, of this manuscript. Silvia Cassinelli performed all the experiments and the data analysis of this article except the membrane trafficking analysis in CY15 samples.

* Silvia Cassinelli and Sara Roig are first co-authors, contributing equally to this work.

Chapter I

Oligomerization and subcellular compartimentalization of Kvβs modulatory subunits

S-acylation-dependent membrane microdomain localization of the regulatory Kvβ2.1 subunit

Sara R. Roig[1,2] , Silvia Cassinelli[1], María Navarro-Pérez[1], Mireia Pérez-Verdaguer[1,3] · Irene Estadella[1] · Jesusa Capera[1,4] · Antonio Felipe[1]

[1] Molecular Physiology Laboratory, Departament de Bioquímica i Biomedicina Molecular, Institut de Biomedicina (IBUB), Universitat de Barcelona, Avda. Diagonal 643, 08028 Barcelona, Spain

[2] Imaging Core Facility, Biozentrum University of Basel, 4056 Basel, Switzerland

[3] Department of Cell Biology, School of Medicine, University of Pittsburgh, 3500 Terrace Street, Pittsburgh, PA 15261, USA

[4] Kennedy Institute of Rheumatology, University of Oxford, Oxford OX3 7FY, UK

ORIGINAL ARTICLE

S-acylation-dependent membrane microdomain localization of the regulatory Kvβ2.1 subunit

Sara R. Roig[1,2] · Silvia Cassinelli[1] · María Navarro-Pérez[1] · Mireia Pérez-Verdaguer[1,3] · Irene Estadella[1] · Jesusa Capera[1,4] · Antonio Felipe[1]

Abstract

The voltage-dependent potassium (Kv) channel Kvβ family was the first identified group of modulators of Kv channels. Kvβ regulation of the α-subunits, in addition to their aldoketoreductase activity, has been under extensive study. However, scarce information about their specific α-subunit-independent biology is available. The expression of Kvβs is ubiquitous and, similar to Kv channels, is tightly regulated in leukocytes. Although Kvβ subunits exhibit cytosolic distribution, spatial localization, in close contact with plasma membrane Kv channels, is crucial for a proper immune response. Therefore, Kvβ2.1 is located near cell surface Kv1.3 channels within the immunological synapse during lymphocyte activation. The objective of this study was to analyze the structural elements that participate in the cellular distribution of Kvβs. It was demonstrated that Kvβ peptides, in addition to the cytoplasmic pattern, targeted the cell surface in the absence of Kv channels. Furthermore, Kvβ2.1, but not Kvβ1.1, targeted lipid raft microdomains in an S-acylation-dependent manner, which was concomitant with peptide localization within the immunological synapse. A pair of C-terminal cysteines (C301/C311) was mostly responsible for the specific palmitoylation of Kvβ2.1. Several insults altered Kvβ2.1 membrane localization. Therefore, growth factor-dependent proliferation enhanced surface targeting, whereas PKC activation impaired lipid raft expression. However, PSD95 stabilized Kvβ2.1 in these domains. This data shed light on the molecular mechanism by which Kvβ2.1 clusters into immunological synapses during leukocyte activation.

Keywords Potassium channels · Regulatory subunits · Palmitoylation · Immunological synapse · Lymphocytes

Introduction

Voltage-gated potassium channels (Kv) control action potentials in muscles and nerves. Furthermore, Kv plays fundamental functions during leukocyte activation, proliferation and apoptosis. In addition, the association with different accessory proteins further increases their functional diversity. These ancillary interactions affect not only the electrophysiological properties of the channels, but also their localization, trafficking and turnover [1, 2].

The Kvβ family was the first group of proteins identified as Kv channel regulatory subunits. Three different genes (*KCNAB1*, *KCNAB2* and *KCNAB3*) encode this family, including different splicing variants [1]. The crystal structure of the Kv1.2 channel in the presence of Kvβ2.1 confirmed the soluble nature of these Kvβ peptides [3]. These cytoplasmic proteins, via their conserved C-terminal domain, associate with α-subunits by interacting with an N-terminus preserved structure in Kv [4]. In addition to regulating the electrophysiological properties, some Kvβ members alter the trafficking of Kv channels. Therefore, an increase in Kv channels at the cell surface claims chaperone-like effects [5, 6].

✉ Antonio Felipe
afelipe@ub.edu

1   Molecular Physiology Laboratory, Departament de Bioquímica i Biomedicina Molecular, Institut de Biomedicina (IBUB), Universitat de Barcelona, Avda. Diagonal 643, 08028 Barcelona, Spain

2   Imaging Core Facility, Biozentrum University of Basel, 4056 Basel, Switzerland

3   Department of Cell Biology, School of Medicine, University of Pittsburgh, 3500 Terrace Street, Pittsburgh, PA 15261, USA

4   Kennedy Institute of Rheumatology, University of Oxford, Oxford OX3 7FY, UK

🖉 Springer

While the modulation of the activity of Kv channels by the Kvβ subfamily has been under intensive investigation, the Kvβ subcellular distribution has been poorly analysed. In addition to cytosolic localization, Kvβ1.1, but not Kvβ2.1, associates with the actin-based cytoskeleton [4]. This interaction, placed in the ball-and-chain N-terminal domain of Kvβ, induces resistance to extraction with nonionic detergents [7] and could explain why Kvβ1.1 increases Kv1.1 current inactivation under depolymerization [8, 9]. However, Kvβ2 polarizes in some tissues in association with the microtubular cytoskeleton [10, 11].

From a functional point of view, Kvβ2, lacking the inactivation ball-and-chain domain, enhances folding, glycosylation, trafficking and axonal targeting of Kv1 channels. However, this function is highly dependent on the α-subunit [5, 12]. In addition, Kvβ2 functions as alpha-keto reductase (AKR) [13, 14]. Genetic ablation of Kvβ2 leads to reduced lifespans, occasional seizures, and cold swim-induced tremors. 1p36 deletion syndrome, with a *KCNAB2* genetic deficiency, triggers childhood seizures and altered electroencephalograms [15]. However, a further Kv1 distribution analysis claims that neither the chaperone-like function nor the AKR-like catalytic activity of Kvβ2 would be responsible for this phenotype, pointing to a more complex scenario [16, 17].

Leukocytes express a limited repertoire of Kv channel proteins, including the Kv1.3 channel and Kvβ1 and Kvβ2 regulatory subunits [18, 19]. Similar to Kv1.3, Kvβ peptides are regulated during proliferation and activation in leukocytes. Kv1.3 targets the immunological synapse (IS) during cellular responses. Although there is no direct experimental proof, because ZIP kinases associate with both Kvβ2 and protein kinase C (PKC) ζ, assembling the PKCζ-ZIP-Kv1.3 complexes, evidence most likely situates Kvβ2 within the interactome of the IS [20–22]. ZIP1 and ZIP2 phosphorylate Kvβ2 by PKCζ forming heteromultimeric complexes. In this scenario, PKC activation displaces Kv1.3 from rafts [23], which are concentrated in the IS [24]. Whether Kvβ2 routes to the cluster either by direct association with Kv1.3, ZIP and PKC or by self-targeting is unknown. This information turns crucial to understanding the complex architecture that configures the IS during the immunological response [20, 22, 25].

This study demonstrates, for the first time, the presence of Kvβ regulatory subunits at the plasma membrane. In addition, Kvβ2, but not Kvβ1, targets lipid raft microdomains and concentrates at the immunological synapse. Kvβ2 routes to these spots in the absence of Kv1.3 but is highly dependent on the S-palmitoylation of two distal C-terminal cysteine residues. Furthermore, proliferation and activation differentially altered Kvβ2 localization. While proliferation concentrates Kvβ2 in these domains,

PKC-dependent activation decreases its abundance. However, PSD95 stabilizes the presence of this regulatory peptide in rafts.

Results

Kvβ localized at the plasma membrane, and Kvβ2.1, but not Kvβ1.1, targeted lipid rafts

The regulatory voltage-gated Kvβ1.1 and Kvβ2.1 peptides are cytosolic proteins that clearly display intracellular phenotypes (Fig. 1Aa–Ah). However, when the Kvβ pattern was analyzed further, pixel-by-pixel analysis revealed some partial colocalization with plasma membrane staining (Fig. 1 Ad and Ah). This Kvβ cell surface expression was further confirmed in enriched plasma membrane preparations (Fig. 1B, C).

Evidence claims that the association of Kvβ1.1, but not Kvβ2.1, with actin filaments would locate Kvβ1.1 near the plasma membrane [7]. Coimmunoprecipitation studies confirmed that, unlike Kvβ2.1, Kvβ1.1 indeed interacted with β-actin (Fig. 1D, E). In addition, the membrane localization of Kvβ subunits was independent of the amount of protein expressed per cell (Fig. S1).

To further study the membrane distribution of Kvβ, cell-unroofing preparations (CUPs) were prepared from HEK cells transfected with Kvβ1.1CFP and Kvβ2.1CFP (Fig. 2A–F). Both Kvβ1.1 (Fig. 2A–C) and Kvβ2.1 (Fig. 2D–F) were clearly detected in CUPs, but their distribution differed. While Kvβ1.1 was distributed evenly, Kvβ2.1 mostly appeared as a punctate pattern. Certain punctate patterns of ion channels indicate protein localization in discrete lipid raft microdomains [26]. Because Kvβ2.1 did not interact with β-actin but was present in the plasma membrane, showing a punctate pattern, whether Kvβ2.1 targeted lipid raft microdomains was postulated (Fig. 2H). Interestingly, while Kvβ2.1 localized in *rafts* (8 ± 2%) Kvβ1.1 did not (Fig. 2G, H). Kvβ2.1 lipid raft targeting was further confirmed by cholera toxin β subunit (CTXβ) staining in both whole cells and CUPs (Fig. S2). Several ion channel proteins, including Kv, target lipid rafts by interacting with caveolin via caveolin-binding domains (CBDs) [27, 28]. A structural analysis of Kvβ2.1 revealed several putative CBDs (Fig. S3A). However, coimmunoprecipitation between both Kvβs and caveolin demonstrated that neither Kvβ1.1 nor Kvβ2.1 showed an association with caveolin (Fig. S3B-C). These results suggested that Kvβ2.1 targets the plasma membrane lipid raft microdomains by specific mechanisms independent of actin filaments and not mediated by caveolin interaction.
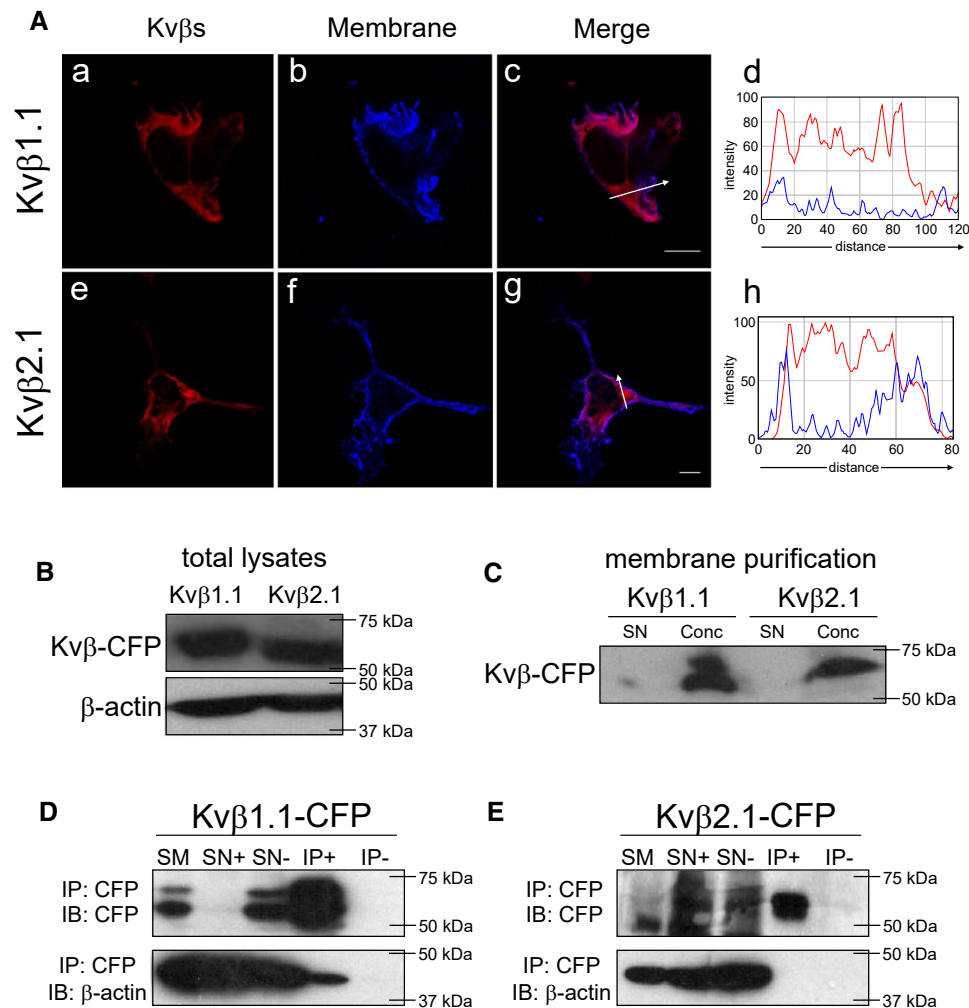
Fig. 1 Cytoplasmic Kvβ1.1 and Kvβ2.1 also target the plasma membrane. HEK 293 cells were transfected with Kvβ1.1CFP and Kvβ2.1CFP, and the cellular expression was studied. **A** Kvβ1.1 (a-c) and Kvβ2.1 (e–g) distribution. (Ad and Ah) Pixel-by-pixel analysis of Kvβs and the membrane marker. Histograms derived from arrow sections in c and g. a and e, Kvβ in red; b and f, membrane in blue; c and g, merge; purple indicates colocalization. Scale bars represent 10 µm. **B** Kvβ1.1CFP and Kvβ2.1CFP expression in whole lysates from HEK cells. **C** Purified membranes from HEK cells expressing Kvβ1.1CFP and Kvβ2.1CFP. SN, supernatants; Conc, concentrated membranes. **D**, **E** Coimmunoprecipitation of Kvβ1.1CFP and Kvβ2.1CFP with β-actin. **D** Coimmunoprecipitation of Kvβ1.1CFP with β-actin. **E** Absence of coimmunoprecipitation of Kvβ2.1CFP with β-actin. Top panels: immunoblot (IB) against CFP (Kvβs). Bottom panels: immunoblot (IB) against β-actin. SM, starting material. SN+, supernatants in presence of antibody. SN-, supernatants in absence of antibody. IP+, immunoprecipitation in the presence of antibody. IP-, immunoprecipitation in the absence of antibody

S-acetylation drives Kvß2.1 to cell plasma membrane lipid raft microdomains

Soluble proteins may attach to the eukaryotic plasma membrane by lipidic posttranslational modifications such as S-acetylation. Palmitoyl acyltransferases (PATs) add palmitate to cysteine residues, which can be reverted by thioesterases. Palmitoylation helps protein–protein interactions and confers protein stability but also improves trafficking and membrane association [29].

Evidence situates Kvβ2.1 at the lymphocyte IS, which is enriched in lipid rafts [20, 24]. Because Kvβ2.1 targeted raft microdomains by actin- and caveolin-independent mechanisms, we analyzed whether Kvβ2.1 could undergo palmitoylation, facilitating membrane targeting. The mKvβ1.1 and mKvβ2.1 structures (https://www.UniProt.org) share five cysteine putative targets for S-acylation (Fig. 3A). Palmitoylation ABE analysis of Kvβ2.1 and Kvβ1.1 showed that both peptides were palmitoylated (Fig. 3B, C). Thus, biotin pulled down (PD) samples, in the presence of hydroxylamine (+HA), which cleaves palmitoyl-cysteine thioester linkages, revealed the palmitoylation of flotillin (positive control, which also targets rafts) and Kvβ2.1, as well as Kvβ1.1 (Fig. 3B, C). A further PLA assay definitely demonstrated
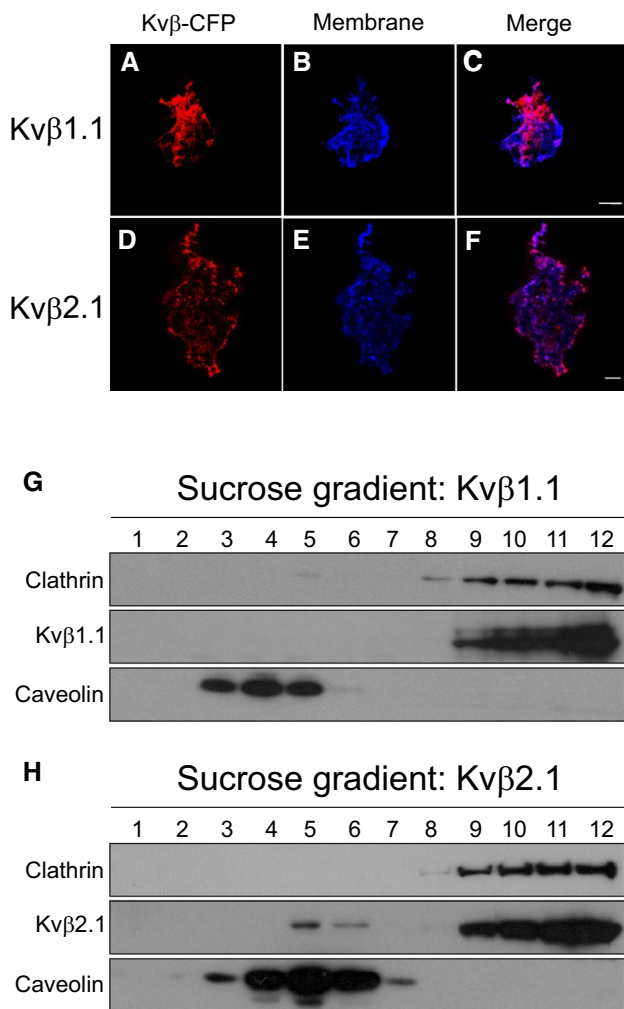
Fig. 2 Kvβ expression in cell-unroofing preparations (CUPs) and lipid raft microdomains. **A–C** Kvβ1.1CFP and the membrane marker in CUPs. **D–F** Kvβ2.1CFP and the membrane marker in CUPs. **A** and **D** Kvβs-CFP in red; **B** and **E** Membrane marker in blue; **C** and **F** merged channel; purple indicates colocalization. Scale bars represent 10 μm. **G** and **H** Lipid raft isolation of HEK cells transfected with Kvβ1.1CFP **G** and Kvβ2.1CFP **H**. Sequential sucrose fractions were extracted from the top (1, lowest density) to the bottom (12, highest density) of the tube and the Kvβ expression analyzed by western blot

that cell surface Kvβ2.1 was indeed S-palmitoylated in HEK 293 cells (Fig. 3D). In fact, membrane colocalization analysis indicated that palmitoylated Kvβ2.1 (Alk-C16) targeted the plasma membrane better than total Kvβ2.1 (Fig. 3E).

The S-acylation of Kvβ2.1 could have no correlation with lipid raft targeting because Kvβ1.1 was also palmitoylated. Therefore, two additional treatments approached lipid raft targeting: 2-bromopalmitate (2-BP) and H_2O_2 (Fig. 4A–C). 2-BP competes against palmitate for the palmitoyltransferase domain of PATs. In addition, H_2O_2, a strong oxidant, impairs palmitoylation on the SH groups by the formation of cistine bonds [30, 31]. Additionally, the Kvβ family exhibits NADPH oxidoreductase activity, which buffers oxidant

reactions. Therefore, by combining both treatments, the presence of Kvβ2.1 in lipid raft domains related to either palmitoylation or oxidation could be analyzed (Fig. 4D). Around 10% of Kvβ2.1 targeted to lipid rafts, but this was impaired by 2-BP (Fig. 4A, B) and H_2O_2 (Fig. 4C) by approximately $83.9\% \pm 9.8$ and $72.3\% \pm 10$, respectively (Fig. 4E). The combination of both treatments (Fig. 4D) triggered a similar reduction ($86.6\% \pm 3.9$). These results pointed to S-palmitoylation as responsible for the lipid raft targeting of Kvβ2.1 independent of oxidoreductase activity.

Human T lymphocytes concentrate palmitoylated Kvß2.1 at the immunological synapse

We showed that palmitoylated Kvβ2.1 targeted plasma membrane lipid raft microdomains. In addition, Kvβ2.1 interacts with ZIP1/2 and PKC, providing an effective phosphorylation cluster for signaling in the IS [20, 22, 25]. During T-cell activation, IS, enriched in lipid rafts, concentrates Kv1.3 channels, which in turn may associate with Kvβ2.1 to fine tune the immune response [32]. However, our data would indicate that Kvβ2.1 is located in IS via palmitoylation, even in the absence of Kv1.3. Therefore, the AKR activity of Kvβ2.1 in addition to further functions would be independent of channel expression. In this scenario, evidence claims Kvβ2.1 localization at IS [20]. Although palmitome studies identify Kvβ2 in brain [33, 34], this protein is not found in some leukocyte analysis [35–39]. Human CD4 + lymphocytes and human Jurkat T cells expressed Kvβ2 (Fig. 5A, C). Biotin pulled down extracts (PD), in the presence of hydroxylamine, revealed that CD4 + lymphocytes (Fig. 5B) and Jurkat cells (Fig. 5D) expressed palmitoylated Kvβ2.1, which was located on the plasma membrane surface (Fig. 5E) and targeted lipid rafts (Fig. 5F) in Jurkat lymphocytes. Cell conjugates between SEE-activated human B lymphocytes (Raji) and human T lymphocytes (Jurkat) demonstrated that while Kvβ2.1 evenly stained the surface of T cells, in the absence of IS, Kvβ2.1 concentrated at the IS once the synapse was achieved (Fig. 5Ga–e). Non-SEE activated Raji cells generate no synapse with Jurkat T cells and Kvβ2 did not accumulate in cell-to-cell contact surfaces (Fig. 5Gf–i).

Distal C-terminal cysteines are responsible for the specific palmitoylation of Kvß2.1

We demonstrated that palmitoylated Kvβ2.1 reached plasma membrane lipid raft microdomains and polarized into IS during the immune response. Because 2-BP is promiscuous and targets PAT enzymes, transporters and many palmitoylated proteins [40], 2-BP's impairment of Kvβ2's targeting to lipid rafts (Fig. 4) must be taken with caution. Therefore, the molecular determinants involved were further analyzed. The five S-acylated putative Cys

Fig. 3 Palmitoylation of Kvβ1.1 and Kvβ2.1. **A** Amino acid sequence alignment of murine Kvβ1.1 and Kvβ2.1. The UniProt (https://www.uniprot.org/) identification number is indicated in brackets. Sequences were analyzed for cysteines. Cysteines are in red. Conserved cysteines are highlighted in yellow. **B**, **C** ABE palmitoilation assay on HEK cells transfected with Kvβ1.1CFP (**B**) and Kvβ2.1CFP (**C**). +HA, presence of hydroxylamine. −HA, absence of hydroxylamine. Top panels, immunoblot against Kvβ1.1 and Kvβ2.1. Bottom panels, immunoblot against flotillin. SM, starting material. PD, pulldown of the palmitoylated proteins. **D** Palmitoylated Kvβ2.1 targets the cell surface. Proximity-ligation-assay (PLA). Palmitic acid 15-hexadecynoic acid was used for Alk-C16 protein palmitoylation. (a) Total Kvβ2.1CFP in green; (b) membrane marker staining in blue; (c) Kvβ2.1CFP Alk-C16 palmitoylation in red; (d) merge panel; (e) colocalization of total Kvβ2.1CFP, in green, with the membrane marker (Mb) in blue; (f) colocalization of Kvβ2.1CFP Alk-C16, in red, with the membrane marker (Mb) in blue. Arrowheads highlight Alk-C16 palmitoylation colocalizing with the cell surface in purple. Scale bars represent 10 μm (**E**) Quantification of membrane (Mb) colocalization with total and palmiyoylated (Alk-C16) Kvβ2.1 using Mander's overlap coefficient (MOC). *$p < 0.05$ (Student's t test) vs. total Kvβ2.1. Values are mean ± SE of 30 cells
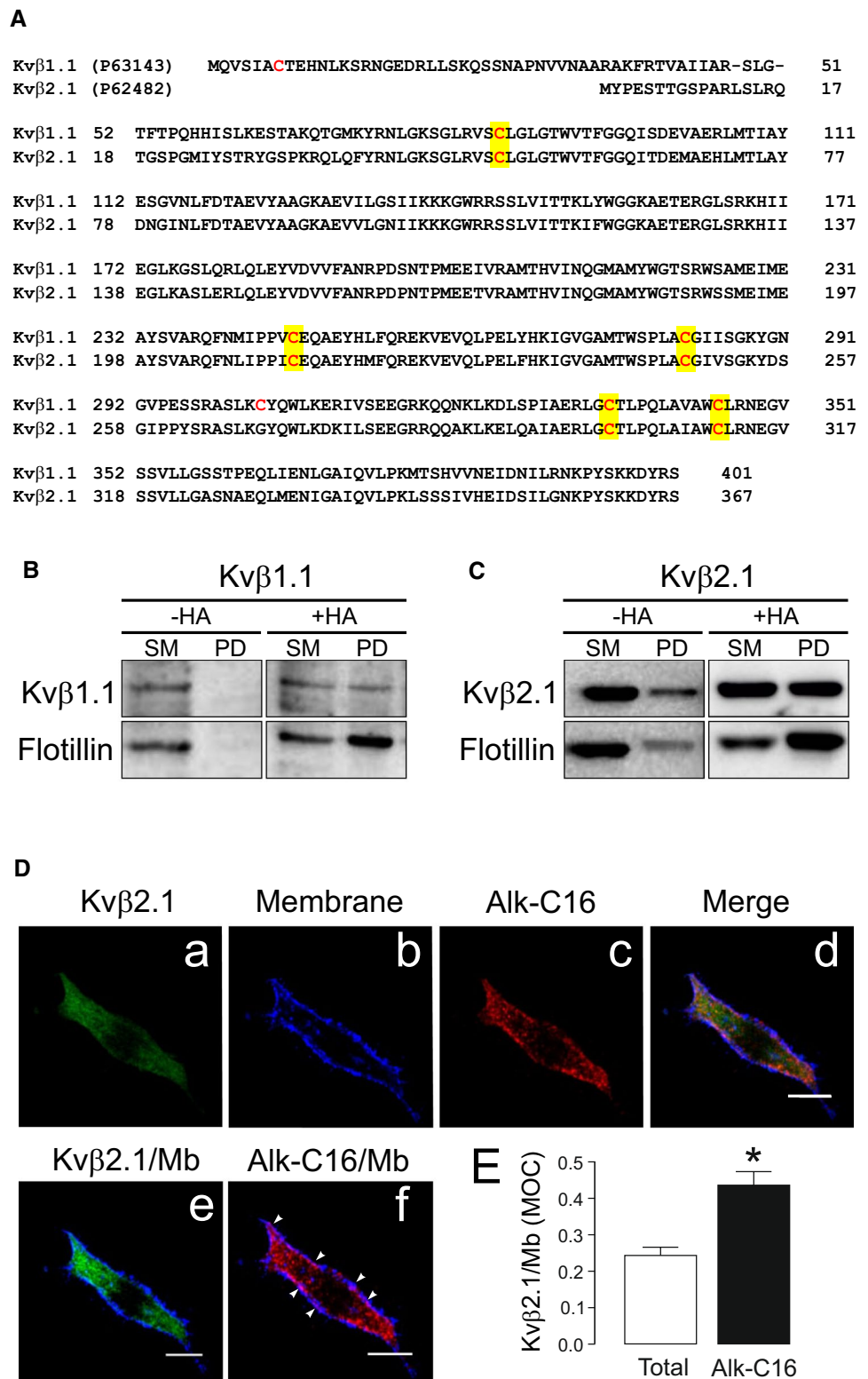
residues in Kvβ2.1 (51, 212, 248, 301 and 311) were mutated to Ser, maintaining structural similarity (Fig. 6A, B). Surprisingly, while C(51–212-248–301)S preserved the regular intracellular pattern of Kvβ2.1, with limited cell surface localization, the introduction of the C311S mutation in combination with the rest of cysteine (C$_{less}$) triggered anomalous plasma membrane distributions (Fig. S4). This altered behavior could be the consequence of
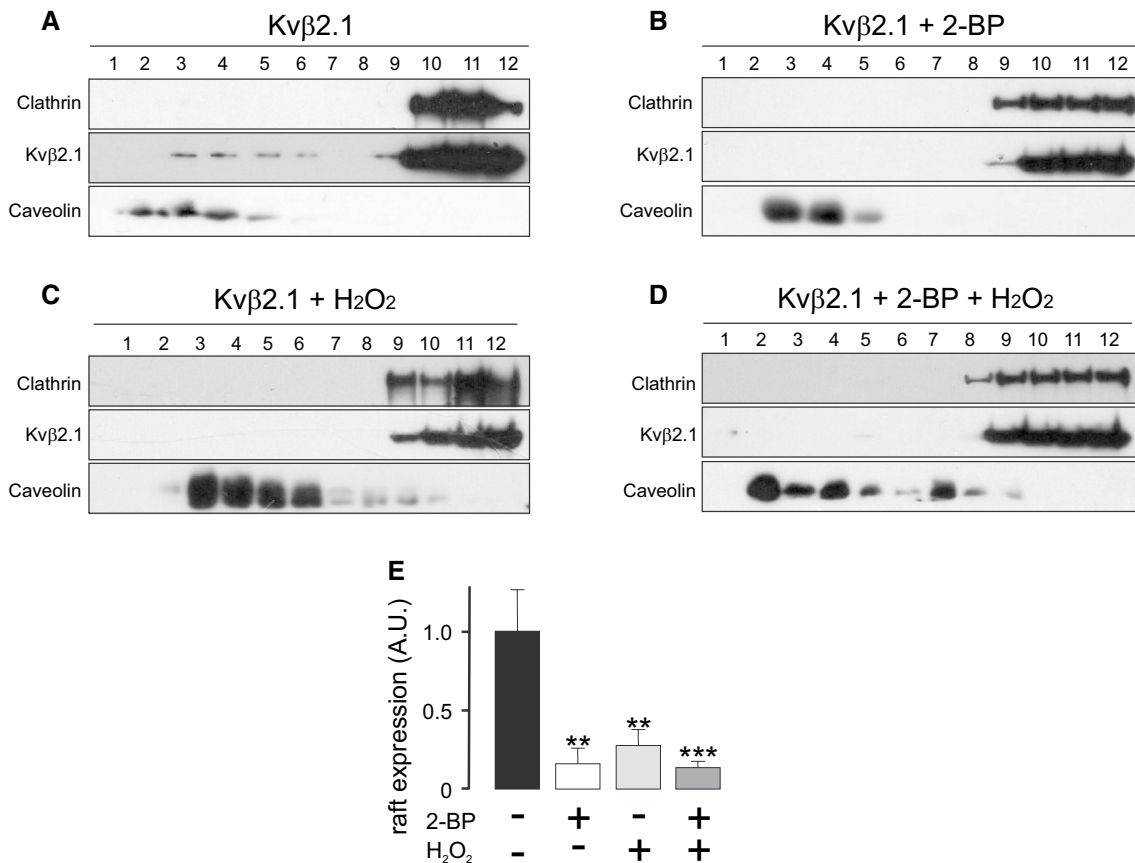
Fig. 4 Palmitoylation-dependent lipid raft targeting of Kvβ2.1. **A–D** Lipid raft microdomains were isolated in the absence (**A**) or presence of (**B**) 2-bromopalmitate (2-BP), (**C**) H_2O_2 or both (**D**), and lipid raft fractions were analyzed for Kvβ2.1CFP by western blot. Lipid raft fractions were sequentially extracted from the top (1, lowest density and highest buoyancy) to the bottom (12, highest density and lowest buoyancy) of the tube. (**E**) Quantification of the expression of Kvβ2.1CFP in low-density fractions, defined by the presence of caveolin, relativized by the total amount of expression. A.U., arbitrary units. $**p < 0.01$; $***p < 0.001$ vs. no additions (Student's t test)

the introduction of an artificial PKC phosphorylation site (Fig. S4B). Therefore, this substitution was discarded, and new Kvβ2.1 C301A, C311A and $C_{less}A$ mutants were generated, which conserved the WT phenotype (Fig. 6C). The sequential substitution of cysteines steadily triggered the loss of membrane localization, which was pronounced when the distal C-term Cys (301 and 311) were mutated (C51-212-248-301S; $C_{less}A$) (Fig. 6D).

Whether S-palmitoylation was concomitant with the cell surface expression of Kvβ2.1 was further investigated. The ABE data showed that only when Cys 301 and 311 were individually substituted (C301A, C311A) or combined with the rest of Cys (C51-212–248-301S; $C_{less}A$) the Kvβ2.1 palmitoylation was clearly impaired (Fig. 7A, B; Fig. S5). Therefore, evidence demonstrated that the C301 and C311 C-terminal distal residues were the main targets for PATs in Kvβ2.1. Furthermore, palmitoylation-dependent lipid raft and plasma membrane targeting was further confirmed. Thus, unlike Kvβ2.1 WT, Kvβ2.1 $C_{less}A$ neither targeted to rafts (Fig. 7C–E) nor to cell surface (Fig. S6).

Proliferation and activation differentially alter Kvβ2.1 localization

Lipid rafts are membrane platforms that initiate cell signaling. These microdomains reduce the spatial distance between signaling proteins and their targets [41]. Considering Kvβ oxidoreductase function and Kv modulation, the positioning of Kvβ2.1 in lipid raft microdomains within the IS was highly relevant. Because Kvβ subunits exhibit differential regulation upon proliferation or activation in macrophages [18], it was wondered whether targeting lipid rafts, which was dependent on S-palmitoylation, underwent regulation. Therefore, HEK cells were cultured in the absence of FBS and analyzed Kvβ2.1 spatial location. In the absence of growth factors (-FBS), the plasma membrane Kvβ2.1 localization slightly decreased (Fig. 8A–I) concomitant with a notable disappearance from floating fractions (Fig. 8J–L).

Evidence demonstrates that PKC initiates signaling events within IS [21]. Previous works from the authors' laboratory report a PMA-dependent exit of Kv1.3 from raft
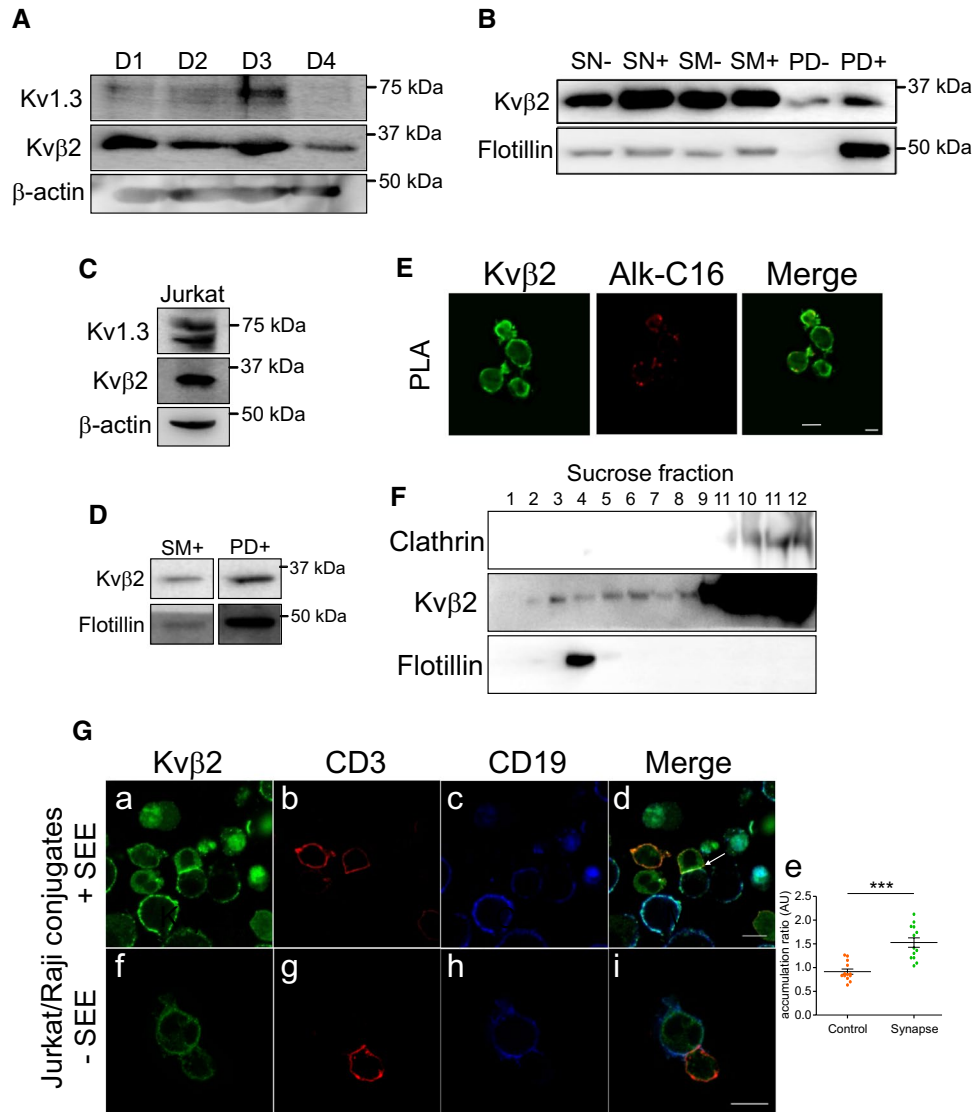
Fig. 5 Human T lymphocytes express palmitoylated Kvβ2.1, which targets lipid raft microdomains and concentrates in the IS during the immunological response. (**A**) Human CD4 + lymphocytes express Kvβ2 and Kv1.3. T lymphocytes from 4 different donors (D1-4) were obtained and analyzed. (**B**) Kvβ2 undergoes palmitoylation in human CD4+T-cells. SN, supernatant in the absence (−) or the presence (+) of HA. SM, starting material in the absence (−) or the presence (+) of HA. PD, pulldown of palmitoylated proteins in the absence (−) or presence (+) of HA. **C** Human Jurkat T lymphocytes express Kvβ2 and Kv1.3. **D** Kvβ2 undergoes palmitoylation in human Jurkat T cells. SM, starting material in the presence of HA. PD, pulldown of palmitoylated proteins in the presence of HA. **E** Proximity ligation assay (PLA) in Jurkat lymphocytes. Palmitic Alk-C16 Kvβ2 palmitoylation. Total Kvβ2 in green; Alk-C16 Kvβ2 palmitoylation in red; merged panel highlights Alk-C16 palmitoylation at the cell surface. **F** Kvβ2 targets lipid rafts in Jukat cells. Lipid raft fractions were sequentially extracted from the top (1, lowest density and highest buoyancy) to the bottom (12, highest density and lowest buoyancy) of the tube. Because T cells lack the expression of caveolin, flotillin identified lipid rafts. **G** Cell conjugates between human Jurkat T cells and human Raji B lymphocytes. (Ga-Ge) SEE-activated B lymphocytes were cocultured in the presence of Jurkat cells. Merged panel showing triple colocalization in white (white arrow) localizes Kvβ2 in the IS. Panel Ge shows the accumulation ratio of Kvβ2 at the IS vs. the entire Kvβ2 cell intensity. Values represent mean ± SE. ***$p < 0.01$ Student's t test. (Gf-Gi) Non-SEE- activated B lymphocytes were cocultured in the presence of Jurkat cells. Note that neither Kvβ2 accumulation nor IS formation is observed. Cells were stained against Kvβ2 (green), CD3 (marker of T cells, red), and CD19 (marker of B cells, blue). Bars are 20 μm

domains prior to endocytosis of the channel [23]. Because Kvβ2.1, which is phosphorylated by PKC [42], was present at lipid rafts, it was analyzed whether PMA would also regulate the location of this auxiliary subunit. Therefore, lipid raft microdomains were isolated in the absence or presence of PMA, and Kvβ2.1 expression was analyzed (Fig. 9 A-D). PMA reduced the distribution of Kvβ2.1 to nonfloating fractions by 67.4% ± 4.3 (Fig. 9E).

MAGUK proteins participate in IS formation, NFAT activation, cytokine secretion and negatively regulate

Fig. 6 Cellular distribution of different Kvβ2.1 mutants. **A** Cartoon of the crystal structure of murine Kvβ2.1 (UniProtKB—P62482), highlighting 5 cysteines in blue. **B** Representative cartoon of Kvβ2.1 mutants. While Ser substitutions are indicated in red, Ala mutations are indicated in green. **C** Cellular staining of Kvβ2.1 WT (a-d), C$^{(52-212-248)}$S (e–h), C$^{(52-212-248-301)}$S (i-l) and Kvβ2.1C$_{less}$A (m-p). Panels d, h, l and p show the pixel-by-pixel analysis of white arrow sections in c, g, k and o, respectively. Scale bars represent 10 μm. **D** Quantification of membrane colocalization using Mander's overlap coefficient (MOC). **$p < 0.01$; ***$p < 0.001$ (Student's t test) vs. WT. Values are mean $\pm$ SE of 20–30 cells
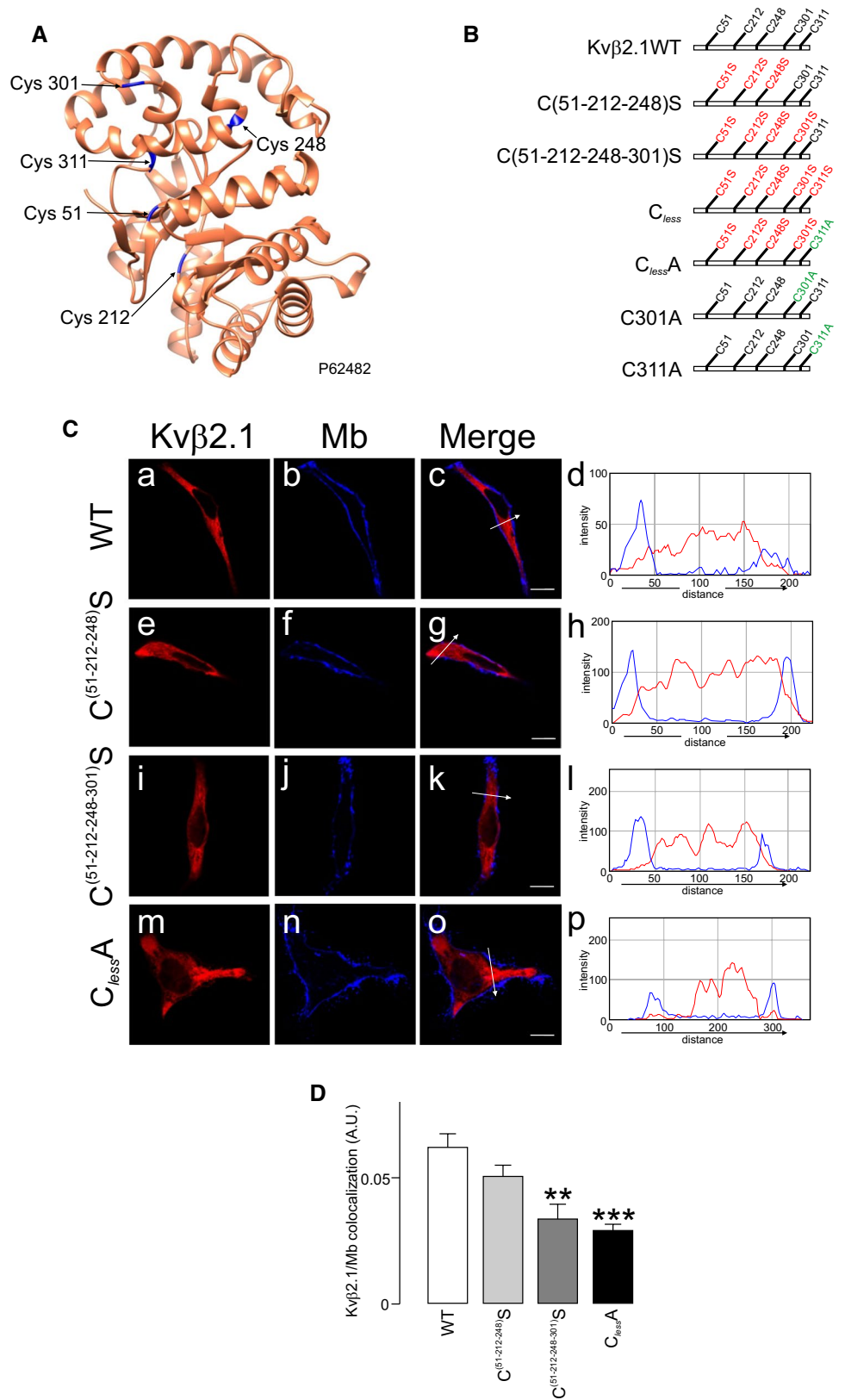
Fig. 7 Palmitoylation of Kvβ2.1 WT and mutants. HEK 293 cells were transfected with Kvβ2.1CFP WT and several cysteine mutants (C$^{(51-212-248)}$S, C$^{(51-212-248-301)}$S and C$_{less}$A), and palmitoylation was analyzed. **A** Representative ABE experiment of Kvβ2.1 WT and C$^{(51-212-248)}$S, C$^{(51-212-248-301)}$S and C$_{less}$A mutants. Flotillin was the positive control. SM, starting material; PD, palmitoylated pull down. **B** Quantification of pulldowns normalized to starting materials. Values are mean ± SE of three independent experiments. **$p < 0.01$; ***$p < 0.001$ (Student's t test) vs. WT. White bar, Kvβ2.1 WT; light gray bar, C$^{(51-212-248)}$S; dark gray bar, C$^{(51-212-248-301)}$S; black bar, Kvβ2.1C$_{less}$A. **C, D** Localization of Kvβ2.1 (**C**) and Kvβ2.1 C$_{less}$A (**D**) in lipid rafts. Lipid raft fractions were sequentially extracted from the top (1, low density and high buoyancy) to the bottom (12, high density and low buoyancy) of the tube. (**E**) Quantification of the abundance of Kvβ2.1CFP in low buoyant fractions, defined by caveolin, relativized by the total amount of expression. ***$p < 0.001$ (Student's t test) vs. WT. Values are mean ± SE of three independent experiments. White bar, Kvβ2.1 WT; black bar, Kvβ2.1C$_{less}$A
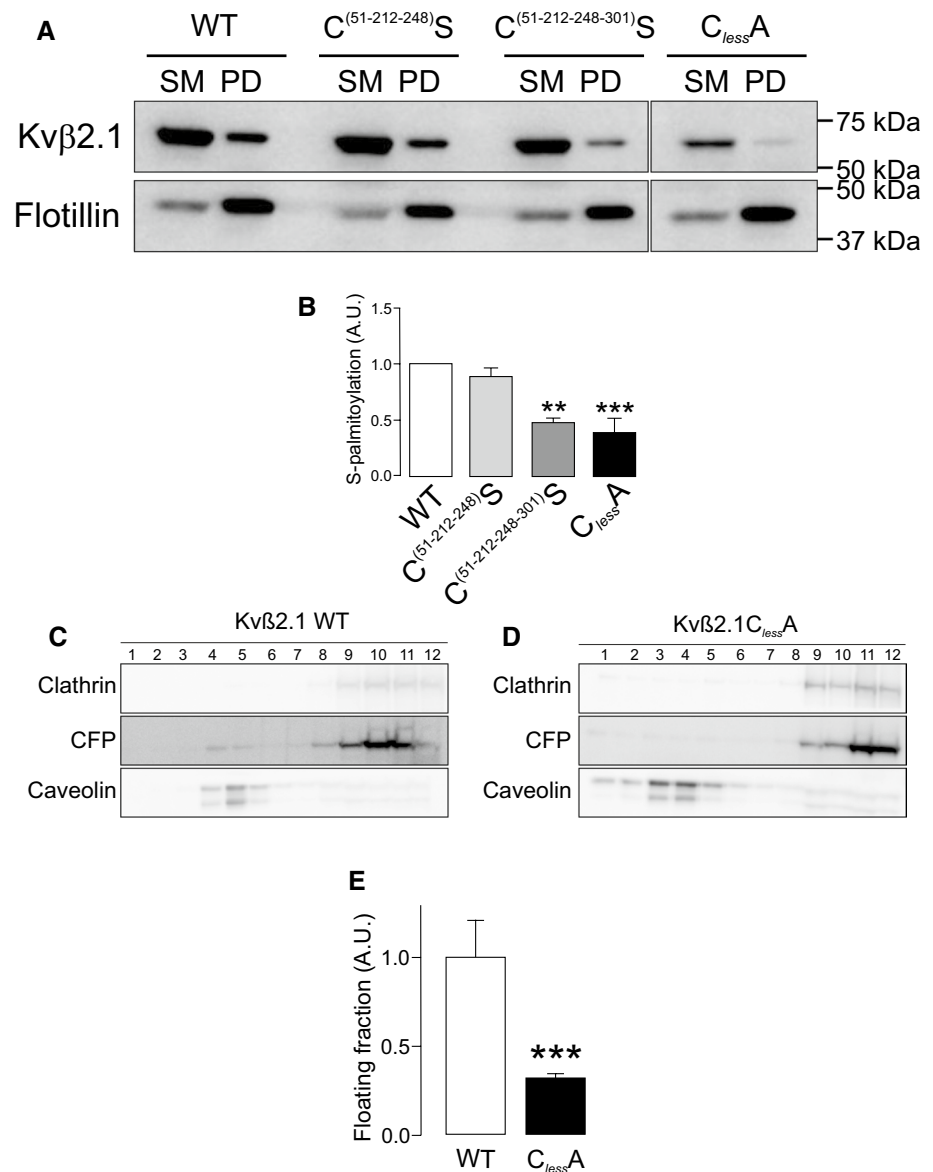
lymphocyte proliferation. hDgl1 (synapse-associated protein 97, SAP97) is located at the IS, and hDgl4 (postsynaptic density protein 95, PSD95) is required for uropod formation in T-cells [43, 44]. Furthermore, PSD95, interacting with Kv1.3 at the IS, stabilizes the channel in rafts upon PKC-dependent endocytosis. Palmitoylated PSD95 targets lipid rafts interacting with PKCα [45–47]. Taking all this in mind, the effect of PSD95 on Kvβ2.1 were analyzed upon PKC-dependent activation. The data indicated that PSD95 stabilized Kvβ2.1 into floating fractions, preventing the PKC-dependent lipid raft displacement observed with PMA (Fig. 9C–E). However, unlike Kv1.3 [23], PSD95 did not interact with Kvβ2.1 (Fig. 9F). Therefore, these results indicated that PSD95 functions on Kvβ2.1 by an indirect mechanism stabilizing lipid rafts buffering PKC effects.

PKC activation triggers Kv1.3 endocytosis, increasing endosomal localization and lysosomal degradation of the channel, which is crucial for Kv1.3-related cell physiology [23]. Although mostly intracellular, Kvβ2.1 shares Kv1.3 spatial distribution and PKC-dependent regulation. Therefore, it was wondered whether PKC activation mediates a similar regulatory mechanism on Kvβ2.1. However, PMA-dependent PKC activation neither increased the presence of Kvβ2.1 in early endosomes nor significantly augmented its ubiquitination (Fig. S7A–D). Furthermore, unlike Kv1.3 (Fig. S7E), the stability of Kvβ2.1 was not altered by PKC-dependent activation. Thus, even after 24 h of PMA incubation neither lysosomal (BA, bafilomycin) nor proteasome MG (MG132) functions altered Kvβ2.1 abundance (Fig. S7 F,G).
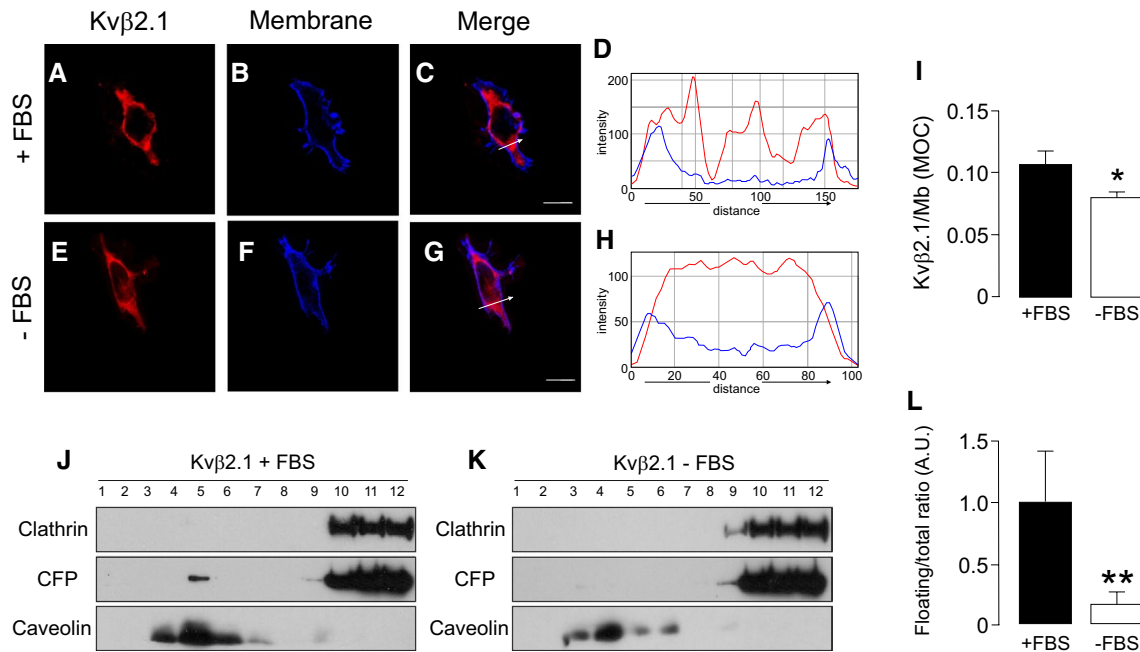
Fig. 8 FBS-dependent proliferation increases Kvβ2.1 membrane and lipid raft targeting. HEK 293 cells were transfected with Kvβ2.1CFP. After 24 h of FBS deprivation, cells were further cultured for 24 h in the presence (**A–D**) or absence (**E–H**) of 10% FBS, and the cellular distribution of Kvβ2.1 was analyzed. **A, E** Kvβ2.1 CFP in red. **B, F** WGA membrane staining in blue. **C, G** merge, purple indicates colocalization. Scale bars represent 10 μm. **D** and **H** Pixel-by-pixel analysis of the arrow sections in **C** and **G**, respectively. **I** Quantification of membrane targeting using Mander's overlap coefficient (MOC). *$p < 0.05$ vs. +FBS (Student's t test). Values are mean of 20–30 cells. **J, K** Lipid raft localization of Kvβ2.1CFP in the presence (**J**) or absence (**K**) of FBS. (**L**) Quantification of Kvβ2.1CFP floatability. Expression of Kvβ2.1CFP in low buoyant fractions (defined by caveolin expression) relative to the total amount. **$p < 0.01$ vs. +FBS (Student's t test). Values are mean of 4 independent experiments. Black bars, presence of FBS; white bars, absence of FBS

Our results indicated that Kvβ2.1, even in the absence of Kv1.3, targets the IS by a palmitoylation-dependent mechanism. S-acylation may also play a role in the functional coupling of Kvβ2 and Kv1.3, as has been for BK channel alpha and beta subunits [48], and such role will be discerned in future studies. The information points to the intrinsic importance of Kvβ2.1 function, independent of Kv1.3, during the immune response. In addition, the data show that palmitoylated Kvβ2.1 targets the lipid raft-enriched IS (Fig. 10). In fact, a signaling complex consisting of CD4, Kv1.3, Kvβ2, SAP97 (hDlg1) and ZIP clusters at the IS in human T cells [20, 22, 25]. In this scenario, PSD95 (also known as SAP90 from the synapse-associated protein—SAP—family), which stabilizes Kv1.3 at rafts, would share effects on Kvβ2.1. However, unlike Kv1.3, the mechanism would not involve direct association. Furthermore, while proliferation increased the amount of Kvβ2.1 in lipid rafts, PKC-dependent activation drove the peptide outside rafts, without compromising the peptide stability (Fig. 10).

Discussion

Voltage-dependent K^+ channels control the resting potential of mammalian cells. In addition, Kv participate in a myriad of physiological functions. To achieve that role, Kv associate with a number of ancillary proteins that further increase their function. The Kvβ regulatory subunit family is the most important group of peptides that, associating with many Kv channels, provide diversity [1]. We found that cytoplasmic Kvβ2.1 was located at the cell surface and, unlike Kvβ1.1, partially targeted lipid rafts in the absence of Kv subunits. This spatial localization, which situates Kvβ2.1 in the IS during the immune response, was mediated by specific S-acylation in two distal C-terminal cysteines (C301 and C311), which are far from the $NADP^+$ binding pocket. S-palmitoylation is related to lipid raft localization, and soluble proteins may route to the cell
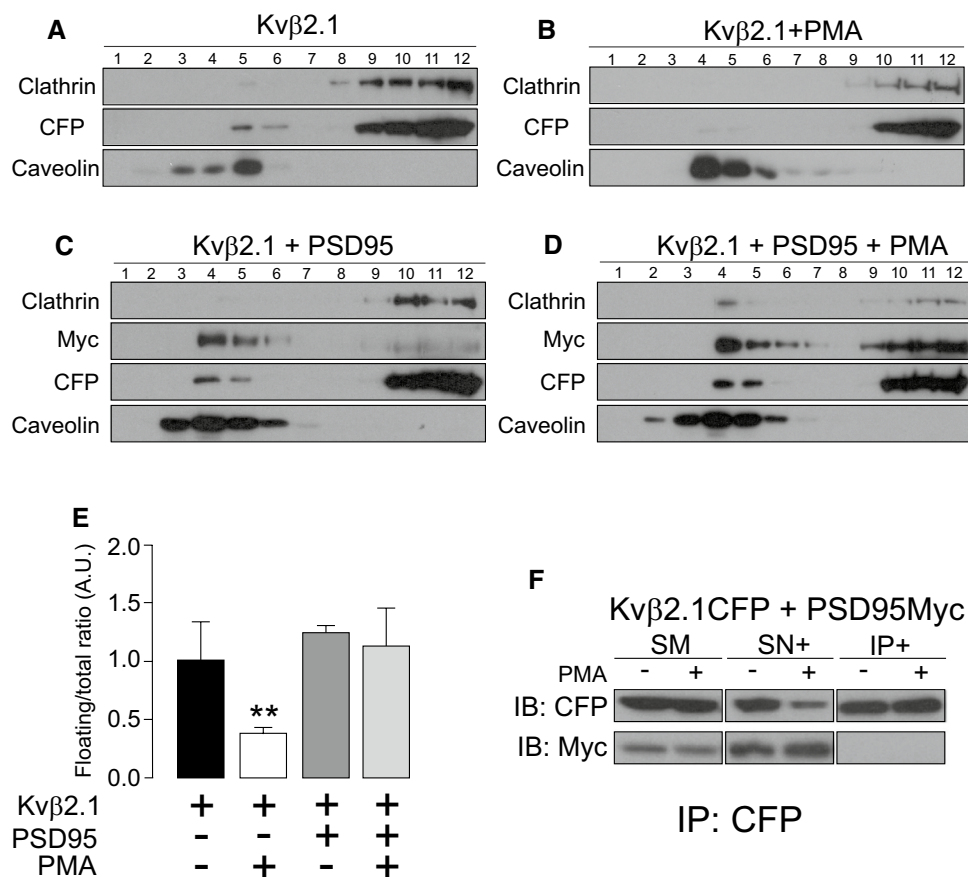
Fig. 9 Lipid raft microdomain expression of Kvβ2.1 in the presence of PMA. HEK 293 cells were transfected with Kvβ2.1CFP. Isolation of lipid rafts was performed after 1 μM PMA incubation for 30 min at 37 °C. **A** Kvβ2.1CFP expression in lipid raft fractions in the absence of PMA. **B** Kvβ2.1CFP expression in the presence of PMA. **C**, **D** HEK 293 cells were cotransfected with Kvβ2.1CFP and Myc-PSD95 in the absence (**C**) or presence (**D**) of PMA. Immunoblot against CFP shows Kvβ2.1CFP. Immunoblot against Myc indicates Myc-PSD95. **E** Quantification of the Kvβ2.1 floatability, indicated by caveolin expression, relativized to the total amount of expression. **p < 0.01 vs. Kvβ2.1 in the absence of PMA (Student's *t* test). Black bar,

Kvβ2.1 alone; white bar, Kvβ2.1 in the presence of PMA; dark gray bar, Kvβ2.1 in the presence of PSD95 but in the absence of PMA; light gray bar, Kvβ2.1 in the presence of PSD95 and PMA. Values are men ± SE of 4 independent experiments. **F** Kvβ2.1 does not interact with PSD95. Cells were cotransfected with Kvβ2.1CFP and Myc-PSD95 in the absence (−) or presence (+) of PMA. Total lysates were coimmunoprecipitated against Kvβ2.1CFP (IP: CFP) and immunoblotted (IB) against CFP (Kvβ2.1) and myc (PSD95). SM, starting material; SN+: supernatant in the presence of antibody. IP+: Immunoprecipitation in the presence of the antibody

surface via this lipidation [49]. Therefore, the results of this study are in line with those of palmitoylated SNAP-25, which routes to the plasma membrane, contributing to the formation of the SNARE complex [50]. Furthermore, the palmitoylation of the DLK kinase, critical for axon-to-soma retrograde signaling upon nerve injury, locates DLK in trafficking vesicles [51].

Kvβ1.1 and Kvβ2.1 are palmitoylated, but only the last targeted to lipid rafts. Although this location may be intriguing for a cytoplasmic protein, evidence situates this peptide in the IS complex in lymphocytes at the onset of the immunological response. Several palmitoyl acyltransferases, such as DHHC18 or DHHC13, are expressed in lymphocytes and may underlie the palmitoylation of Kvβs [35–39]. The data

demonstrated that S-acylation controls the Kvβ2.1 location and concentrates this peptide in this location upon activation in cell conjugates. In addition, the differential lipid raft targeting of Kvβ2.1 by FBS-dependent proliferation or PMA-induced activation suggests that the abundance of Kvβ2.1 in these domains might serve to differentially regulate cell functions. Evidence demonstrates that Kvβ2.1 modulates the Kv1 and Kv4 families [52, 53]. Upon specific combinations of Kvβ2.1/Kv channels, the half-voltage activation switches to more negative values [54]. Although Kvβ2.1 does not contain the ball-and-chain inactivation system, this protein enhances the surface expression of some channels. Therefore, a possible chaperone-like function for Kvβ2.1 was claimed [6]. However, little is known about the role of
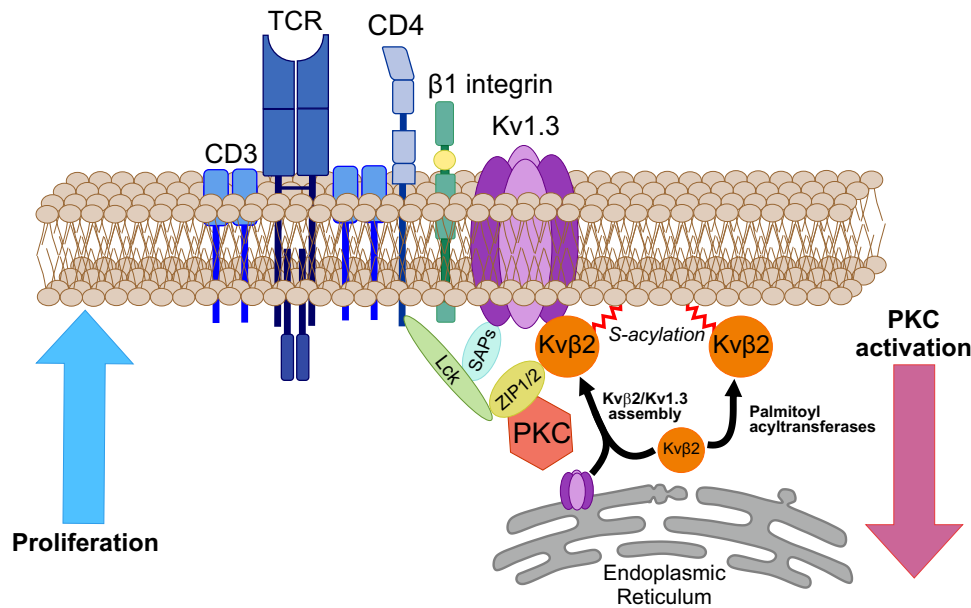
Fig. 10 Cartoon representing the structural Kv1.3-associated proteins in the T-lymphocyte immunological synapse. The Kv1.3 channelosome merges a number of proteins modulating channel function at the IS during immunological synapses. PSD95 (also named synapse-associated protein 90; SAP90), which is encoded by the *hDLG4* (discs large homolog 4) gene, stabilizes Kv1.3 at the IS. SAP97 (synapse-associated protein 97; *hDlg1*) plays similar roles. Therefore, SAP peptides bind to the PDZ domain in the C-terminus of Kv1.3, coupling p56lck to CD4. Kvβ2 links the N-terminus of the Kv1.3 channel to the ZIP1/2 protein, which may interact with several partners, such as p56lck and PKC. CD3 and Kv1.3 are in molecular proximity, and the channel interacts with β1-integrins. Our data indicate that ~ 10% of Kvβ2 targets to lipid rafts either associated or not with Kv1.3 and situate palmitoylated Kvβ2 (red sparkline) at the IS, independent of the Kv1.3 interaction, and stabilized by PSD95. Kvβ2 may link cellular metabolic activity and redox state with calcium signaling in lymphocytes. Kvβ2 also serves as a bridge with ZIP-1/2, which also links the complex to p56lck. Other proteins within IS are the T-cell receptor (TCR), CD3 and CD4 accessory proteins. Kvβ2 in activated T cells concentrates on the IS during synapse formation. Under proliferation, Kvβ2 targets lipid rafts, which are concentrated at the IS. In contrast, PKC activation triggers a lipid raft displacement of Kvβ2, which PSD95 counteracts

this protein in the absence of pore-forming subunits. Computational analysis showed that Kvβ2.1 forms part of the AKR family, and several studies have demonstrated that it is an active enzyme with endogenous substrates [55]. These results suggest putative effects of Kvβ2.1-AKR activity on Kv currents. However, while the interaction with NADPH was required, most likely enhancing the proper folding of Kvβ2.1, the impairment of the enzymatic activity has no major changes on Kvβ2.1 function [56, 57].

Considering that Kvβ2.1 underwent palmitoylation in the absence of α-subunits and that AKR activity is not necessarily coupled to control Kv channels, Kvβ2.1 could act—independent of Kv channels—as a sensor for the redox state of the cell. It was demonstrated that Kvβ1.1 does not target lipid rafts but is placed at the plasma membrane via actin interaction [7]. In this context, Kvβ1.3, closer to Kvβ1.1 than Kvβ2.1, exhibits a slower hydride transfer than Kvβ2.1 [58]. Therefore, the cell could place redox detectors with a specific sensing rate at the plasma membrane. Concomitantly, Kvβ2.1 can preferably reduce aldehydes and ketones of membrane-derived oxidized lipids, highlighting the importance of the Kvβ membrane location [13, 14].

As mentioned above, Kvβ2.1 lipid raft localization was controlled by different insults. Upon proliferation, Kvβ2.1 increased its colocalization in lipid rafts. However, PMA impairs Kvβ2.1 presence in these subcellular domains and, similar to Kv1.3, this was partially counteracted by PSD95. The effect of PSD95 could involve an interaction with PKC rather than associating with Kvβ2.1. Therefore, Kvβ2.1 functions as a redox sensor at IS during the immune response, and MAGUK proteins stabilize the architecture of these multimeric domains. In these spots, several proteins interact with Kvβ2.1 [20, 22]. For instance, ZIP1, ZIP2 and ZIP3 link this protein to PKCζ, which also supports the IS location. These partners may further interact with PKA, EB1, KIF3/kinesin II, TRPV1 and TREK, among others, triggering a complex scenario [11, 21, 59–61]. Because Kvβ2.1 places in lipid rafts following palmitoylation, its partners may be translocated to those domains. This idea suggests that the Kvβ family, in the absence of Kv channels, could exert functions of signaling platforms. Kvβ2.1 interacts with TRPV1, augmenting channel trafficking to the plasma membrane [60]. This balance could be even more complex because other ion channel ancillary subunits, such as Navβ1,

CaM, caveolin and KCNE4, modulate Kv1.3 [62–64]. In this context, the control of Kvβ2.1 distribution by FBS and PKC activation would fine-tune the Kv1.3 channelosome architecture. Further experiments need to be performed to decipher the redox control of these multicomplexes.

Evidence highlights the idea that some functions of Kvβ2.1 have yet to be discovered. Kvβ2.1 null mice exhibit mild effects compared with severe consequences by annihilating Kv1.1 and Kv1.2 at the nervous system [16]. However, Kvβ2.1 association with Kv channels triggers sensitivity to hypoxia either by direct (Kv4.3) or indirect (Kv2.1) associations [65]. Furthermore, the fact that Kvβ2.1 AKR activity does not exert major changes in the control of Kv channels, suggesting that Kvβ2.1 could function as either a moonlighting protein or a scaffolding hub [56]. The $NADP^+$ binding ability of Kvβ subunits is required for cell surface trafficking of Kv1 channels in mammalian cells as well as axonal targeting [10, 56]. The fact that palmitoylated Kvβ2 concentrates in IS during the immune response, also associating to many partners such as Kv1.3, ZIP1/2 and PKC in these microdomains, suggests an exciting yet deciphered physiological role.

Materials and methods

Expression plasmids and site-directed mutagenesis

mKvβ1.1 and mKvβ2.1 were provided by M.M. Tamkun (Colorado State University). mKvβ1.1 and mKvβ2.1 were subcloned into pECFP-N1 (Clontech). mKvβ2.1CFP mutants were generated using QuikChange lightning multisite-directed mutagenesis kits (Stratagene). All constructs and mutants were verified using automated DNA sequencing. Myc-PSD95 was a generous gift from Dr. F. Zafra (Centro de Biología Molecular Severo Ochoa, Madrid).

Cell culture, transfections and pharmacological treatments

HEK-293 cells were cultured on DMEM (LONZA) containing 10% fetal bovine serum (FBS) supplemented with penicillin (10.000 U/ml), streptomycin (100 µg/ml) and 4 mM L-glutamine (Gibco). Human Jurkat T lymphocytes and Raji B cells were cultured in RPMI 1640 medium (Life Technologies) supplemented with 10% FBS and antibiotics. In some experiments, human CD4 + T cell subsets were used. Cells were isolated from peripheral whole blood using a negative selection Rosette Sep™ kit from STEMCELL™ Technologies. Human T lymphocytes were cultured at 37 °C and 5% CO_2 in RPMI 1640 medium (Life Technologies) supplemented with 10% FCS, 1% glutamine, 1% penicillin–streptomycin (Gibco), 1 × nonessential amino acid

solution (Thermo Fisher Scientific), 10 mM HEPES (Life Technologies) and 50 U/ml IL-2 (Bionova). To generate T cell blasts, the Dynabeads Human T-Activator CD3/CD28 for T cell expansion and activation kit (Life Technologies) was used following the manufacturer's instructions. Human T cell blasts were used after 6–7 days of the expansion protocol. No IL-2 was supplemented in media the day before an experiment.

For confocal imaging and coimmunoprecipitation experiments, cells were seeded (70–80% confluence) in six-well dishes containing polylysine-coated coverslips or 100 mm dishes 24 h before transfection. Lipotransfectin® (Attendbio Research) was used for transfection according to the supplier's instructions. The amount of transfected DNA was 4 µg for a 100 mm dish and 500 ng/well of a six-well dish (for coverslip use). Next, 4–6 h after transfection, the mixture was removed from the dishes and replaced with new fresh culture media. All experiments were performed 24 h after transfection.

In some experiments, 24 h transfected HEK cells were incubated with 1 µM PMA at 37 °C for indicated times. For 2-bromopalmitate treatment, HEK-transfected cells were starved for 3 h with DMEM supplemented with 1% dialyzed FBS, and 60 nM 2-bromopalmitate was added for 3 more hours at 37 °C. H_2O_2 (400 µM) was added for 30 min at 37 °C.

Protein extraction, membrane-enriched preparations, coimmunoprecipitation and western blotting

Cells were washed twice in cold PBS (phosphate-buffered saline; 137 mM NaCl, 2.7 mM KCl, 8 mM Na_2HPO_4, and 2 mM KH_2PO_4, pH 7.4) and lysed on ice with lysis buffer (5 mM HEPES, 150 mM NaCl, 1% Triton X-100, pH 7.5) supplemented with 1 µg/ml aprotinin, 1 µg/ml leupeptin, 1 µg/ml pepstatin and 1 mM phenylmethylsulfonyl fluoride as protease inhibitors. Lysates were incubated for 20 min at 4 °C and further spun for 20 min at 14,000 rpm. The protein content of the supernatant was determined using the Bio–Rad Protein Assay (Bio–Rad).

Membrane-enriched preparations were purified from 24 h transfected HEK 293 cells. Cells were washed twice in cold PBS and scrapped in 1 mL of HB buffer (20 mM HEPES pH 7.4, 1 mM EDTA, 255 mM sucrose) supplemented with 1 µg/ml aprotinin, 1 µg/ml leupeptin, 1 µg/ml pepstatin and 1 mM phenylmethylsulfonyl fluoride as protease inhibitors. Samples were passed through a 25-gauge needle ten times, and lysates were centrifuged for 5 min at 3000 × g and 4 °C. The supernatant was diluted three times with HB buffer. To enrich the membrane fraction, lysates were centrifuged for 90 min at 150,000 × g. Finally, the pellet was resuspended in 30 µL 30 mM HEPES and analyzed by western blot.

For coimmunoprecipitation, 1 mg of protein was brought up to 500 µl with lysis buffer (NaCl 150 mM, HEPES 50 mM, Titron X-100 1%, pH 7.4) supplemented with protease inhibitors. Precleaning was performed with 40 µl of protein A Sepharose beads (GE Health care) for 1 h at 4 °C. Next, samples were incubated in a chromatography column (BioRad Micro spin Chromatography Columns), which contained 2.5 µg of anti-GFP antibody (Genescript) previously crosslinked to protein A Sepharose beads, for 2 h at room temperature (RT), with continuous mixing. Next, the columns were centrifuged for 30 s at $1000 \times g$. The supernatant (SN) was kept and stored at -20 °C. Columns were washed four times with 500 µl of lysis buffer and centrifuged for 30 s at $1000 \times g$. Finally, elution was performed by incubating the columns with 100 µl of 0.2 M glycine pH 2.5 and spun for 30 s at $1000 \times g$. Eluted proteins (IPs) were prepared for western blotting by adding 20 µl of loading buffer (5×) and 5 µl of 1 M Tris–HCl pH 10.

Irreversible crosslinking of the antibody to the sepharose beads was performed by mixing the antibody with protein A sepharose beads for 1 h at RT. Next, the beads were incubated with 500 µl of dimethyl pimelimidate (DMP, Pierce) for 30 min at RT. Columns were washed four times with 500 µl of 1×TBS, four times with 500 µl of 0.2 M glycine pH 2.5 and three more times with 1×TBS. Finally, columns were incubated with protein lysates to perform immunoprecipitation, following the protocol described before.

Protein samples (50 µg), SN and IP were boiled in Laemmli SDS loading buffer and separated by 10% SDS–PAGE. Next, samples were transferred to nitrocellulose membranes (Immobilon-P, Millipore) and blocked in 0.2% Tween-20-PBS supplemented with 5% dry milk before immunoreaction. Filters were immunoblotted with antibodies against anti-GFP (1:1,000, Roche), Kvβ1.1 (1/1,000, NeuroMab), Kvβ2.1 (1/1,000, NeuroMab), Kv1.3 (1/200, Neuromab), β-actin (1/50,000, Sigma), ubiquitin (1/500, Santa Cruz), flotillin (1/1,000, BD Transduction), clathrin (1/1,000, BD Transduction), caveolin (1/1,000, BD transduction) or myc (1/1,000, Sigma). Finally, the filters were washed with 0.05% Tween-20-PBS and incubated with horseradish peroxidase-conjugated secondary antibodies (BioRad).

Confocal microscopy and image analysis

For confocal analysis, cells were seeded on polylysine-coated coverslips 24 h prior to transfection. The next day, the cells were washed twice with PBS without K$^+$ (PBS-K$^+$), fixed with 4% paraformaldehyde for 10 min, and washed three times for 5 min with PBS-K$^+$. Finally, coverslips were mounted on microscope slides (Acefesa) with house Mowiol mounting media. Coverslips were dried at RT for at least 1 day before imaging.

Staining with FITC-labeled cholera toxin β subunit (CTXβ) for lipid raft microdomains and wheat germ agglutinin (WGA)-Texas red (Invitrogen) for the plasma membrane was performed under non-permeabilized conditions [66]. Live cells (on ice) were quickly washed with PBS at 4 °C and stained with a dilution of WGA-Texas Red (1/1,500) in DMEM supplemented with 30 mM HEPES for 10 min at 4 °C. Subsequently, the cells were quickly washed twice and fixed with 4% paraformaldehyde in PBS for 10 min. Next, the cells were washed and mounted as described before. The EEA1 marker was used to stain early endosomes. Fixed cells were further permeabilized with 0.1% Triton X-100 for 10 min. After 60 min of incubation with blocking solution (10% goat serum, 5% nonfat powdered milk and 0.05% Triton X-100), primary mouse anti-EEA1 (1:500) antibody was added at 4 °C overnight (BD Transduction Laboratories) in 10% goat serum and 0.05% Triton X-100. Next, the cells were incubated with secondary goat anti-mouse antibody conjugated with Alexa Fluor 660 for 2 h at RT. Mounting as previously described [27].

All images were acquired with a Leica TCS SL laser scanning confocal spectral microscope (Leica Microsystems) equipped with argon and helium–neon lasers. All experiments were performed with a 63×oil-immersion objective lens NA 1.32. Colocalization offline image analysis was performed using ImageJ software (https://imagej.nih.gov/ij/). A pixel-by-pixel colocalization study using JACoP (Just Another Colocalization Plugin) was used, and Mander's overlap coefficient (MOC) was calculated.

Immunological synapse formation

To analyze the Kvβ2 distribution during IS formation, human B cell lymphoma Raji cells were used as antigen-presenting cells. B cells were incubated with 10 µg/mL *Staphylococcus* enterotoxin E (SEE, Toxin Technologies) for 30 min. Next, Raji cells were mixed with Jurkat T cells (1:1) to form cell conjugates and spun at $200 \times g$ for 1 min at 37 °C. Samples were plated on poly-L-lysine-coated coverslips and incubated for 15 min at 37 °C. The cells were washed once with PBS and fixed with 2% PFA in PBS for 10 min. Cells were rinsed three times with PBS between steps. Next, conjugates were labeled with anti-Kvβ2.1 (1/100, NeuroMab), anti-CD3 Alexa 647-conjugated antibody and anti-CD19 Alexa 488-conjugated antibody (1/100, BioLegend). Antibodies were diluted in PBS supplemented with 1% BSA and incubated for 2 h. Coverslips were rinsed and mounted in Mowiol.

Kvβ2 localization at the immune synapse was analyzed using ImageJ software. Briefly, region of interest (ROI) including the whole IS and equal surface areas in both Jurkat and Raji cell membranes outside the IS were drawn. The

Kvβ2 signal intensity was measured in each membrane section and the intensity ratio calculated as follows:

$$(\text{K}v\beta2 \text{ intensity at the IS})/((\text{K}v\beta2 \text{ intensity in Jurkat ROI})$$

$$+ (\text{K}v\beta2 \text{ intensity in Raji ROI})).$$

Therefore, ratios above 1 indicated that Kvβ2 intensities at the IS were higher than the sum of both Kvβ2 intensities in Jurkat and Raji membranes outside IS.

Cell unroofing preparations (CUP)

HEK-293 cells were seeded in poly-D-lysine-treated glass coverslips. Twenty-four hours after transfection, samples were cooled on ice for 5 min and washed twice in PBS-K$^+$. Next, samples were incubated for 5 min in KHMgE buffer (70 mM KCl, 30 mM HEPES, 5 mM MgCl$_2$, 3 mM EGTA, pH 7.5) diluted three times and gently washed with nondiluted KHMgE to induce hypotonic shock. Bursted cells were removed from the coverslip by intensive pipetting up and down. After two washes with KHMgE buffer, only membrane sheets remained attached. Preparations were fixed and mounted as previously described [67].

Lipid-raft isolation

Low-density Triton-insoluble complexes were isolated as previously described [68] from Jurkat T cells and HEK293 cells transiently transfected with Kvβ1.1CFP, Kvβ2.1CFP and the Kvβ2.1CFP^{ClessA} mutant. Cells were homogenized in 1 ml of MBS (150 mM NaCl, 25 mM 2-morpholinoethanesulfonic acid 1-hydrate (MES), pH 6.5) 0.1% Triton X-100, and sucrose was added to a final concentration of 40%. A 5–30% linear sucrose gradient was layered on top and further centrifuged (39,000 rpm) for 20–22 h at 4 °C in a Beckman SW41-Ti rotor. Gradient fractions (1 ml) were sequentially collected from the top of the tube and analyzed by western blotting. While clathrin identified the nonbuoyant fractions, caveolin and flotillin labeled the floating fractions (lipid rafts) in HEK 293 cells and Jurkat T lymphocytes, respectively.

Ubiquitination assay

Cells were washed twice in cold PBS and frozen at − 80 °C for at least one night. Cells were lysed on ice for 20 min with 2 mL of lysis buffer (50 mM HEPES, 150 mM NaCl, 1% Triton X-100, 10% glycerol, pH 7.5) supplemented with 12.5 mg NEM (Nethylmaleimide, Sigma), 0.2 mM MG132, 1 mM EGTA, 1 mM EDTA, 20 mM NaF, 1% NaOV and 2 mM DTT containing 1 μg/ml aprotinin, 1 μg/ml leupeptin, 1 μg/ml pepstatin and 1 mM phenylmethylsulfonyl fluoride as protease inhibitors. Next, the cells were scrapped and

centrifuged at $14,000 \times g$ for 15 min. Immunoprecipitation assays were performed as described above.

Half-life studies

Cells were preincubated with 100 μg/ml cycloheximide (CHX) for 3 h at 37 °C to halt protein synthesis. Next, cells were incubated in the presence or absence of 1 μM PMA at the indicated times. To inhibit lysosomal and proteasomal degradation, 60 nM bafilomycin A1 (BA) or 5 μM MG132 (MG), respectively, was added. Finally, the cells were washed twice with cold PBS, and protein extraction was performed as described above.

Acyl-biotin exchange (ABE) palmitoylation assay

Detection of protein palmitoylation by acyl-biotin exchange (ABE) was described previously [69]. Briefly, human CD4 + lymphocytes, Jurkat T cells and HEK 293 cells transfected with Kvβ2.1 wild type (WT) and Kvβ2.1 cysteine mutants were washed with cold PBS and harvested in buffer A (150 mM NaCl, 50 mM Tris HCl, 0.2% Triton X-100, 5 mM EDTA, pH 7.4) containing protease inhibitors and 10 mM NEM. Lysates were collected by scraping samples on ice, passed ten times through a 25-gauge needle and incubated for 1 h at 4 °C before centrifugation at $16,000 \times g$ for 15 min. Supernatants were chloroform–methanol precipitated, and the pellet was allowed to air dry for 2–3 min. The pellet was resuspended in 300 μl of buffer B (4% SDS, 50 mM Tris HCl, 5 mM EDTA, pH 7.4) supplemented with 10 mM NEM and diluted fourfold in buffer A containing 1 mM NEM. Samples were incubated at 4 °C overnight with gentle agitation. NEM was removed by performing three sequential chloroform–methanol precipitations. Next, the pellet was resuspended in 500 μL of buffer B. The sample was split in two volumes, and 250 μL was diluted with 950 μL of buffer C (50 mM Tris–HCl, 1 mM HPDP-biotin, 0.2% Triton X-100, 100 μM PMSF) containing 0.7 M hydroxylamine (+ HA). The other 250 μL was diluted in buffer C without hydroxylamine (− HA). Samples were incubated at RT with gentle rocking for 1 h. Three rounds of chloroform–methanol precipitation were performed, and the final pellets were resuspended in 300 μL buffer B and diluted with 900 μL buffer D (150 mM NaCl, 50 mM Tris–HCl, 5 mM EDTA, 0.2 mM HPDP-biotin, 0.2% Triton X-100, pH 7.4). Samples were incubated at RT with gentle agitation for 1 h prior to 3 more sequential chloroform–methanol precipitations. The final pellet was resuspended in 120 μL of buffer E (2% SDS, 50 mM Tris HCl, 0,2% Triton X-100, 5 mM EDTA, pH 7.4) and diluted to 0.1% SDS with buffer A. Biotin-labeled proteins were captured with 50 μL of NeutrAvidin agarose beads,

previously washed with 400 μL of buffer A and centrifuged for 1 min at $2000 \times g$. NeutrAvidine beads were pelleted by centrifugation at $2{,}000 \times g$ for 30 s. After washing the beads four times with 400 μL of buffer A, captured proteins were boiled in 100 μL $1 \times$ Laemmli buffer and 2% β-mercaptoethanol. Samples were then analyzed by SDS–PAGE western blot.

Proximity-ligation-assay (PLA)

Palmitic acid (15-yne) 15-hexadecynoic acid (Avanti Polar Lipids) was used for Alk-C16 protein palmitoylation. Jurkat T lymphocytes and HEK-293 cells expressing Kvβ2.1CFP for 4 h were incubated for 18 h with 100 μM 15-yne and further sonicated for 15 min. Next, the cells were quickly washed three times with PBS-K$^+$ and fixed with 2% paraformaldehyde for 10 min, followed by cold methanol for 5 min. After fixation, the cells were washed twice, and a freshly prepared click reaction (0.1 mM biotin-azide (carboxamide-6-azidohexanyl biotin, Invitrogen), 0.1 mM TCEP (Tris(2-carboxyethyl)phosphine hydrochloride, Sigma–Aldrich) and 0.1 mM CuSO$_4$ (Sigma–Aldrich)) was added with gentle rocking for 1 h at RT. After five washes with PBS-K$^+$, cells were incubated with blocking solution (5% BSA, 0.3% Triton) for 1 h at RT. Cells were further washed three times with PBS-K$^+$, incubated with anti-Kvβ2.1 (1:50, Neuromab) and anti-Biotin (1:300, Sigma–Aldrich) antibodies and diluted in Duolink blocking solution 1X (Sigma–Aldrich) at 4 °C overnight. Next, the cells were washed three times and incubated for 1 h at 37 °C with 100 μL of freshly prepared secondary PLA antibodies (20 μL Duolink in situ PLA probe anti-goat MINUS, 20 μL Duolink in situ PLA probe anti-mouse PLUS and 60 μL Duolink antibodies diluent 1X; Sigma–Aldrich). Cells were washed five times and incubated for 30 min at 37 °C with 100 μL ligation-PLA-solution (2.5 U of Duolink ligase, Sigma–Aldrich). After ligation and five further PBS-K$^+$ washes, cells were incubated for 100 min at 37 °C with 100 μl amplification-PLA-solution (12.5 U Duolink Polymerase in $1 \times$ Duolink Far Red amplification buffer, Sigma–Aldrich) in the dark. Finally, after four more washes (PBS-K$^+$), samples were mounted with in-house Mowiol and dried for 1 day before imaging.

Availability of data and material The raw data and datasets generated during and/or analyzed during the current study are available from the corresponding author (afelipe@ub.edu) on reasonable request.

Declarations

Conflict of interest The authors declare no competing interests.

Ethics approval and consent to participate The protocol was reviewed and approved by the Ethics Committee of the Universitat de Barcelona and the Banc de Sang i Teixits de Catalunya (BST). Institutional Review Board (IRB00003099). All procedures followed the rules of the Declaration of Helsinki Guidelines. All donors signed a written informed consent and samples were totally anonymous and untraceable.

Consent for publication Not applicable.

References

1. Pongs O, Schwarz JR (2010) Ancillary subunits associated with voltage-dependent K+ channels. Physiol Rev 90:755–796. https://doi.org/10.1152/physrev.00020.2009

2. Capera J, Serrano-Novillo C, Navarro-Perez M, Cassinelli S, Felipe A (2019) The potassium channel odyssey: mechanisms of traffic and membrane arrangement. Int J Mol Sci. https://doi.org/10.3390/ijms20030734

3. Gulbis JM, Mann S, MacKinnon R (1999) Structure of a voltage-dependent K+ channel beta subunit. Cell 97:943–952. https://doi.org/10.1016/s0092-8674(00)80805-3

4. Rettig J, Heinemann SH, Wunder F, Lorra C, Parcej DN, Dolly JO, Pongs O (1994) Inactivation properties of voltage-gated K+ channels altered by presence of beta-subunit. Nature 369:289–294. https://doi.org/10.1038/369289a0

5. Nagaya N, Papazian DM (1997) Potassium channel alpha and beta subunits assemble in the endoplasmic reticulum. J Biol Chem 272:3022–3027. https://doi.org/10.1074/jbc.272.5.3022

6. Shi G, Nakahira K, Hammond S, Rhodes KJ, Schechter LE, Trimmer JS (1996) Beta subunits promote K+ channel surface expression through effects early in biosynthesis. Neuron 16:843–852. https://doi.org/10.1016/s0896-6273(00)80104-x

7. Nakahira K, Matos MF, Trimmer JS (1998) Differential interaction of voltage-gated K+ channel beta-subunits with cytoskeleton is mediated by unique amino terminal domains. J Mol Neurosci 11:199–208. https://doi.org/10.1385/JMN:11:3:199

8. Levin G, Chikvashvili D, Singer-Lahat D, Peretz T, Thornhill WB, Lotan I (1996) Phosphorylation of a K+ channel alpha subunit modulates the inactivation conferred by a beta subunit Involvement of cytoskeleton. J Biol Chem 271:29321–29328. https://doi.org/10.1074/jbc.271.46.29321

9. Jing J, Peretz T, Singer-Lahat D, Chikvashvili D, Thornhill WB, Lotan I (1997) Inactivation of a voltage-dependent K+ channel by beta subunit. Modulation by a phosphorylation-dependent interaction between the distal C terminus of alpha subunit and cytoskeleton. J Biol Chem 272:14021–14024. https://doi.org/10.1074/jbc.272.22.14021

10. Gu Y, Gu C (2010) Dynamics of Kv1 channel transport in axons. PLoS One 5:e11931. https://doi.org/10.1371/journal.pone.0011931

11. Gu C, Zhou W, Puthenveedu MA, Xu M, Jan YN, Jan LY (2006) The microtubule plus-end tracking protein EB1 is required for Kv1 voltage-gated K+ channel axonal targeting. Neuron 52:803–816. https://doi.org/10.1016/j.neuron.2006.10.022

12. Accili EA, Kiehn J, Yang Q, Wang Z, Brown AM, Wible BA (1997) Separable Kvbeta subunit domains alter expression and gating of potassium channels. J Biol Chem 272:25824–25831. https://doi.org/10.1074/jbc.272.41.25824

13. Tipparaju SM, Barski OA, Srivastava S, Bhatnagar A (2008) Catalytic mechanism and substrate specificity of the beta-subunit of the voltage-gated potassium channel. Biochemistry 47:8840–8854. https://doi.org/10.1021/bi800301b

14. Xie Z, Barski OA, Cai J, Bhatnagar A, Tipparaju SM (2011) Catalytic reduction of carbonyl groups in oxidized PAPC by Kvbeta2 (AKR6). Chem Biol Interact 191:255–260. https://doi.org/10.1016/j.cbi.2011.01.032

15. Heilstedt HA, Burgess DL, Anderson AE, Chedrawi A, Tharp B, Lee O, Kashork CD, Starkey DE, Wu YQ, Noebels JL et al (2001) Loss of the potassium channel beta-subunit gene, KCNAB2, is associated with epilepsy in patients with 1p36 deletion syndrome. Epilepsia 42:1103–1111. https://doi.org/10.1046/j.1528-1157.2001.08801.x

16. McCormack K, Connor JX, Zhou L, Ho LL, Ganetzky B, Chiu SY, Messing A (2002) Genetic analysis of the mammalian K+ channel beta subunit Kvbeta 2 (Kcnab2). J Biol Chem 277:13219–13228. https://doi.org/10.1074/jbc.M111465200

17. Connor JX, McCormack K, Pletsch A, Gaeta S, Ganetzky B, Chiu SY, Messing A (2005) Genetic modifiers of the Kv beta2-null phenotype in mice. Genes Brain Behav 4:77–88. https://doi.org/10.1111/j.1601-183X.2004.00094.x

18. Vicente R, Escalada A, Soler C, Grande M, Celada A, Tamkun MM, Solsona C, Felipe A (2005) Pattern of Kv beta subunit expression in macrophages depends upon proliferation and the mode of activation. J Immunol 174:4736–4744. https://doi.org/10.4049/jimmunol.174.8.4736

19. McCormack T, McCormack K, Nadal MS, Vieira E, Ozaita A, Rudy B (1999) The effects of Shaker beta-subunits on the human lymphocyte K+ channel Kv1.3. J Biol Chem 274:20123–20126. https://doi.org/10.1074/jbc.274.29.20123

20. Panyi G, Varga Z, Gaspar R (2004) Ion channels and lymphocyte activation. Immunol Lett 92:55–66. https://doi.org/10.1016/j.imlet.2003.11.020

21. Gong J, Xu J, Bezanilla M, van Huizen R, Derin R, Li M (1999) Differential stimulation of PKC phosphorylation of potassium channels by ZIP1 and ZIP2. Science 285:1565–1569. https://doi.org/10.1126/science.285.5433.1565

22. Beeton C, Wulff H, Standifer NE, Azam P, Mullen KM, Pennington MW, Kolski-Andreaco A, Wei E, Grino A, Counts DR et al (2006) Kv13 channels are a therapeutic target for T cell-mediated autoimmune diseases. Proc Natl Acad Sci USA 103:17414–17419. https://doi.org/10.1073/pnas.0605136103

23. Martinez-Marmol R, Styrczewska K, Perez-Verdaguer M, Vallejo-Gracia A, Comes N, Sorkin A, Felipe A (2017) Ubiquitination mediates Kv1.3 endocytosis as a mechanism for protein kinase C-dependent modulation. Sci Rep 7:42395. https://doi.org/10.1038/srep42395

24. Bi K, Tanaka Y, Coudronniere N, Sugie K, Hong S, van Stipdonk MJ, Altman A (2001) Antigen-induced translocation of PKC-theta to membrane rafts is required for T cell activation. Nat Immunol 2:556–563. https://doi.org/10.1038/88765

25. Chandy KG, Norton RS (2017) Peptide blockers of Kv1.3 channels in T cells as therapeutics for autoimmune disease. Curr Opin Chem Biol 38:97–107. https://doi.org/10.1016/j.cbpa.2017.02.015

26. Bahamonde MI, Valverde MA (2003) Voltage-dependent anion channel localises to the plasma membrane and peripheral but not perinuclear mitochondria. Pflugers Arch 446:309–313. https://doi.org/10.1007/s00424-003-1054-7

27. Capera J, Perez-Verdaguer M, Peruzzo R, Navarro-Perez M, Martinez-Pinna J, Alberola-Die A, Morales A, Leanza L, Szabo I, Felipe A (2021) A novel mitochondrial Kv13-caveolin axis controls cell survival and apoptosis. Elife. https://doi.org/10.7554/eLife.69099

28. Couet J, Li S, Okamoto T, Ikezu T, Lisanti MP (1997) Identification of peptide and protein ligands for the caveolin-scaffolding domain. Implications for the interaction of caveolin with caveolae-associated proteins. J Biol Chem 272:6525–6533. https://doi.org/10.1074/jbc.272.10.6525

29. Daniotti JL, Pedro MP, Valdez Taubas J (2017) The role of S-acylation in protein trafficking. Traffic 18:699–710. https://doi.org/10.1111/tra.12510

30. Webb Y, Hermida-Matsumoto L, Resh MD (2000) Inhibition of protein palmitoylation, raft localization, and T cell signaling by 2-bromopalmitate and polyunsaturated fatty acids. J Biol Chem 275:261–270. https://doi.org/10.1074/jbc.275.1.261

31. Levental I, Lingwood D, Grzybek M, Coskun U, Simons K (2010) Palmitoylation regulates raft affinity for the majority of integral raft proteins. Proc Natl Acad Sci USA 107:22050–22054. https://doi.org/10.1073/pnas.1016184107

32. Panyi G, Vamosi G, Bacso Z, Bagdany M, Bodnar A, Varga Z, Gaspar R, Matyus L, Damjanovich S (2004) Kv13 potassium channels are localized in the immunological synapse formed between cytotoxic and target cells. Proc Natl Acad Sci USA 101:1285–1290. https://doi.org/10.1073/pnas.0307421100

33. Sanders SS, Martin DD, Butland SL, Lavallee-Adam M, Calzolari D, Kay C, Yates JR, Hayden MR (2015) Curation of the mammalian palmitoylome indicates a pivotal role for palmitoylation in diseases and disorders of the nervous system and cancers. PLoS Comput Biol 11:e1004405. https://doi.org/10.1371/journal.pcbi.1004405

34. Wan J, Savas JN, Roth AF, Sanders SS, Singaraja RR, Hayden MR, Yates JR, Davis NG (2013) Tracking brain palmitoylation change: predominance of glial change in a mouse model of Huntington's disease. Chem Biol 20:1421–1434. https://doi.org/10.1016/j.chembiol.2013.09.018

35. Morrison E, Kuropka B, Kliche S, Brugger B, Krause E, Freund C (2015) Quantitative analysis of the human T cell palmitome. Sci Rep 5:11598. https://doi.org/10.1038/srep11598

36. Morrison E, Wegner T, Zucchetti AE, Alvaro-Benito M, Zheng A, Kliche S, Krause E, Brugger B, Hivroz C, Freund C (2020) Dynamic palmitoylation events following T-cell

receptor signaling. Commun Biol 3:368. https://doi.org/10.1038/s42003-020-1063-5

37. Ivaldi C, Martin BR, Kieffer-Jaquinod S, Chapel A, Levade T, Garin J, Journet A (2012) Proteomic analysis of S-acylated proteins in human B cells reveals palmitoylation of the immune regulators CD20 and CD23. PLoS One 7:e37187. https://doi.org/10.1371/journal.pone.0037187

38. Martin BR, Cravatt BF (2009) Large-scale profiling of protein palmitoylation in mammalian cells. Nat Methods 6:135–138. https://doi.org/10.1038/nmeth.1293

39. Wilson JP, Raghavan AS, Yang YY, Charron G, Hang HC (2011) Proteomic analysis of fatty-acylated proteins in mammalian cells with chemical reporters reveals S-acylation of histone H3 variants. Mol Cell Proteomics. https://doi.org/10.1074/mcp.M110.001198

40. Davda D, El Azzouny MA, Tom CT, Hernandez JL, Majmudar JD, Kennedy RT, Martin BR (2013) Profiling targets of the irreversible palmitoylation inhibitor 2-bromopalmitate. ACS Chem Biol 8:1912–1917. https://doi.org/10.1021/cb400380s

41. Dart C (2010) Lipid microdomains and the regulation of ion channel function. J Physiol 588:3169–3178. https://doi.org/10.1113/jphysiol.2010.191585

42. Wang X, Zhang J, Berkowski SM, Knowleg H, Chandramouly AB, Downens M, Prystowsky MB (2004) Protein kinase C-mediated phosphorylation of Kv beta 2 in adult rat brain. Neurochem Res 29:1879–1886. https://doi.org/10.1023/b:nere.0000042215.92952.3d

43. Shaw AS, Filbert EL (2009) Scaffold proteins and immune-cell signalling. Nat Rev Immunol 9:47–56. https://doi.org/10.1038/nri2473

44. Ludford-Menting MJ, Oliaro J, Sacirbegovic F, Cheah ET, Pedersen N, Thomas SJ, Pasam A, Iazzolino R, Dow LE, Waterhouse NJ et al (2005) A network of PDZ-containing proteins regulates T cell polarity and morphology during migration and immunological synapse formation. Immunity 22:737–748. https://doi.org/10.1016/j.immuni.2005.04.009

45. Cho KO, Hunt CA, Kennedy MB (1992) The rat brain postsynaptic density fraction contains a homolog of the Drosophila discs-large tumor suppressor protein. Neuron 9:929–942. https://doi.org/10.1016/0896-6273(92)90245-9

46. Wong W, Schlichter LC (2004) Differential recruitment of Kv1.4 and Kv4.2 to lipid rafts by PSD-95. J Biol Chem 279:444–452. https://doi.org/10.1074/jbc.M304675200

47. O'Neill AK, Gallegos LL, Justilien V, Garcia EL, Leitges M, Fields AP, Hall RA, Newton AC (2011) Protein kinase Calpha promotes cell migration through a PDZ-dependent interaction with its novel substrate discs large homolog 1 (DLG1). J Biol Chem 286:43559–43568. https://doi.org/10.1074/jbc.M111.294603

48. Duncan PJ, Bi D, McClafferty H, Chen L, Tian L, Shipston MJ (2019) S-Acylation controls functional coupling of BK channel pore-forming alpha-subunits and beta1-subunits. J Biol Chem 294:12066–12076. https://doi.org/10.1074/jbc.RA119.009065

49. Charollais J, Van Der Goot FG (2009) Palmitoylation of membrane proteins (review). Mol Membr Biol 26:55–66. https://doi.org/10.1080/09687680802620369

50. Greaves J, Prescott GR, Gorleku OA, Chamberlain LH (2010) Regulation of SNAP-25 trafficking and function by palmitoylation. Biochem Soc Trans 38:163–166. https://doi.org/10.1042/BST0380163

51. Holland SM, Collura KM, Ketschek A, Noma K, Ferguson TA, Jin Y, Gallo G, Thomas GM (2016) Palmitoylation controls DLK localization, interactions and activity to ensure effective axonal injury signaling. Proc Natl Acad Sci USA 113:763–768. https://doi.org/10.1073/pnas.1514123113

52. Yang EK, Alvira MR, Levitan ES, Takimoto K (2001) Kvbeta subunits increase expression of Kv4.3 channels by interacting with their C termini. J Biol Chem 276:4839–4844. https://doi.org/10.1074/jbc.M004768200

53. Li Y, Um SY, McDonald TV (2006) Voltage-gated potassium channels: regulation by accessory subunits. Neuroscientist 12:199–210. https://doi.org/10.1177/1073858406287717

54. Heinemann SH, Rettig J, Graack HR, Pongs O (1996) Functional characterization of Kv channel beta-subunits from rat brain. J Physiol 493(Pt 3):625–633. https://doi.org/10.1113/jphysiol.1996.sp021409

55. Kilfoil PJ, Tipparaju SM, Barski OA, Bhatnagar A (2013) Regulation of ion channels by pyridine nucleotides. Circ Res 112:721–741. https://doi.org/10.1161/CIRCRESAHA.111.247940

56. Campomanes CR, Carroll KI, Manganas LN, Hershberger ME, Gong B, Antonucci DE, Rhodes KJ, Trimmer JS (2002) Kv beta subunit oxidoreductase activity and Kv1 potassium channel trafficking. J Biol Chem 277:8298–8305. https://doi.org/10.1074/jbc.M110276200

57. Weng J, Cao Y, Moss N, Zhou M (2006) Modulation of voltage-dependent Shaker family potassium channels by an aldo-keto reductase. J Biol Chem 281:15194–15200. https://doi.org/10.1074/jbc.M513809200

58. Tipparaju SM, Liu SQ, Barski OA, Bhatnagar A (2007) NADPH binding to beta-subunit regulates inactivation of voltage-gated K(+) channels. Biochem Biophys Res Commun 359:269–276. https://doi.org/10.1016/j.bbrc.2007.05.102

59. Croci C, Brandstatter JH, Enz R (2003) ZIP3, a new splice variant of the PKC-zeta-interacting protein family, binds to GABAC receptors, PKC-zeta, and Kv beta 2. J Biol Chem 278:6128–6135. https://doi.org/10.1074/jbc.M205162200

60. Bavassano C, Marvaldi L, Langeslag M, Sarg B, Lindner H, Klimaschewski L, Kress M, Ferrer-Montiel A, Knaus HG (2013) Identification of voltage-gated K(+) channel beta 2 (Kvbeta2) subunit as a novel interaction partner of the pain transducer transient receptor potential vanilloid 1 channel (TRPV1). Biochim Biophys Acta 1833:3166–3175. https://doi.org/10.1016/j.bbamcr.2013.09.001

61. Kisselbach J, Schweizer PA, Gerstberger R, Becker R, Katus HA, Thomas D (2012) Enhancement of K2P2.1 (TREK1) background currents expressed in Xenopus oocytes by voltage-gated K+ channel beta subunits. Life Sci 91:377–383. https://doi.org/10.1016/j.lfs.2012.08.011

62. Roig SR, Sole L, Cassinelli S, Colomer-Molera M, Sastre D, Serrano-Novillo C, Serrano-Albarras A, Lillo MP, Tamkun MM, Felipe A (2021) Calmodulin-dependent KCNE4 dimerization controls membrane targeting. Sci Rep 11:14046. https://doi.org/10.1038/s41598-021-93562-5

63. Nguyen HM, Miyazaki H, Hoshi N, Smith BJ, Nukina N, Goldin AL, Chandy KG (2012) Modulation of voltage-gated K+ channels by the sodium channel beta1 subunit. Proc Natl Acad Sci USA 109:18577–18582. https://doi.org/10.1073/pnas.1209142109

64. Kubota T, Correa AM, Bezanilla F (2017) Mechanism of functional interaction between potassium channel Kv1.3 and sodium channel NavBeta1 subunit. Sci Rep 7:45310. https://doi.org/10.1038/srep45310

65. Coppock EA, Martens JR, Tamkun MM (2001) Molecular basis of hypoxia-induced pulmonary vasoconstriction: role of voltage-gated K+ channels. Am J Physiol Lung Cell Mol Physiol 281:L1-12. https://doi.org/10.1152/ajplung.2001.281.1.L1

66. Sole L, Roura-Ferrer M, Perez-Verdaguer M, Oliveras A, Calvo M, Fernandez-Fernandez JM, Felipe A (2009) KCNE4 suppresses Kv1.3 currents by modulating trafficking, surface expression and channel gating. J Cell Sci 122:3738–3748. https://doi.org/10.1242/jcs.056689

67. Oliveras A, Serrano-Novillo C, Moreno C, de la Cruz A, Valenzuela C, Soeller C, Comes N, Felipe A (2020) The unconventional biogenesis of Kv7.1-KCNE1 complexes. Sci Adv 6:4472. https://doi.org/10.1126/sciadv.aay4472

68. Martinez-Marmol R, Villalonga N, Sole L, Vicente R, Tamkun MM, Soler C, Felipe A (2008) Multiple Kv1.5 targeting to membrane

surface microdomains. J Cell Physiol 217:667–673. https://doi.org/10.1002/jcp.21538

69. Wan J, Roth AF, Bailey AO, Davis NG (2007) Palmitoylated proteins: purification and identification. Nat Protoc 2:1573–1584. https://doi.org/10.1038/nprot.2007.225

S-acylation-dependent membrane microdomain localization of the regulatory Kvβ2.1 subunit

Sara R. Roig[1,2], Silvia Cassinelli[1], Mireia Pérez-Verdaguer[3], María Navarro-Pérez[1], Irene Estadella[1], Antonio Felipe[1].

[1]Molecular Physiology Laboratory, Departament de Bioquímica i Biomedicina Molecular, Institut de Biomedicina (IBUB), Universitat de Barcelona, Avda. Diagonal 643, 08028 Barcelona, Spain. [2]Imaging Core Facility, Biozentrum, University of Basel, 4056 Basel, Switzerland; [3]Department of Cell Biology, School of Medicine, University of Pittsburgh, 3500 Terrace Street, Pittsburgh, PA 15261, United States.

*Corresponding author: Antonio Felipe, e-mail address: afelipe@ub.edu

SUPPLEMENTARY INFORMATION
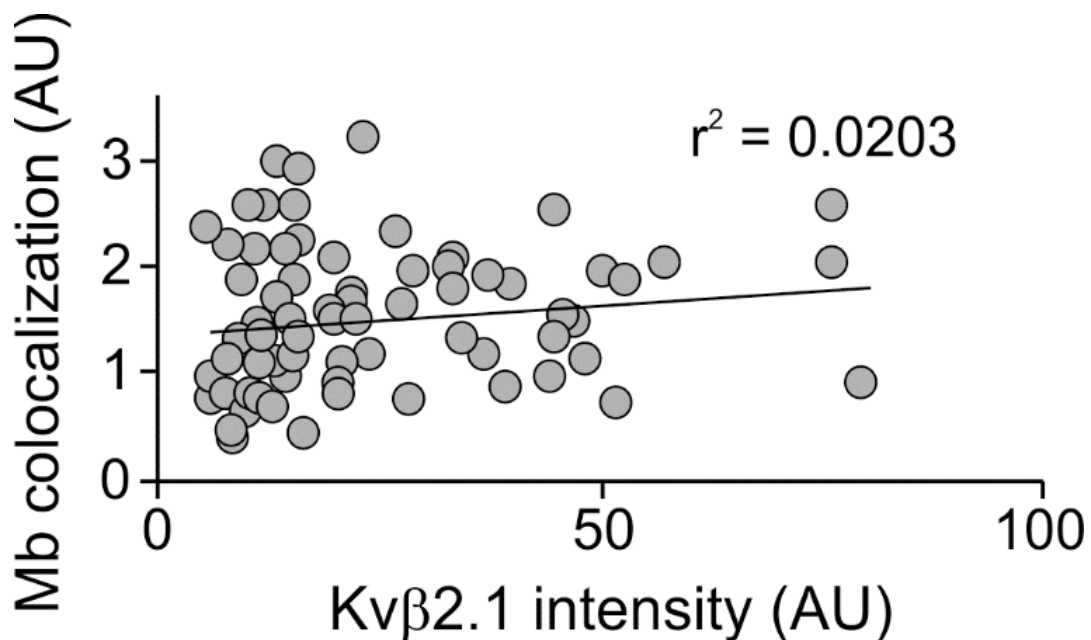
Figure S1. Kvβ2.1 membrane targeting is dose-independent. HEK 293 cells were transfected with Kvβ2.1CFP. The plasma membrane was stained with WGA, and Kvβ2.1 expression and membrane colocalization were measured. Plot of membrane colocalization of Kvβ2.1CFP (Mb) vs. intensity level of Kvβ2.1CFP in the entire cell. A calculated r^2 of 0.0203 indicates no correlation.

A

```
Kvβ1.1 (P63143)         MQVSIACTEHNLKSRNGEDRLLSKQSSNAPNVVNAARAKFRTVAIIAR-SLG-   51
Kvβ2.1 (P62482)                              MYPESTTGSPARLSLRQ   17

Kvβ1.1  52  TFTPQHHISLKESTAKQTGMKYRNLGKSGLRVSCLGLGTWVTFGGQISDEVAERLMTIAY   111
Kvβ2.1  18  TGSPGMIYSTRYGSPKRQLQFYRNLGKSGLRVSCLGLGTWVTFGGQITDEMAEHLMTLAY    77

Kvβ1.1 112  ESGVNLFDTAEVYAAGKAEVILGSIIKKKGWRRSSLVITTKLYWGGKAETERGLSRKHII   171
Kvβ2.1  78  DNGINLFDTAEVYAAGKAEVVLGNIIKKKGWRRSSLVITTKIFWGGKAETERGLSRKHII   137

Kvβ1.1 172  EGLKGSLQRLQLEYVDVVFANRPDSNTPMEEIVRAMTHVINQGMAMYWGTSRWSAMEIME   231
Kvβ2.1 138  EGLKASLERLQLEYVDVVFANRPDPNTPMEETVRAMTHVINQGMAMYWGTSRWSSMEIME   197

Kvβ1.1 232  AYSVARQFNMIPPVCEQAEYHLFQREKVEVQLPELYHKIGVGAMTWSPLACGIISGKYGN   291
Kvβ2.1 198  AYSVARQFNLIPPICEQAEYHMFQREKVEVQLPELFHKIGVGAMTWSPLACGIVSGKYDS   257

Kvβ1.1 292  GVPESSRASLKCYQWLKERIVSEEGRKQQNKLKDLSPIAERLGCTLPQLAVAWCLRNEGV   351
Kvβ2.1 258  GIPPYSRASLKGYQWLKDKILSEEGRRQQAKLKELQAIAERLGCTLPQLAIAWCLRNEGV   317

Kvβ1.1 352  SSVLLGSSTPEQLIENLGAIQVLPKMTSHVVNEIDNILRNKPYSKKDYRS      401
Kvβ2.1 318  SSVLLGASNAEQLMENIGAIQVLPKLSSSIVHEIDSILGNKPYSKKDYRS      367
```

B

Kvβ1.1-CFP

SM SN+ SN- IP+ IP-

IP CFP
IB CFP

IP CFP
IB Cav

C

Kvβ2.1-CFP

SM SN+ SN- IP+ IP-

IP CFP
IB CFP

IP CFP
IB Cav
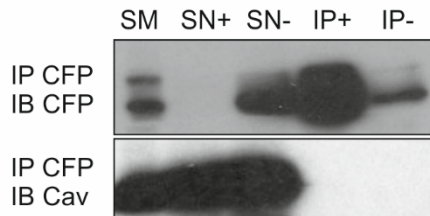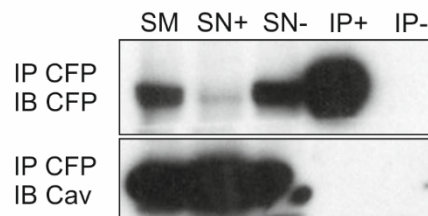
Figure S2. Kvβ2.1 does not interact with caveolin. (A) Amino acid sequence alignment of murine Kvβ1.1 and Kvβ2.1. The UniProt (https://www.uniprot.org/) identification number is indicated in brackets. Sequences were analyzed for putative CBD. Aromatic residues are highlighted in red, and putative hydrophobic CBD clusters are boxed in gray. Alternative hydrophobic residues within clusters are colored in blue. Bold black residues highlight identical amino acids. (B and C) HEK 293 cells were transfected with Kvβ1.1CFP and Kvβ2.1CFP, and the caveolin interaction was analyzed. (B) Kvβ1.1 does not coimmunoprecipitate with caveolin. (C) Kvβ2.1 does not coimmunoprecipitate with caveolin. Lysates were immunoprecipitated (IP) against CFP (Kvβ1.1 and Kvβ2.1) and immunoblotted (IB) against CFP (Kvβ1.1 and Kvβ2.1, top panels) and caveolin (cav, bottom panels). SM, staring materials. SN+, supernatant in presence of antibody. SN-, supernatant in absence of antibody. IP+, immunoprecipitation in the presence of antibody. IP-, immunoprecipitation in the absence of antibody.

A

Kvβ2.1WT

Kvβ2.1C$_{less}$

B
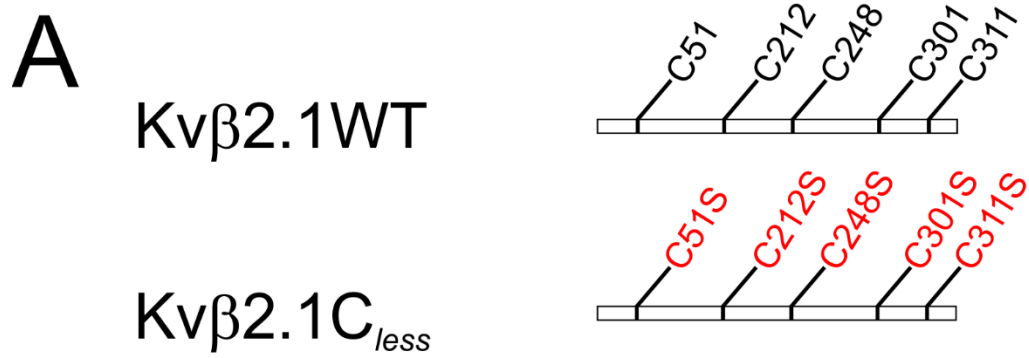
Kvβ2.1 300 G**C**TLPQLAIAW**C**LRNEGV 317
C$_{less}$ 300 G**S**TLPQLAIAW**S**LRNEGV 317
       PKC *consensus*   X**S**X**R**

C

Kvβ2.1 Mb Merge

WT

C$_{less}$

D
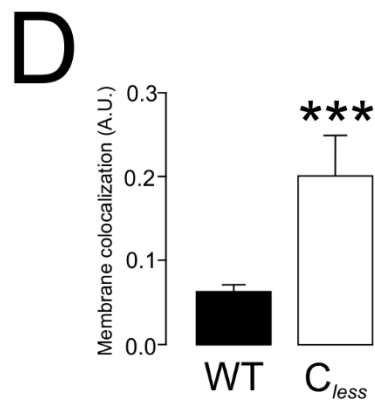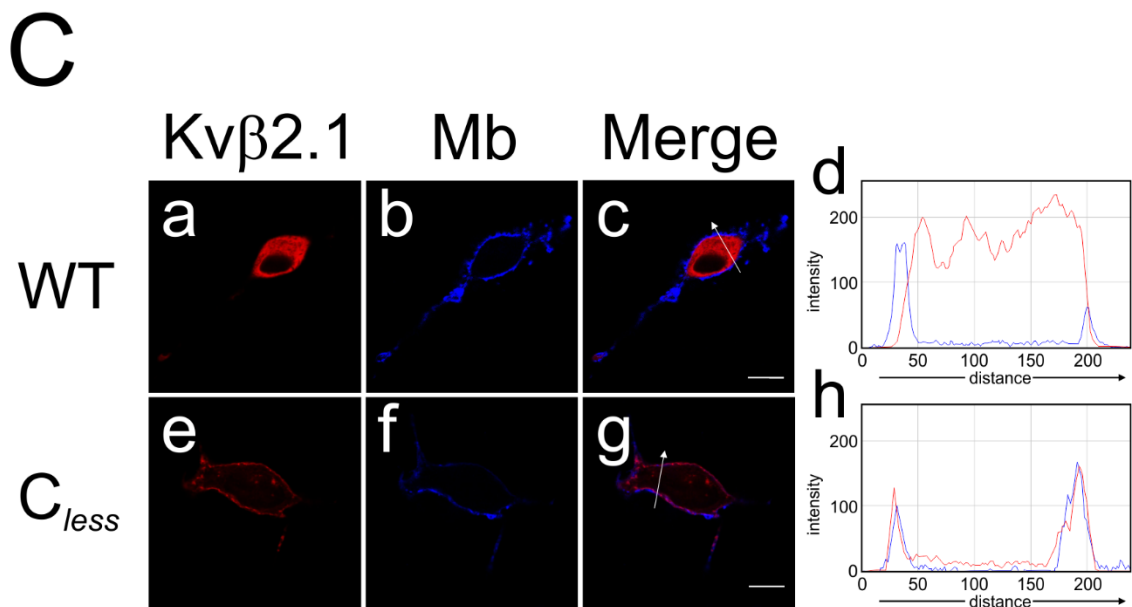
Figure S3 (previous page). Schematic representation and aberrant behavior of the mutant Kvβ2.1C$_{less}$.(A)Representative cartoon. Serine substitutions are shown in red. (B) Sequence analysis of the amino acid residues highlighting the *de novo* introduction of a potential PKC site. (C) Representative images of Kvβ2.1 WT and C$_{less}$ mutant. HEK 293 cells were transfected with Kvβ2.1CFP WT and C$_{less}$ mutant, and the subcellular distribution was analyzed. Kvβ2.1 in red; WGA membrane surface labeling in blue; merge shows colocalization in purple. Panels d and h show the pixel-by-pixel analysis of white arrow sections in c and g, respectively. Scale bars represent 10 μm. (D) Quantification of membrane colocalization using Mander's overlap coefficient (MOC). ***p<0.001 (Student's t-test) vs. WT. Values are mean $\pm$ SE of 30 cells. Black bar, Kvβ2.1 WT; white bar, Kvβ2.1C$_{less}$.
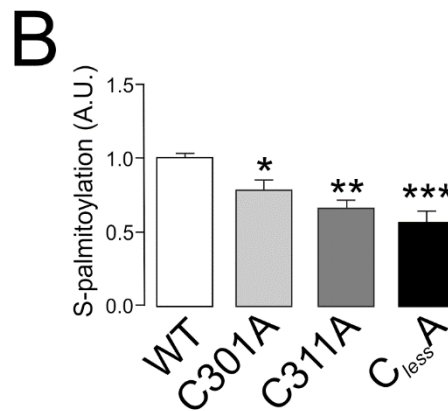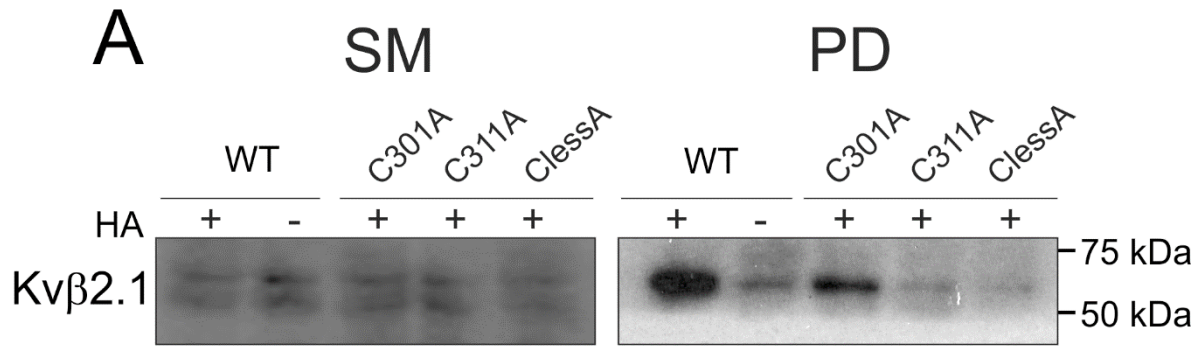
Figure S4. Palmitoylation of Kvβ2.1 WT and single cysteine mutants. HEK 293 cells were transfected with Kvβ2.1CFP WT, single cysteine mutants (C301A, C311A) and C*less*A. (A) Representative ABE experiment. SM, starting material immunoblotted with an anti-Kvβ2 antibody; PD, palmitoylated pull down. (B) Quantification of pulldowns relative to starting materials. Values are mean $\pm$ SE of 3 independent experiments. *, p<0.05; **, p<0.01; ***, p<0.001 (Student's t-test) vs. WT. White bar, Kvβ2.1 WT; light gray bar, C301A; dark gray bar, C311A; black bar, Kvβ2.1C*less*A.
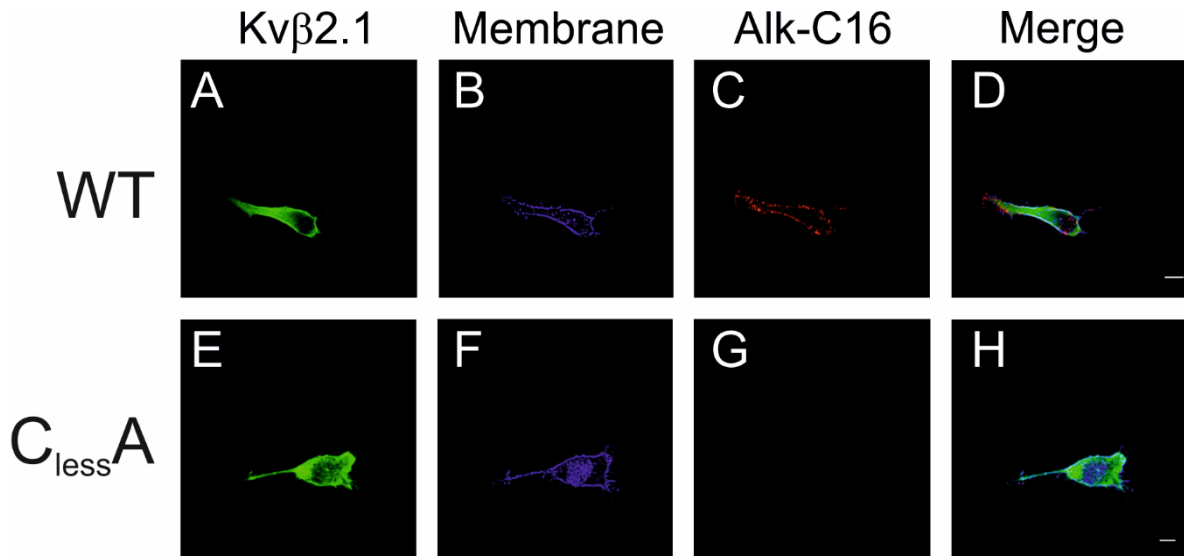
Figure S5. Palmitoylation-dependent cell surface targeting of Kvβ2.1. Proximity-ligation-assay (PLA). Palmitic acid 15-hexadecynoic acid was used for Alk-C16 protein palmitoylation. HEK 293 cells were transfected with Kvβ2.1CFP WT (A-D) and $C_{less}A$ (E-H). (A, E) Total Kvβ2.1CFP in green. (B, F) membrane marker staining in blue. (C, G) Kvβ2.1CFP Alk-C16 palmitoylation in red. (D, H) merge panel highlights Alk-C16 palmitoylation colocalizing with the cell surface. Scale bars represent 10µm.
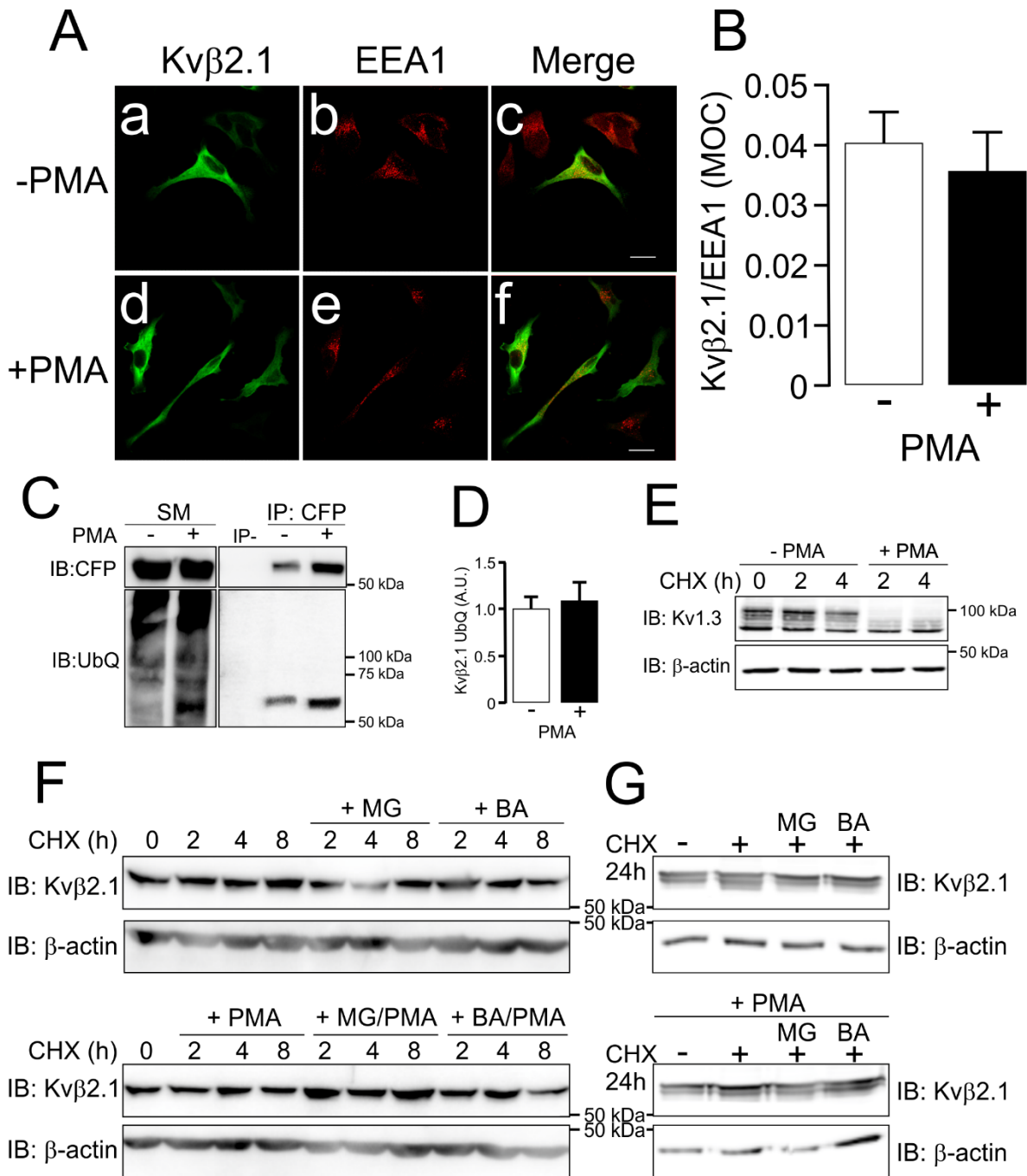
Figure S6. Localization, ubiquitination and stability of Kvβ2.1 upon PMA treatment. HEK 293 cells were transfected with Kvβ2.1CFP, and the early endocytosis location, ubiquitination and degradation fate were analyzed under PMA incubation. (A) Cellular distribution and colocalization with EEA1 of Kvβ2.1 in the absence (-) or presence (+) of PMA. Cells were incubated with PMA for 30 min. Kvβ2.1 CFP in green; EEA1 in red; merged panels, yellow indicates colocalization. Scale bars represents 10 μm. (B)

Quantification of Kvβ2.1/EEA-1 colocalization using Mander's overlap coefficient (MOC). Values are mean $\pm$ SE of 20-30 cells. (C) Kvβ2.1 ubiquitination in the absence (-) or presence (+) of PMA for 30 min. The right panel shows immunoprecipitation (IP) of CFP (Kvβ2.1) and immunoblot (IB) against CFP (top panel) and UbQ (bottom panel). Left panel shows immunoblot (IB) against CFP and UbQ. SM, starting material; IP-, immunoprecipitation in the absence of anti-CFP antibody; IP+, immunoprecipitation in the presence of anti-CFP antibody. (D) Quantification of ubiquitinated Kvβ2.1 upon PMA treatment. Ubiquitinated Kvβ2.1 (IB: UbQ) values, in arbitrary units (A.U.) were relativized to the total immunoprecipitated Kvβ2.1 (IB: CFP). (E) HEK 293 cells were transfected with Kv1.3YFP and its stability was measured in the presence (+) or the absence (-) of PMA at different times (h). Cells were incubated with cycloheximide (CHX) 30 min prior PMA addition and the protein synthesis inhibitor was further present all times. Note that while Kv1.3 abundance slightly decreased at 4 h in the absence of PMA, it almost disappeared as soon as 2 h after PMA treatment. (F) Analysis of the proteasomal and lysosomal degradation of Kvβ2.1 upon PMA treatment at different times (h). Cells were incubated in the absence or presence of MG (MG-132, proteasome inhibitor) and BA (bafilomycin A1, lysosomal inhibitor). (G) Analysis of the Kvβ2.1 stability upon PMA treatment during 24h. Lysates were immunoblotted against Kvβ2.1 (IB: Kvβ2.1). Kvβ2.1 abundancy in the absence (top panels) or presence (bottom panels) of PMA. Note that no Kvβ2.1 changes were observed throughout the experiment.

Oligomerization and Spatial Distribution of Kvβ1.1 and Kvβ2.1 Regulatory Subunits

Sara R. Roig[1,2] , Silvia Cassinelli[1] , Andre Zeug[3] , Evgeni Ponimaskin[3] and Antonio Felipe[1]

[1] Molecular Physiology Laboratory, Departament de Bioquímica i Biomedicina Molecular, Institut de Biomedicina (IBUB), Universitat de Barcelona, Avda. Diagonal 643, 08028 Barcelona, Spain

[2] Imaging Core Facility, Biozentrum University of Basel, 4056 Basel, Switzerland

[3] Department of Cellular Neurophysiology, Hannover Medical School, Hannover, Germany

[4] Kennedy Institute of Rheumatology, University of Oxford, Oxford OX3 7FY, UK

Oligomerization and Spatial Distribution of Kvβ1.1 and Kvβ2.1 Regulatory Subunits

Sara R. Roig[1,2], Silvia Cassinelli[1], Andre Zeug[3], Evgeni Ponimaskin[3] and Antonio Felipe[1]*

[1]Molecular Physiology Laboratory, Departament de Bioquímica i Biomedicina Molecular, Institut de Biomedicina (IBUB), Universitat de Barcelona, Barcelona, Spain, [2]Imaging Core Facility, Biozentrum, University of Basel, Basel, Switzerland, [3]Department of Cellular Neurophysiology, Hannover Medical School, Hannover, Germany

Members of the regulatory Kvβ family modulate the kinetics and traffic of voltage-dependent K^+ (Kv) channels. The crystal structure of Kv channels associated with Kvβ peptides suggests a α4/β4 composition. Although Kvβ2 and Kvβ1 form heteromers, evidence supports that only Kvβ2.1 forms tetramers in the absence of α subunits. Therefore, the stoichiometry of the Kvβ oligomers fine-tunes the activity of hetero-oligomeric Kv channel complexes. We demonstrate that Kvβ subtypes form homo- and heterotetramers with similar affinities. The Kvβ1.1/Kvβ2.1 heteromer showed an altered spatial distribution in lipid rafts, recapitulating the Kvβ1.1 pattern. Because Kvβ2 is an active partner of the Kv1.3-TCR complex at the immunological synapse (IS), an association with Kvβ1 would alter this location, shaping the immune response. Differential regulation of Kvβs influences the traffic and architecture of the Kvβ heterotetramer, modulating Kvβ-dependent physiological responses.

Keywords: regulatory subunits, oligomerization, potassium channels, lipid rafts, leukocytes

INTRODUCTION

The association of α-conducting subunits with β regulatory peptides determines the functional diversity of voltage-gated potassium (Kv) currents. Thus, changes in the expression of a subunit shape the channel composition and the physiological properties of the channelosome (Pongs and Schwarz, 2010).

Three genes (Kvβ1-3) encode the Kvβ family, some undergoing alternative splicing (i.e., Kvβ1.1–Kvβ1.3). Kvβs exhibit 85% similarity, mostly at the C-terminus. However, several functional differences, focused on Kv modulation, have been described (Kilfoil et al., 2013). While Kvβ1 and Kvβ3 accelerate the fast inactivation of Kv channels, using a ball-and-chain mechanism (Heinemann et al., 1995; Leicher et al., 1996), Kvβ2 increases the surface expression of the complex (Shi et al., 1996). Kvβ peptides exhibit aldo-keto reductase (AKR) activity by binding to NADP(H) and are included in the AKR6A subfamily within the AKR superfamily (Hyndman et al., 2003). Biochemical and structural evidence confirmed the presence of more than one Kvβ subunit in a tetrameric Kv channel configuration (Parcej et al., 1992; Gulbis et al., 1999). Scarce information is available regarding the oligomeric formation of Kvβ peptides. Evidence suggests that Kvβ1 and Kvβ2 form homo and hetero-oligomeric compositions (Xu et al., 1998; Nystoriak et al., 2017). Atomic force and electron microscopy support that the complex architecture is a tetramer with possible intermediate structures (van Huizen et al., 1999). The Kvβ2 crystal determines not only the macromolecular structure but also the orientation of units (Gulbis et al., 1999).

The molecular determinants for Kvβ2 oligomeric formation are mainly located within the core region. Kvβ1.1 and Kvβ2.1 share most of the C-terminal sequence, but Kvβ1.1 presents no interacting domains. Regarding the function of Kv, evidence shows that the higher the expression of Kvβ1 is, the larger the inactivation rate. Therefore, the variable stoichiometry of $\alpha_4\beta_n$ (4 α-subunits with a flexible number of β-subunits) would exert important physiological consequences (Xu et al., 1998). Thus, Kvβ2 inhibits the Kvβ1-mediated inactivation of Kv channels. This effect requires the core part of the subunit, which is necessary not only for homo- and hetero-oligomerization but also for interaction with the channel. Kvβ2 interacts with Kv channels in a tetrameric structure displacing Kvβ1, leading to a nonconcentration dependence of Kv modulation (Xu and Li, 1997). However, similar to Kvβ2, the capacity of Kvβ1.2 to form homo-oligomers has also been documented. Therefore, hybrids of both proteins with Kv channels induce intermediate inactivation patterns on Kv1.2 (Accili et al., 1997). This function could be of special relevance in immune system physiology, where Kvβ peptides are tightly regulated under insults (McCormack et al., 1999; Vicente et al., 2005). Kvβ2 concentrates with Kv1.3 at the immunological synapse (IS) (Beeton et al., 2006; Roig et al., 2022). Furthermore, Kvβ2, located in lipid rafts, may cluster in these spots, independent of the channel, during the immune response (Roig et al., 2022). Unlike Kvβ1, this spatial regulation is dependent on palmitoylation. The fact that Kvβ1.1 may alter the Kvβ2 spatial location at the IS, influencing the Kv1.3-dependent physiological consequences, could be crucial during the immune response.

Evidence suggest that Kvβ peptides could have physiological functions, such as REDOX sensors and clustering targeting proteins to specific spots, without the participation of Kv α subunits (Beeton et al., 2006; Roig et al., 2022). In this context, our results demonstrated that Kvβ1.1, as well as Kvβ2.1, are tetramers. In addition, we found that the affinity to form Kvβ homo- and hetero-oligomers is similar. Both Kvβ subunits reach the cell surface in homo- and heteromeric forms but with different plasma membrane distributions. While Kvβ2.1 partially targets lipid rafts, the combination with Kvβ1.1 mistargeted these domains. Therefore, Kvβ1, whose abundance is under tight regulation, would fine-tune the final fate and stoichiometry of the functional Kvβ complex, thereby shaping Kv1.3-dependent physiological responses.

MATERIALS AND METHODS

Expression Plasmids, Cell Culture and Transfections

mKvβ1.1 and mKvβ2.1 were provided by M.M. Tamkun (Colorado State University). mKvβ1.1 and mKvβ2.1 were subcloned into pEYFP-N1 and pECFP-N1 (Clontech). All constructs were verified by sequencing.

HEK-293 cells were cultured in DMEM (Lonza) containing 10% fetal bovine serum (FBS) supplemented with penicillin (10,000 U/ml), streptomycin (100 µg/ml) and L-glutamine

(4 mM) (Gibco). Human Jurkat T-lymphocytes and the murine CY15 dendritic cell line were cultured in RPMI culture medium (Lonza) containing 10% heat-inactivated FBS and supplemented with 10,000 U/ml penicillin, 100 µg/ml streptomycin and 2 mM L-glutamine (Gibco). Human CD4+ T-cell subsets were isolated from peripheral whole blood using a negative selection Rosette Sep™ kit from STEMCELL™ Technologies. Human T lymphocytes were cultured as previously described (Capera et al., 2021). Murine bone marrow-derived macrophages (BMDMs) from 6- to 10-week-old BALB/c mice (Charles River Laboratories) were used. The cells were isolated and cultured as described elsewhere (Sole et al., 2013).

For confocal imaging and coimmunoprecipitation experiments, cells were seeded (70–80% confluence) in 6-well dishes containing polylysine-coated coverslips or 100 mm dishes 24 h before transfection with selected cDNAs. Lipotransfectina® (Attendbio Research) was used for transfection according to the supplier's instructions. The amount of transfected DNA was 4 µg for a 100 mm dish and 500 ng for each well of a 6-well dish (for coverslip use). Next, 4–6 h after transfection, the mixture was removed from the dishes and replaced with fresh culture medium. All experiments were performed 24 h after transfection.

Protein Extraction, Coimmunoprecipitation and Western Blotting

All experimental protocols were approved by the ethical committee of the Universitat de Barcelona in accordance with the European Community Council Directive 86/609 EEC. We also confirm that all experiments were carried out in compliance with the ARRIVE guidelines (https://arriveguidelines.org). Rats and mice were briefly anesthetized with isoflurane, and brains and femurs were extracted immediately after euthanasia. The brain was homogenized in RIPA lysis buffer (1% Triton X-100, 1% sodium deoxycholate, 0.1% SDS, 50 mM Tris-HCl pH 8.0, 150 mM NaCl) supplemented with protease inhibitors. Total lysates were spun for 10 min at ×10,000 g to remove debris. Supernatants were used to analyze protein expression by western blotting.

Cells were washed twice in cold PBS and lysed on ice with lysis buffer (5 mM HEPES, 150 mM NaCl, 1% Triton X100, pH 7.5) supplemented with 1 µg/ml aprotinin, 1 µg/ml leupeptin, 1 µg/ml pepstatin and 1 mM phenylmethylsulfonyl fluoride as protease inhibitors. Cells were scraped and transferred to a 1.5 ml tube. Then, they were incubated for 20 min at the orbital at 4°C and spun for 20 min at 14,000 rpm. The supernatant was transferred to a new tube, and the protein contents were determined by using the Bio−Rad Protein Assay (Bio−Rad).

For coimmunoprecipitation, 1 mg of protein from each condition was separated and brought up to a volume of 500 µL with lysis buffer for IPs (150 mM NaCl, 50 mM HEPES, 1% Triton X-100, pH 7.4) supplemented with protease inhibitors. Precleaning was performed with 40 µL of protein A Sepharose beads (GE Healthcare) in an orbital shaker for 1 h at 4°C. Next, each sample was incubated in a small chromatography column (Bio−Rad Microspin

Chromatography Columns), which contained 2.5 μg of anti-GFP antibody (Genescript) previously crosslinked to protein A Sepharose beads, for 2 h at room temperature (RT) with continuous mixing. Next, columns were centrifuged for 30 s at ×1,000 g. The supernatant (SN) was kept and stored at −20°C. The columns were washed four times with 500 μL of lysis buffer and centrifuged for 30 s at ×1,000 g. Finally, elution was performed by incubating the columns with 100 μL of 0.2 M glycine pH 2.5 and spun 30 s at ×1,000 g. The eluted proteins (IP) were prepared for western blotting by adding 20 μL of loading buffer (×5) and 5 μL of 1 M Tris-HCl pH 10.

Irreversible crosslinking of the antibody to the Sepharose beads was performed after 1 h of incubation at RT of the antibody with protein A Sepharose beads, incubating the beads with 500 μL of dimethyl pimelimidate (DMP, Pierce) for 30 min at RT. Next, the columns were washed four times with 500 μL of ×1 TBS, four times with 500 μL of 0.2 M glycine pH 2.5 and three times more with ×1 TBS. Next, the columns were incubated with the protein lysates to perform immunoprecipitation following the above-described protocol.

Protein samples (50 μg), SN and IP were boiled in Laemmli SDS loading buffer and separated by 10% SDS–PAGE. For the nondenaturing technique, no boiling step was applied, and the SDS–PAGE gel was 8%. Next, samples were transferred to nitrocellulose membranes (Immobilon-P, Millipore) and blocked in 0.2% Tween-20-PBS supplemented with 5% dry milk before immunoreaction. Filters were immunoblotted with antibodies against Kvβ1.1 (1/1,000, Neuromab), Kvβ2.1 (1/1,000, Neuromab), Clathrin (1/1,000, BD Transduction) or Caveolin (1/1,000, BD transduction). Finally, the filters were washed with 0.05% Tween 20 PBS and incubated with horseradish peroxidase-conjugated secondary antibodies (Bio–Rad).

Confocal Microscopy and Image Analysis

For confocal microscopy, cells were seeded on poly-lysine-coated coverslips and transfected 24 h later. The next day, the cells were quickly washed twice, fixed with 4% paraformaldehyde for 10 min, and washed three times for 5 min with PBS-K+. Finally, coverslips were mounted on microscope slides (Acefesa) with house Mowiol mounting media. Coverslips were dried at RT at least 1 day before imaging.

The fluorescence resonance energy transfer (FRET) via the acceptor photobleaching technique was measured in a discrete region of interest (ROI). Fluorescent proteins from fixed cells were excited with the 458 nm or the 514 nm lines using low excitation intensities. Next, 475–495 nm bandpass and >530 nm longpass emission filters were applied. The YFP was bleached using maximum laser power with a yield of approximately 80% acceptor bleaching. After photobleaching of the acceptor, images of the donors and acceptors were captured. The FRET efficiency was calculated using the equation.

$[(F_{CFPafter} - F_{CFPbefore})/F_{CFPafter}] \times 100$, where $F_{CFPafter}$ and $F_{CFPbefore}$ are the fluorescence of the donor after and before bleaching, respectively. The loss of fluorescence as a result of the scans was corrected by measuring the CFP intensity in the unbleached part of the cell. All images were acquired with a Leica

TCS SL laser scanning confocal spectral microscope (Leica Microsystems) equipped with argon and helium–neon lasers. All experiments were performed with a ×63 oil-immersion objective lens NA 1.32. All offline image analyses were performed using ImageJ software.

Cell Unroofing Preparations

HEK-293 cells were seeded in poly-D-lysine-treated glass coverslips. Twenty-four hours after transfection, they were cooled on ice for 5 min and washed twice in PBS without K+. Next, the samples were incubated for 5 min in KHMgE buffer (70 mM KCl, 30 mM HEPES, 5 mM MgCl$_2$, 3 mM EGTA, pH 7.5) diluted three times and then gently washed with nondiluted KHMgE to induce hypotonic shock. Burst cells were removed from the coverslip by intensively pipetting up and down. After two washes with KHMgE buffer, only membrane sheets remained attached. Preparations were fixed and mounted as previously described (Oliveras et al., 2020).

Lipid Raft Isolation

Low density Triton-insoluble complexes were isolated as previously described (Martinez-Marmol et al., 2008) from HEK-293 cells transiently transfected with Kvβ1.1CFP and Kvβ2.1CFP. Cells were homogenized in 1 ml of 1% Triton X-100, and sucrose was added to a final concentration of 40%. A 5–30% linear sucrose gradient was layered on top and further centrifuged (×390,000 g) for 20–22 h at 4°C in a Beckman SW41Ti rotor. Gradient fractions (1 ml) were sequentially collected from the top and analyzed by western blotting.

Spectral Lux-Fluorescence Resonance Energy Transfer Analysis in Living Cells

Linear unmixing FRET (lux-FRET) described in (Wlodarczyk et al., 2008; Prasad et al., 2013) is a quantitative spectral FRET approach, based on two excitations, preferentially but not necessary where donor and acceptor are best excited, respectively. Lux-FRET treats the variety of possible distances, i.e., FRET states, of donor and acceptor as superposition of free donor and acceptor, and DA complexes. Since lux-FRET is based on spectral unmixing, references of donor only and acceptor only are required. Furthermore, like in other spectral FRET approaches, lux-FRET requires one tandem construct with a fixed one-to-one stoichiometry of donor and acceptor fluorophore. Because the calibration of the tandem construct is independent of the FRET efficiency, the information about the FRET efficiency of the tandem construct is not necessary. With the knowledge of the fluorescence quantum yield of the donor and acceptor fluorophores, lux-FRET is able to deduce the apparent FRET efficiencies Ef_D and Ef_A, where $f_D = \frac{[DA]}{[D^t]}$ and $f_A = \frac{[DA]}{[A^t]}$ are the fractions of donors and acceptors in complexes, respectively; the donor molar fraction ($x_D = \frac{[D^t]}{[D^t]+[A^t]}$); and the total donor (D) and acceptor (A) quantities, $[D^t]$ and $[A^t]$, scaled to the reference concentrations. For that, HEK-293 cells were cotransfected with Kvβ1.1YFP and Kvβ2.1CFP. Twenty-four

hours after transfection, the cells were resuspended in PBS. All lux-FRET measurements were recorded with the fluorescence spectrometer Fluorog-3.22 (Horiba) equipped with a xenon lamp (450 W, 950 V) and two double monochromators. Following configuration and settings were used: 5-mm pathway quartz cuvettes at 37°C in "front face" arrangement, dual excitation 440 and 488 nm, with emission spectra 450–600 nm and 500–600 nm, respectively, 0.5 s integration time. The spectral contributions from light scattering and nonspecific fluorescence of the cells were taken into account by subtracting the emission spectra of non-transfected cells (background) from each measured spectrum. Before the measurements, the spectrofluorometer was calibrated for the xenon lamp spectrum and Raman scattering peak position. To determine the apparent FRET efficiency for Kvβ1.1 and Kvβ2.1, we used a method described in detail previously (Renner et al., 2012; Prasad et al., 2013)). In short, we obtained relative excitation strengths $r^{ex,1}$ and $r^{ex,2}$ of the donor and acceptor from cells expressing, e.g., Kvβ1.1CFP or Kvβ2.1YFP only and did a non-negative linear unmixing with the corresponding characteristic, the Mock and the Raman spectrum. In the same way we received the donor and acceptor contributions δ^i and α^i, for both excitations i from co-expressions of donor and acceptor of various relative expression levels. The relative experimental donor to acceptor brightness $R_{TC} = \frac{\alpha^1_{TC} \cdot r^{ex,2} - \alpha^2_{TC} \cdot r^{ex,1}}{\Delta r \cdot \delta^1_{TC} + \Delta \alpha_{TC}}$, with $\Delta r = r^{ex,2} - r^{ex,1}$ and $\Delta \alpha = \alpha^2 - \alpha^1$, required for further calculations, we obtained from a tandem construct TC with one-to-one stoichiometry of donor and acceptor. From that, we calculated the total concentration ratio $[A^t]/[D^t] = \frac{\alpha^1 \cdot r^{ex,2} - \alpha^2 \cdot r^{ex,1}}{R_{TC} \cdot (\Delta r \cdot \delta^1 + \Delta \alpha)}$ of the donor and acceptor, the donor molar fraction (x_D) $x_D = \frac{[D^t]}{[D^t] + [A^t]} = 1/\frac{1}{1 + [A^t]/[D^t]}$ and the apparent FRET efficiencies $Ef_D = \frac{\Delta \alpha}{\Delta r \cdot \delta^1 + \Delta \alpha}$ and $Ef_A = R_{TC} \cdot \frac{\Delta \alpha}{\alpha^1 \cdot r^{ex,2} - \alpha^2 \cdot r^{ex,1}}$ (Wlodarczyk et al., 2008). The model characterizing apparent FRET efficiency (Ef$_D$) as a function of donor mole fraction (x$_D$) for oligomeric structures was developed previously (Veatch and Stryer, 1977) following $Ef_D = E(1 - x_D^{n-1})$. Fitting this model to experimental data yields the true transfer efficiency (E) and provides information about the number of units (n) interacting within the oligomeric complex. This model was slightly augmented for use with $Ef_A = E \frac{x_D}{x_D - 1}(1 - x_D^{n-1})$ (Meyer et al., 2006). The oligomerization model, yielding the total FRET efficiency, the basic subunit formation and the affinity constants, was previously described (Renner et al., 2012).

RESULTS

Kvβ1.1 and Kvβ2.1 are able to Homo- and Heteroligomerize

The nervous and immune systems express members of the voltage-gated regulatory subunit family Kvβ (McCormack et al., 1999; Vicente et al., 2005; Pongs and Schwarz, 2010). Kvβ1 and Kvβ2 are involved in controlling Kv inactivation and spatial distribution, such as axonal targeting and IS location (Gu

FIGURE 1 | Kvβ1 and Kvβ2 expression in the brain and leukocytes. Total lysates from rat brain and different leukocytes were immunoblotted against Kvβ1 and Kvβ2. Mouse dendritic CY15, human Jurkat T cells, human CD4+ lymphocytes, and murine BMDM samples were obtained and processed as described in the methods. Top panel, Kvβ1; middle panel, Kvβ2; bottom panel, β-actin as a control. Note that representative western blots are shown only for qualitative purposes. No comparison among groups due to species, cell type and sample processing is intended.

et al., 2003; Beeton et al., 2006; Roig et al., 2022). Therefore, we confirmed that the brain and leukocytes expressed the Kvβ1 and Kvβ2 subunits. As expected, not only the rat brain but also a wide repertoire of leukocytes, such as mouse CY15 dendritic cells, human Jurkat T cells, human CD4+ lymphocytes and primary murine bone marrow-derived macrophages (BMDMs), expressed both Kvβ1 and Kvβ2 regulatory subunits (**Figure 1**). Therefore, Kvβs are ubiquitously expressed within the immune system.

Most of the work related to the Kvβ family addresses the regulation of Kv channels (Pongs and Schwarz, 2010). Some studies address the modulation, *via* AKR activity, of the α-subunits. However, scarce information is available on the putative oligomeric formation of Kvβs. Evidence indicates that Kvβ2, but not Kvβ1, forms complexes. Kvβ1 controls channel activity in a concentration-dependent manner, and Kvβ2, by trapping Kvβ1 in those complexes, could impair its function on the α-subunits (Xu and Li, 1997; Xu et al., 1998). Structural studies indicate a prevalent tetrameric composition for the Kvβ2 complexes (Gulbis et al., 1999; van Huizen et al., 1999). Although evidence demonstrates that Kvβ2.1 forms homo- and heteromers with Kvβ1, no Kvβ1 oligomers have been detected in the absence of Kv channels. In this scenario, coimmunoprecipitation assays were performed in HEK cells transfected with Kvβ1.1CFP/Kvβ1.1, Kvβ2.1CFP/Kvβ2.1 and Kvβ1.1CFP/Kvβ2.1. Our data showed that in the absence of any Kv α subunit, Kvβ2.1, as well as Kvβ1.1, showed significant homo- and heterocoimmunoprecipitation (**Figures 2A–C**).

To explore further oligomeric associations, a series of FRET experiments were performed (see representative Kvβ1.1CFP/Kvβ2.1YFP in **Figure 2D**). Cells were transfected with KvβsCFP (Kvβ1.1CFP, **Figure 2Da**) and KvβsYFP (Kvβ2.1YFP, **Figure 2Db**) used as donor and acceptor fluorophores, respectively. Positive colocalization spots (**Figure 2Dc**) were subject to the acceptor bleach (white square in **Figure 2Dd**). FRET values confirmed that, similar to the tetrameric Kv1.3 channel (positive control), Kvβ1.1CFP/
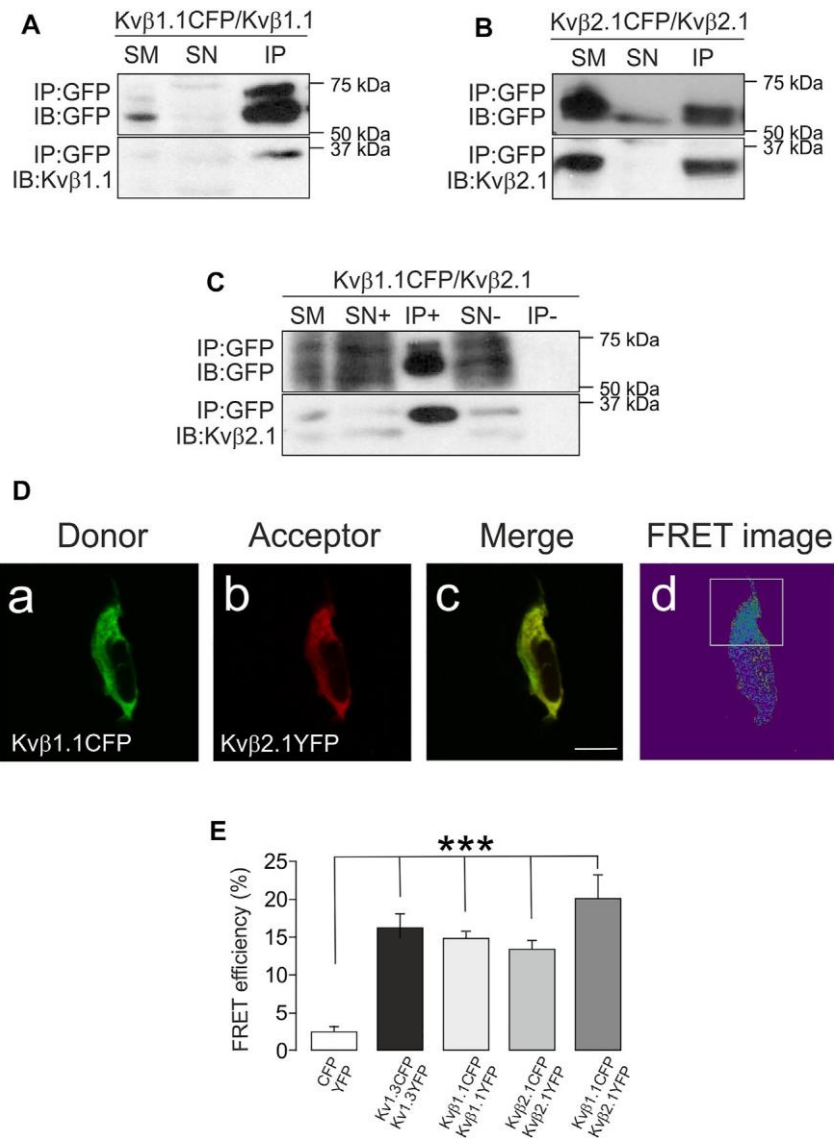
FIGURE 2 | Kvβ1.1 and Kvβ2.1 form oligomers. HEK 293 cells were transfected with Kvβ1.1 and Kvβ2.1. (A) Coimmunoprecipitation assay against Kvβ1.1CFP in the presence of Kvβ1.1. (B) Coimmunoprecipitation assay against Kvβ2.1CFP in the presence of Kvβ2.1. (C) Coimmunoprecipitation assay against Kvβ1.1CFP in the presence of Kvβ2.1. (C). Top panels: immunoprecipitation (IP) of CFP and immunoblot (IB) against CFP. Bottom panels: IB against Kvβ1.1 (A) and Kvβ2.1 (B,C). SM: starting material. SN+: supernatant in the presence of the antibody. IP+: Immunoprecipitation in the presence of the antibody. SN-: supernatant in the absence of the antibody. IP-: immunoprecipitation in the absence of the antibody. (D) Kvβ1.1 and Kvβ2.1 form homo- and hetero-oligomers. Representative image of Kvβ1.1 and Kvβ2.1 cotransfection. (Da) Donor, Kvb1.1CFP; (Db) Acceptor, Kvb2.1 YFP; (Dc) merge, yellow indicates colocalization; (Dd) FRET image obtained from the relationship between the donor prebleach versus postbleach after acceptor photobleaching. The white square highlights the bleached section. The bar represents 20 μm. (E) FRET efficiencies (%) calculated from the acceptor photobleaching experiments. Values are the mean ± SE of >30 cells. ***$p < 0.01$ vs. CFP/YFP negative control (Student's t test).

Kvβ1.1YFP, Kvβ2.1CFP/Kvβ2.1YFP and Kvβ1.1CFP/Kvβ2.1YFP form homo- and hetero-oligomeric complexes (Figure 2E).

Kvβ Homo- and Hetero-Oligomerization Affinities are Similar

Evidence suggests a preferred configuration of Kvβ complexes containing Kvβ2. However, our data indicated that Kvβ1 would also form oligomers in the absence of α-units. To decipher the affinity of the Kvβ complexes, we applied the linear unmixing FRET (lux-FRET) technique, which provides the apparent donor and acceptor FRET efficiencies, stoichiometry and affinity constants of interactions (Wlodarczyk et al., 2008). Experiments were performed in cell suspensions transfected with different donor molar ratios (Figure 3).

Coexpression of Kvβ1.1CFP/Kvβ1.1YFP raised three different complexes: homomeric Kvβ1.1CFP, homomeric Kvβ1.1YFP and

FIGURE 3 | Kvβ1.1 and Kvβ2.1 exhibit high FRET efficiencies for homo- and hetero-oligomerization with a basic unit of two peptides per complex. (A) Kvβ1.1CFP/ Kvβ1.1YFP. (B) Kvβ2.1CFP/Kvβ2.1YFP. (C) Kvβ1.1YFP/Kvβ2.1CFP. (D) Kvβ1.1CFP/Kvβ2.1YFP. Left panels, schematic representation of possible interactions upon cotransfection. Right panels, plot of Ef_D (blue circles), Ef_D fitting (solid line), Ef_A (green circles), Ef_A fitting (dashed line) vs. the donor molar ratio (x_D). (E) Values obtained from lux-FRET experiments performed on Kvβ combinations represented in orange squares in (A–D). E, FRET efficiency (%); N, number of units per complex; ROI, number of ROIs analyzed. Green shapes, Kvβ1.1; purple shapes, Kvβ2.1. Yellow represents YFP; blue represents CFP.

Kvβ1.1CFP/Kvβ1.1YFP heteromers. FRET confirmed the formation of heteromeric complexes (orange box in Figure 3A). In this case, lux-FRET values demonstrated an inverse correlation between the FRET efficiency of the donor (Ef_D) and the donor molar fraction (solid line, Figure 3A). The apparent FRET efficiency of the acceptor (Ef_A) was the opposite. Thus, the higher the donor molar fraction, the higher the apparent FRET efficiency (dashed line, Figure 3A). From these data, the FRET efficiency (E) and stoichiometry (N) of the complex were calculated. The FRET efficiency was 30.2%, and the basic unit involved two Kvβ1.1 subunits ($n = 1.93$) (Figure 3E). Kvβ2.1CFP/Kvβ2.1YFP exhibited a similar

pattern (Figure 3B), showing 22.3% FRET efficiency and a basic unit of two Kvβ2.1 peptides ($n = 2.09$) (Figure 3E).

We next analyzed Kvβ1.1CFP/Kvβ2.1YFP and reciprocal Kvβ2.1CFP/Kvβ1.1YFP (Figures 3C,D). The Kvβ1.1CFP/ Kvβ2.1YFP plot shifted to a lower x_D due to a slightly lower expression of Kvβ1.1CFP compared with Kvβ2.1YFP (Figure 3C). In this case, the calculated FRET efficiency was 32.5% with a basic unit of two proteins ($n = 1.88$) per complex (Figure 3E). Kvβ2.1CFP/Kvβ1.1YFP shifted in the opposite x_D direction due to the same effect by the lowest Kvβ2.1CFP expression (Figure 3D). In this context, Kvβ2.1 again presented a value of a basic unit of two ($n = 1.99$) and a FRET of 30.4% (Figure 3E).

FIGURE 4 | Kvβ1.1 and Kvβ2.1 can form homo- and heteromeric complexes with similar affinities. (A) Model of the interaction between donor and acceptor proteins. (B) Model of Kvβ1.1 and Kvβ2.1 oligomerization. (C). The calculated plot was based on the formula developed in the MATLAB program to find the affinity constants. Plot of the different parameters [DA], [DD], [AA], [D], [A], f_D and f_A depending on the donor molar fraction when a model presents the same affinity for forming three different complexes. [β2.1-β1.1], concentration of donor-acceptor complexes. [β2.1-β2.1], concentration of donor-donor complexes. [β1.1-β1.1], concentration of acceptor-acceptor complexes. [β2.1], donor concentration, [β1.1], acceptor concentration. $f_{β2.1}$, apparent donor efficiency. $f_{β1.1}$, apparent acceptor efficiency.

Kvβ1.1 and Kvβ2.1 Form Tetramers by Dimer Dimerization

Our data established that the basic unit for oligomerization was two peptides. This result implies that two different possibilities for the complex dynamics existed: 1) Kvβs form dimers; 2) these dimers oligomerize to form tetrameric structures (Figure 5A). Our results also indicated no trimeric structures (Figure 3E). Because Kvβ2.1 forms tetramers in the absence of the α-subunit, we wondered whether this also applies to the Kvβ1.1 subunit. Semidenaturating gel electrophoresis was implemented in HEK cells transfected with Kvβ1.1CFP and Kvβ2.1CFP (van Huizen et al., 1999). Monomeric structures were detected in all four conditions tested, but unlike YFP-transfected cells (Figure 5B), dimers and tetramers were found in Kv1.3YFP, Kvβ1.1YFP and Kvβ2.1YFP (Figures 5C,D). Kv1.3YFP was used as a control because of its tetrameric architecture. Thus, monomers, some dimers and tetramers were clearly visible (Figure 5C). Similarly, Kvβ1.1 and Kvβ2.1 analysis triggered monomeric, dimeric and tetrameric forms (Figure 5D). Therefore, in agreement with the lux-FRET data, no trimeric complexes were detected. Taken together, our data showed that both Kvβ1.1 and Kvβ2.1 could form tetramers by a dimeric interaction.

Surface Spatial Localization of Oligomeric Kvβ Compositions

Kvβ1.1 and Kvβ2.1 target the membrane surface, but only Kvβ2.1 is located in lipid rafts, independent of Kv1.3, in a palmitoylation-dependent manner (Roig et al., 2022). This spatial localization is crucial because Kvβ2.1 clusters at the IS during the immune system response (Beeton et al., 2006; Roig et al., 2022). Therefore, putative oligomeric Kvβ compositions, whose stoichiometry would depend on variable protein expression, could fine-tune leukocyte physiology. In this context, we sought to decipher whether Kvβ subunits target the plasma membrane in the absence of Kvα subunits as homo- or hetero-oligomeric complexes. CUPs were purified from HEK transfected cells, and FRET between Kvβs was analyzed (Figure 6). Only the negative CFP-YFP control was measured in a whole-cell configuration because CFP-YFP is a soluble peptide (Figures 6A–C). The tetrameric Kv1.3CFP/Kv1.3YFP channel was used as a positive control (Figures 6D–F). The FRET efficiency values of Kvβ1.1CFP/Kvβ1.1YFP (Figures 6G–I), Kvβ2.1CFP/Kvβ2.1YFP (Figure 6J–L) and Kvβ1.1CFP/Kvβ2.1YFP (Figures 6M–O) were clearly positive (Figure 6P). These results demonstrated that homo- and hetero-oligomeric Kvβ structures target the plasma membrane.

Kvβ2.1, but not Kvβ1.1, is locate in lipid rafts (Roig et al., 2022). Because the Kvβ affinity for homo- and heteromultimerization was similar, we investigated whether Kvβ2.1 and Kvβ1.1 would target rafts in a hetero-oligomeric configuration. Low-buoyancy membrane fractions from transfected HEK-293 cells were analyzed. While Kvβ1.1 was not present in raft domains (Figure 7A), Kvβ2.1 exhibited partial localization in these fractions (Figure 7B). Coexpression of both subunits (Kvβ1.1/Kvβ2.1) triggered

The calculation of the affinity constants was based on the model presented in Figure 4A. The mixture between a donor and an acceptor yields three different complexes. Each complex is formed to a greater or lesser extent depending on their affinity constants (Renner et al., 2012). This model was implemented to solve the Kvβ1.1/Kvβ2.1 affinity (Figure 4B). The system relies on previous evaluation of homomeric forms. Next, the different affinity constants could be defined by using the following formula.

$$\left(-K_{DD} + \sqrt{K_{DD}^2 + 8K_{DD}\left([D_t] - [DA]\right)} \right) \times \left(-K_{AA} + \sqrt{K_{AA}^2 + 8K_{AA}\left([A_t] - [DA]\right)} \right) = 16K_{DA}[DA]$$

Our abovementioned data were concomitant with the plot in Figure 4C, which suggests that the 3 affinity constants (k) in our model were similar. Thus, unlike 5-HT receptors, the absence of tilted ends in our plots indicated no differences in affinities, and therefore no preferences, between Kvβ1.1 and Kvβ2.1 forming homo- and hetero-oligomers (Renner et al., 2012).
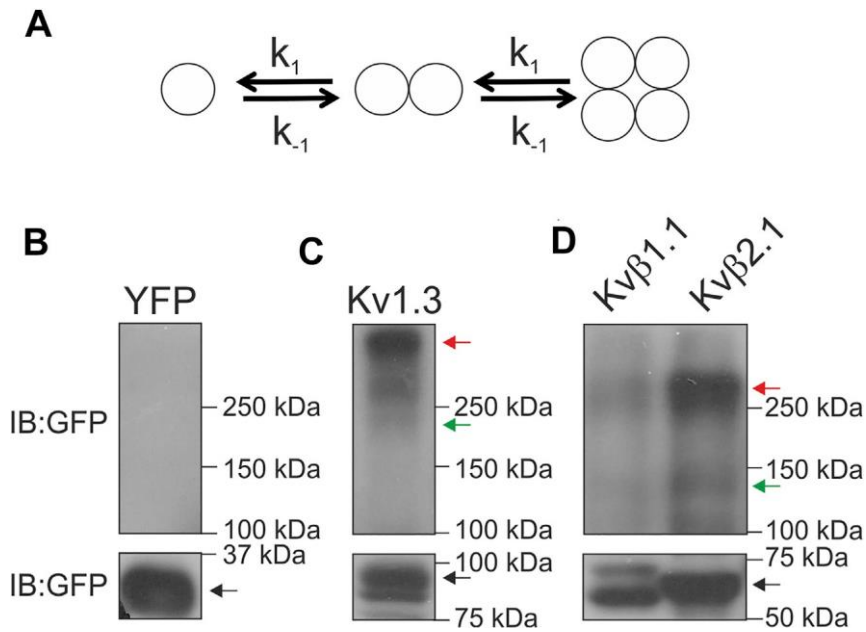
FIGURE 5 | Kvβ1.1 and Kvβ2.1 form dimeric and tetrameric structures. (A) Model representing the two putative options for Kvβ oligomerization. Kvβ forms dimers, and Kvβ forms tetrameric structures by association. The affinity constant (k) for every step would be the same in all conditions. (B–D) HEK 293 cells were transfected with YFP, Kv1.3YFP, Kvβ1.1YFP and Kvβ2.1YFP. Total lysates were analyzed in semidenaturing conditions. (B) YFP, (C) Kv1.3YFP, (D) Kvβ1.1YFP and Kvβ2.1YFP. Immunoblots (IB) were performed with an anti-GFP antibody. Blots were split into two for low- and high-molecular-weight forms for better visualization. The black arrow indicates monomeric forms. The green arrow indicates dimeric forms. The red arrow highlights tetrameric forms.

Kvβ2.1 to no longer traffic to raft microdomains (Figure 7C). Therefore, Kvβ1.1 hetero-oligomerization altered Kvβ2.1 membrane localization in lipid rafts.

DISCUSSION

The physiological function of Kv channels is tightly regulated by regulatory β subunits (Pongs and Schwarz, 2010). The composition and stoichiometry of the α-β complex ultimately determine the kinetics and gating of potassium channels as well as their cellular traffic and distribution (Pongs and Schwarz, 2010). We demonstrated that Kvβ1.1 and Kvβ2.1 form heteromeric complexes. Both peptides present over 85% similarity, and the regions involved in oligomerization are highly conserved. Although the homomeric composition for Kvβ2 was described early (Xu et al., 1998; van Huizen et al., 1999), the tetrameric ability of Kvβ1 subunits is a subject of debate (Accili et al., 1997). The crystal structure of Kvβ2 sustains a tetrameric architecture that was also inferred for Kvβ1 (Gulbis et al., 1999). However, hetero-oligomeric complexes always contain Kvβ2 (Nystoriak et al., 2017). Our work demonstrates that both Kvβs may form homotetramers. The tetramer is generated by dimerization of dimers. Both the homo- and heterotetrameric complexes exhibit similar affinity constants for both Kvβs. Therefore, differential abundance of Kvβs would shape the stoichiometry. In addition, Kvβ2, but not Kvβ1, targets lipid raft microdomains, and the heteromeric composition of the complex impairs the raft location of the Kvβ1/Kvβ2 structure. Given that Kvβ2 clusters at the IS, which concentrates lipid rafts, participating during the immunological response, the Kvβ1 interaction would fine-tune the physiological function by misallocating Kvβ2 from these signaling spots (Figure 8).

Our study also sheds light on the dynamic formation of Kvβ complexes. We found that the tetrameric composition Kvβs follows two sequential steps: 1) dimeric formation and 2) dimer dimerization to form the final tetrameric configuration. Although early evidence suggested trimeric structures (van Huizen et al., 1999), our results can only be fitted to a sequential dimerization of dimers, which would be in agreement with what was described for Kvβ2 homotetramers. Our findings would thereby be concomitant with the oligomerization that Kv α units undergo to form a conducting entity (Hille, 2001). A putative low oligomerization affinity would explain the negative homomeric Kvβ1.1 associations previously documented. In this context, because only Kvβ2 forms tetramers, upon elevated expression, homomeric Kvβ2 complexes displace Kvβ1, impairing its function (Xu and Li, 1997). However, we found that Kvβ1.1 formed oligomers with similar affinity, and the same was true for Kvβ1/Kvβ2 heterotetramerization. In fact, Kvβ1/Kvβ2 heteroligomers are expressed in coronary arterial myocytes, regulating Kv1.5 fine-tuning of the trafficking and membrane
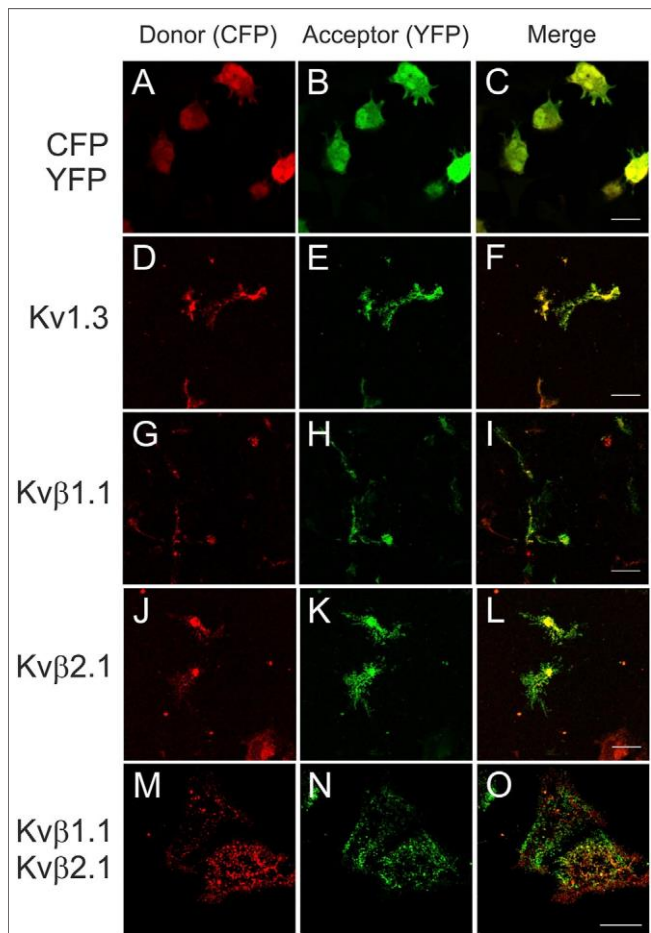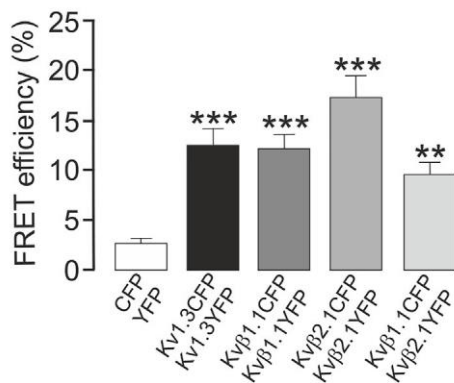
FIGURE 6 | Kvβ1.1 and Kvβ2.1 form heteromeric complexes at the plasma membrane. HEK 293 cells were transfected with Kv1.3YFP-Kv1.3CFP, Kvβ1.1YFP-Kvβ1.1CFP and Kvβ2.1YFP-Kvβ2.1CFP. After transfection, CUPs were purified, and FRET was analyzed. (A–C) CFP-YFP-transfected cells were used as negative controls. Note that CFP-YFP was analyzed in entire cells. (D–F) Kv1.3CFP-Kv1.3YFP. (G–I) Kvβ1.1CFP-Kvβ1.1YFP. (J–L) Kvβ2.1CFP-Kvβ2.1YFP. (M–O) Kvβ1.1CFP-Kvβ2.1YFP. Red panels, CFP; green panels, YFP; merged panels, yellow indicates colocalization. (P) FRET efficiency (%). **, $p < 0.01$; ***, $p < 0.001$ versus CFP-YFP (Student's t test). Values are the mean of 20–30 cells. Scale bars represent 10 µm.

localization of the channel (Nystoriak et al., 2017). We confirm previous evidence, but our contribution further shows that Kvβ2.1 and Kvβ1.1 form hetero-oligomers with similar affinities in the absence of the Kv channel. Thus, the unique factor governing multiple stoichiometries would be the differential regulation of both Kvβ peptides. In this scenario, the pattern of Kvβ subunit expression in macrophages depends upon proliferation and the mode of activation (Vicente et al., 2005). Therefore, Kv modulation depends on the final composition of the Kvβ heterotetramer architecture. Several proteins exhibit oligomeric composition control depending on the amount of each partner. For instance, ZIP1/ZIP2/ZIP3 are established hetero- and homodimers depending on the expression level upon different insults (Gong et al., 1999; Croci et al., 2003). In this vein, the heterotetrameric Kv1.3/Kv1.5 channel of professional antigen-presenting cells, such as dendritic cells and macrophages, follow the same fate (Vicente et al., 2006; Villalonga et al., 2007; Vallejo-Gracia et al., 2021). Because two different subunits can govern one unique channel, fine-tuning Kvβ concentrations would trigger a repertoire of functional channels (Pongs and Schwarz, 2010).
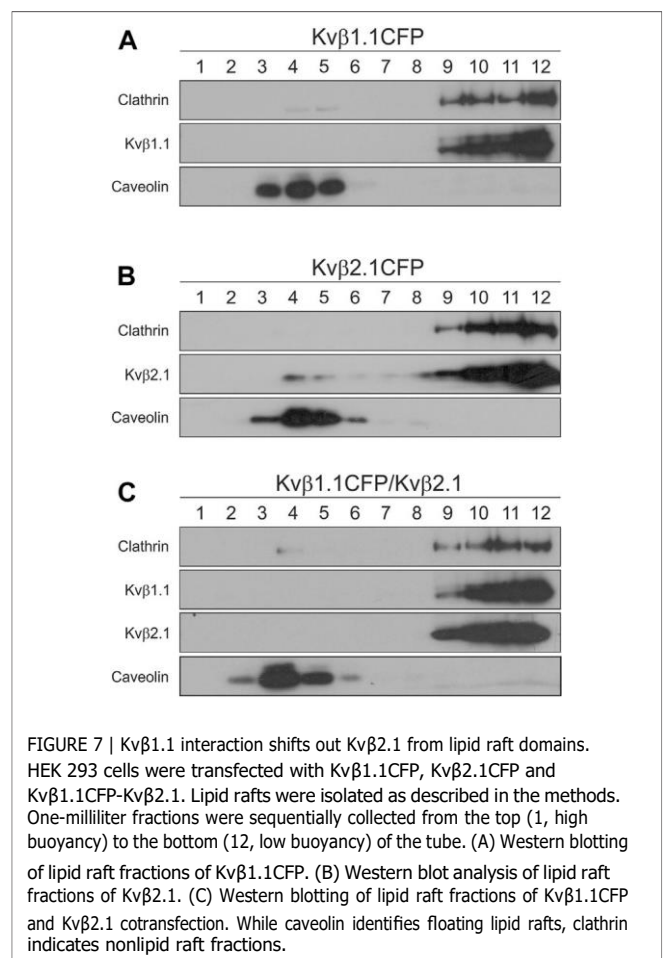
FIGURE 7 | Kvβ1.1 interaction shifts out Kvβ2.1 from lipid raft domains. HEK 293 cells were transfected with Kvβ1.1CFP, Kvβ2.1CFP and Kvβ1.1CFP-Kvβ2.1. Lipid rafts were isolated as described in the methods. One-milliliter fractions were sequentially collected from the top (1, high buoyancy) to the bottom (12, low buoyancy) of the tube. (A) Western blotting of lipid raft fractions of Kvβ1.1CFP. (B) Western blot analysis of lipid raft fractions of Kvβ2.1. (C) Western blotting of lipid raft fractions of Kvβ1.1CFP and Kvβ2.1 cotransfection. While caveolin identifies floating lipid rafts, clathrin indicates nonlipid raft fractions.
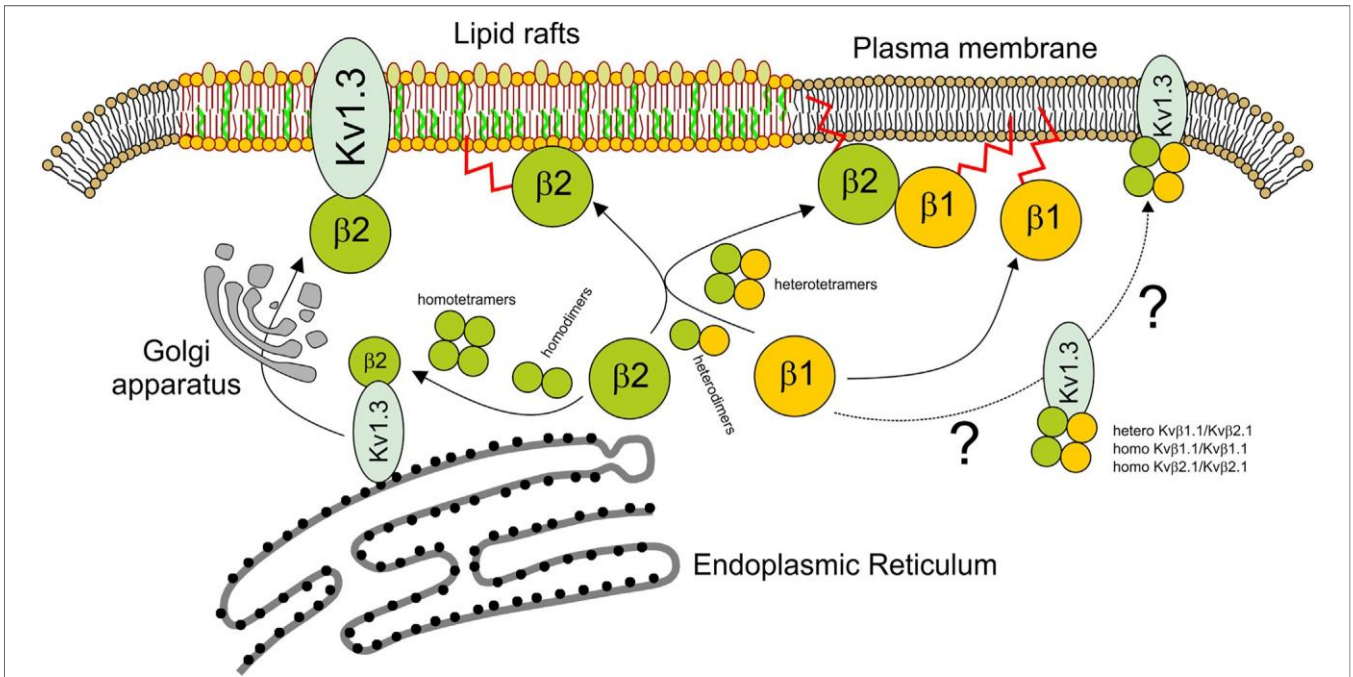
FIGURE 8 | Scheme representing the homo- and heteromeric Kvβ fate. While the tetrameric Kv1.3 channel is assembled early at the ER, soluble Kvβ is synthesized in the cytoplasm. Kvβ would form homo- and heterodimers. Kvβ tetramers would be formed by dimerization of dimers. Kvβ tetramers, especially Kvβ2, interact early with Kv1.3 to target lipid rafts via the Golgi apparatus. The extent to which Kv1.3 associated with Kvβ1.1 or Kvβ1.1/Kvβ2.1 tetramers follows different destinies outside lipid rafts is uncertain. In the absence of a channel, Kvβ2.1 tetramers target lipid rafts in a palmitoylation-dependent manner. However, Kvβ2.1 could also interact with Kvβ1.1, forming heterotetramers. In this context, not only homo-Kvβ1.1 but also Kvβ1.1–Kvβ2.1 heterotetramers would be displaced from lipid rafts targeting other plasma membrane surface locations. By this mechanism, Kvβ1.1 fine-tunes the Kvβ2.1-dependent physiological mechanisms at specific cell surface spots. Blue shape, Kv1.3; green balls, Kvβ2.1; yellow balls, Kvβ1.1. Kvβ palmitoylation (red sparkline).

Homo- and hetero-oligomers of Kvβ1.1/Kvβ2.1 targeted the membrane surface, but their microdomain localization was different. While Kvβ1.1 is associated with the actin cytoskeleton (Nakahira et al., 1998), Kvβ2.1 partially resides in lipid rafts (Roig et al., 2022). Both Kvβ proteins are palmitoylated, and palmitoylation of Kvβ2 is crucial for its location in these domains (Roig et al., 2022). This is of physiological relevance because Kvβ2 clusters at the IS, which are enriched in lipid rafts, representing an essential hub for signaling during the immune response (Beeton et al., 2006). Kvβ2 is situated in the IS, either modulating Kv1.3 or functioning as a hub for protein−protein interactions. Heterooligomeric interactions between Kvβ1 and Kvβ2 misplace the latter from lipid rafts and impair the function of Kvβ2 in these microdomains. In addition, the presence of Kvβ1 altered the function of Kvβ2 in a concentration-dependent manner. Therefore, the Kvβ1 interaction might fine-tune the Kvβ2-dependent physiological consequences during the immune response. In addition to regulating Kv channels and cluster protein interactions, Kvβs are also AKRs; therefore, redox variations can be sensed (Kilfoil et al., 2013). The different distribution of Kvβ throughout the cell surface would provide a differential redox sensitivity in different microdomains. Moreover, the diverse affinity for NADPH determines differential spatial triggers. Kvβ2 forms part of the signaling complex, which interacts with CD4, Kv1.3, ZIP1/2 and PSD proteins and clusters at the immunological synapse in human

T cells (Beeton et al., 2006; Roig et al., 2022). In addition, within these locations, Kvβ2 is regulated by PKC, p56lck and other signaling kinases (Kwak et al., 1999; Wang et al., 2004; Kim et al., 2005; Roepke et al., 2007; Ishii et al., 2013). Therefore, any spatial alteration in the localization of Kvβ2, as well as changes in Kvβ2-dependent enzymatic functions, such as modulating the Kv1.3 channelosome, surely would have essential consequences for leukocyte physiology.

DATA AVAILABILITY STATEMENT

The original contributions presented in the study are included in the article/Supplementary Material, further inquiries can be directed to the corresponding author.

ETHICS STATEMENT

The studies involving human participants were reviewed and approved by the Ethics Committee of the Universitat de Barcelona and the Banc de Sang i Teixits de Catalunya (BST). Institutional Review Board (IRB00003099). All procedures followed the rules of the Declaration of Helsinki Guidelines. The patients/participants provided their written informed consent to participate in this study. The animal study was

reviewed and approved by Universitat de Barcelona in accordance with the European Community Council Directive 86/609 EEC.

AUTHORS' CONTRIBUTIONS

SR, SC, and AZ performed experiments. SR, AZ, EP and AF designed the experiments. SR, AZ and AF wrote the manuscript. EP and AF directed the work. All the authors discussed the findings and revised the final version of the paper.

FUNDING

ACKNOWLEDGMENTS

SUPPLEMENTARY MATERIAL

The Supplementary Material for this article can be found online at: https://www.frontiersin.org/articles/10.3389/fphys.2022.930769/full#supplementary-material

REFERENCES

Accili, E. A., Kiehn, J., Wible, B. A., and Brown, A. M. (1997). Interactions Among Inactivating and Noninactivating Kvβ Subunits, and Kvα1.2, Produce Potassium Currents with Intermediate Inactivation. *J. Biol. Chem.* 272 (45), 28232–28236. doi:10.1074/jbc.272.45.28232

Beeton, C., Wulff, H., Standifer, N. E., Azam, P., Mullen, K. M., Pennington, M. W., et al. (2006). Kv1.3 Channels Are a Therapeutic Target for T Cell-Mediated Autoimmune Diseases. *Proc. Natl. Acad. Sci. U.S.A.* 103 (46), 17414–17419. doi:10.1073/pnas.0605136103

Capera, J., Pérez-Verdaguer, M., Peruzzo, R., Navarro-Pérez, M., Martínez-Pinna, J., Alberola-Die, A., et al. (2021). A Novel Mitochondrial Kv1.3-caveolin axis Controls Cell Survival and Apoptosis. *Elife* 10. doi:10.7554/eLife.69099

Croci, C., Brandstätter, J. H., and Enz, R. (2003). ZIP3, a New Splice Variant of the PKC-ζ-Interacting Protein Family, Binds to GABAC Receptors, PKC-ζ, and Kvβ2. *J. Biol. Chem.* 278 (8), 6128–6135. doi:10.1074/jbc.M205162200

Gong, J., Xu, J., Bezanilla, M., Huizen, R. v., Derin, R., and Li, M. (1999). Differential Stimulation of PKC Phosphorylation of Potassium Channels by ZIP1 and ZIP2. *Science* 285 (5433), 1565–1569. doi:10.1126/science.285.5433.1565

Gu, C., Jan, Y. N., and Jan, L. Y. (2003). A Conserved Domain in Axonal Targeting of Kv1 (Shaker) Voltage-Gated Potassium Channels. *Science* 301 (5633), 646–649. doi:10.1126/science.1086998

Gulbis, J. M., Mann, S., and MacKinnon, R. (1999). Structure of a Voltage-dependent K+ Channel β Subunit. *Cell* 97 (7), 943–952. doi:10.1016/s0092-8674(00)80805-3

Heinemann, S. H., Rettig, J., Wunder, F., and Pongs, O. (1995). Molecular and Functional Characterization of a Rat Brain Kv Beta 3 Potassium Channel Subunit. *FEBS Lett.* 377 (3), 383–389. doi:10.1016/0014-5793(95)01377-6

Hille, B. (2001). *Ion Channels of Excitable Membranes.* Sunderland, Massachusetts: Sinauer Associates.

Hyndman, D., Bauman, D. R., Heredia, V. V., and Penning, T. M. (2003). The Aldo-Keto Reductase Superfamily Homepage. *Chemico-Biological Interact.* 143-144, 621–631. doi:10.1016/s0009-2797(02)00193-x

Ishii, T., Warabi, E., Siow, R. C. M., and Mann, G. E. (2013). Sequestosome1/p62: a Regulator of Redox-Sensitive Voltage-Activated Potassium Channels, Arterial Remodeling, Inflammation, and Neurite Outgrowth. *Free Radic. Biol. Med.* 65, 102–116. doi:10.1016/j.freeradbiomed.2013.06.019

Kilfoil, P. J., Tipparaju, S. M., Barski, O. A., and Bhatnagar, A. (2013). Regulation of Ion Channels by Pyridine Nucleotides. *Circ. Res.* 112 (4), 721–741. doi:10.1161/CIRCRESAHA.111.247940

Kim, Y., Park, M.-K., Uhm, D.-Y., Shin, J., and Chung, S. (2005). Modulation of Delayed Rectifier Potassium Channels by α1-adrenergic Activation via Protein Kinase C ζ and P62 in PC12 Cells. *Neurosci. Lett.* 387 (1), 43–48. doi:10.1016/j.neulet.2005.07.016

Kwak, Y.-G., Hu, N., Wei, J., George, A. L., Jr., Grobaski, T. D., Tamkun, M. M., et al. (1999). Protein Kinase A Phosphorylation Alters Kvβ1.3 Subunit-Mediated Inactivation of the Kv1.5 Potassium Channel. *J. Biol. Chem.* 274 (20), 13928–13932. doi:10.1074/jbc.274.20.13928

Leicher, T., Roeper, J., Weber, K., Wang, X., and Pongs, O. (1996). Structural and Functional Characterization of Human Potassium Channel Subunit β1 (KCNA1B). *Neuropharmacology* 35 (7), 787–795. doi:10.1016/0028-3908(96)00133-5

Martínez-Mármol, R., Villalonga, N., Solé, L., Vicente, R., Tamkun, M. M., Soler, C., et al. (2008). Multiple Kv1.5 Targeting to Membrane Surface Microdomains. *J. Cell. Physiol.* 217 (3), 667–673. doi:10.1002/jcp.21538

McCormack, T., McCormack, K., Nadal, M. S., Vieira, E., Ozaita, A., and Rudy, B. (1999). The Effects of Shaker β-Subunits on the Human Lymphocyte K+ Channel Kv1.3. *J. Biol. Chem.* 274 (29), 20123–20126. doi:10.1074/jbc.274.29.20123

Meyer, B. H., Segura, J.-M., Martinez, K. L., Hovius, R., George, N., Johnsson, K., et al. (2006). FRET Imaging Reveals that Functional Neurokinin-1 Receptors Are Monomeric and Reside in Membrane Microdomains of Live Cells. *Proc. Natl. Acad. Sci. U.S.A.* 103 (7), 2138–2143. doi:10.1073/pnas.0507686103

Nakahira, K., Matos, M. F., and Trimmer, J. S. (1998). Differential Interaction of Voltage-Gated K+ Channel β-Subunits with Cytoskeleton Is Mediated by Unique Amino Terminal Domains. *Jmn* 11 (3), 199–208. doi:10.1385/JMN:11:3:199

Nystoriak, M. A., Zhang, D., Jagatheesan, G., and Bhatnagar, A. (2017). Heteromeric Complexes of Aldo-Keto Reductase Auxiliary K V β Subunits (AKR6A) Regulate Sarcolemmal Localization of K V 1.5 in Coronary Arterial Myocytes. *Chemico-Biological Interact.* 276, 210–217. doi:10.1016/j.cbi.2017.03.011

Oliveras, A., Serrano-Novillo, C., Moreno, C., de la Cruz, A., Valenzuela, C., Soeller, C., et al. (2020). The Unconventional Biogenesis of Kv7.1-KCNE1 Complexes. *Sci. Adv.* 6 (14), eaay4472. doi:10.1126/sciadv.aay4472

Parcej, D. N., Scott, V. E. S., and Dolly, J. O. (1992). Oligomeric Properties of .alpha.-Dendrotoxin-Sensitive Potassium Ion Channels Purified from Bovine Brain. *Biochemistry* 31 (45), 11084–11088. doi:10.1021/bi00160a018

Pongs, O., and Schwarz, J. R. (2010). Ancillary Subunits Associated with Voltage-dependent K+Channels. *Physiol. Rev.* 90 (2), 755–796. doi:10.1152/physrev.00020.2009

Prasad, S., Zeug, A., and Ponimaskin, E. (2013). Analysis of Receptor-Receptor Interaction by Combined Application of FRET and Microscopy. *Methods Cell Biol.* 117, 243–265. doi:10.1016/B978-0-12-408143-7.00014-1

Renner, U., Zeug, A., Woehler, A., Niebert, M., Dityatev, A., Dityateva, G., et al. (2012). Heterodimerization of Serotonin Receptors 5-HT1A and 5-HT7 Differentially Regulates Receptor Signalling and Trafficking. *J. Cell Sci.* 125 (Pt 10), 2486–2499. doi:10.1242/jcs.101337

Roepke, T. A., Malyala, A., Bosch, M. A., Kelly, M. J., and Rønnekleiv, O. K. (2007). Estrogen Regulation of Genes Important for K+ Channel Signaling in the Arcuate Nucleus. *Endocrinology* 148 (10), 4937–4951. doi:10.1210/en.2007-0605

Roig, S. R., Cassinelli, S., Navarro-Pérez, M., Pérez-Verdaguer, M., Estadella, I., Capera, J., et al. (2022). S-acylation-dependent Membrane Microdomain Localization of the Regulatory Kvβ2.1 Subunit. *Cell. Mol. Life Sci.* 79 (5), 230. doi:10.1007/s00018-022-04269-3

Shi, G., Nakahira, K., Hammond, S., Rhodes, K. J., Schechter, L. E., and Trimmer, J. S. (1996). βSubunits Promote K+ Channel Surface Expression through Effects Early in Biosynthesis. *Neuron* 16 (4), 843–852. doi:10.1016/s0896-6273(00)80104-x

Solé, L., Vallejo-Gracia, A., Roig, S. R., Serrano-Albarrás, A., Marruecos, L., Manils, J., et al. (2013). KCNE Gene Expression Is Dependent on the Proliferation and Mode of Activation of Leukocytes. *Channels* 7 (2), 85–96. doi:10.4161/chan.23258

Vallejo-Gracia, A., Sastre, D., Colomer-Molera, M., Solé, L., Navarro-Pérez, M., Capera, J., et al. (2021). KCNE4-dependent Functional Consequences of Kv1.3-related Leukocyte Physiology. *Sci. Rep.* 11 (1), 14632. doi:10.1038/s41598-021-94015-9

van Huizen, R., Czajkowsky, D. M., Shi, D., Shao, Z., and Li, M. (1999). Images of Oligomeric Kvβ2, a Modulatory Subunit of Potassium Channels. *FEBS Lett.* 457 (1), 107–111. doi:10.1016/s0014-5793(99)01021-2

Veatch, W. R., and Stryer, L. (1977). Effect of Cholesterol on the Rotational Mobility of Diphenylhexatriene in Liposomes: A Nanosecond Fluorescence Anisotropy Study. *J. Mol. Biol.* 117 (4), 1109–1113. doi:10.1016/s0022-2836(77)80017-x

Vicente, R., Escalada, A., Soler, C., Grande, M., Celada, A., Tamkun, M. M., et al. (2005). Pattern of Kvβ Subunit Expression in Macrophages Depends upon Proliferation and the Mode of Activation. *J. Immunol.* 174 (8), 4736–4744. doi:10.4049/jimmunol.174.8.4736

Vicente, R., Escalada, A., Villalonga, N., Texidó, L., Roura-Ferrer, M., Martín-Satué, M., et al. (2006). Association of Kv1.5 and Kv1.3 Contributes to the Major Voltage-dependent K+ Channel in Macrophages. *J. Biol. Chem.* 281 (49), 37675–37685. doi:10.1074/jbc.M605617200

Villalonga, N., Escalada, A., Vicente, R., Sánchez-Tilló, E., Celada, A., Solsona, C., et al. (2007). Kv1.3/Kv1.5 Heteromeric Channels Compromise

Pharmacological Responses in Macrophages. *Biochem. Biophysical Res. Commun.* 352 (4), 913–918. doi:10.1016/j.bbrc.2006.11.120

Wang, X., Zhang, J., Berkowski, S. M., Knowleg, H., Chandramouly, A. B., Downens, M., et al. (2004). Protein Kinase C-Mediated Phosphorylation of Kv 2 in Adult Rat Brain. *Neurochem. Res.* 29 (10), 1879–1886. doi:10.1023/b:nere.0000042215.92952.3d

Wlodarczyk, J., Woehler, A., Kobe, F., Ponimaskin, E., Zeug, A., and Neher, E. (2008). Analysis of FRET Signals in the Presence of Free Donors and Acceptors. *Biophysical J.* 94 (3), 986–1000. doi:10.1529/biophysj.107.111773

Xu, J., and Li, M. (1997). Kvβ2 Inhibits the Kvβ1-Mediated Inactivation of K+ Channels in Transfected Mammalian Cells. *J. Biol. Chem.* 272 (18), 11728–11735. doi:10.1074/jbc.272.18.11728

Xu, J., Yu, W., Wright, J. M., Raab, R. W., and Li, M. (1998). Distinct Functional Stoichiometry of Potassium Channel β Subunits. *Proc. Natl. Acad. Sci. U.S.A.* 95 (4), 1846–1851. doi:10.1073/pnas.95.4.1846

Chapter II

Molecular interaction at
the KCNE4 C-terminus

Calmodulin-dependent KCNE4 dimerization controls membrane targeting

Sara R. Roig[1,2], Laura Solé[1,3], Silvia Cassinelli[1] , Magalí Colomer-Molera[1] , Daniel Sastre[1] , Clara Serrano-Novillo[1] , Antonio Serrano-Albarrás[1] , M. Pilar Lillo[4] , Michael M.Tamkun[3] & Antonio Felipe[1]

[1] Molecular Physiology Laboratory, Dpt. de Bioquímica I Biomedicina Molecular, Institut de Biomedicina (IBUB), Universitat de Barcelona, Avda. Diagonal 643, 08028 Barcelona, Spain.

[2] Imaging Core Facility, Biozentrum, University of Basel, 4056 Basel, Switzerland.

[3] Department of Biomedical Sciences, Colorado State University, Fort Collins, CO 80523, USA.

[4] Instituto de Química Física Rocasolano, CSIC, 28006 Madrid, Spain.

.

scientific reports

Check for updates

OPEN

Calmodulin-dependent KCNE4 dimerization controls membrane targeting

Sara R. Roig[1,2], Laura Solé[1,3], Silvia Cassinelli[1], Magalí Colomer-Molera[1], Daniel Sastre[1], Clara Serrano-Novillo[1], Antonio Serrano-Albarrás[1], M. Pilar Lillo[4], Michael M. Tamkun[3] & Antonio Felipe[1✉]

The voltage-dependent potassium channel Kv1.3 participates in the immune response. Kv1.3 is essential in different cellular functions, such as proliferation, activation and apoptosis. Because aberrant expression of Kv1.3 is linked to autoimmune diseases, fine-tuning its function is crucial for leukocyte physiology. Regulatory KCNE subunits are expressed in the immune system, and KCNE4 specifically tightly regulates Kv1.3. KCNE4 modulates Kv1.3 currents slowing activation, accelerating inactivation and retaining the channel at the endoplasmic reticulum (ER), thereby altering its membrane localization. In addition, KCNE4 genomic variants are associated with immune pathologies. Therefore, an in-depth knowledge of KCNE4 function is extremely relevant for understanding immune system physiology. We demonstrate that KCNE4 dimerizes, which is unique among KCNE regulatory peptide family members. Furthermore, the juxtamembrane tetraleucine carboxyl-terminal domain of KCNE4 is a structural platform in which Kv1.3, Ca^{2+}/calmodulin (CaM) and dimerizing KCNE4 compete for multiple interaction partners. CaM-dependent KCNE4 dimerization controls KCNE4 membrane targeting and modulates its interaction with Kv1.3. KCNE4, which is highly retained at the ER, contains an important ER retention motif near the tetraleucine motif. Upon escaping the ER in a CaM-dependent pattern, KCNE4 follows a COP-II-dependent forward trafficking mechanism. Therefore, CaM, an essential signaling molecule that controls the dimerization and membrane targeting of KCNE4, modulates the KCNE4-dependent regulation of Kv1.3, which in turn fine-tunes leukocyte physiology.

Voltage-dependent potassium (Kv) channels participate in the resting membrane potential and repolarization of excitable cells[1]. Furthermore, Kv channels mediate additional cellular functions, such as control of cell cycle progression, cell activation and apoptosis[2]. Kv1.3 is mainly expressed in the nervous and immune systems. Leukocytes present a limited repertoire of potassium channels, and Kv1.3 is essential during the immune system response[3,4]. T lymphocyte activation triggers the translocation of the channel to the immunological synapse between T lymphocytes and antigen-presenting cells, maintaining the driving force for sustained calcium signaling[5].

Regulatory subunits modulate the function, trafficking and subcellular localization of Kv channels[6]. The KCNE family contains five single-span membrane auxiliary peptides (KCNE1-5) that modulate potassium channels[7]. KCNEs are present in the immune system, and their expression is regulated by several insults, highlighting the importance of this peptide family in leukocytes[8,9]. KCNE4, the largest member of the family, triggers dominant-negative effects on Kv channels. For instance, this subunit decreases Kv1.1, Kv1.3, Kv2.1 and Kv7.1 potassium current[10–12]. KCNE4 inhibits Kv7.1 current, not by altering the surface abundance of the channel but by altering the channel localization in lipid raft microdomains[13,14]. Functional interactions between KCNE4 and Kv7.1 require the presence of calmodulin (CaM). In fact, KCNE4 interacts with Ca^{2+}/CaM through a tetraleucine domain in the juxtamembrane of the KCNE4 C-terminus[15].

Evidence demonstrates that alterations in Kv1.3 and KCNE4 are associated with immune system pathologies[16–18]. KCNE4, tightly regulated in leukocytes, inhibits Kv1.3 function by hindering the surface

[1]Molecular Physiology Laboratory, Dpt. de Bioquímica I Biomedicina Molecular, Institut de Biomedicina (IBUB), Universitat de Barcelona, Avda. Diagonal 643, 08028 Barcelona, Spain. [2]Imaging Core Facility, Biozentrum, University of Basel, 4056 Basel, Switzerland. [3]Department of Biomedical Sciences, Colorado State University, Fort Collins, CO 80523, USA. [4]Instituto de Química Física Rocasolano, CSIC, 28006 Madrid, Spain. ✉email: afelipe@ub.edu

expression and lipid raft localization of the channel[19]. Kv1.3 and KCNE4 interact via the C-terminal domains of both proteins[20,21]. While the implicated molecular determinants of Kv1.3 are not evident, the tetraleucine domain of KCNE4 clearly participates in this interaction[20,21]. The tetraleucine motif hub forms a competing mechanism that directs the KCNE4 association with either CaM or Kv1.3, tuning the membrane targeting of the channel. The fact that several dileucine-rich domains participate in protein–protein interactions and that the tetraleucine signature of KCNE4 facilitates the association with CaM and Kv1.3 points to whether this element could be involved in further interactions regulated by CaM. In fact, KCNE4 does not inhibit Kv7.1 by impairing the association to CaM[15]. Furthermore, CaM interaction improves the surface targeting of Kv7.2[22]. Therefore, the evidence suggests that the CaM interaction, and hence the molecular determinants involved, is an important intracellular signaling mechanism of ion channel function.

We show in this work that the tetraleucine motif in the juxtamembrane region of the KCNE4 C-terminus functions as a multiple platform for subunit assembly and protein interaction. In contrast with other members of the KCNE family, KCNE4 forms stable dimers. The tetraleucine domain, unique to KCNE4, mediates this dimerization. The association of KCNE4 with CaM, as well as with Kv1.3, disrupts the dimer and facilitates the cell surface expression of KCNE4. CaM fine-tunes the association capacity of KCNE4 with Kv1.3, thereby modulating channel-dependent immune responses. Our data are of physiological relevance because CaM, a very important intracellular signaling molecule, controls Kv1.3-dependent KCNE4-related immunological events.

Results

KCNE4, broadly expressed in mammalian tissues, specifically inhibits Kv1.3. In addition to cardiac action potentials and synaptic transmission, Kv channels participate in many physiological functions throughout the body. The expression of these proteins is not limited to excitable cells, and tight modulation by regulatory subunits is essential to achieve a plethora of actions. The association with regulatory peptides adds complexity to the channel architecture, further increasing their function. In this scenario, KCNE4 modulates many Kv channels, and KCNE4 mRNA expression is ubiquitous[10,11,23]. However, no protein data are available. We showed that KCNE4 was differentially expressed in several rat tissues and leukocytes (Fig. 1A). As previously mentioned[10,11], we confirmed the expression of KCNE4 in the uterus, which is not surprising because the uterus exhibits ion channel proteins, such as KCNE1 or Nav2.3 [24,25]. KCNE4 was also present in some epithelium-like tissues, such as the colon and lung (Fig. 1Aa), where the movement of ions and water is achieved by multiple ion channels. The presence of KCNE4 in the brain and heart is in accordance with several Kv proteins, such as Kv1.1, Kv1.3, Kv2.1, and Kv7.1, which are targets of this regulatory peptide[23]. Within the immune system, in contrast to Jurkat T lymphocytes, KCNE4 expression in spleen and mononuclear phagocytes, such as CY15 dendritic cells (Fig. 1Aa) and bone marrow-derived macrophages (Fig. 1Ab), was notable. Although KCNE4 is widely expressed in the immune system, KCNE4 regulation is unique. Leukocytes express both Kv1.3 and Kv1.5 to govern cell responses[3,26], but KCNE4 selectively regulates only Kv1.3 when expressed in HEK-293 cells (Fig. 1B, C).

KCNE peptides exhibit important structural motifs in the juxtamembrane region of the C-terminus. KCNE regulatory peptides, sharing a notable ER retention, cause a differential effect on the plasma membrane targeting of Kv channels[13,14]. Thus, while KCNE1 interaction mostly improves Kv channel membrane targeting[27], KCNE4 transfers to the Kv1.3 complex ER retention motifs crucial for the control of the surface expression of the channel[20,21]. Because of the physiological relevance of these effects on the immune response, we characterized the intracellular retention mechanisms of KCNE4 by using KCNE1, the most documented KCNE subunit, as a reference. The membrane targeting of KCNE1 was low and similar to that observed with KCNE4 (Fig. 2A), and both KCNEs markedly colocalized with the ER (Fig. 2B). Our data further support and extend the evidence suggesting that KCNEs share ER retention motifs in their structure. A sequence alignment of their primary structures clearly shows basic clusters canonically associated with ER retention located in the juxtamembrane region of the KCNE C-terminus (Fig. 2C). In this context, KCNE3 and KCNE4 motifs contained larger motifs, which could suggest a major capacity of transfer intracellular retention to the associated Kv complex. Interestingly, KCNE4 is unique within the KCNE family because it presents a tetraleucine motif (L69-72) known to participate in the CaM-dependent modulation of channels, such as Kv7.1 and Kv1.3[15,20].

KCNE4 dimerization. Because dileucine motifs are critical for multiple protein–protein interactions, we wondered whether the tetraleucine signature mediates homo-oligomerizations of KCNE4. If it does, then this subunit is unique within the KCNE family, conferring distinctive structural features to this peptide that may fine-tune its Kv1.3-specific physiological functions. The molecular modeling of KCNE4, based on the KCNE1 structure (PBD ID: 2K21)[28], suggested that the tetraleucine motif, containing four consecutive hydrophobic residues, forms an accessible loop for different protein–protein interactions, e.g. Kv1.3 and CaM (Fig. 3A). This model is highly reliable because, although it is based on the KCNE1 structure[28], it is quite similar to that obtained for KCNE3 by cryo-EM[29]. Protein analysis in the presence of the DMP cross-linking reagent revealed that KCNE4 and Kv1.3 form oligomeric structures, which indicates several protein–protein interactions (Fig. 3B). Thus, the tetrameric Kv1.3-YFP complex forms large molecules. Similarly, KCNE4 exhibited large forms, which indicate multimeric complexes detectable only with DMP. The formation of these structures was confirmed by coimmunoprecipitation showing that KCNE4-YFP and KCNE4-HA interact (Fig. 3C) and FRET studies of KCNE4-YFP and KCNE-4CFP (Fig. 3D and E). This result was specific for KCNE4 because KCNE1 showed no positive FRET values (Fig. 3E).

To characterize the KCNE4 oligomers further, we performed a TIRF-derived single bleaching step assay[30]. Kv1.3-loopBAD-GFP, KCNE4-loopBAD-GFP and KCNE1-loopBAD-GFP were expressed in HEK 293 cells, and GFP fluorescent immobile spots were monitored (Fig. 4). Kv1.3 was used as the control (Fig. 4A–C). Experimental
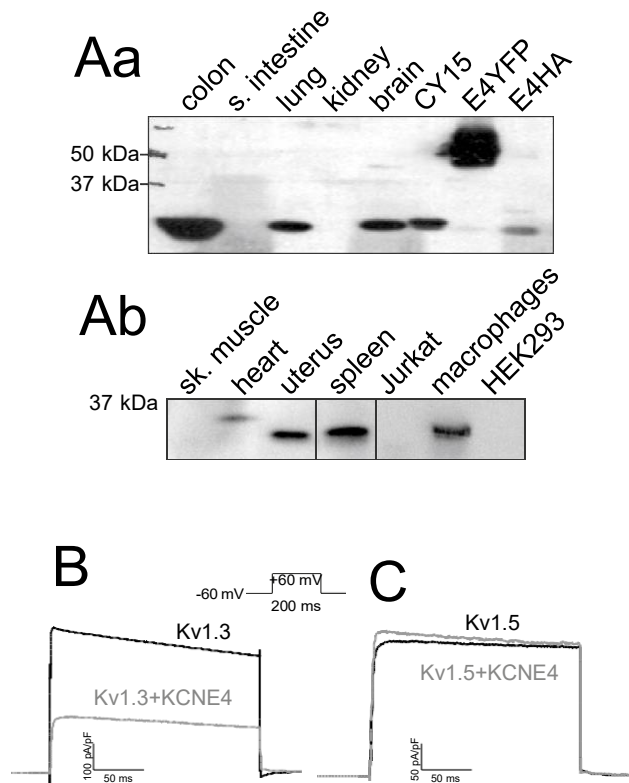
Figure 1. KCNE4, which specifically regulates Kv1.3, is differentially expressed in tissues and leukocytes. (**A**) Protein expression of KCNE4 in different rat tissues and cell lines. HEK-293 cells were used as negative control, and HEK cells transfected with KCNE4-YFP (E4YFP) and KCNE4-HA (E4HA) were used as positive controls. Different western blots with the same KCNE4-YFP and KCNE4-HA controls from different origins were merged for better visualization. Fifty micrograms of protein was loaded in each lane, and filters were immunoblotted with anti-KCNE4 antibody. Differential β-actin expression among tissues and cell lines (not shown) invalidated this protein as a control. Therefore, a KCNE4 abundance comparison among samples should not be considered. The results must be considered as qualitative data. Representative cropped blots, clearly separated by vertical black lines, are shown only for qualitative purposes. (**B**, **C**) Representative patch-clamp recordings of HEK-293 cells transfected with Kv1.3 and Kv1.5 in the absence or presence (+KCNE4) of KCNE4. Cells were hold at -60 mV and voltage-dependent K$^+$ currents were elicited by applying 200 ms depolarizing pulses to +60 mV. (B) Kv1.3 +/- KCNE4. (C) Kv1.5 +/- KCNE4. Gray lines, presence of KCNE4 (+KCNE4); black lines, absence of KCNE4. Data analysis was performed using FitMaster (HEKA) and SigmaPlot 10.0 software (Systat Software).

bleaching steps in selected ROIs demonstrated the canonical Kv1.3 tetrameric architecture (Fig. 4B). We calculated the expected distribution of the tetrameric channels with different p values (probability of fluorescing GFP), and the best fit was obtained with a GFP folding efficiency of 67% (*p* = 0.67) (Fig. 4C), indicating a tetrameric architecture as previously described[30–32]. However, KCNE4 mostly exhibited two unique possible structures (Fig. 4D–F). That is, monomeric and dimeric forms of KCNE4 were detected (Fig. 4D and E). The best fit for the expected distribution and the experimental data revealed that KCNE4 is present in monomeric and dimeric forms (Fig. 4F). In contrast, using the same approach, we found that KCNE1 was present only in monomeric form (Fig. 4G, H), as previously demonstrated[33,34].

The juxtamembrane tetraleucine motif facilitates CaM‑dependent protein–protein interactions and membrane targeting of KCNE4. The tetraleucine motif of KCNE4 is an interacting platform that defines the CaM modulation of the KCNE4-dependent regulation of Kv1.3 and Kv7.1[15,20]. In this context, we wanted to know whether this unique motif among KCNE peptides facilitates KCNE4 dimerization. To examine this possibility, we generated several KCNE4 mutants that disrupted the tetraleucine motif either alone (KCNE4(L69-72A)) or in combination with ERRM signaling (KCNE4(RM&L)). KCNE2, which neither contains tetraleucine motifs nor associates with Kv1.3, has been widely characterized[20]. Therefore, a KCNE2 mutant (KCNE2(L83-86)) with an embedded tetraleucine motif was also used (Fig. 5A). In contrast to WT KCNE4, disruption of the tetraleucine motif (KCNE4(L69-72A)) impaired KCNE4 dimerization, as observed by coimmunoprecipitation (Fig. 5B), non-denaturing polyacrylamide gel electrophoresis (Fig. 5C) and further supported by FRET assays (Fig. 5D). In addition, coimmunoprecipitation experiments with the KCNE2(L83-86) mutant showed that the addition of the leucine cluster to KCNE2 triggered the dimerization of KCNE2 with KCNE4 (Fig. 5E).

A Cell Surface

KCNE1 | KCNE | Merge
KCNE1 | MB | Merge

KCNE4 | KCNE | Merge
KCNE4 | MB | Merge

MB colocalization
0.8
0.6
0.4
0.2
0.0
E1 E4

B Endoplasmic Reticulum

KCNE1 | KCNE | Merge
KCNE1 | ER | Merge

KCNE4 | KCNE | Merge
KCNE4 | ER | Merge

ER colocalization
0.8
0.6
0.4
0.2
0.0
E1 E4

C

```
P23299|KCNE1_MOUSE  -MSLPNST--------TVLPFLARLWQE----------TA--EQGGNVSGLA-RKSQLRD  38
Q9D808|KCNE2_MOUSE  MATLANLTQTLEDAFKKIFITYMDSWRR----------NT--TAEEQ--ALQ--ARVDAE  44
Q9WTW2|KCNE3_MOUSE  -METSNGTETWYMSLHAVLKALNTTLHS-HLLCRPGPGPGPDN-----QTEDRRASLPG  52
Q9WTW3|KCNE4_MOUSE  MLRMEPLN--------S-------TYPS---------AA--ASSS---PLESHVPSNSS  30
Q9QZ26|KCNE5_MOUSE  -MNCSESQ-----RLQTLLNRLLLELHHRGNASGLGIGTGPSMGMGVVPDPFVGREATSA  54

P23299|KCNE1_MOUSE  DSKLEALYIILMVLGFFGFFTLGIMLSYIRSKKLEHS.DPFNVYIES-DAWQEKGKAVFQA  97
Q9D808|KCNE2_MOUSE  NFYYVILYLMVMIGMFSFIVVAILVSTVKSKRREHS'HPYHQYIVE--DWQEKYKSQILH  102
Q9WTW2|KCNE3_MOUSE  RNDNSYMYILFVMFLFAVTVGSLILGYTRSRKVDKRSDPYHVYIKNRVSMI---------  103
Q9WTW3|KCNE4_MOUSE  GNGNEYFYILVVMSFYGVFLIGIMLGYMKSKRREKKSSLLLLYKDEERLWGEAMKPLPMM  90
Q9QZ26|KCNE5_MOUSE  KGNDAYLYILLIMIFYACLAGGLILAYTRSRKLVEAKDEPPLACVAEQEWVPAAIASADP  114

P23299|KCNE1_MOUSE  RVLESFRACYVIE---------------NQAA-----VEQPATHLPELK---------126
Q9D808|KCNE2_MOUSE  --LEDSKAT-IHE---------------NMGA-----TGF------TVS---------122
Q9WTW2|KCNE3_MOUSE  ----------------------------------------------------------
Q9WTW3|KCNE4_MOUSE  SGLRSGQVPMMLNMLQESVAPALSCTLCSMEGDSVSSESSSPDVHLPIQEEGADDELEET  150
Q9QZ26|KCNE5_MOUSE  ---ENGQGLLA-E-------------------GG-----HQLAAGALPALAQGAERV---143

P23299|KCNE1_MOUSE  ---PLS--------------129
Q9D808|KCNE2_MOUSE  ---P----------------123
Q9WTW2|KCNE3_MOUSE  -------------------------
Q9WTW3|KCNE4_MOUSE  SETPLNDSSEGSSENIHQNS 170
Q9QZ26|KCNE5_MOUSE  -------------------------
```

Figure 2. KCNE1 and KCNE4 exhibit notable endoplasmic reticulum retention. Representative confocal images of HEK-293 cells transfected with KCNE1 and KCNE4. (**A**) KCNE-transfected cells were cotransfected with a plasma membrane marker (MB). (**B**) KCNE-transfected HEK-293 cells were cotransfected with an endoplasmic reticulum marker (ER). Right panels, KCNE1; center panels, KCNE4; left panels, histograms showing the colocalization between KCNEs (E1 and E4) and markers (MB and ER) based on Mander's coefficient analysis. The values represent the mean of > 40 cells. Green, KCNEs; red, cell markers; yellow, merged image. Bars represent 10 μm. (**C**) Sequence alignment of murine KCNE peptides. KCNE1 (UniProtKB: P23299); KCNE2 (UniProtKB: Q9D808); KCNE3 (UniProtKB: Q9WTW2); KCNE4 (UniProtKB: Q9WTW3); KCNE5 (UniProtKB: Q9QZ26). Mouse sequences are shown because murine isoforms were used throughout the study, and the results obtained were similar to the results with human isoforms. Transmembrane segments are highlighted in red. The ER-retention motifs are boxed in yellow. The specific tetraleucine motif identified in KCNE4 is colored gray.

Our data indicated that the tetraleucine motif of KCNE4 is a hub for protein–protein interactions governing the dimerization of this peptide. In addition, this cluster is involved in Kv1.3 and CaM associations[20]. Both Kv and CaM interactions with KCNE4 are important for the physiological function of Kv channels[15]. Therefore, we wanted to analyze whether KCNE4 dimerization has a competitive effect fine-tuning the association of KCNE4

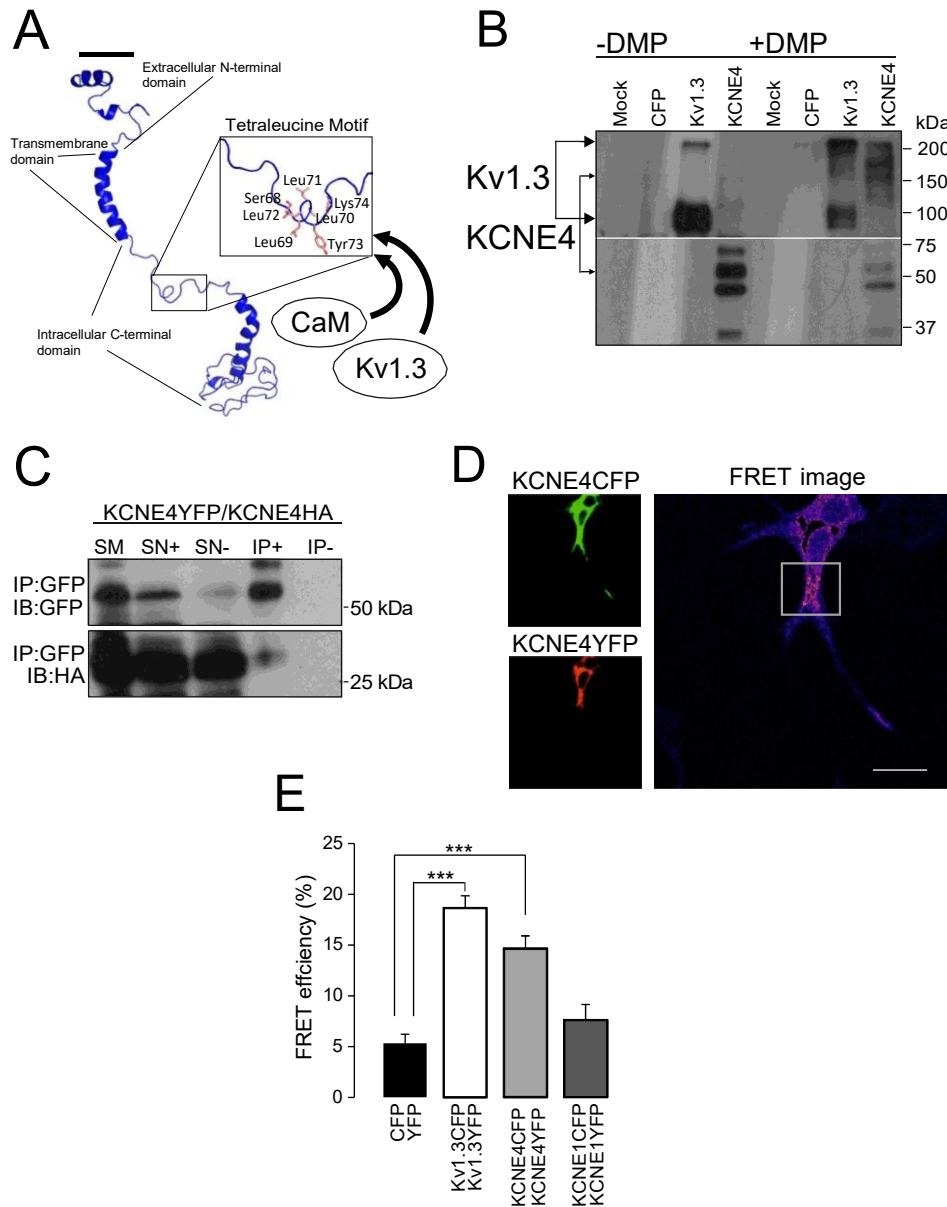**Figure 3.** KCNE4 homo-oligomerization. HEK-293 cells were transfected with different KCNE4-tagged peptides, and their homo-oligomeric formation ability was studied. (**A**) Molecular simulation of KCNE4 using the KCNE1 template (PDB code 2K21) as described in the Materials and Methods. The inset highlights the tetraleucine signature (L69-72A) where CaM and Kv1.3 associate. (**B**) Oligomerization of KCNE4. Cell lysates were incubated in the absence (−) or presence (+) of DMP (dimethyl pimelimidate). Filters were immunoblotted against CFP (Kv1.3-CFP, KCNE4-CFP). Lower Kv1.3 arrow, Kv1.3 monomers. Upper Kv1.3 arrow, Kv1.3 tetramers. Lower KCNE4 arrow, KCNE4 monomers. Upper KCNE4 arrow, KCNE4 oligomers. Mock- and CFP-transfected cells were used as negative controls. (**C**) HEK-293 cells were cotransfected with KCNE4-YFP and KCNE4-HA. Immunoprecipitation was performed for KCNE4-YFP (IP: GFP). Top panel: Immunoblot (IB) against GFP. Bottom panel: immunoblot (IB) against HA. SM: starting material. SN +, supernatant in the presence of antibody. SN-, supernatant in the absence of antibody. IP +, Immunoprecipitation in the presence of the anti-GFP antibody. IP- Immunoprecipitation in the absence of the anti-GFP antibody. (**D**, **E**) HEK-293 cells were transfected with Kv1.3-, KCNE1- and KCNE4-tagged (CFP/YFP) proteins. Homo-oligomerization of Kv1.3 and KCNE4, but not KCNE1, as analyzed by the FRET acceptor-photobleaching technique. (**D**) Green, representative image of a KCNE4-CFP donor. Red, representative image of a KCNE4-YFP acceptor. FRET image, white square highlights a ROI showing FRET image obtained after photobleaching. Bars represent 10 µm. (**E**) Quantification of the FRET efficiency (%). CFP/YFP, negative control; Kv1.3CFP/Kv1.3YFP, positive control. ***, $p < 0.001$ vs CFP/YFP (Student's t-test). The values represent the mean ± SEM of 22 (CFP/YFP), 33 (Kv1.3CFP/Kv1.3YFP), 28 (KCNE4CFP/KCNE4YFP) and 25 (KCNE1CFP/KCNE1YFP) cells.
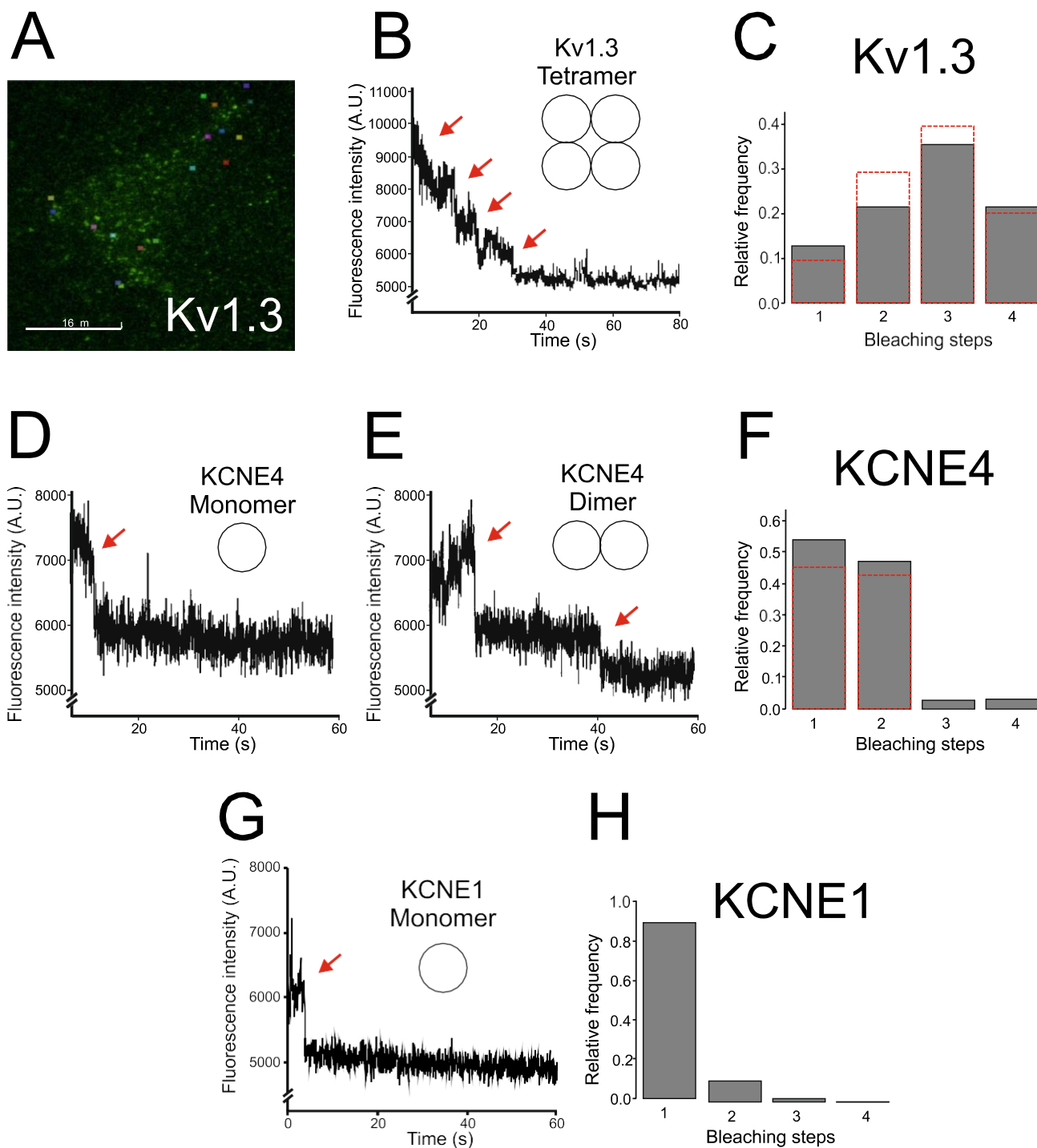
Figure 4. GFP bleaching steps from HEK-293 cells transfected with Kv1.3, KCNE4 and KCNE1. (**A**–**C**) Cells were transfected with Kv1.3 loopBADGFP. (**A**) Representative snapshot from the TIRFM video (488 nm laser). Colored ROIs (6×6 pixels) indicate representative analyzed unmoving spots. Scale bar represents 16 μm. (**B**) Representative graph of bleaching steps from different spots that were analyzed. Red arrows point to 4 bleaching steps. (**C**) Relative frequency of 1–4 bleaching events counted per spot. Gray bars correspond to the experimental frequency observed. Red dashed lines correspond to the theoretical distribution of the bleaching steps with p=0.67. (**D**–**F**) GFP bleaching steps with HEK-293 cells transfected with KCNE4 loopBADGFP. (**D**, **E**) Representative graphs of the bleaching steps from different KCNE4 spots that were analyzed. (**D**) Red arrows point to one bleaching step, indicating a KCNE4 monomer. (**E**) Two bleaching steps demonstrating KCNE4 dimers. (**F**) Relative frequency of 1–4 bleaching events counted per spot. Gray bars correspond to the experimental frequency observed. Red dashed lines correspond to the theoretical distribution of bleaching steps showing a dimer. (**G**, **H**) GFP bleaching steps from HEK-293 cells transfected with KCNE1 loopBADGFP. (**G**) Representative graph showing one bleaching step suggesting KCNE1 monomers. (**H**) Relative frequency of 1–4 bleaching events counted per spot. Gray bars correspond to the experimental frequency observed, demonstrating a KCNE1 monomeric structure.

Figure 5. The juxtamembrane tetraleucine motif is critical for KCNE4 dimerization. (**A**) Representative cartoon showing the sequence alignment of the juxtamembrane segment of KCNE4 and KCNE2 and the comparison with the int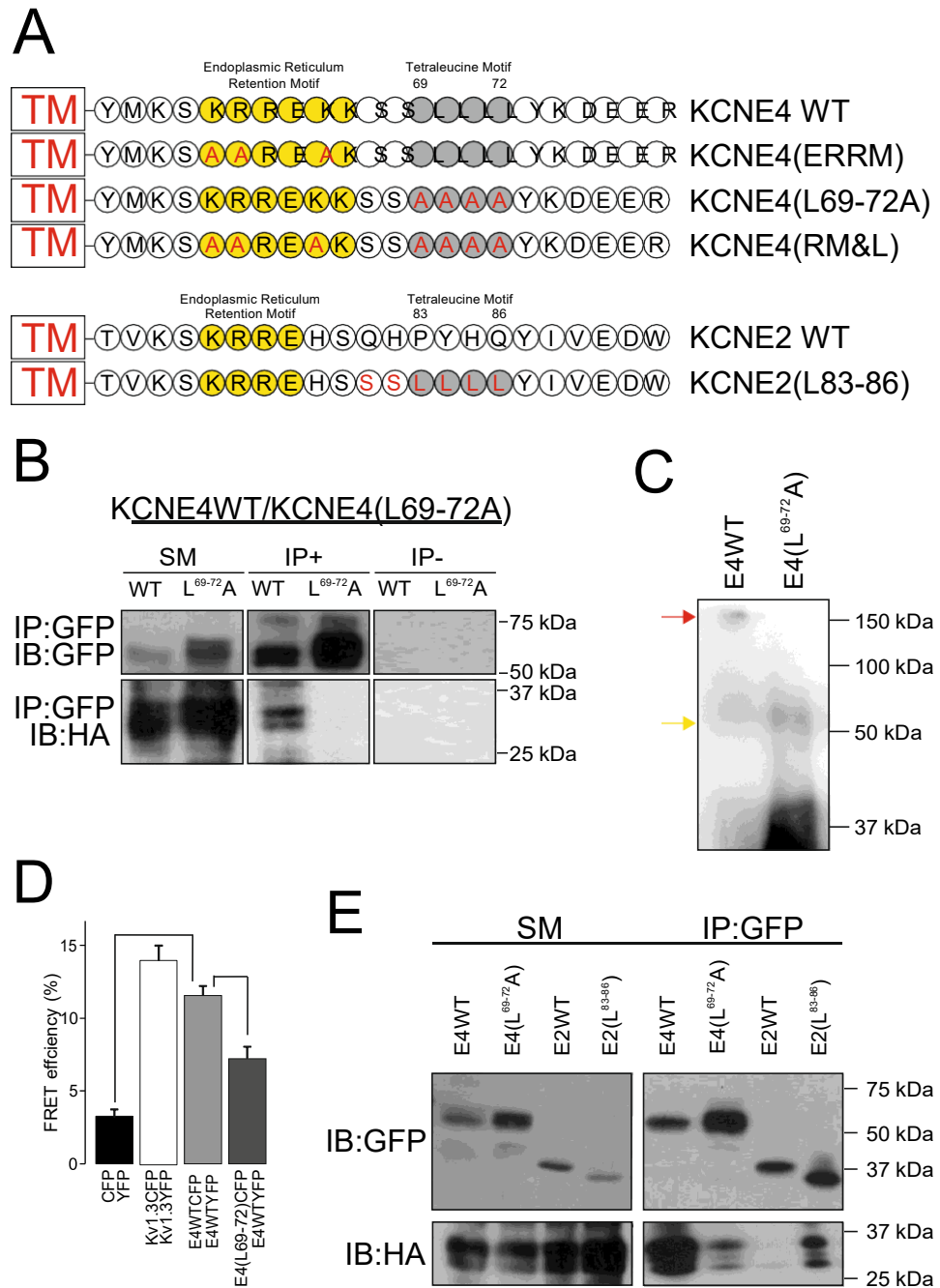roduced mutations. The transmembrane domain (TM) is shown in a box in red. The KCNE ERRMs are in yellow. The tetraleucine signature is colored gray. Amino acid substitutions are highlighted in red. For KCNE4 (ERRM), the ERRM of KCNE4 was disrupted with alanine residues (in red). For KCNE4 (L69-72A), the tetraleucine motif (gray) was also mutated to alanine (in red). For KCNE4(RM&L), both the ERRM and the tetraleucine L69-72A motifs were disrupted by alanine substitutions. The tetraleucine motif of KCNE4 was introduced in the same location in KCNE2 (KCNE2(L83-86)). (B-D) HEK-293 cells were transfected with KCNE4CFP, KCNE2-HA, Kv1.3-(CFP/YFP) and different KCNE mutants. (**B**) Coimmunoprecipitation assay against KCNE4-CFP and KCNE4(L69-72A)CFP in the presence of KCNE4-HA (IP:GFP). Top panel: Immunoblot against CFP (IB:GFP). Bottom panel: immunoblot against HA (IB:HA). SM: starting material. IP+: Immunoprecipitation in the presence of the anti-GFP antibody. IP-: Immunoprecipitation in the absence of the anti-GFP antibody. KCNE4-HA coimmunoprecipitates with KCNE4CFP (KCNE4WT) but not with KCNE4(L69-72A)CFP. Representative cropped blots are clearly separated by vertical white lines. (**C**) Non-denaturing SDS-PAGE. HEK 293 cells were transfected with KCNE4WT-CFP and KCNE4(L69-72A)CFP and cell lysates immunoblotted against GFP. Note that while KCNE4WT-CFP exhibited large molecular mass forms (red arrow), KCNE4(L69-72A)CFP only appeared as monomers (yellow arrow). (**D**) Quantification of the FRET efficiency of KCNE4 dimerization. Cells were cotransfected with CFP/YFP (negative controls), Kv1.3CFP/Kv1.3-YFP (positive control), KCNE4WT (CFP/YFP) and KCNE4WT-YFP and KCNE4(L69-72A)CFP. The values represent the mean±SE of n> 25 cells. ***$p < 0.001$ Student's *t*-test. (E) HEK-293 cells were cotransfected with KCNE4WT-HA/ KCNE4(L69-72A)CFP and KCNE4WT-HA and either KCNE2WT-CFP or KCNE2(L83-86)-CFP. Top panels: Immunoblot against CFP (IB: GFP). Bottom panel: immunoblot against HA (IB: HA). SM: starting material. IP: GFP: Immunoprecipitation in the presence of the anti-GFP antibody. KCNE4-HA coimmunoprecipitates with KCNE2(L83-86)-CFP but not with KCNE2WT-CFP.
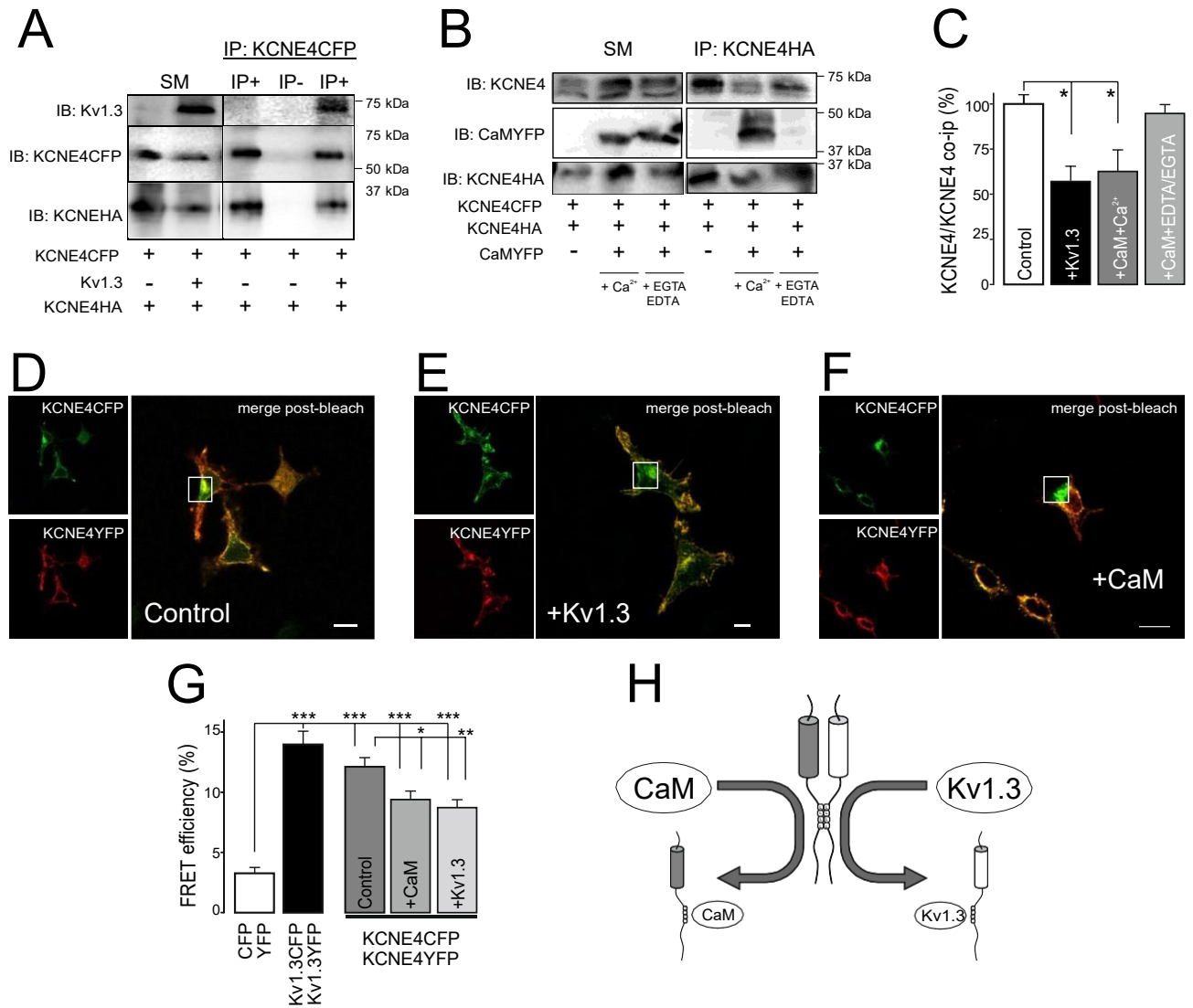
92

Figure 6. The presence of CaM and Kv1.3 impairs the dimerization of KCNE4. Coimmunoprecipitation of KCNE4-CFP and KCNE4-HA in the presence (+) or absence (-) of Kv1.3 (**A**) and CaM (**B**). The experiment in the presence of CaM (+CaM) was performed in the absence (+2 mM EDTA/2 mM EGTA) or the presence (+ Ca^{2+}) of 2 mM Ca^{2+}. KCNE4 was immunoprecipitated (IP) with select anti-tag antibodies (anti-GFP and anti-HA), and membranes were blotted (IB) against Kv1.3, KCNE4 and CaM with the indicated primary antibodies (anti-Kv1.3, anti-KCNE4, anti-GFP or anti-HA). Representative cropped blots are clearly separated by vertical white lines. (**C**) Relative KCNE4/KCNE4 coimmunoprecipitation in the presence of Kv1.3 and CaM. Control represents KCNE4/KCNE4 with no additions. The values represent the mean of 4 independent experiments. *$p < 0.05$ vs control (KCNE4-CFP/KCNE4-HA in the absence of further additions, Student's t-test). (**D–F**) Representative FRET experiments between KCNE4YFP and KCNE4CFP in the absence (D, control) or presence of + Kv1.3 (**E**) or + CaM (**F**). Green panels, KCNE4-CFP (donor); red panels, KCNE4-YFP (acceptor); merged postbleach panels; yellow indicates colocalization; white square highlights the acceptor photobleached ROI analyzed. Bars represent 10 μm. (**G**) FRET efficiency quantification of KCNE4-CFP/KCNE4-YFP in the presence of CaM and Kv1.3. The values represent the mean of 20–30 cells. *$p < 0.05$; **$p < 0.01$; ***$p < 0.001$ (Student's t-test). Control, no additions; + CaM, presence of CaM; + Kv1.3, presence of Kv1.3. CFP/YFP, negative controls; Kv1.3YFP/Kv1.3CFP, positive controls. (**H**) Schematic showing the interfering associations impairing KCNE4 dimer formation due to multiple tetraleucine motif interactions. The presence of either CaM or Kv1.3 would disrupt KCNE4 association, inhibiting dimer formation.

with CaM and Kv1.3. KCNE4 coimmunoprecipitation studies in the presence of either Kv1.3 (Fig. 6A) or CaM (Fig. 6B) indicated that the dimerization of KCNE4 is altered by both proteins (Fig. 6C). Thus, the presence of Kv1.3 decreased the KCNE4 dimer by one-half. In addition, Ca^{2+} is essential for KCNE4-dependent CaM-related Kv7.1 and Kv1.3 regulation[15,20]. Thus, CaM inhibited the dimerization of KCNE4 in the presence but not in the absence (EDTA/EGTA) of Ca^{2+} (Fig. 6C). Furthermore, FRET data, which indicated the molecular proximity
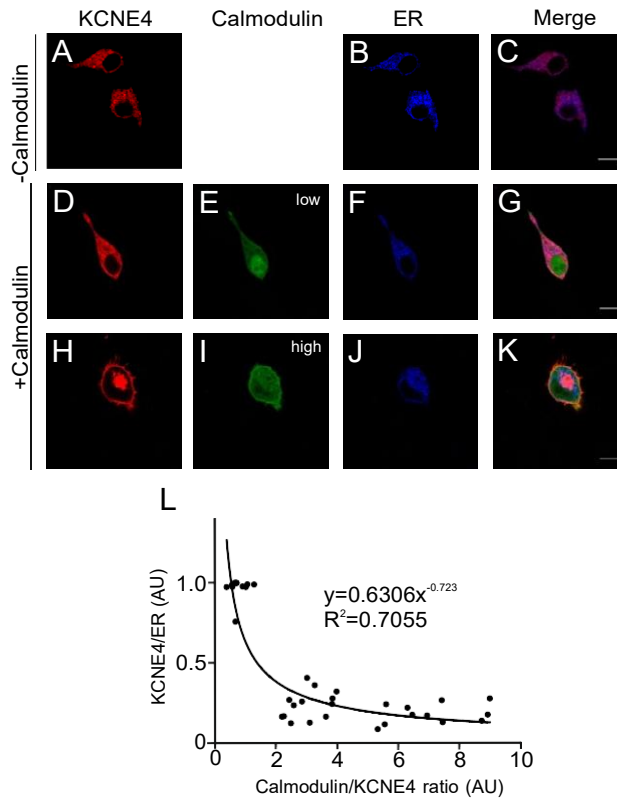
Figure 7. Endoplasmic reticulum colocalization of KCNE4 in the presence of CaM. HEK-293 cells were cotransfected with KCNE4-CFP, CaM-YFP and pDsRed-ER. (**A–C**) Colocalization of KCNE4 to the ER in the absence of CaM. (**D–K**) Colocalization of KCNE4 to the ER in the presence of CaM. (**D–G**) Representative images of a cell expressing low levels of CaM. (**H–K**) Representative images of a cell expressing high levels of CaM. (**A, D, H**) KCNE4-CFP, red; (**E, I**) CaM-YFP in green; (**B, F, J**) ER, blue; (**C, G, K**) merged panels. Purple indicates colocalization of KCNE4 and ER markers. Yellow, colocalization of KCNE4 and CaM. White and light pink indicate triple colocalization. Scale bars represented 10 μm. (**L**) ER colocalization of KCNE4 plotted against the CaM/KCNE4 ratio. All images were captured with the same laser intensity and photomultiplication parameters. A pixel-by-pixel analysis was performed to determine the relative KCNE4/ER and the CaM/KCNE4 ratios. The regression curve and a high R^2 value are indicated. Values were from 20–30 cells. Note: High levels of CaM correspond to low ER colocalization of KCNE4.

between KCNE4-CFP/KCNE4-YFP, further supported that the dimerization of KCNE4 was also displaced by the presence of either Kv1.3 or CaM (Fig. 6D–G).

Keeping all these results and the previous evidence in mind, we postulated a model (Fig. 6H). KCNE4 dimerizes via its juxtamembrane C-terminal tetraleucine motif. In addition, this region is involved in the Kv1.3 association and CaM interaction. The dimerization of KCNE4 would balance oligomeric interactions fine-tuning the KCNE4 physiological effects. Therefore, the association with Kv1.3 and CaM would be in competition with the KCNE4 dyad formation.

Recent evidence indicates that increasing amounts of KCNE4 steadily decrease Kv1.3 abundance at the cell surface[30]. Furthermore, CaM facilitates the membrane expression of Kv7 channels[22]. CaM also competes with Kv1.3 for KCNE4 tetraleucine motif association, facilitating Kv1.3 escape from KCNE4-dependent ER retention. We wondered whether CaM, impairing KCNE4 dimerization, affects the cellular distribution of KCNE4. The ER colocalization of KCNE4 in the absence (Fig. 7A–C) or presence of variable (low, Fig. 7D–G; high, Fig. 7H–K) CaM expression was analyzed. All images were captured using the same parameters of laser intensity and photomultiplication. Therefore, a pixel-by-pixel analysis of both CaM and KCNE4 intensities was performed, and the data were plotted against the ER localization of KCNE4. The data fitted with an exponential decay showed a strong correlation. Therefore, we found that increasing amounts of CaM triggered a notable decrease in KCNE4 ER localization concomitant with an increase in the cell surface staining of KCNE4 (Fig. 7H–L).

Our data indicated that CaM facilitated the targeting of KCNE4 to the plasma membrane. Thus, we wanted to identify the mechanism that promoted KCNE4 forward trafficking to the cell surface. Although KCNE peptides exhibit notable intracellular retention, KCNE1 reaches the cell surface via COPII-dependent machinery[27]. KCNE1 and KCNE4 behave similarly, but only the latter contains the tetraleucine signature that facilitates CaM-dependent membrane surface expression. Therefore, we analyzed whether the COPII machinery mediated KCNE4 membrane targeting (Fig. 8). KCNE4 exhibited intracellular retention and minor membrane staining (Fig. 8A–C). The coexpression of Sar1 (H79G), which disrupts ER-to-Golgi trafficking[27], did not alter the amount
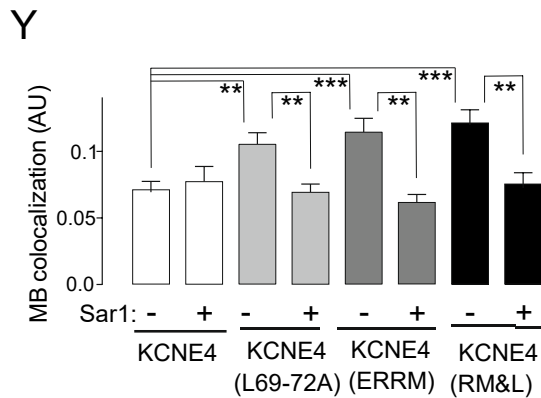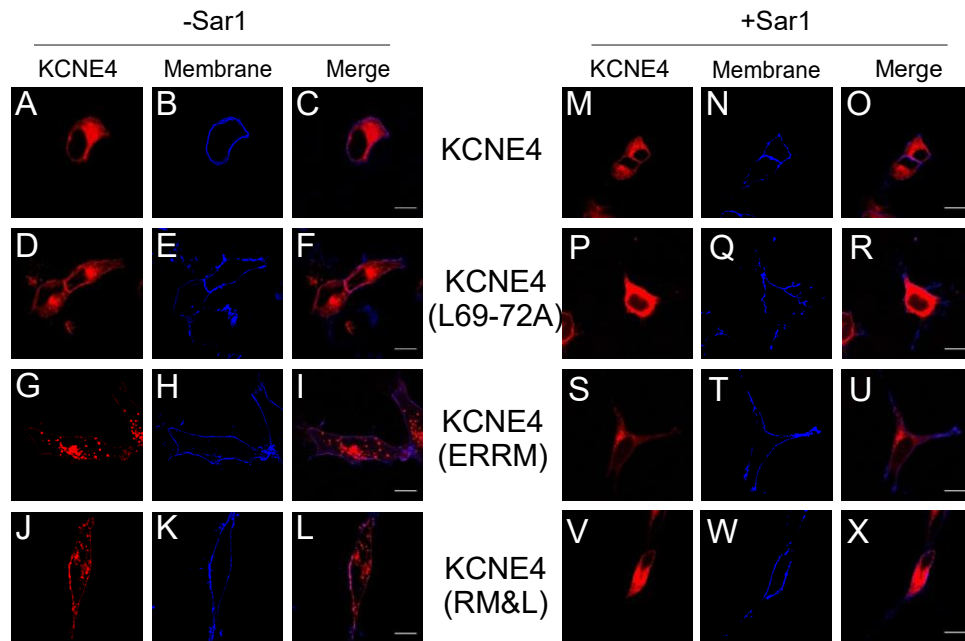
Figure 8. KCNE4 traffics to the plasma membrane via *a COPII-dependent mechanism*. HEK-293 cells were cotransfected with KCNE4WT and mutants (KCNE4(L69-72A), KCNE4(ERRM) and KCNE4(RM&L)) and the Akt-PH-pDsRed membrane marker in the absence (-Sar1, A-L) or the presence (+Sar1, M-X) of HA-Sar1H79G. (A-C and M–O) KCNE4WT colocalization with the membrane marker. (D-F and P-R) KCNE4(L69-72A) colocalization with the membrane marker. (G-I and S-U) KCNE4(ERRM) colocalization with the membrane marker. (J-L and V-X) KCNE4(RM&L) membrane colocalization. Red panels, KCNE4. Blue panels, stained membrane. In the merged panels, purple indicates colocalization. Scale bars represent 10 μm. (Y) Quantification of membrane (MB) colocalization of KCNE4 in the absence (−) or presence (+) of HA-Sar1H79G (Sar1) using Mander's coefficient. White columns, KCNE4 WT; light gray, KCNE4(L69-72A); dark gray, KCNE4(ERRM); black columns, KCNE4(RM&L). The values represent the mean of 20–30 cells. $**p < 0.01$; $***p < 0.001$ One-way ANOVA and post hoc Tukey's test.

of KCNE4 localized at the membrane (Fig. 8A–C, Y). KCNE4(L69-72A) showed improved membrane targeting, similar to that obtained with KCNE4(ERRM), which has the ER retention motif disrupted, and KCNE4(RM&L), with both the ERRM and the tetraleucine signals altered (Fig. 8D–X). Interestingly, Sar1(H79G) clearly prevented membrane targeting under all conditions (Fig. 8Y). Therefore, our data suggest that, in addition to the tetraleucine motif, ERRM cooperates in the ER retention of KCNE4. In addition, we show that KCNE4, escaping the ER, is routed via conventional COPII-dependent anterograde trafficking to the cell plasma membrane.

Discussion

The voltage-gated potassium channel Kv1.3 is crucial in the physiology of the immune system. The channel controls the membrane potential, driving Ca^{++} entry during the immune response. The abundance of Kv1.3 at the cell surface is in accordance with the magnitude of the cellular reaction[35]. KCNE4 is a regulatory subunit that controls the expression of Kv1.3 in the plasma membrane, fine-tuning this response[30]. Because KCNE4 is

important for controlling channel functionality, its mechanism of action and architecture are of physiological relevance. Here, we demonstrate that, unlike other KCNE peptides, KCNE4 forms dimers. Dimerization is mediated by the tetraleucine motif in the C-terminal domain. Interestingly, this unique structural element creates a platform where protein-to-protein interactions take place. Thus, the capacities for KCNE4 interaction with Kv1.3 and CaM with and KCNE4 dimerization are determined at this motif. CaM-dependent dimerization of KCNE4 tunes KCNE4 ER retention and the KCNE4-Kv1.3 association. Dimerization provides additional ERRM to the complex that balances the CaM association. Furthermore, the evidence indicates that the forward trafficking of KCNE4 to reach the membrane surface is realized through the COPII-dependent machinery. Our data are of physiological relevance because the dimerization attenuates the effects of the KCNE4 regulatory subunit on Kv1.3. In addition, the KCNE4 interaction with CaM, which hides the tetraleucine motif, situates this important signaling molecule to balance Kv1.3 physiological functions.

The tetraleucine motif at the juxtamembrane domain of the KCNE4 C-terminus is a structural platform where essential proteins for Kv1.3-dependent physiology interface. Thus far, this KCNE4 feature is unique within the KCNE family. Dileucine motifs promote endocytosis, protein–protein interactions or basolateral trafficking[36–39]. In this context, leucine-enriched domains mediate the oligomerization of Toll-like receptors[40]. However, leucine residues are mainly located at every third amino acid position in these domains[41]. The KCNE4 tetraleucine signature forms a coil-like domain that can be transferred to other KCNE peptides. Moreover, our data demonstrated that this mechanism acts as a trafficking modulator. Mutation of this cluster, as well as the ERRM, facilitates plasma membrane targeting of KCNE4. Dimerization provides redundant signals to the KCNE4 dyad, retaining a pool of peptides at the ER. Thus, not only the interaction with Kv1.3, but also with CaM, is controlled[20]. Upon association with CaM or Kv1.3, KCNE4 units may travel either with CaM to the membrane or, by masking the forward traffic motifs of Kv1.3, retain the channel within in the cell, thereby tuning the channel expression at the cell surface. Both mechanisms reveal as important players controlling Kv1.3-asociated cellular responses[42,43].

Evidence links dileucine clusters with protein trafficking. For instance, the ClC-2 chloride channel, which might compensate for the malfunction of CFTR in absorptive epithelia during cystic fibrosis, contains a dileucine motif. Mutations of this signature alter the basolateral targeting of the channel[44]. Similarly, the dileucine motif of human organic solute transporter beta plays a critical role in its association with the alpha subunit and cell surface polarization[37]. However, similar to that of KCNE4, other evidence raises an alternative possibility. The acid-sensing ion channel ASIC2a has a double dileucine motif (LLDLL) in the C-terminal juxtamembrane region. Altering the LLDLL sequence, either full or in part, increases the surface levels of the channel[45]. Moreover, mutation of the carboxyl terminal dileucine sequence of the LHβ subunit increases trafficking and exocytosis[46]. In this context, our data indicated that disrupting or masking the tetraleucine motif hinders dimerization, thereby facilitating membrane targeting of KCNE4. Therefore, in a KCNE4 monomer, although it contains an ERRM, the strength of the retention signal may be counterbalanced by associating with CaM. This mechanism is in agreement with the Ca^{2+}/CaM-dependent regulation of KCNE4 of Kv channels, such as Kv7.1 or Kv1.3. CaM, upon calcium stimuli, can interact with KCNE4 at the tetraleucine motif[15,20]. Therefore, CaM fine-tunes the dimerization and promotes KCNE4 anterograde trafficking through a COPII-dependent mechanism. Thus, Ca^{2+} signaling controls the final fate of KCNE4, which in turn modulates Kv1.3 function, which is profoundly related to the Ca^{2+} trigger in leukocytes. The precise balance between several interactions in a unique cluster, masking the interaction sites to prevent competing associations, fine-tunes the final function of a multitask channel such as Kv1.3[16]. A similar cloaking mechanism is evident for E-cadherin. A dileucine motif in the juxtamembrane cytoplasmic domain is required for E-cadherin endocytosis. When mutated, this protein cannot be internalized. P-120, an E-cadherin interactor, associates and masks this motif, inhibiting endocytosis[47]. Furthermore, our data indicate that KCNE4 contains routing information to the plasma membrane via COPII-dependent mechanisms. KCNEs, which contain strong ERRM signals at their C-terminus, share a notable intracellular retention capacity. Surprisingly, without canonical sequences, the COPII-dependent mechanism is a major characteristic of KCNE peptides because, similar to KCNE4, KCNE1 uses this route[27]. In this sense, N-glycosylation facilitates KCNE anterograde trafficking through the secretory pathway, but the specific mechanisms have not been dissected[48]. The balance between forward trafficking and retention signaling is highly skewed toward the latter in KCNEs. Regardless of whether the assembly of KCNE and Kv channels takes place at the cell surface or through the secretory pathway, CaM controls cell surface channels by modulating KCNE4 trafficking[15,27,49].

We demonstrated that Kv1.3, KCNE4 and CaM are closely related because they interact via the tetraleucine cluster in KCNE4. A balanced competition warrants no tripartite complexes[20]. Our data support the dimerization of KCNE4 as a regulating mechanism for such interactions and CaM displaced KCNE4 dyad formation. These data, similar to those of Kv7.1/KCNE1 and Kv7.1/KCNE3, further support that single monomeric forms of KCNE4 occupy the cleavage between subunits within the Kv tetrameric structure[20,28,29]. However, in contrast to Kv7.1, Kv1.3 does not need CaM to associate with KCNE4[15]. CaM indirectly interacts with Kv1.3 in a Ca^{2+}-dependent manner, forming a multiprotein complex with CaM kinase II (CaMKII)[50,51]. Although the regulation of Kv1.3 by Ca^{2+}/CaM in leukocytes is under debate, CaM-dependent KCNE4 dimerization situates this important signaling molecule in the equation. Ca^{2+}- and CaM-dependent signaling pathways are key to T cell activation. The immunological synapses enriched in lipid rafts concentrate Ca^{2+}-dependent targets. KCNE4, retaining Kv1.3 at the ER, impairs the localization of Kv1.3 to lipid rafts. Therefore, our data are of physiological relevance because indicates that the KCNE4 tetraleucine motif is an associative platform in which different targets may compete for signaling interactions fine-tuning the cell physiology.

Methods

Expression plasmids, chimeric channels and site-directed mutagenesis. The rKv1.3 in pRc-CMV, provided by T.C. Holmes (University of California, Irvine), was subcloned into pEYFP-C1, pECFP-C1 and pEGFP-C1 (Clontech). hKv1.5 has been widely analyzed[26]. Mouse KCNE4 in pSGEM was obtained from M. Sanguinetti (University of Utah, Salt Lake City, UT). mKCNE4 was introduced into pEYFP-N1, pECFP-N1 and pEGFP-N1 (Clontech). hKCNE1-HA and hKCNE2-HA, obtained from S. de la Luna (CRG, Barcelona, Spain), were introduced into pECFP-N1, pEYFP-N1 and pEGFP-N1 (Clontech). CaMYFP was obtained from A. Villar-roel (Universidad País Vasco-CSIC). An endoplasmic reticulum marker (pDsRed-ER), soluble cyan fluorescent protein (pECFP-N1), green fluorescent protein (pEGFP-N1) and yellow fluorescent protein (pEYFP-N1) were obtained from Clontech. The plasma membrane marker Akt-PH-pDsRed (pDsRed-tagged pleckstrin homology (PH) domain of Akt) was a kind gift from F. Viana (Universidad Miguel Hernández, Spain). The dominant-negative GTPase mutant HA-Sar1H79G was provided by R. Pepperkok (EMBL, Germany)[19–21].

For counting the bleaching steps in nonmoving spots, a loopBAD-tag was added. The loop-BAD tag was introduced into GFP-Kv1.3, KCNE1-GFP and KCNE4-GFP at NruI restriction sites. The Kv2.1-loopBAD-YFP and BirA coding plasmids were previously described[30,52].

The KCNE4-CFP tetraleucine motif (L69–72) was mutated to alanine by single-site–directed mutagenesis using a QuikChange multisite-directed mutagenesis kit (Agilent Technologies), generating the KCNE4(L69–72A)-CFP mutant. A tetraleucine motif similar to that in KCNE4 was incorporated into KCNE2-CFP (KCNE2(L83–86)-CFP). KCNE4 (ERRM), with ERRM disruption, and KCNE4 (RM&L), containing both modified ERRM and tetraleucine motifs, have been fully characterized previously[20]. All constructs and mutants were verified by automated DNA sequencing.

Cell culture and transient transfection. HEK-293 cells (Sigma-Aldrich) were cultured in DMEM (LONZA) containing 10% fetal bovine serum (FBS) supplemented with penicillin (10,000 U/ml), streptomycin (100 μg/ml) (Gibco), 4.5 g/l glucose and L-glutamine (4 mM).

For confocal imaging and coimmunoprecipitation experiments, cells were seeded (70–80% confluence) in either 6-well dishes containing poly-D-lysine-coated coverslips or 100-mm dishes. Metafectene PRO (Biontex) was used for transfection according to the supplier's instructions. The amount of transfected DNA was 4 μg for a 100-mm dish and 500 ng for each well of a 6-well dish. Next, 4–6 h after transfection, the mixture was removed from the dishes and replaced with fresh culture medium. All experiments were performed 24 h after transfection[20,21].

For patch-clamp experiments, trypsinized cells from a confluent culture in a 100-mm dish were electroporated with 1 μg of DNA using a Bio-Rad Gene Pulser Xcell system with a 0.2-cm gap cuvette and a single 110-V 25-ms pulse[30].

For total internal reflection fluorescence (TIRF) microscopy experiments, trypsinized cells from a confluent culture in a 100-mm dish were electroporated with 25–100 ng of the desired DNA plus 100 ng of BirA DNA (encoding a biotin ligase to biotinylate the loopBAD-tagged proteins) using a Bio-Rad Gene Pulser Xcell system, as previously described. Transfected cells were plated on 35-mm glass-bottom dishes (MatTek) previously coated with collagen and EZ-Link NHS-PEG12-Biotin (Pierce, Thermo Scientific). The next day, TIRF experiments were performed after incubation of the cells with neutravidin (50 nM) to immobilize channels onto glass as previously described[20,35].

Protein extraction, coimmunoprecipitation and western blotting. HEK-293 cells were washed twice in cold PBS and lysed on ice with a lysis solution (1% Triton X-100, 10% glycerol, 50 mM HEPES, 150 mM NaCl at pH 7.2) supplemented with protease inhibitors (1 μg/ml aprotinin, 1 μg/ml leupeptin, 1 μg/ml pepstatin and 1 mM phenylmethylsulfonyl fluoride). Lysates were gently mixed for 10 min and spun (10 min at 12,000 × g). The supernatant was transferred to a new tube, and the protein contents were determined by using a Bio-Rad protein assay[20,21].

For coimmunoprecipitation, 1 mg of protein added to lysis buffer at a final concentration of 500 μl and used for immunoprecipitation (150 mM NaCl, 50 mM HEPES, 1% Triton X-100 at pH 7.4) supplemented with protease inhibitors. Samples were precleared with 50 μl of protein A-Sepharose beads (GE Healthcare) for 1 h at 4 °C with gentle mixing. Next, each sample was incubated in a small chromatography column (Bio-Rad Micro Bio-Spin™ chromatography columns), which contained 2.5 μg of anti-GFP antibody previously cross-linked to protein A-Sepharose beads, for 2 h at room temperature (RT) with gentle mixing. The columns were centrifuged for 30 s at 1,000 × g. Supernatants were stored at -20 °C. The columns were washed four times with 500 μl of lysis buffer and centrifuged for 30 s at 1,000 × g. Finally, the columns were incubated with 100 μl of 0.2 M glycine (pH 2.5) and spun for 30 s at 1,000 × g for elution[19–21].

Irreversible cross-linking of the antibody to the Sepharose beads was performed after incubation of the antibody with protein A-Sepharose beads for 1 h at RT. The beads were then incubated with 500 μl of 5.2 mg/ml dimethyl pimelimidate (Pierce) for 30 min at RT with gentle mixing. The columns were then washed four times with 500 μl of 1 × TBS, four times with 500 μl of 0.2 M glycine (pH 2.5) and three more times with 1 × TBS (0.1% Triton X-100, 10% glycerol, 150 mM NaCl, 50 mM HEPES at pH 7.4). Finally, the columns were incubated with protein lysates to perform immunoprecipitation as described above.

For the coimmunoprecipitation experiments in the presence of CaM, the samples were precleared for 1 h at 4 °C by mixing samples with 50 μl of protein A-Sepharose beads (GE Healthcare) previously washed with 1 × TBS and centrifuged for 30 s at 5,000 × g. Next, supernatants were incubated for 2 h at RT with 8 ng of anti-HA antibody (Proteintech) previously cross-linked to Protein A-Sepharose beads. The samples were centrifuged (30 s, 5.000 × g), and the pellet was washed 3 times with 1 × TBS buffer. Finally, proteins were eluted upon the

addition of 20 μl of SDS Laemmli loading buffer (5x) and 80 μl of H$_2$O and boiled for 7 min. Elutions were briefly centrifuged, and the supernatans were prepared for western blotting[19–21].

All experimental protocols were approved by the ethical committee of the Universitat de Barcelona in accordance with the European Community Council Directive 86/609 EEC. We also confirm that all experiments were carried out in compliance with the ARRIVE guidelines (https://arriveguidelines.org). Rats were briefly anesthetized with isoflurane, and tissues were extracted immediately after euthanasia. Tissues were homogenized in RIPA lysis buffer (1% Triton X-100, 1% sodium deoxycholate, 0.1% SDS, 50 mM Tris–HCl pH 8.0, 150 mM NaCl) supplemented with protease inhibitors. Total lysates were spun for 10 min at 10,000 × g to remove debris. Supernatants were used to analyze protein expression by western blot.

Protein samples (50 μg), supernatants, immunoprecipitates and total tissue lysates were boiled in Laemmli SDS loading buffer and separated by 10–15% SDS-PAGE. Next, the proteins were transferred to PVDF membranes (Immobilon-P; Millipore) and blocked in 0.2% Tween-20-PBS supplemented with 5% dry milk before immunoreaction with antibodies. Filters were immunoblotted with antibodies against Kv1.3 (1/500, NeuroMab), HA (1/1,000, Sigma), KCNE4 (1/800, Proteintech), GFP (1/1,000, Roche) or calmodulin (1/600, Millipore). Finally, the membranes were washed with 0.05% Tween 20 PBS and incubated with horseradish peroxidase-conjugated secondary antibodies (Bio-Rad).

The dimerization of KCNE4 WT-CFP and KCNE4 (L69–72A)-CFP was analyzed in non-denaturing conditions. Briefly, total lysates were mixed with sample buffer (50 mM Tris–HCl pH 6.8, 10% glycerol, 0.2% bromophenol blue) and loaded in a non-denaturing SDS-PAGE (5% acrylamide/bis-acrylamide (30%-0.8% w/v), 0.29 M Tris–HCl pH 8.8, 0.1% SDS, 0.1%). Western Blot was performed as abovementioned and PVDF membranes were incubated with anti-GFP (1/1,000, Roche) and horseradish peroxidase-conjugated secondary antibodies (Bio-Rad).

DMP cross-linking protocol. Twenty-four hours after transfection, HEK-293 cells were washed twice in cold PBS and lysed on ice with lysis buffer (50 mM boric acid, 100 mM K acetate, 2 mM MgCl$_2$, 1 mM EGTA and 1% Triton X-100; pH 8.5). One-half of the proteins was incubated with 5 mM DMP (dimethyl pimelimidate) for 1 h, while the other half was maintained for use as controls. The reaction was stopped by adding 1 ml of 0.5 M (pH 6.8). Protein samples (50 μg) were boiled in Laemmli SDS loading buffer and separated on 7% SDS-PAGE gels.

Electrophysiology. HEK-293 cells were trypsinized 24 h after transfection and plated on 35-mm glass-bottom dishes coated with Matrigel[30]. After 2–4 h, the cells were washed extensively with whole-cell external recording solution containing (in mM) 150 NaCl, 5 KCl, 10 CaCl$_2$, 2 MgCl$_2$, 10 glucose, and 10 HEPES at pH 7.4. Whole-cell currents were recorded using the patch-clamp technique in the whole-cell configuration with a HEKA EPC10 USB amplifier (HEKA Elektronik). PatchMaster software (HEKA) was used for data acquisition. We applied a stimulation frequency of 50 kHz and a filter at 10 kHz. The capacitance and series resistance compensation were optimized. In most experiments, we obtained 80% compensation of the effective access resistance. Micropipettes were prepared from borosilicate glass capillaries (Harvard Apparatus) using a P-97 puller (Sutter Instrument) and fire polished. The pipettes had a resistance of 2–4 MΩ when filled with a solution containing (in mM): 4 NaCl, 150 KCl, 1 MgCl$_2$, 0.5 EGTA, 5 K$_2$ATP, and 10 HEPES at pH 7.4. Cells were clamped at a holding potential of − 80 mV. To evoke voltage-gated currents, cells were stimulated with 200 ms square pulses to + 60 mV. Data analysis was performed using FitMaster (HEKA) and SigmaPlot 10.0 software (Systat Software). All recordings were performed at room temperature (21–23 °C).

KCNE4 complex modeling. KCNE4 was modeled using high-resolution templates of homologs available from the Protein Data Bank (http://www.rcsb.org/pdb). The N-terminus, transmembrane domain and proximal C-terminus (residues 1–98), which contains the tetraleucine motif, were modeled with KCNE1 (PDB ID: 2K21). The final molecular graphic representation was created using PyMOL v1.4.1 (http://pymorl.org/) as previously described[20].

Confocal microscopy, image analysis and FRET. For confocal image acquisition, cells were seeded on polylysine-coated coverslips and transfected 24 h later. The next day, the cells were quickly washed twice, fixed with 4% paraformaldehyde for 10 min, and washed three times for 5 min each time with PBS-K$^+$. Finally, coverslips were added to microscope slides (ACEFESA) with house Mowiol mounting media. The coverslips were allowed to dry for at least one day before imaging. All procedures were performed at RT. All images were acquired with a Leica TCS SP2 AOBS microscope (Leica Microsystems) equipped with argon and helium–neon lasers. All experiments were performed with a 63 × oil-immersion objective lens NA 1.32. Colocalization analysis was performed with ImageJ software (NIH, Bethesda, MD, USA) as previously described. A pixel-by-pixel colocalization study using JACoP (Just Another Colocalization Plugin) was used. Mander's overlap coefficients (MOC), which are proportional to the amount of fluorescence of the colocalizing pixels in each color channel, were obtained[19–21]. In some experiments the colocalization of KCNE4 with some subcellular markers was analyzed. HEK 293 cells were co-transfected with KCNE4 and the endoplasmic reticulum marker (ER, pDsRed-ER) and the plasma membrane marker (MB, Akt-PH-pDsRed). In addition, KCNE4 transfected cells were further processed for immunocytochemistry. Thus, after fixation, cells were further permeabilized with 0.1% Triton X-100 for 20 min. After 60 min of incubation with blocking solution (10% goat serum, 5% nonfat milk, and 0.05% Triton X-100), the cells were incubated with anti-GM130 (1:1000; BD Transduction Laboratories) and anti-TGN46 2F11 (1:100; bioNova científica) in 10% goat serum and 0.05% Triton X-100 overnight at 4 °C for

cis-Golgi and trans-Golgi networks respectively. Next, the cells were incubated with Cy5-conjugated secondary antibodies for 2 h at RT and further mounted with Mowiol.

The fluorescence resonance energy transfer (FRET) via the acceptor photobleaching technique was measured in discrete ROIs (regions of interest). Fluorescent proteins from fixed cells were excited with the 458 nm or 514 nm beam lines using low excitation intensities. Next, 475 to 495 nm bandpass and > 530 nm longpass emission filters were applied. The YFP protein was bleached using maximum laser power. We obtained acceptor intensity bleaching of approximately 80%. Posteriorly, images of the donors and acceptors were taken. The FRET efficiency was calculated using the equation $[(F_{CFPafter} - F_{CFPbefore})/F_{CFPbefore}]*100$, where $F_{CFPafter}$ was the fluorescence of the donor after bleaching and $F_{CFPbefore}$ was the fluorescence before bleaching. The loss of fluorescence as a result of scanning was corrected by measuring the CFP intensity in the unbleached part of the cell[20].

TIRF and bleaching steps of single fluorescent protein complexes. The single bleaching quantitative approach was first described by Isacoff and collaborators[31] and is based on TIRF microscopy to visualize single GFP-tagged proteins on the cell surface, as previously described[20,35]. To immobilize proteins and analyze the number of bleaching steps, cells were transfected with loopBAD-tagged proteins in the presence of BirA, which encodes DNA for tag biotinylation. The cells seeded in a biotin-collagen-coated glass-bottom dish were incubated with neutravidin (50 nM) at 37 °C for 30 min before imaging. Neutravidin binds the cell surface biotinylated Kv1.3-, KCNE1- and KCNE4-loopBAD-GFP and, simultaneously, the biotinylated glass surface, fixing the cell surface proteins to monitor the fluorescently immobile GFP spots. The amount of DNA transfected was adjusted to achieve a low membrane density for imaging and counting. Multiple spots were imaged, but the density was low enough to minimize the probability of two channels lying within the same diffraction-limited spot. Transfected HEK-293 cells were imaged within 24 h after electroporation in HEK physiological saline buffer consisting of (in mM) 146 NaCl, 4.7 KCl, 2.5 CaCl$_2$, 1 MgCl$_2$, 10 glucose, and 10 HEPES at pH 7.4. Videos were processed and analyzed using Volocity software. The intensity of the 6×6 pixel ROIs was added and calculated for all durations of the videos. The intensity of the ROIs was plotted against time. The GFP bleaching steps were counted and statistically analyzed. GFP bleaching experiments were performed with a Nikon Eclipse Ti Perfect-Focus system equipped with a TIRF/wide-field fluorescence microscope and AOTF-controlled 405, 488, 561 nm diode lasers (100 mW each), and an Intensilight wide-field light source. A $100 \times$ PlanApo TIRF, 1.49 NA, objective lens was used for image acquisition. Emissions were collected through a Sutter Lambda 10–3 filter wheel containing the appropriate bandpass filters. The microscope was equipped with an Andor iXonEMCCD DU-897 camera, 512×512. For TIRF image acquisition, an incident angle of 63.3° was used[30,35,52].

Statistics. The results are expressed as the means ± SE. Student's *t*-test, one-way ANOVA and Tukey's post hoc test and two-way ANOVA were used for statistical analysis (GraphPad PRISM v5.01). $P < 0.05$ was considered statistically significant.

References

1. Hille, B. *Ion channels of excitable membranes*. 3rd edn, 72 (Sinauer, Sunderland, Mass., 2001).
2. Serrano-Novillo, C. *et al.* Implication of voltage-gated potassium channels in neoplastic cell proliferation. *Cancers* **11**, 287 (2019).
3. Felipe, A., Soler, C. & Comes, N. Kv15 in the immune system: the good, the bad, or the ugly?. *Front. Physiol.* **1**, 152 (2010).
4. Panyi, G., Beeton, C. & Felipe, A. Ion channels and anti-cancer immunity. *Philosophical Trans. Royal Soc Lond. Ser. B Biol. Sci.* **369**, 20130106 (2014).
5. Panyi, G., Varga, Z. & Gaspar, R. Ion channels and lymphocyte activation. *Immunol. Lett.* **92**, 55–66 (2004).
6. Martens, J. R., Kwak, Y. G. & Tamkun, M. M. Modulation of Kv channel alpha/beta subunit interactions. *Trends Cardiovasc. Med.* **9**, 253–258 (1999).
7. Pongs, O. & Schwarz, J. R. Ancillary subunits associated with voltage-dependent K+ channels. *Physiol. Rev.* **90**, 755–796 (2010).
8. Sole, L. & Felipe, A. Does a physiological role for KCNE subunits exist in the immune system?. *Commun. Integrat. Biol.* **3**, 166–168 (2010).
9. Sole, L. *et al.* KCNE gene expression is dependent on the proliferation and mode of activation of leukocytes. *Channels (Austin)* **7**, 85–96 (2013).
10. Grunnet, M. *et al.* KCNE4 is an inhibitory subunit to the KCNQ1 channel. *J. Physiol.* **542**, 119–130 (2002).
11. Grunnet, M. *et al.* KCNE4 is an inhibitory subunit to Kv1.1 and Kv1.3 potassium channels. *Biophys. J.* **85**, 1525–1537 (2003).
12. McCrossan, Z. A. & Abbott, G. W. The MinK-related peptides. *Neuropharmacology* **47**, 787–821 (2004).
13. Kanda, V. A. & Abbott, G. W. KCNE regulation of K(+) channel trafficking—a sisyphean task?. *Front. Physiol.* **3**, 231 (2012).
14. Roura-Ferrer, M. *et al.* Impact of KCNE subunits on KCNQ1 (Kv7.1) channel membrane surface targeting. *J. Cellular Physiol.* **225**, 692–700 (2010).
15. Ciampa, E. J., Welch, R. C., Vanoye, C. G. & George, A. L. Jr. KCNE4 juxtamembrane region is required for interaction with calmodulin and for functional suppression of KCNQ1. *J. Biol. Chem.* **286**, 4141–4149 (2011).
16. Serrano-Albarras, A., Estadella, I., Cirera-Rocosa, S., Navarro-Perez, M. & Felipe, A. Kv1.3: a multifunctional channel with many pathological implications. *Exp. Opin. Therapeutic Targets* **22**, 101–105 (2018).
17. Freidin, M. B. *et al.* Genome-wide association study of allergic diseases in Russians of Western Siberia. *Mol. Biol.* **45**, 464–472 (2011).
18. Trevino, L. R. *et al.* Germline genomic variants associated with childhood acute lymphoblastic leukemia. *Nat. Genet.* **41**, 1001–1005 (2009).
19. Sole, L. *et al.* KCNE4 suppresses Kv13 currents by modulating trafficking, surface expression and channel gating. *J. Cell Sci.* **122**, 3738–3748 (2009).

20. Sole, L. *et al.* The calmodulin-binding tetraleucine motif of KCNE4 is responsible for association with Kv1.3. *FASEB J. Official Publ. Federation Am. Soc. Exp. Biol.* **33**, 8263–8279 (2019).
21. Sole, L. *et al.* The C-terminal domain of Kv1.3 regulates functional interactions with the KCNE4 subunit. *J. Cell Sci.* **129**, 4265–4277 (2016).
22. Gomis-Perez, C. *et al.* An unconventional calmodulin-anchoring site within the AB module of Kv7.2 channels. *J. Cell Sci.* **128**, 3155–3163 (2015).
23. Abbott, G. W. KCNE4 and KCNE5: K(+) channel regulation and cardiac arrhythmogenesis. *Gene* **593**, 249–260 (2016).
24. Felipe, A., Knittle, T. J., Doyle, K. L. & Tamkun, M. M. Primary structure and differential expression during development and pregnancy of a novel voltage-gated sodium channel in the mouse. *J. Biol. Chem.* **269**, 30125–30131 (1994).
25. Felipe, A., Snyders, D. J., Deal, K. K. & Tamkun, M. M. Influence of cloned voltage-gated K+ channel expression on alanine transport, Rb+ uptake, and cell volume. *Am. J. Physiol.* **265**, C1230-1238 (1993).
26. Vicente, R. *et al.* Association of Kv1.5 and Kv1.3 contributes to the major voltage-dependent K+ channel in macrophages. *J. Biol. Chem.* **281**, 37675–37685 (2006).
27. Oliveras, A. *et al.* The unconventional biogenesis of Kv7.1-KCNE1 complexes. *Sci. Adv.* **6**, eaay4472 (2020).
28. Kang, C. *et al.* Structure of KCNE1 and implications for how it modulates the KCNQ1 potassium channel. *Biochemistry* **47**, 7999–8006 (2008).
29. Sun, J. & MacKinnon, R. Structural Basis of Human KCNQ1 Modulation and Gating. *Cell* **180**, 340–349 (2020).
30. Sole, L. *et al.* Functional consequences of the variable stoichiometry of the Kv1.3-KCNE4 complex. *Cells* **9**, 1833 (2020).
31. Ulbrich, M. H. & Isacoff, E. Y. Subunit counting in membrane-bound proteins. *Nat. Methods* **4**, 319–321 (2007).
32. Nakajo, K., Ulbrich, M. H., Kubo, Y. & Isacoff, E. Y. Stoichiometry of the KCNQ1 - KCNE1 ion channel complex. *Proc. Natl. Acad. Sci. U.S.A.* **107**, 18862–18867 (2010).
33. Plant, L. D., Xiong, D., Dai, H. & Goldstein, S. A. Individual IKs channels at the surface of mammalian cells contain two KCNE1 accessory subunits. *Proc. Natl. Acad. Sci. U.S.A.* **111**, E1438-1446 (2014).
34. Um, S. Y. & McDonald, T. V. Differential association between HERG and KCNE1 or KCNE2. *PLoS ONE* **2**, 933 (2007).
35. Perez-Verdaguer, M. *et al.* Caveolar targeting links Kv1.3 with the insulin-dependent adipocyte physiology. *Cellular Mol. Life Sci. CMLS* **75**, 4059–4075 (2018).
36. Govers, R., van Kerkhof, P., Schwartz, A. L. & Strous, G. J. Di-leucine-mediated internalization of ligand by a truncated growth hormone receptor is independent of the ubiquitin conjugation system. *J. Biol. Chem.* **273**, 16426–16433 (1998).
37. Xu, S. *et al.* A novel di-leucine motif at the N-Terminus of human organic solute transporter beta is essential for protein association and membrane localization. *PLoS ONE* **11**, e0158269 (2016).
38. Wang, Q., Zhu, F. & Wang, Z. Identification of EGF receptor C-terminal sequences 1005–1017 and di-leucine motif 1010LL1011 as essential in EGF receptor endocytosis. *Exp. Cell Res.* **313**, 3349–3363 (2007).
39. de la Fuente-Ortega, E. *et al.* Basolateral sorting of chloride channel 2 is mediated by interactions between a dileucine motif and the clathrin adaptor AP-1. *Mol. Biol. Cell* **26**, 1728–1742 (2015).
40. Berglund, N. A., Kargas, V., Ortiz-Suarez, M. L. & Bond, P. J. The role of protein-protein interactions in Toll-like receptor function. *Prog. Biophys. Mol. Biol.* **119**, 72–83 (2015).
41. Afzal, A. J. *et al.* Homo-dimerization and ligand binding by the leucine-rich repeat domain at RHG1/RFS2 underlying resistance to two soybean pathogens. *BMC Plant Biol.* **13**, 43 (2013).
42. Capera, J., Serrano-Novillo, C., Navarro-Perez, M., Cassinelli, S. & Felipe, A. The potassium channel odyssey: mechanisms of traffic and membrane arrangement. *Int. J. Mol. Sci.* **20**, 734 (2019).
43. Serrano-Albarras, A., Cirera-Rocosa, S., Sastre, D., Estadella, I. & Felipe, A. Fighting rheumatoid arthritis: Kv1.3 as a therapeutic target. *Biochem. Pharmacol.* **165**, 214–220 (2019).
44. Pena-Munzenmayer, G. *et al.* Basolateral localization of native ClC-2 chloride channels in absorptive intestinal epithelial cells and basolateral sorting encoded by a CBS-2 domain di-leucine motif. *J. Cell Sci.* **118**, 4243–4252 (2005).
45. Wu, J. *et al.* Two di-leucine motifs regulate trafficking and function of mouse ASIC2a. *Mol. Brain* **9**, 9 (2016).
46. Jablonka-Shariff, A. & Boime, I. A dileucine determinant in the carboxyl terminal sequence of the LHbeta subunit is implicated in the regulated secretion of lutropin from transfected GH3 cells. *Mol. Cell. Endocrinol.* **339**, 7–13 (2011).
47. Miyashita, Y. & Ozawa, M. Increased internalization of p120-uncoupled E-cadherin and a requirement for a dileucine motif in the cytoplasmic domain for endocytosis of the protein. *J. Biol. Chem.* **282**, 11540–11548 (2007).
48. Malaby, H. L. & Kobertz, W. R. Molecular determinants of co- and post-translational N-glycosylation of type I transmembrane peptides. *Biochem. J.* **453**, 427–434 (2013).
49. Vanoye, C. G., Welch, R. C., Tian, C., Sanders, C. R. & George, A. L. Jr. KCNQ1/KCNE1 assembly, co-translation not required. *Channels (Austin)* **4**, 108–114 (2010).
50. Chang, M. C., Khanna, R. & Schlichter, L. C. Regulation of Kv1.3 channels in activated human T lymphocytes by Ca(2+)-dependent pathways. *Cell Physiol. Biochem.* **11**, 123–134 (2001).
51. Fanger, C. M. *et al.* Calmodulin mediates calcium-dependent activation of the intermediate conductance KCa channel, IKCa1. *J. Biol. Chem.* **274**, 5746–5754 (1999).
52. Tamkun, M. M., O'Connell, K. M. & Rolig, A. S. A cytoskeletal-based perimeter fence selectively corrals a sub-population of cell surface Kv21 channels. *J. Cell Sci.* **120**, 2413–2423 (2007).

Acknowledgements

Author contributions

S.R.R., L.S., S.C., M.C.M., D.S., C.S.N., A.S.A. performed the experiments. S.R.R., L.S., P.L., M.M.T. and A.F. designed the experiments. P.L. and M.M.T. provided tools and facilities. S.R.R. and A.F. wrote the manuscript. All authors debated and edited the final form of the manuscript. A.F. directed the study.

Competing interests

The authors declare no competing interests.

Additional information

Supplementary Information The online version contains supplementary material available at https://doi.org/10.1038/s41598-021-93562-5.

Supplementary Information

Calmodulin-dependent KCNE4 dimerization controls membrane targeting

Sara R. Roig[1,2], Laura Solé[1,3], Silvia Cassinelli[1], Magalí Colomer-Molera[1], Daniel Sastre[1], Clara Serrano-Novillo[1], Antonio Serrano-Albarrás[1], M. Pilar Lillo[4], Michael M Tamkun[3], Antonio Felipe[1]

[1]Molecular Physiology Laboratory, Dpt. de Bioquímica i Biomedicina Molecular, Institut de Biomedicina (IBUB), Universitat de Barcelona, Avda. Diagonal 643, 08028 Barcelona,Spain. [2]Imaging Core Facility, Biozentrum, University of Basel, 4056 Basel, Switzerland; [3]Department of Biomedical Sciences, Colorado State University, Fort Collins, Colorado 80523. [4]Instituto de Química Física Rocasolano, CSIC, 28006 Madrid, Spain.

Supplementary Figure 1. Subcellular localization of KCNE4. Representative confocal images of HEK-293 cells transfected with KCNE4. (Aa-c) KCNE4-transfected cells were cotransfected with a plasma membrane marker (MB). (Ad-f) KCNE4-transfected HEK-293 cells were cotransfected with an endoplasmic reticulum marker (ER). (Ag-i) KCNE4- transfected cells were further stained against cis-Golgi network (GM130). (Aj-l) KCNE4- transfected HEK-293 cells were further stained against trans-Golgi (TGN46). Left panels, KCNE4 in green; center panels, cellular markers in red; right panels, merge in yellow. Bars represent 10 ☐m. (B) Histogram showing the colocalization between KCNE4 and the markers based on Mander's overlap coefficient (MOC). The values represent mean + SE of >40 cells.
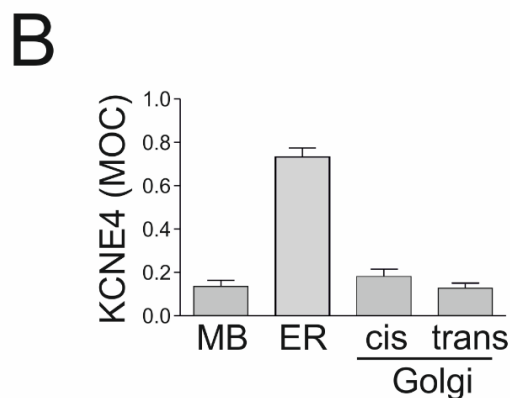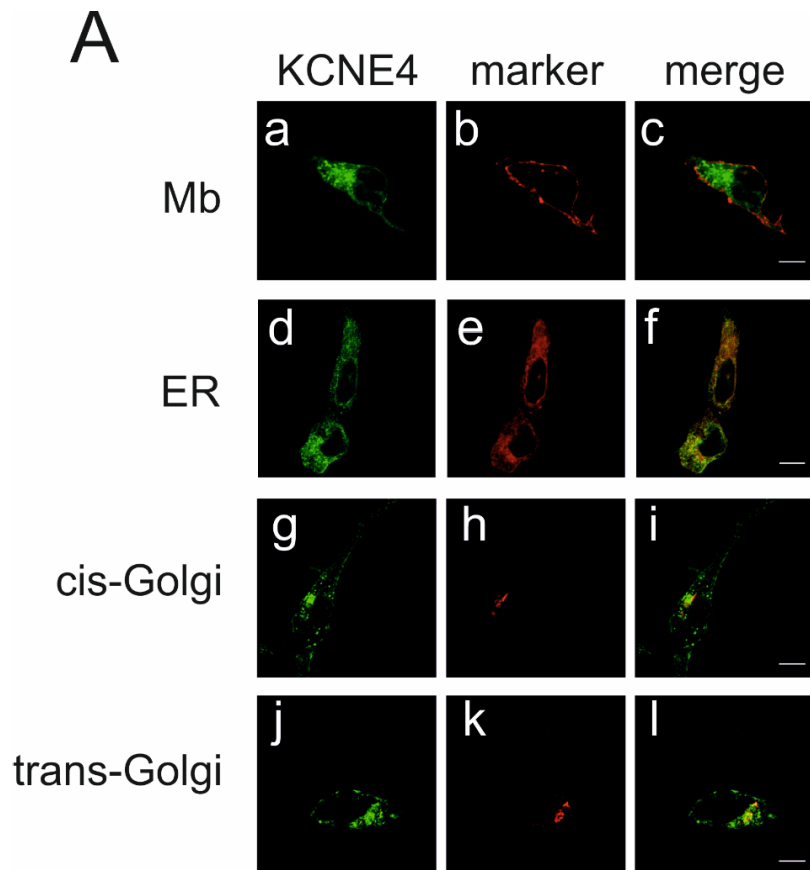
Chapter III

Effects of S-acylation within the Kv1.3 interactome

Palmitoylation regulates the architecture and cellular targeting of KCNE4

Silvia Cassinelli[1], Carla Viñola-Renart[1], Alexine. De Wit[2], María Navarro-Pérez[1], Jesusa Capera[1,3], Geert Van Den Bogaart[2], Antonio Felipe[1]

[1] Molecular Physiology Laboratory, Departament de Bioquímica i Biomedicina Molecular, Institut de Biomedicina (IBUB), Universitat de Barcelona, Avda. Diagonal 643, 08028 Barcelona, Spain.

[2] Molecular Immunology Laboratory, Department of Molecular Immunology, P.O.Box 11103. GBB, University of Groningen. 9700 CC Groningen, the Netherlands.

[3] The Kennedy Institute of Rheumatology, Nuffield Department of Orthopaedics Rheumatology & Musculoskeletal Sciences, University of Oxford, Oxford, United Kingdom.

Palmitoylation regulates the architecture and cellular targeting of KCNE4

Silvia Cassinelli[1], Carla Viñola-Renart[1], Alexine. De Wit[2], María Navarro-Pérez[1], Jesusa Capera[1,3], Geert Van Den Bogaart[2], Antonio Felipe[1].

[1] Molecular Physiology Laboratory, Departament de Bioquímica i Biomedicina Molecular, Institut de Biomedicina (IBUB), Universitat de Barcelona, Avda. Diagonal 643, 08028 Barcelona, Spain.

[2] Molecular Immunology Laboratory, Department of Molecular Immunology, P.O.Box 11103. GBB, University of Groningen. 9700 CC Groningen, the Netherlands.

[3] The Kennedy Institute of Rheumatology, Nuffield Department of Orthopaedics Rheumatology & Musculoskeletal Sciences, University of Oxford, Oxford, United Kingdom.

Abstract. Voltage-gated potassium channels play pleiotropic roles in both excitable and non-excitable cells. The functions of these channels are further expanded by the interaction with numerous regulatory proteins, which are in turn modulated by a number post-translational modifications. Kv1.3 localizes in membrane lipid-rafts and accumulates at the immunological synapse during cell activation, controling the membrane potential and triggering down-stream calcium-signalling pathways. KCNE4 acts as a dominant negative regulatory subunit on Kv1.3 causing intracellular retention. Palmitoylation is a reversible post-translational mechanism, increasing the hydrophobicity of protein domains and facilitating their membrane association, protein–protein interactions and subcellular trafficking among membrane organelles and within specific lipid-rafts. Our data showed that KCNE4 underwent S-acylation and the palmitate attachment causes spatial rearrangements, decreasing the protein distribution within the endoplasmic reticulum. Therefore, affecting the regulation of Kv1.3. Moreover, KCNE4 traffics to the cell surface associated with Kv1.3 in activated dendritic cells, but altering the immunological synapse location. This work points to the KCNE4 palmitoylation as an important component in regulating protein subcellular segregation and oligomeric state, affecting in turn the channel membrane expression. Since Kv1.3 is considered an immunomodulatory target, our results provide new insights for future pharmacological studies.

Introduction

Voltage-gated potassium channels (Kv) contribute to the membrane potential in excitable cells (*1*). However, this function is also crucial in cells with no action potentials (*2*). Thus, Kv are involved in the proliferation, apoptosis and activation of immune cells (*3*) (*4*). They are also involved in the development of different inflammatory autoimmune diseases, such as rheumatoid arthritis, asthma, multiple sclerosis among others (*5*) (*6*) (*7*). Kv functions are further expanded by the interaction with numerous regulatory proteins, affecting not only the cellular distribution, but also kinetics. Therefore, understanding the molecular interactions between β-subunits and regulated channels could be crucial for clinical-pharmacology studies (*8*). The macromolecular complexes are modulated in turn by a number of post-translational modifications, influencing both the cellular trafficking and the gating within the complex (*9*) (*10*). During immune response most cytokines and transcription factors, as well as ion channels, undergo specific modifications fine tuning their appropriate function. Between members of the NF-kB protein family, the transcriptional activity of p65 is strongly affected by its phosphorylation (*11*) (*12*). In calcium-activated potassium (BK) channels, the membrane inclusion depends on an interplay between palmitoylation of the STREX motif and the PKA-dependent phosphorylation of channels C-terminus (*13*). Palmitoylation, is one of the most common form of fatty acylation, consisting in the esterification of palmitates to cysteine side chains. Palmitoylation is a reversible process, catalysed by palmitoyl acyl transferases (*14*) and reversed by protein acyl-thioesterases (APTs) (*15*). Among multitudes of biological processes, palmitoylation can directly affects membrane curvature, promotes the clustering and internalization of both proteins and lipids and can regulate the affinity of proteins for cellular

membranes dependent on their shape (*16*). Furthermore, it may promote protein-protein interactions (*17*) and participate in the traffic and inclusion of soluble and transmembrane proteins at the plasma membrane and specific lipid-rafts, during immunological synapse formation (*18*) (*19*). In addition, palmitoylation assumes central roles in the regulation of ion channels, controlling different phases of the protein life cycle (*20*) and the modulation by β-subunits. Acylation and de-acylation cycles of these ancillary peptides may critically affect the regulation of α-subunits, altering both the electrophysiological properties and cellular fate (*21*). In this context, Kv1.3, highly expressed in leukocytes, is responsible for the K^+ efflux during cell activation, contributing to the electrogenic force, essential for a proper immune response (*22*). This feature facilitates the precision of pharmacological strategies, pointing up to Kv1.3 as an attractive target for the immunotherapy (*23*). The channel activity is regulated by the action of numerous regulatory proteins, such as Kvβs or KCNEs (*24*) (*25*). Considering this last group, KCNEs are five single-span membrane proteins, which some are expressed in the immune system and leukocytes (*26*). KCNE4 is the biggest member, presenting a disordered C-terminal domain and acting as a dominant negative on Kv1.3, by causing the endoplasmic reticulum (ER) retention and enhancing the channel inactivation (*27*). Given the importance of protein acylation, both during molecular immune responses and in the regulation of ion channels, in this work we aimed to elucidate the effects of palmitoylation on the KCNE4 modulatory peptide and the Kv1.3/KCNE4 complex. We also studied the distribution of the proteins by using the murine histiocytic tumor CY15 (*28*) cell line, and the traffic of KCNE4 to immunological synapses between human monocytes-derived (moDCs) dendritic cells and Jurkat T-cells, upon activation.

Materials and Methods

Cell culture, Expression plasmids, and site directed mutagenesis. rKv1.3 in pRcCMV was provided by T.C. Holmes and subcloned into pEYFP-C1 (Clontech). Mouse KCNE4 in pSGEM was obtained from M. Sanguinetti (*29*) and included into pEYFP-N1 and pECFP-N1 (Clontech). mKCNE4-HA was introduced into pcDNA3-N1 (Clontech). Soluble cyan fuorescent protein (pECFP-N1), green fuorescent protein (pEGFP-N1) and yellow fuorescent protein (pEYFP-N1) were obtained from Clontech. The plasma membrane marker Akt-PH-pDsRed (pDsRed-tagged pleckstrin homology (PH) domain of Akt) was a kindly donated by F. Viana (Universidad Miguel Hernández, Spain). The KCNE4-ClessS mutant was obtained by mutation of Cysteines to Serines by single-site–directed mutagenesis, using a QuikChange multisite-directed mutagenesis kit (Agilent Technologies). All constructs and mutants were verified by DNA sequencing. HEK-293 cells were cultured in DMEM (Lonza) medium supplemented with 10% fetal bovine serum (FBS), penicillin (10.000 U/ml), streptomycin (100 μg/ml) (GIBCO), and L-glutamine (4 mM). The murine histiocytic tumor cell line CY15 was kindly provided by R. Vicente, (Universitat Pompeu Fabra, Spain) and cultured in Lonza™ BioWhittaker™ RPMI 1640 medium containing L-Glutamine, supplemented with 10% FBS, penicillin (10,000 U/mL) and streptomycin (100 μg/mL). Buffy Coat cells from healthy donor patients were obtained from Sanquin.org Blood Supply, University Medical Center Groningen, Hanzeplein 1, (Ingang 47 a/d Oostersingel), 9713 GZ Groningen, The Netherlands. moDCs were isolated at the Molecular Immunology Laboratory, Department of Molecular Immunology (MIMY), University of Groningen, The Netherlands. Jurkat NY-ESO1 T cells were kindly donated by G. Van den Bogaart (University of Groningen, The Netherlands).

Transient transfection and pharmacological treatments. For all the experiments, cells were seeded up to 70–80% confluence, in 6-well dishes containing poly-D-lysine-coated coverslips and 100-mm dishes, respectively. Transfections were performed using Lipotransfectina (Attendbio Research) for a total amount of 4μgDNA per condition. HEKs-293 were transfected with Kv1.3-YFP or Kv1.3-HA, KCNE4-CFP WT and ClessS DNA. After 4-6 h of transfection, the mixture was replaced with fresh culture medium. In some experiment, cells were treated with 5 [μg/μL] of Brefeldin-A during 4h, before to start the protocol. In CY15, cells were incubated in the presence or not of 100 ng/mL of lipopolysaccharide (LPS, Sigma-Aldrich) for 24 h, to induce metabolic activation.

Protein extraction, membrane protein biotinylation, co-immunoprecipitation and western blotting. HEK-293 and CY15 cells were washed twice with cold Phosphate-buffered saline (PBS) and lysed with lysis buffer (5 mM HEPES, 150 mM NaCl, 1%

Triton X-100, pH7.5). After incubation, they were centrifuged and Bio-Rad Protein assays (Bio-Rad) were performed to determine the protein concentration. For co-immunoprecipitation, 1000 µg of protein were separated and complemented with lysis buffer up to a final volume of 500 µL, in order to distribute each sample in the same volume. For membrane-biotinylation assays, cells were transfected 24h and incubated 30 min with EZ-Link Sulfo-NHS-SS-Biotin (sulfosuccinimidyl-2-[biotinamido]ethyl-1,3-dithiopropionate). After scraping, cell lysates were immunoprecipitated with Neutravidin Beads (ThermoFisher). Western Blot was performed boiling the resulting samples in Laemmli SDS loading buffer and separated (50 µg) on 10% SDS-PAGE. Next, samples were transferred to nitrocellulose membranes (Millipore) and blocked in 0.2% Tween-20-PBS supplemented with 5% dry milk. Immunoreactions were performed using antibodies against KCNE4 (Proetintech, 1:1000), Kv1.3 (Neuromab, 1:200), GFP (Alomone, 1:500), iNOS (1:100, Santa Cruz Biotechnology). Anti-Calnexin antibody (1:100; BD Transduction Laboratories) was used to determine intracellular protein fractions. Anti-Flotillin (1/1,000, BD Biosciences) and anti-Clathrin (1/1,000, BD Biosciences) antibodies were used as a marker of lipid raft and non-floating fractions, respectively. (1/1,000, BD Biosciences). Anti-β-actin ans anti-GAPDH were used as loading control of proteins expression (1/50,000, Sigma). Anti-iNOS was used as a positive control of dendritic cells metabolic activation (1:100, Santa Cruz Biotechnology).

ABE palmitoylation assay. After transfection HEK-293 cells were lysate in buffer A (150 mM NaCl, 50 mM Tris HCl, 0,2% Triton X-100, 5 mM EDTA, pH 7.4) containing 10mM NEM (Nethylmaleimide, Sigma) and passed through a 25-gauge needle to expose free-cysteine chains of proteins. Next, samples were chloroform-methanol (C/M) precipitated and pellets were left to dry. Thus, pellets were re-suspended in 300 µL of buffer B (4% sodium dodecyl sulfate, 50 mM Tris HCl, 5 mM EDTA, pH 7.4) and diluted four fold in buffer A containing 10mM NEM. Therefore, samples were incubated at 4°C overnight in the orbital shaker. The next day, the excess of NEM was removed by performing three sequential chloroform-methanol precipitations. Following the last precipitation, pellets were re-suspended in 500 µL of buffer B and splitted in two: 250 µL were diluted with 950uL of buffer C, supplemented with 0.7 M hydroxylamine (*30*) (50mM

Tris-HCl, 1 mM HPDP-biotin, 0.2% Triton X-100, 100µM PMSF). This compound hydrolyses the thioester bond and resulting in a free sulfhydryl group at the site at which the cysteine residue was palmitoylated. The remaining samples were diluted in buffer C without hydroxylamine (-HA) as negative control. The Buffer C incubation (*30*) has been at room temperature, shaking for one hour. To clean samples from HA excesses, three (C/M) precipitation were performed and the final pellets were incubated with 900 buffer D (150 mM NaCl, 50 mM TrisHCl, 5 mM EDTA, 0.2 mM HPDP-biotin, 0.2% Triton X-100, pH 7.4), for one hour at room temperature. Next, three last C/M precipitations were performed and the final pellets were re-suspended in 120 µL of buffer E (2% SDS, 50 mM Tris HCl, 0,2% Triton X-100, 5 mM EDTA, pH 7.4). Functional groups released by HA are now free, and can therefore be contacted by HPDP-biotin. Upon complete resuspension, samples were diluted up to 0.1% SDS in buffer A for cleaning, during 30 minutes. Finally, Biotin-labelled proteins were pulled down overnight, using 50 µL of NeutrAvidin agarose beads previously washed with 400µL of buffer A and centrifuged 1 min at 2000gs. The next day, the beads were washed four times with 400µL of buffer A and pellets were boiled in 100µL Laemmli buffer 1x and 2% β-mercaptoethanol. Samples were analysed by Western Blot and processed with Fiji ImageJ software, for quantification.

Immunocytochemistry and image analysis. HEK-293 cells were seeded on poly-lysine-coated coverslips and transfected with fluorescent-labelled proteins. Twenty-four hours later, two quick washes were performed, with PBS-K$^+$-less and fixed with paraformaldehyde 4%, during 10 min. after three additional washes of 5 min, coverslips were mounted on microscope slides (Acefesa) using home-made Mowiol mounting media. All the procedure was performed at RT. Confocal images were acquired after complete slides drying, with a Zeiss 880 confocal microscope. Images were analysed using Fiji ImageJ software (NIH, Bethesda, MD, USA). To obtain Mander's overlap coefficients (MOC), which are proportional to the amount of fluorescence of the colocalizing pixels in each colour channel (*31*) and pixel-by-pixel colocalization studies, the plugin JACoP (Just Another Colocalization Plugin) was used. For CY15 immunocytochemistry experiments, twenty-four hours after seeding, the supplemented RPMI cell-culture medium was replaced with fresh

medium, and a 100 ng/mL of lipopolysaccharide (LPS, Sigma-Aldrich) treatment was added to the +LPS condition in order to induce activation. The next day, cells were washed with cold PBS Ø K+ and incubated with binding solution (RPMI supplemented with Hepes 30 mM and WGA-Alexa555 1/1500) for 5 min at 4°C. Cells were then quickly washed three times with PBS Ø K+ and fixated for 10 min with 4% paraformaldehyde at room temperature. Next, the cells were washed three times with 20 mM glycine PBS Ø K+ (5 min/wash) and permeabilized for 10 min with 20 mM glycine 0.1% Triton X-100 PBS Ø K+. Thus, cells were incubated with blocking solution (PBS Ø K+ with 20 mM glycine, 0,05% Triton X-100, and 1% BSA) for 1 h at room temperature. After that, cells were incubated with blocking solution supplemented with primary antibodies anti-KCNE4 (1/200, Proteintech) and anti-Kv1.3 (1/25, Neuromab) for 90 min in a dark, humid chamber at room temperature. Hence, smaples were washed three times with 0.05% Triton X-100 20 mM glycine PBS Ø K+ during 5 min and incubated for 1 h at room temperature in a dark, humid chamber with secondary antibodies 1/200 Goat Anti Mouse Alexa-660 and 1/400 Goat Anti Rabbit Alexa-488. Finally, cells were washed with PBS Ø K+ 20 mM glycine 0,05% Triton X-100 for three times, during 5 min. Nuclei were stained with 1 µg/ml DAPI for two minutes. Again, cells were thrice washed, and mounted on coverslips (ACEFESA) with homemade Mowiol mounting media containing DABCO anti-fading reagent. The KCNE4-Kv1.3 colocalization analysis was performed by ImageJ software. An IJ1 Macro implemented in the laboratory was used to create a mask of the colocalization between the Kv1.3 and KCNE4 signal. These colocalization points were then analyzed by means of JACoP to calculate the MOCs between the plasma membrane and KCNE4/Kv1.3 colocalized points.

Förster Resonance Energy Transfer (FRET) Acceptor Photobleaching. FRET efficiency was measured 24h after transfection, in specific ROIs (regions of interest). Fluorescent CFP-YFP proteins from fixed cells were excited with the 458 nm or 514 nm beam lines, using low excitation intensities. Then, 475 to 495 nm bandpass and > 530 nm longpass emission filters were applied, using the maximum laser power for the YFP-bleaching. The acceptor intensity bleaching was 100%. Thus, donors and acceptors images were acquired and FRET efficiencies (*Fe*) were obtained. *Fe* and bleaching percentages were obtained following the steps proposed by Zimmermann T. *Methods Mol Biol*. 2019 (*32*). The equation applied was: $Fe = [(Fe\mathrm{CFP_{post}} - Fe\mathrm{CFP_{pre}})/Fe\mathrm{CFP_{post}}]$ where $\mathrm{FeCFP_{post}}$ represents the fluorescence of the donor after bleaching and $\mathrm{FeCFP_{pre}}$ the fluorescence before bleaching. Cells with bleaching percentages lower than 80% were analysed applying the correction factor (b) equation: $b = 1 - (\mathrm{Acceptor_{post}} / \mathrm{Acceptor_{pre}})$ and $\mathrm{Fe_{corr}} = Fe / b$ (29). The loss of fluorescence because of scanning was corrected by measuring the CFP intensity in the unbleached part of the cell, using the same bleaching-ROIs size. Analysis was performed using FIJI-ImageJ.

Cell unroofing preparations (CUPs). Membrane sheets were obtained by osmotic shock. HEK-293 cells were seeded on poly-D-lysine-treated glass coverslips and transfected 24 h with KCNE4 CFP and / or Kv1.3 YFP. The next day, in order to induce hypotonic shock, cells were cooled on ice 5 minutes and rapidly washed in PBS1X K$^+$-deficient, twice. Then, cells were incubated during 5 additional minutes in threefold-diluted KHMgE buffer (70 mM KCl, 30 mM HEPES, 5 mM MgCl2, 3 mM EGTA, pH 7.5). Lysed cells were removed from the coverslips by pipetting 8 times up and down. After two washes with 1XKHMgE buffer, only plasma membrane compartments remained attached on the coverslip, thus, samples were fixed with 4% PFA for 10 minutes at RT and mounted on coverslips by using home-made Mowiol, until complete drying.

Electrophysiology. Transfected HEK-293 cells were trypsinized and replated on a perfusion chamber. After 15 min, cells were washed with extracellular solution (in mM: 145 NaCl, 4 KCl, 1 MgCl2, 1.8 CaCl2, 10 HEPES Na, and 10 glucose. pH 7.40 adjusted with NaOH). Borosilicate electrodes were from glass capillaries (1.2 OD x 0.94 x 100 L mm) (Harvard Apparatus) with a P-97 puller (Sutter Instruments) and fire-polished with a MF 830 Microforge (Narishige) to achieve a resistance of 2-4 MΩ. The intracellular pipette solution contained (in mM: 80 AspK, 42 KCl, 10 KH2PO4, 5 EGTA-K and 5 HEPES-K adjusted to pH 7 with KOH, 3 P-creatine, and 3 ATP-Mg). Gigaseal formation was achieved by suction and the membrane patch was ruptured with an additional brief suction. Cells were clamped at a holding potential of -80 mV. Experiments took place at RT using the whole-cell configuration of the patch clamp technique with an EPC-10 amplifier (Harvard

Bioscience), waiting 45 s between pulses to allow completely recovery of Kv1.3 from inactivation. Cells were stimulated with 250 ms square pulses ranging from +60 to -80 mV in 10-mV steps to elicit voltage-gated currents. Peak current was relativized by cell capacitance to obtain measures of current density.

Buffy Coat and Cell-Conjugates preparation. These experiment have been entirely performed at the MIMY Laboratory, University of Groningen. To isolate monocytes from healthy donors, 40 mL of fresh blood were transferred to T75 culture flask and diluted with Dilution Solution (1x PBS, 0.5M EDTA) in 1:1 ratio. Thus, 20 mL of Ficoll solution were added through the insert of 5 SepMate-50 tubes (ThermoFisher) and 20 mL of blood were pipetted on the top of the ficoll layer. Cells were centrifuged for 22 min at 1250x g, at room temperature (*33*). Then, the top layer containing peripheral blood mononuclear cells was poured into a new 50mL tube and diluting solution was added until a total volume of 50mL. After spinning down for 10 min, at 1700rpm, RT, the supernatant was removed and pellets were resuspended in Wash Buffer (1x PBS cold, 10% BSA, 0,5M EDTA). Samples were then centrifuged during 5 min at 4 °C at 300xg and the process was repeated until supernatants clear up. Thus, suspensions were collected in 2 separated 50mL tubes and a series of wash steps were repeated until supernatants become lighter. Next, cells were pulled and counted (order of 200-400 x 10e6) by using 10uL of isolated cells and 90uL of Turks solution, to exclude lymphocytes from counting. After that, suspensions were centrifuged 10 min at 300xg, supernatants were completely aspirated and positive selection of CD14$^+$ monocytes was performed for each donor, using MACS separator (Milteny Biotec). For magnetic separation LS Columns were prepared by rising 3 mL of MACS BSA stock solution (1x PBS pH 7.2, 0.5% bovine serum albumin (BSA), 2 mM EDTA) diluted in 1:20 autoMACS® Rinsing solution. For the CD14-positive cells selection, pellets were resuspended with 80 uL of cold MACS-BSA-Rising buffer and mixed with 20 uL of CD14$^+$-MicroBeads per 10^7 total cells. Then, samples were incubated during 15 min at 4 °C, thereby washed twice with 2 mL of the MACS-BSA-Rising buffer, and centrifuged at 300xg, for 10 min. Pellets were resuspended up to 10^8 cells in wash buffer and suspensions were applied onto an LS column by using a p1000 pipette, to avoid clamp formations. Then, total effluents containing the unlabelled cells (negative selection) were collected and columns were washed three times. Columns were next separated from the magnet and placed on a suitable collection tube. Hence, 5 mL of MACS-BSA-Rising buffer were added and magnetically labelled cells were flushed out, by pushing the plunger into the column. The collection tubes now contain the CD14$^+$ monocytes. 1x10e^6 monocytes were plated in a T75 culture flask, in RPMI 1640 (GIBCO) supplemented with 10% FBS, 2mM L-Glutamine and 1x Gibco Anti-anti. To induce the monocyte-derived (moDCs) dendritic cells differentiation, Interleukin-4 (IL4-300U/mL) and granulocyte-macrophage colony-stimulating factor (GM-CSF- 450U/mL) were added and cells were cultured during 6 days at 37 °C. After this time moDCs were treated with 100 ng/mL LPS in the presence or not of 20 nM tumor-selective cancer testis antigen 1A (NY-ESO-1), overnight. The day after, Jurkat-T cells engineered with a specific TCR to MHC-epitope complex recognizing NY-ESO-1, were added in a 1:2 ratio, in order to force the immune clusters organization. After 4h, samples were permeabilized by using CLSM buffer (1xPBS, 3%BSA, 10mM glycine) supplemented with Saponin 0.1% and stained against KCNE4 (Proteintech), Phalloidin (ThermoFisher) as membrane marker and α-tubulin (ThermoFisher) labelling the actin cytoskeleton. Thus, samples were fixed with 4% PFA and mounted on coverslip for confocal microscopy analyses, by using Moviowl mounting media supplemented with DABCO anti-fade reagent, until complete drying. MTOC distance to the IS measurements were obtained using ImageJ software, applying the formula: *MTOC distance to IS / Ø^{Feret} DCs*. Where Ø^{Feret} is the Feret's diameter of dendritic cells, calculated with a specific ImageJ plugin. Quantification of Phalloidin and KCNE4 aggregates at the IS was performed by using the following formulae: *IS$_{IN}$ / (IS$_{OUT}$ DCs + IS$_{OUT}$ JCs) w*here DCs and JCs mean Dendritic and Jurkat cells, respectively. IN and OUT indicate the intensity of proteins signals within specific ROIs, which were drawn INSIDE (IS$_{IN}$) the synaptic interface or OUTSIDE (IS$_{OUT}$) the synaptic interface.

Statistical analysis. Student's t-test or one-way ANOVA and Tukey's post hoc test were analysed using GraphPad PRISM v5.01. The results represent the means±SEM resulting from >15 analysed cells. P values * <0.05, ** <0.005, **<0.0005 were considered statistically significant. Experiments involving <15 analysed cells were analysed uning a Kruskal-Wallis and Dunn's no-parametric tests. For

CY15 confocal analyses, a Mann-Whitney non-parametric test was used for samples smaller than 15 cells or samples with no normal distributions, while, parametric unpaired test was used for quantifications of >15 cells, and positive for a normal distribution. A value of $p < 0.05$ was considered significant.

Results

1. The absence of KCNE4 S-acylation increases the targeting to plasma membrane.

S-acylation plays essential roles during the immunological synapse formation concentrating many signalling proteins into lipid rafts, where Kv1.3 is recruited upon immune cell activation (27). Therefore, this modification is of interest within the Kv1.3 channelosome and may affect some ancillary subunits. In order to analyse whether KCNE members may undergo palmitoylation, a full sequence alignment was performed using Clustal Omega (CLUSTALO) from the European Bioinformatics Institute site (34) (https://www.ebi.ac.uk/Tools/msa/clustalo/).

The analysis showed that KCNE4 has two cysteine residues. On the contrary, KCNE1 contains only one and KCNE2 completely lacks of cysteines (Fig.1 A). Thus, to investigate the S-acylation of KCNE4, we first analysed its palmitoylation, using KCNE2 as a negative control. We transfected HEK-293 cells with CFP-KCNEs (1, 2 and 4) and performed the ABE-palmitoylation assay. Unlike KCNE4, KCNE1 and KCNE2 showed negligible S-palmitoylation (Fig.1B). We generated a ClessS mutant, by substituting the two C-terminal cysteines of KCNE4 to serines, in order to keep maximum amino acid similarity (Fig. 1Ca) and we performed an ABE-palmitoylation assay in HEK-293 (Fig.1 Cb). As expected, the ClessS palmitoylation was minimal. Next, we analysed the protein distribution by confocal analysis (Fig.1 Da-Dg). The KCNE4 ClessS was mainly retained intracellularly (Fig.1 Dd, Dh). However, the pixel-by-pixel and quantification analyses showed an increase with the colocalization of the membrane marker vs the wild-type protein (Fig.1 d, h, j). Furthermore, Fig. 1E confirmed a positive correlation between the palmitoylation rate and the protein membrane trafficking (p= 0.0279, pearson coeff.). Single cysteine to serine mutants (C115S, C118S) were also studied (Fig. 2). All mutants exhibited comparable and intermediate results, suggesting that both distal cysteines were

palmitoylated and, in addition, pointing at C118 as the major residue involved in the KCNE4's plasma membrane targeting (Fig. 2). Similar extensive analysis performed on the alternative C115A mutant, in which A was introduced instead S, confirmed that modulations observed on both KCNE4 and Kv1.3 are due to a direct effect of palmitoylation's impairment (Supplementary Fig.1).

KCNE4 presents a strong endoplasmic reticulum retention motif (ERRM) placed at the C-terminus (35). DNA sequencing confirmed that mutations included in KCNE4 ClessS were not affecting this domain. However, KCNE4 ClessS showed lower ER localization (Fig.3). It is tempting to speculate that in addition to the ERRM, a palmitate addition at the large C-terminus could anchor this domain to the ER membrane.

To further investigate this data, we treated HEK-293 cells with Brefeldin-A (BFA), a chemical compound that blocks the sorting from the ER to the Golgi apparatus. We then repeated both confocal analyses and ABE-palmitoylation assays. Unlike KCNE4 WT, KCNE4 ClessS enhanced the ER distribution in the presence of BFA (Fig.4 A, B). Furthermore, the palmitoylation rate was incremented by two-fold for KCNE4 WT upon blocking protein secretion (Fig.4 C, D), suggesting that the retention of KCNE4 at the ER increased the palmitoylation of the protein. Hence, the modification could act as an additional anchor for the intrinsically disordered C-terminal domain of KCNE4 to the ER membrane facilitating the palmitoylation in this compartment.

2. KCNE4 palmitoylation increases the protein homodimerization.

Protein acylation influences different functions of transmembrane proteins, including conformational changes and oligomerization within the resident membrane (36). Molecular dynamics and computational simulation assays show that palmitoylation of the human dopamine transporter directly influences the abundance of dimers involving the transmembrane-12 domain, while, the palmitate addition on a single cysteine residue (C797) of the oncogenic Epidermal growth factor receptor (EGFR) is essential for its dimerization and activation (37) (38). DHHCs and APTs are the implicated enzymes and, themselves, are also regulated by changing their oligomeric state (32). KCNE4 dimerises at early states of the secretory pathway at the ER (39).

A CLUSTAL O(1.2.4) multiple sequence alignment

```
sp|Q9WTW3|KCNE4_MOUSE    MLRMEPLN--------S-------TYPSAAASSS---PLESHVPSNSSGNGNEYFYILVV   42
sp|P23299|KCNE1_MOUSE    -MSLPNST--------TVLPFLARLWQETAEQGGNVSGLA-RKSQLRDDSKLEALYILMV   50
sp|Q9D808|KCNE2_MOUSE    MATLANLTQTLEDAFKKIFITYMDSWRRNTTAEEQ-ALQ--ARVDAENFYYVILYLMVM   56
                                  :     .         :       :          ..    :*::::

sp|Q9WTW3|KCNE4_MOUSE    MSFYGVFLIGIMLGYMKSKRREKKSSLLLLYKDEERLWGEAMKPLPMMSGLRSGQVPMML   102
sp|P23299|KCNE1_MOUSE    LGFFGFFTLGIMLSYIRSKKLEHSHDPFNVYIES-DAWQEKGKAVFQARVLESFRACYVI   109
sp|Q9D808|KCNE2_MOUSE    IGMFSFIVVAILVSTVKSKRREHSQHPYHQYIVE--DWQEYKSQILH--LEDSKAT-IH   111
                         :.:.:.:  :: *::. ::**: *:.        *   . * *  *        *.. ::

sp|Q9WTW3|KCNE4_MOUSE    NMLQESVAPALSCTLCSMEGDSVSSESSSPDVHLPIQEEGADDELEETSETPLNDSSEGS   162
sp|P23299|KCNE1_MOUSE    E--------NQAA----VEQPATHLPELK-------------PLS------   129
sp|Q9D808|KCNE2_MOUSE    E--------NMGA----TGF------TVS-------------P------   123
                         :                                             *
```

```
sp|Q9WTW3|KCNE4_MOUSE    SENIHQNS   170
sp|P23299|KCNE1_MOUSE    --------   129
sp|Q9D808|KCNE2_MOUSE    --------   123
```

B

Ca

```
                        340        350
                        C115 *     C118 *
KCNE4 WT    TGTCCTGCACTCTTTGCTCGAT
f ClessS    TGTCCAGCACTCTTAGCTCGAT
```

Cb

D

j

E

P= 0.0279 *
r = -0.7857
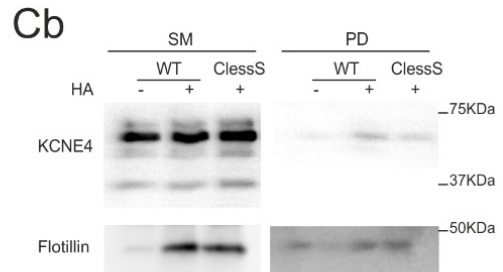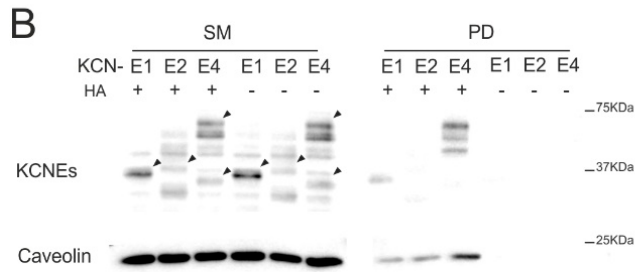
Figure 1. KCNE4 is S-acylated in HEK293 cells and the absence of the modification leads to the protein's plasma membrane traffic. (A) Sequence alignment of some murine KCNE peptides; KCNE1 (UniProtKB: P23299); KCNE2 (UniProtK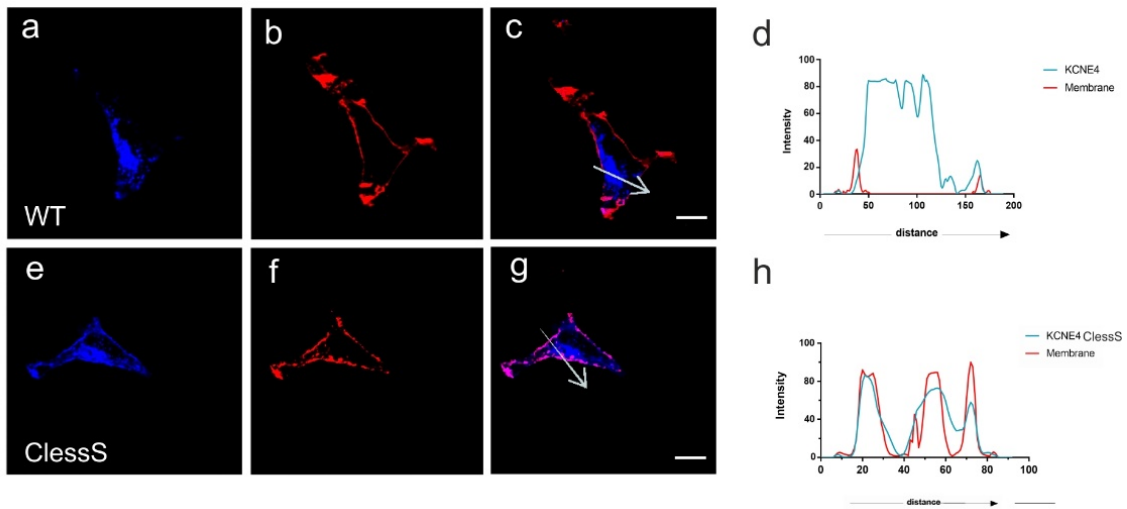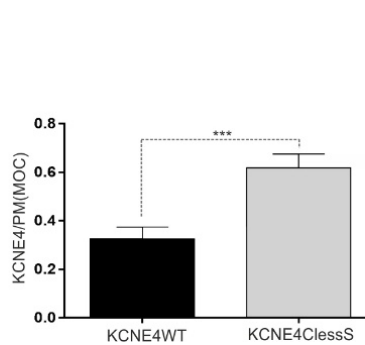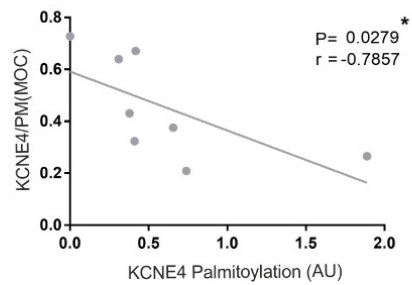B: Q9D808); KCNE4 (UniProtKB: Q9WTW3); mouse sequences are shown because murine isoforms were used for the study; similar outputs were obtained with human isoforms; cysteines are highlighted by black rectangles. Unlike KCNE2, KCNE4 presents two distal and KCNE1 a single cysteine residue. (B) ABE-palmitoylation assay of HEK293 cells transfected with KCNE1,2 and 4 in a peCFP-C1 plasmids; +/- HA means the presence or absence of Hydroxylamine; SM: Starting Material; PD: Pull down of palmitoylated proteins; caveolin is used as positive control. (Ca) KCNE4ClessS mutant generation by mutating all the protein's cysteines to serines, because of similarity. (Cb) Western blot representing palmitoylatyon analysis of KCNE WT and the ClessS mutant in HEK293 cells; flotillin is used as positive control. (D) Membrane colocalization analisys of CFP-KCNE4 WT and ClessS. (a-c) CFP-KCNE4 WT; (e-g) CFP-KCNE4 ClessS; (d, h) pixel-by-pixel analysis of the white arrow in merged panels; membrane is labelled by dsRED (red colour); merge means colocalizing channels. (j) Quantification of the plasma membrane (PM) colocalization by Mander's overlap coefficient (MOC) resulting from 30 cells analysis; ***, p<0.005 (One-way ANOVA, Tukey's multiple comparisons tests); scale bar represents 10μm. (E) Correlation analysis between KCNE4 WT/ClessS MOCs and four independent rounds of ABE-palmitoylation assay; r indicates association between data; P indicates the significance of r; * p<0.05.
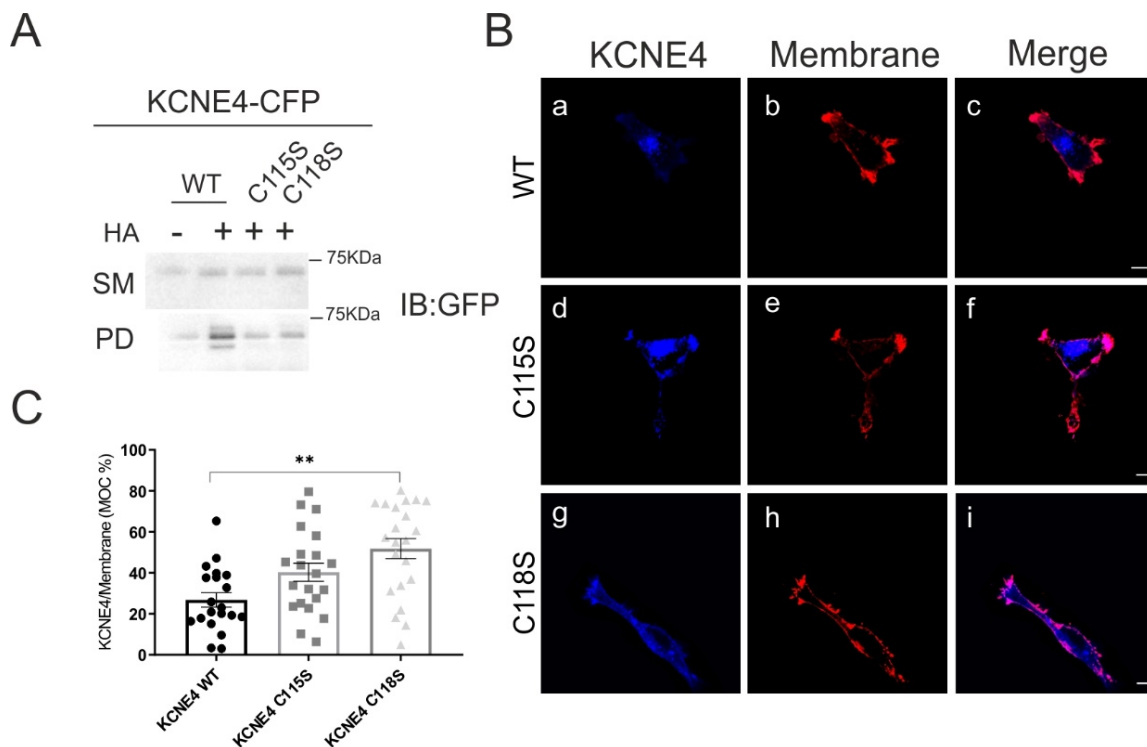
Figure 2. Membrane trafficking of KCNE4 single cysteine mutants. (A) Representative western blot of ABE-palmitoylation assay in HEK293 cells transfected with KCNE4 WT, C115S, C118S and ClessS. +/- HA, presence or absence of Hydroxylamine respectively; SM: Starting Material; PD: Pull down of palmitoylated proteins, note that mutants showed a basal palmitolylation. (B) Confocal microscopy performed in HEK293 cells transfected with KCNE4 and single cysteine mutants. (a-i) CFP-KCNE4 WT and CFP-KCNE4 C115S and C118S are indicated in blue; membrane is labelled by ds-RED and merge means overlapping between channels. (C) Quantification of MOCs resulting from 20-23 analysis; **p<0.005 (One-way ANOVA and Dunnet's multiple comparison tests) vs WT. All the mutants showed enhanced membrane trafficking.

Taking all this in mind, we next evaluated whether the palmitoylation would alter the dimerization capacity of KCNE4. For this purpose, we performed co-immunoprecipitation assays and *acceptor-photobleaching* FRET in HEK-293. Fig. 5 A confirmed a basal protein dimerization between KCNE4 CFP and KCNE4 HA. However, KCNE4 ClessS showed a two-fold increase in dimers

formation respect to the WT protein (Fig.5 B, C). Thus, palmitoylation is affecting both the intracellular trafficking and the oligomeric state of KCNE4.

Since the protein dimerization occurs at intracellular levels, we speculate that the palmitate addition may lead to conformational rearrangements, which would mask the structural motifs required for KCNE4 oligomerization. Nevertheless, we cannot exclude the presence of KCNE4 dyad at the plasma membrane.

Unlike most of KCNE members, KCNE4 exerts a strong downregulation on Kv1.3 controlling both fast inactivation and plasma membrane expression. Therefore, we wondered whether the palmitoylation of KCNE4 would affect the channel behaviour. For this purpose, we studied the Kv1.3 membrane expression in the presence of either KCNE4 WT or ClessS. HEK-293 cells were transfected with Kv1.3-YFP, KCNE4 WT, KCNE4 ClessS-CFP and membrane dsRED. To ensure that the absence of
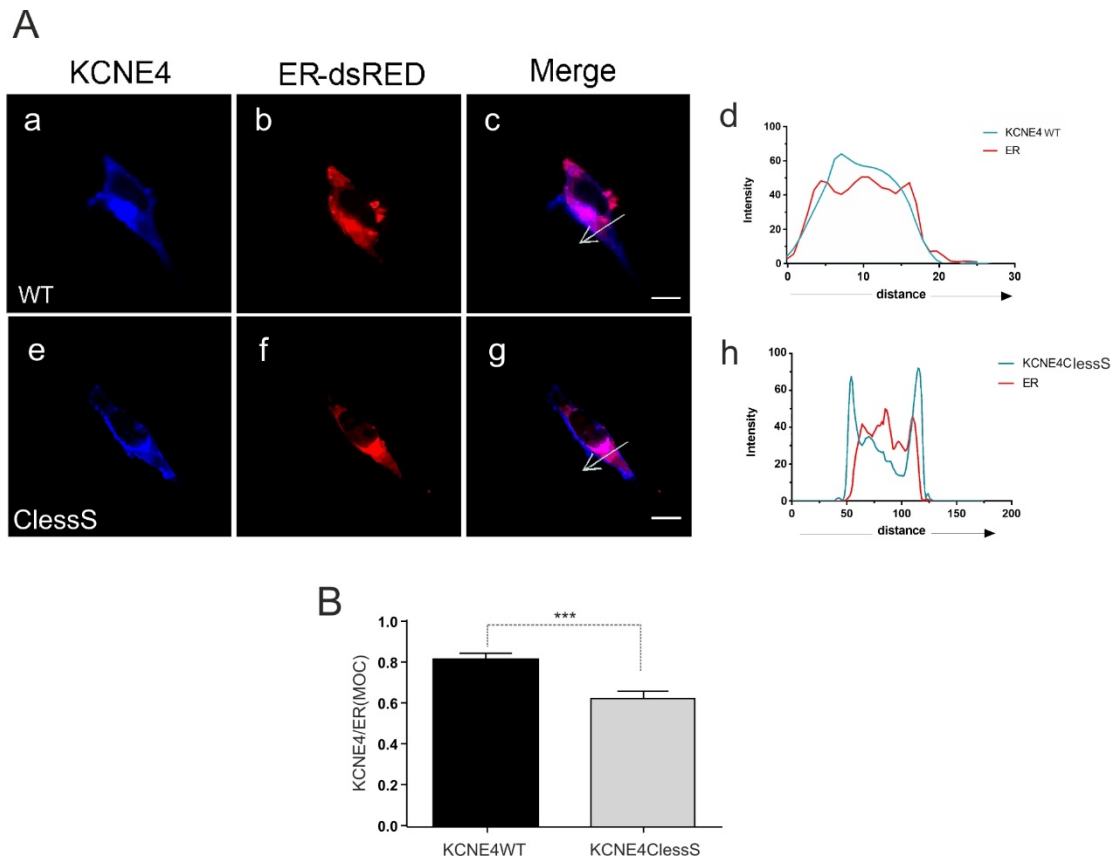

Figure 3. KCNE4 ClessS decreases the ER localization. (A) Representative confocal images of KNCE4 WT and ClessS. (a-c) CFP-KCNE4WT indicated by blue colour; (e-g) CFP-KCNE4 ClessS in blue; dsRED labelling the endoplasmic reticulum (ER); merge means colocalization between channels; (d, h) pixel-by-pixel analysis of white arrows. (B) Quantification of the ER-colocalization by MOCs, resulting from 30 cells analysis; ***, p<0.005 (Student's t-test); scale bar represents 10μm.

3. The lack of KCNE4 S-acylation alters the Kv1.3 intracellular retention.

Kv1.3 activity is crucial during a number of physiological processes. In microglia, as well as in T-lymphocytes, Kv1.3 repolarizes the plasma membrane exiting K^+ ions and maintaining the calcium's driving force required for cell activation and proliferation. Therefore, the Kv1.3 inhibition impairs T-cell activation, supporting, in turn, an immunological suppression (40) (41).

palmitoylated cysteines did not alter the association with Kv1.3, we first analysed the co-immunoprecipitation (Fig.6 A). Figure 6 B showed no significant changes between KCNE4WT and ClessS associating with Kv1.3. However, membrane-biotinylation assays indicated a lower Kv1.3 membrane expression in the presence of KCNE4 ClessS (Fig.6 C, D). Despite that, confocal experiments presented a greater surface distribution for Kv1.3 in the presence of KCNE4 ClessS (Fig.6 E). As indicated by pixel by pixel analyses the channel
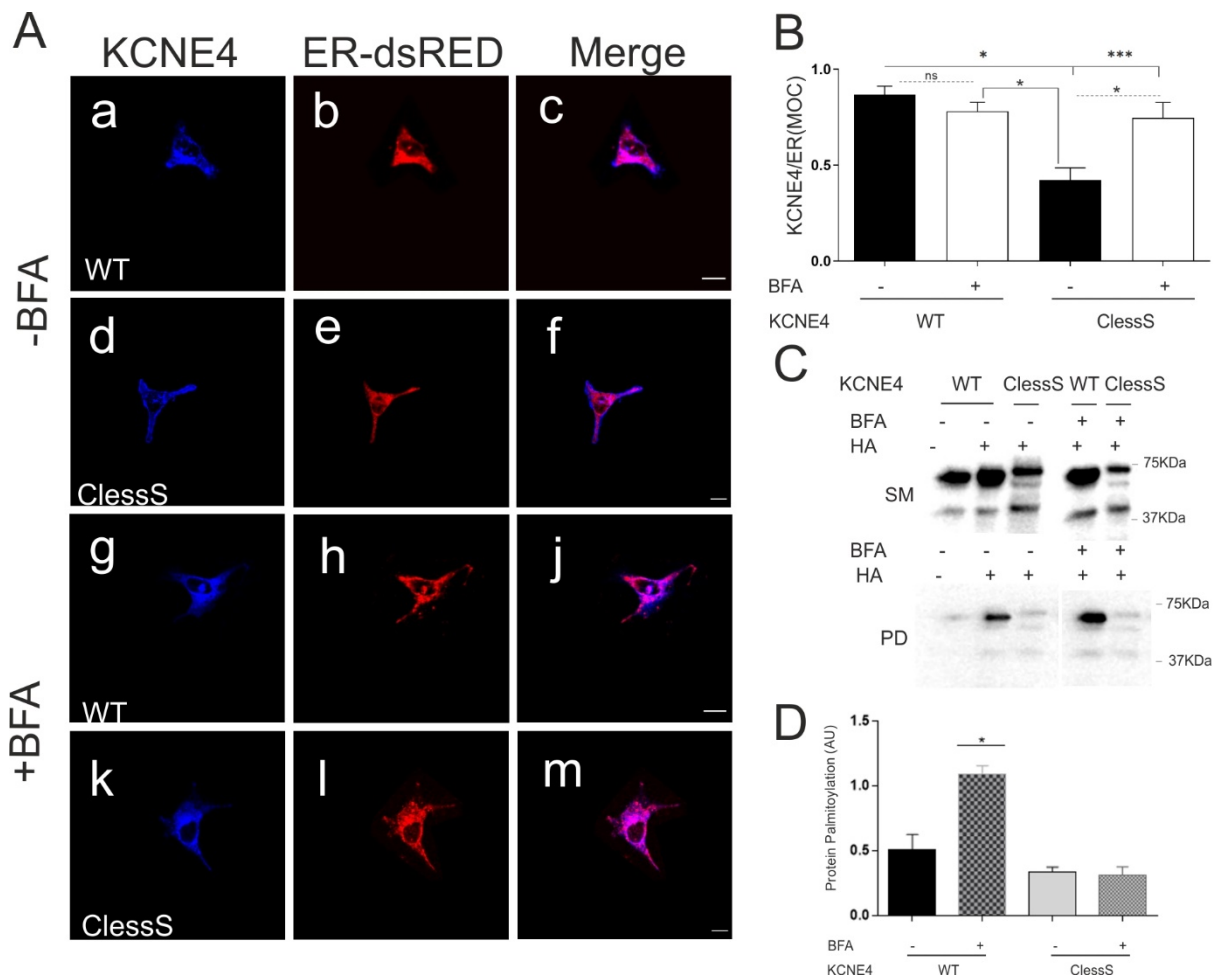
Figure 4. KCNE4 requires S-acylation for a proper ER-membrane anchoring. (A) Confocal analysis of HEK293 cells transfected with KCNE4WT and ClessS. (a-c) KCNE4 WT indicated by blue colour, in absence of BFA treatment; (d-f) KCNE4 ClessS indicated by blue colour, in absence of BFA treatment; (g-j) KCNE4 WT indicated by blue colour, in the presence of Brefeldin-A (BFA) treatment; (k-m) KCNE4 ClessS indicated by blue colour, in the presence of of BFA treatment; merge means colocalizing channels. ER is labelled by dsRED. (B) Quantification of MOCs resulting from 15 cells analysis; ***, p<0.005 (Kruskal-Wallis and Dunn's tests); scale bar represents 10µm. (C) Western blot of two independent rounds of ABE-palmitoylation assay in HEK293, treated or not with BFA and transfected with KCNE4 WT or ClessS. HA; hydroxylamine, SM: starting material, PD: pull down of palmitoylated proteins. (D) Quantification of the two independent rounds; *, p < 0.005 Student's t-test.

presented notable overlapping with the membrane marker in absence of KCNE4 palmitoylation (Fig.6 Ed, Ei, En). Additionally, Fig. 6 F shows approximately a threefold increase of membrane colocalization, when the channel (black bars) was co-transfected with KCNE4ClessS respect to the wild-type protein (white bars).

To support this data, we further analyzed the plasma membrane by performing cell-unroofing preparations (CUPs). As it shown in Fig. 7A, this protocol fixes on a coverslip only the plasma membrane fraction via hypotonic shock, and intensive burst. Samples were analysed by confocal microscopy and the intensity of each protein was quantified. Kv1.3 nicely targets the plasma membrane, thereby we firstly examined the channel distribution, confirming a notable surface expression (Fig.7 B). We next repeated the analysis by co-transfecting KCNE4 WT or ClessS (Fig.7 C) with Kv1.3. In agreement with Fig.6 E-F, Kv1.3 and KCNE4 ClessS targeted the plasma membrane, presenting a threefold increase in the surface distribution (Fig.7 D, E). These results suggested that because the abundance of KCNE4 ClessS in the ER is lower, the intracellular channel retention decreases.

4. Kv1.3 and KCNE4 ClessS would route independently the plasma membrane.
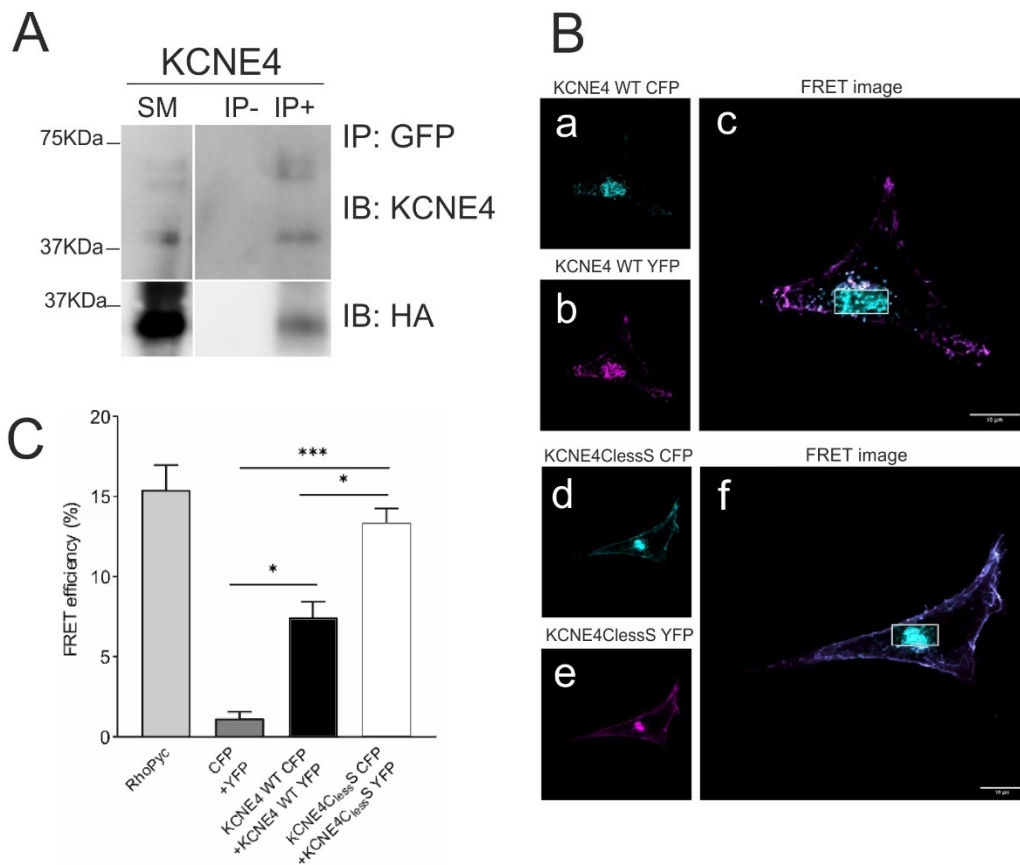
Figure 5. KCNE4 ClessS enhances the formation of dyads. *(*A) Representative western blot of Immunoprecipitation assay in HEK293 cells transfected with KCNE4-CFP and KCNE4-HA. IP: immunoprecipitation of CFP-tagged proteins; SM: starting material collected immunoprecipitation; IB means immunoblots against anti-KCNE4 and anti-HA, the peptides showed association. (B) FRET images of HEK-293 cells transfected with KCNE4-tagged CFP and YFP proteins. The Homo-dimerization was analysed by the FRET acceptor-photobleaching technique. (a, d) Cyan colour labels the donor KCNE4-CFP WT or ClessS; (b, e) magenta indicate the acceptor KCNE4-YFP WT or ClessS; white square highlights a ROI showing FRET images obtained after photobleaching; bars represent 10 µm. (C) Quantification of the FRET efficiency. CFP/YFP, negative control; RhoPyc, positive control; values are mean ± SEM of 15-30 cells. *$p < 0.05$; ***$p < 0.001$ (Kruskal-Wallis test followed by Dunn's multiple comparisons test).

To further corroborate the effects of the palmitoylation of KCNE4 on Kv1.3, we next investigated the channel association by *acceptor photobleaching-FRET* and Patch clamp experiments. Fig. 8A shows that the peak current density elicited by Kv1.3-YFP was 50% lower than in the presence of either KCNE4 subunit. Despite that, Kv1.3 currents, upon co-transfection of KCNE4 ClessS, doubled the pA/pF values obtained by KCNE4 WT (Fig. 8 B). FRET measurements in CUPs (Fig. 9) showed while Kv1.3/KCNE4WT interacted at the plasma membrane level, no physical association was observed between Kv1.3 and KCNE4ClessS. Hence, the proteins reached cell surface independently (Fig.

9 A, B). These results, together with co-immunoprecipitation in Fig. 6 A and B*,* suggested that the mutant binds and retains Kv1.3 intracellularly. Nonetheless, KCNE4ClessS generated twice the Kv1.3 current density respect to the wild-type protein. Thus we would speculate that an amount of unpalmitoylated KCNE4 would escape the ER upon structural reorganizations, targeting the cell surface separately from Kv1.3. This would agree with the idea that, since the intracellular supply of KCNE4 is reduced, the channel retention decreases. Given that KCNE4 suppresses Kv1.3 functions, these data may offer new insights in the channel-related immunotherapy.
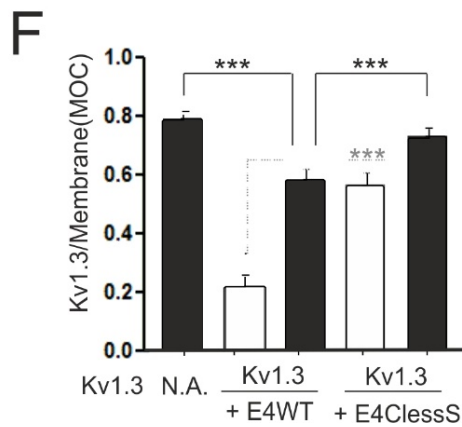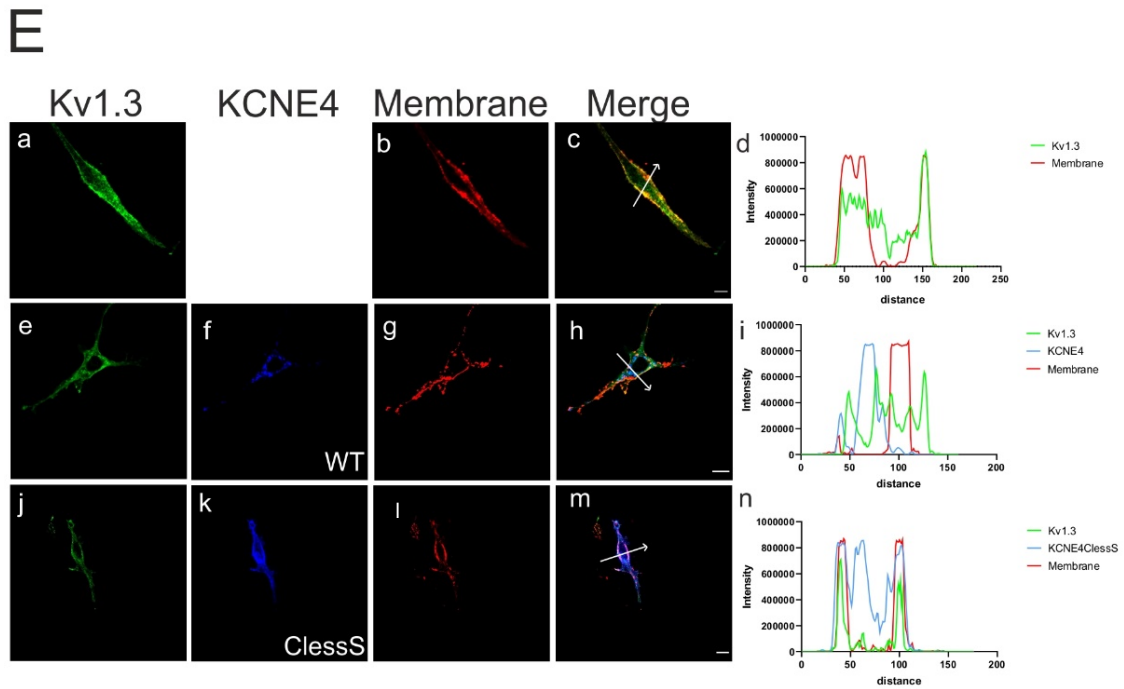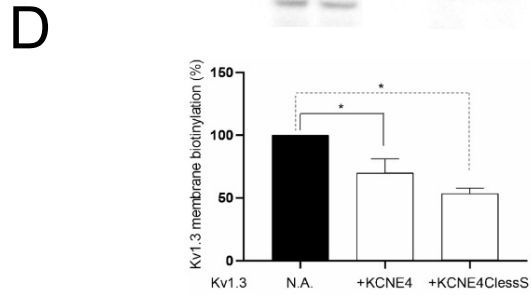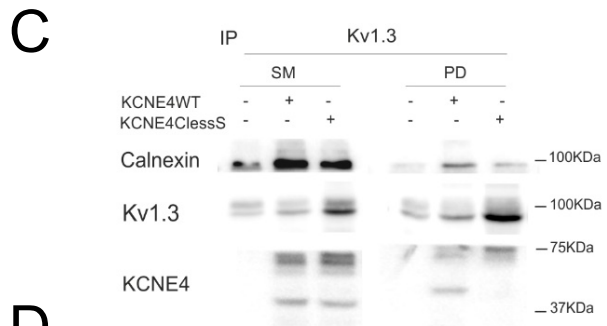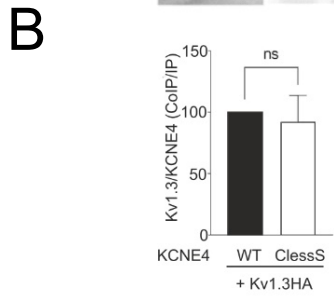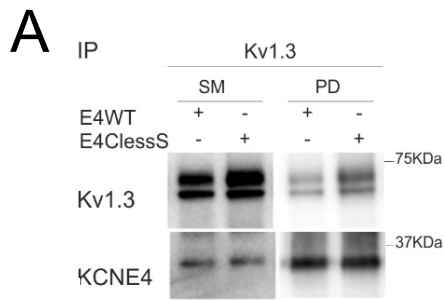
Figure 6. Membrane biotinylation assay and membrane colocalization of Kv1.3, KCNE4 WT and ClessS. (A) Representative western blot of co-immunoprecipitation assay in HEK-293 cells transfected with Kv1.3-pcDNA3 and KCNE4s-CFP. Kv1.3 was the immunoprecipitated (IP) protein; SM: starting material collected before immunoprecipitation; PD: pull-down of immunoprecipitated proteins; IB: immunoblots against Kv1.3 (upper) and KCNE4 (bottom). (B) Quantification of the two rounds. (C) Western blot representing Membrane Biotinylation assay of Kv1.3 in the presence or not of KCNE4 mutants. SM: starting material; PD: pull down of biotinylated proteins; calnexin is used as negative loading control. (D) Quantification of membrane biotinylation, Kv1.3 decreased the membrane expression in the presence of KCNE4ClessS. (E) Membrane colocalization analysis of HEK293 cells transfected with Kv1.3 YFP and KCNE4WT or ClessS-CFP. (a, e, j) Kv1.3 is indicated by green colour; (f, k) KCNE4 WT or ClessS are labelled by blue colour; (b, g, n) membrane is labelled by dsRED; (c, h, m) merge means colocalization between proteins and membrane markers; (d, i, n) pixel-by-pixel analysis of the white arrows. (F) Quantification of the colocalization MOCs resulting from 30 cells analysis; ***, p<0.005 (One-way-Anova, Tukey's multiple comparisons tests); scale bar represents 10µm. Black columns represent Kv1.3; white columns represent the presence of KCNE4 WT, or ClessS.
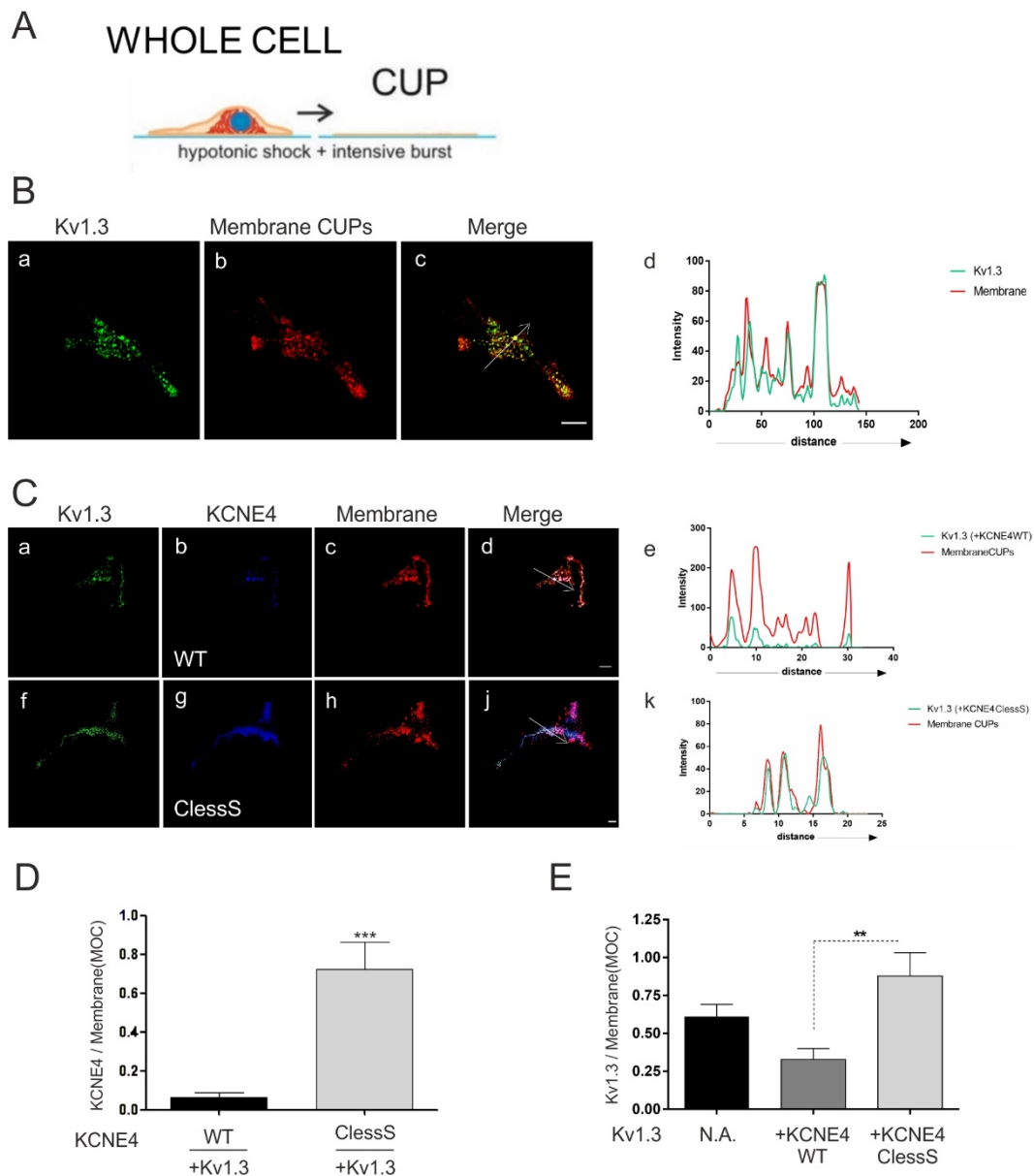
Figure 7. Kv1.3 and KCNE4ClessS enhance the membrane expression in CUPs. (A) Representative cartoon of CUPs protocol. Hypotonic shock and intensive burst leads to plasma membrane isolation. (B) Confocal images of Kv1.3 membrane distribution (a-c) in CUPs resulting from transfected HEK293 cells. The channel is indicated in green, the membrane in red by dsRED. Merge means merged channels. (d) Pixel-by pixel analisys of the white arrow. (C) Confocal images of Kv1.3 membrane distribution (green, a-c) co-transfected or not with KCNE4 WT (blue, a-d) or ClessS (blue, f-j). The membrane-dsRED is indicated in red. Merge: merged channels. (d, e, k) Pixel-by-pixel analyses of Kv1.3 colocalizing with the plasma membrane marker indicates by the white arrows. (D) MOCs resulting from 15-20 cells analysis. ***, p < 0.005 Student's t-test. (E) Quantification of the colocalization by MOCs resulting. ***, p <0.005 (Kruskal-Wallis test followed by Dunn's multiple comparisons test). Scale bars represents 10μm.
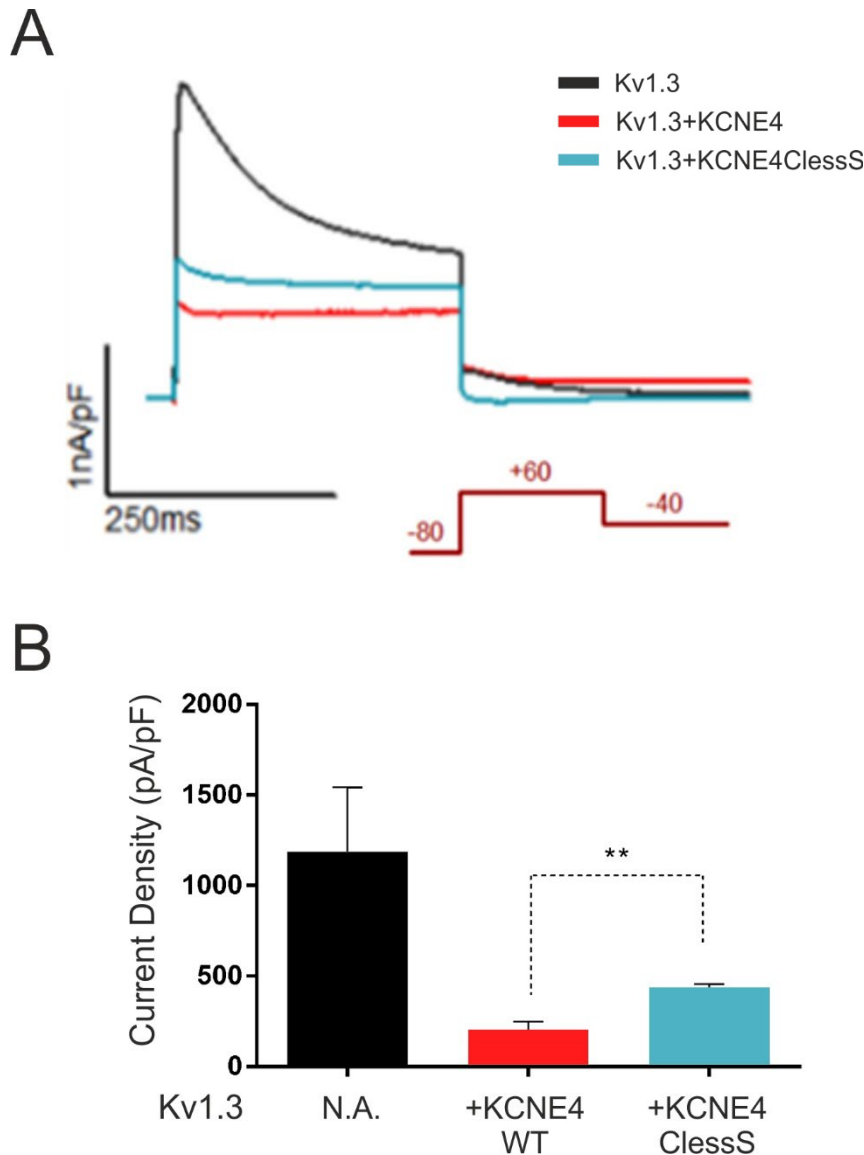
Figure 8. Current density of Kv1.3 in the presence of KCNE4WT or ClessS. Currents were recorded using the whole cell-patch clamp technique, by applying a 250 ms pulse to +60 mV from a holding potential of -80 mV. (A) Representative traces at +60 mV of Kv1.3 currents in the presence or the absence of KCNE4WT or ClessS in HEK293 cells. (B) Quantification of current density measurements; black line indicates Kv1.3; red line is Kv1.3 + KCNE4WT; blue line labels Kv1.3 + KCNE4ClessS. Values are the mean ± SEM of 4 independent cells per condition **, p < 0.01 Kv1.3_KCNE4WT vs Kv1.3_KCNE4 ClessS (Students t test).

5. KCNE4 and Kv1.3 in antigen presenting (APCs) cells.

Kv1.3 is an essential component of the immune response, in particular in CCR7-deficient effector memory T cells, during activation (*42*). The physiology of both T-cells and antigen-presenting cells (APCs), such as dendritic cells and macrophages, depends on Kv1.3 functioning (*43*).

DCs nicely express KCNE4 (*44*), whose alteration may result in a number of clinical disease, including colon adenocarcinoma and idiopathic pulmonary arterial hypertension (*45*) (*46*) (*47*). Hence, we
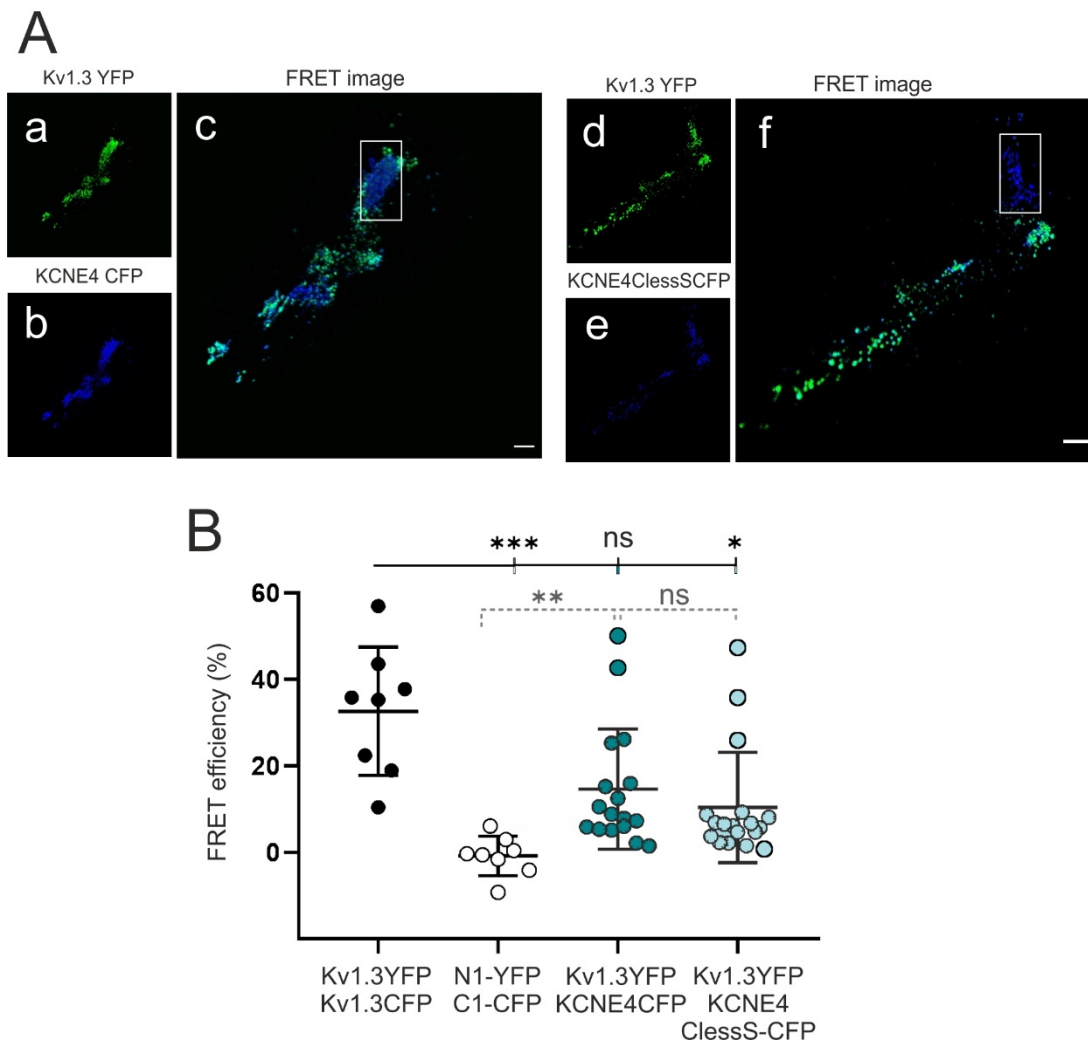
Figure 9. Molecular interaction of Kv1.3 with KCNE4 WT and ClessS. (A) Representative confocal and FRET images of HEK-293 cells transfected with Kv1.3-tagged YFP and KCNE4-tagged CFP proteins. (a, d) Green colour labelled the acceptor molecule, Kv1.3-YFP; (b, e) blue colour indicates the donor molecule, KCNE4 CFP. The Homo-dimerization was analysed by the FRET acceptor-photobleaching technique. (c, f) White square highlights a ROI showing FRET images obtained after photobleaching; bars represent 10 μm. (B) Quantification of the FRET efficiency. CFP/YFP is the negative control; Kv1.3YFP-Kv1.3CFP tetramers were used as positive control. Values are mean ± SEM of 8-20 cells. *$p < 0.05$; ***$p < 0.001$ (Kruskal-Wallis followed by Dunn's multiple comparisons tests).

wondered how expression and membrane traffic of Kv1.3-KCNE4 complexes behaved during immune cell activation. We used CY15 DCs, a model of immature DCs developed from a malignant murine histiocytic tumour (*28*). CY15 cell were activated with 100 ng/mL of LPS. Twenty-four h later, extended cell dendrites and higher expression of inducible nitric oxide synthase (iNOS) were observed (Fig. 10 A, B). These features pointed to a clear cell activation. Moreover, in accordance to earlier laboratory findings, we tested the expression of KCNE4 and Kv1.3. Unlike KCNE4, cell activation increased Kv1.3 expression. Since the quantity of

KCNE4 remained constant (Fig. 10B), we next evaluated the effects of LPS-activation on the proteins hetero-oligomerization and the plasma membrane trafficking. Co-immunoprecipitation of Kv1.3 and KCNE4 in activated or immature CY15 cells showed a comparable protein association under both conditions (Fig. 10C). Therefore, the LPS treatment did not alter the protein association. Thus, we checked the membrane colocalization by staining cells against nuclei, plasma membrane, KCNE4 and Kv1.3 (Fig. 10D). Panels in Fig. 10 De, Dl highlighted a mask of colocalization between KCNE4 and Kv1.3 (KCNE4-Kv1.3). We used this mask to quantify the membrane
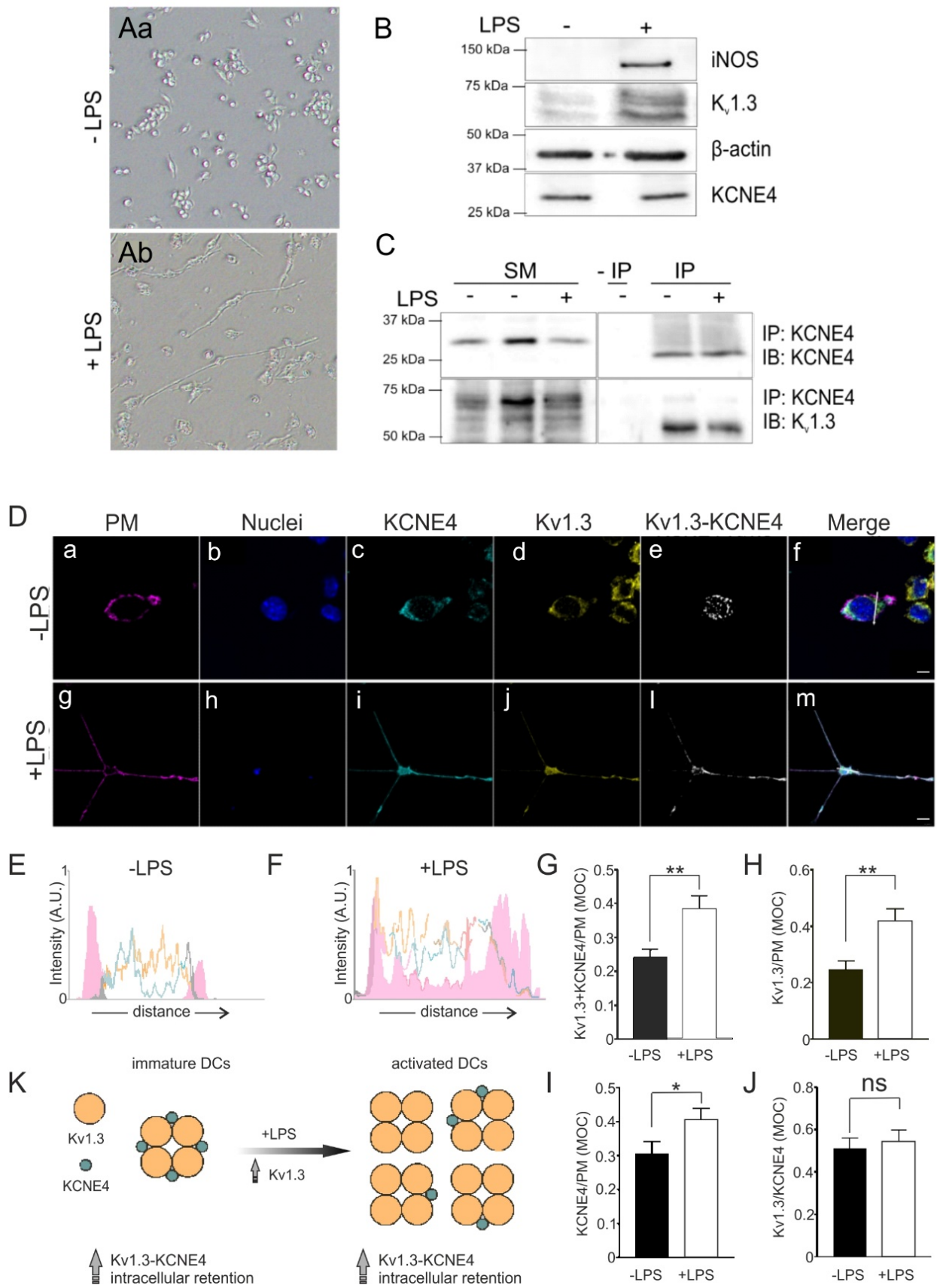
Figure 10. Kv1.3/KCNE4 in CY15 dendritic cells. (A) Optical microscopy images displaying cell morphology changes between immune cells. (Aa) Immature DCs; (Ab)LPS-activated DCs. (B) Representative western blot showing iNOS, KCNE4 and Kv1.3 expression in CY15 in the presence (+) and absence (-) of LPS; β-actin was used as a loading control. (C) Western blot showing co-immunoprecipitation of Kv1.3 and KCNE4 in CY15 dendritic cells treated (+) or not (-) with LPS. IP: Cells immunoprecipitated against KCNE4; IB: immunoblots against KCNE4 and Kv1.3; SM: starting materials; IP: immunoprecipitation; IP-: immunoprecipitation in the absence of KCNE4 antibody. (D) Membrane colocalization analysis of Kv1.3 and KCNE4 in immature or activated CY15. (a-f) Membrane trafficking of YFP-labelled Kv1.3 and CFP-labelled KCNE4 in absence of (-) LPS treatment; (g-m) Membrane trafficking of YFP-labelled Kv1.3 and CFP-labelled KCNE4 in the presence of (+) LPS treatment. The plasma membrane (PM) was labelled by WGA in magenta colour, while nuclei by DAPI in blue colour. (E, F) Pixel-by-pixel analysis of the white arrows; scale bars represent 5 μm; KCNE4-Kv1.3 represents the overlap points between the Kv1.3 and KCNE4 signals; merged panels show colocalization between channels, excluding KCNE4-Kv1.3 overlapping spots. (G) MOCs indicate the fraction of Kv1.3- KCNE4 complexes colocalizing with PM. (H, I) MOCs resulting from individual Kv1.3 and KCNE4, colocalizing with the PM. (J) Quantification of KCNE4 MOCs colocalizing with Kv1.3. Values are mean ± SEM of n > 20 cells; ns, no significant (p>0.05), * p<0.01 vs -LPS (Student's t-Test). (K) Cartoon representing how the increase of Kv1.3 expression in activated CY15 would affect KCNE4's capacity to retain Kv1.3-KCNE4 complexes intracellularly. A decreased KCNE4/Kv1.3 ratio upon cell activation would increase the plasma membrane trafficking of these complexes.

portion of KCNE4 overlapping Kv1.3. Although the single proteins and complexes appeared mostly intracellular in the absence of LPS (Fig. 10E), the membrane distribution of both individual KCNE4, Kv1.3, and hetero-oligomers significantly increased after 24h of treatments (Fig. 10D, Fig. 10 F-I). These findings agreed with a recent publication from the laboratory, demonstrating that a noticeable amount of Kv1.3 escapes the KCNE4-related Kv1.3 intracellular retention during cell activation, because of alterations in their relative expression (*27*). In this case, no changes in KCNE4/Kv1.3 association were observed (Fig. 10J), implying that the majority of KCNE4 molecules are bound to Kv1.3, prior to proteins delivery. Taking all this in mind, we suggest that the LPS activation may lead to an increment of the Kv1.3/KCNE4 ratio and this would result in a lower fraction of KCNE4 subunits bound to each Kv1.3 complex (Fig. 10K). In this scenario, the bigger amount of Kv1.3 tetramers would bypass the ER-retention mediated by KCNE4, increasing in turn the forward trafficking.

Considering the higher membrane targeting of Kv1.3/KCNE4 complexes and the channel participation in immunological synapses (IS) formation, we finally studied the presence of KCNE4 in these spots. We performed cell conjugates between human monocytes-derived dendritic cells (moDCs) and an engineered Jurkat-T cells line presenting a TCR specific to the MHC-epitope complex, used to improve T cell-APC recognition. Particularly, it recognizes the tumor-selective cancer testis antigen

1A (NY-ESO1), classified as one of the most immunogenic cancer/testis antigens (*48*). For this purpose, we isolated blood human monocytes and induced the dendritic cell differentiation (moDCs) (*43*), confirming KCNE4 expression (Fig. 11A). Next, we performed cell conjugates by treating cells with LPS, in the presence or not of NY-ESO1. When APCs contact a T-cell TCR, the tubulin cytoskeleton undergoes structural changes, promoting the translocation of the microtubule-organizing center MTOC toward the IS region (*49*). Moreover, phalloidin, a toxic cyclopeptide produced by the green mushroom *Amanita phalloides*, may accumulates at the interface between T- and B-cells by binding the F-actin filaments (*50*). Thus, we used those structures as synapses detectors, considering cells incubated with single LPS (+LPS) as negative control, since they lack of the specific antigen recognized by these engineered Jurkat cells. According to that, we observed mostly contacting cells without neither MTOC organization nor aggregation of phalloidin in +LPS-samples (Fig. 11 Ba-Bd). Otherwise, upon LPS and NY-ESO1 treatments (+LPS+NY-ESO1), Jurkat NYESO1-TCRs recognized the antigen and the majority of cells showed MTOC polarization and phalloidin clustering (Fig. 11 Be-Bh), with a lower distance between the MTOC and the IS region, as well as a major aggregation of phalloidin (Fig. 11 C and D). Thus, we selected cells forming immunological spots and analysed the KCNE4 intensity at the immune interface. Our results indicated that, despite the major membrane targeting of KCNE4/Kv1.3 hetero-

oligomers, KCNE4 did not target the IS (Fig. 11E). Given that IS regions are enriched in lipid-rafts, this result would be in agreement with published data showing that KCNE4 impairs the targeting of Kv1.3 to these domains and to the IS in KCNE4 overexpressing T-cells (*44*).
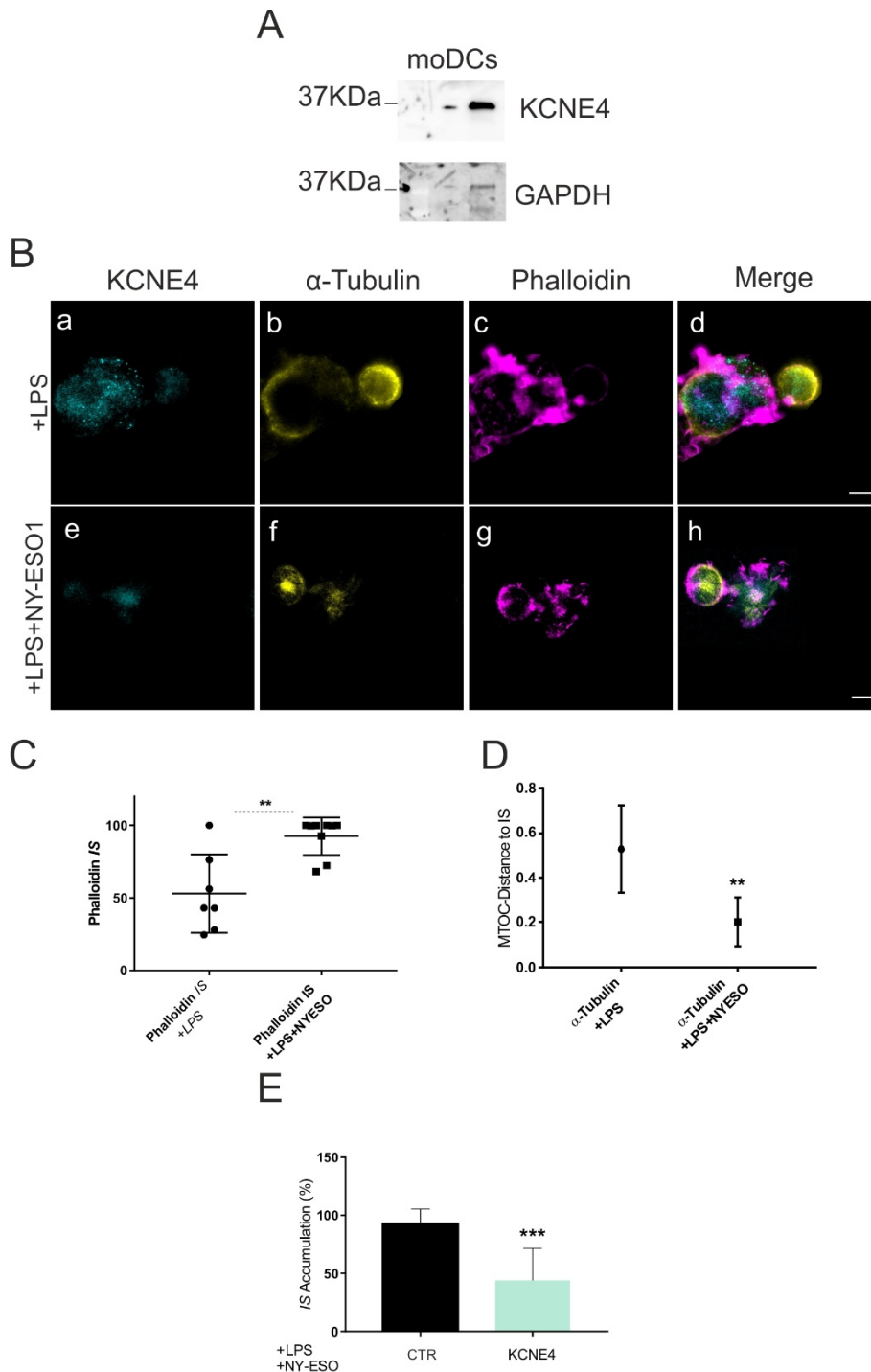
Figure 11. KCNE4 distribution at immunological synapses (IS). (A) Western blot showing KCNE4 expression in human monocytes blood-derived dendritic cells (moDCs); GAPDH was used as positive loading control. (A) Confocal images of cell conjugates between moDCs and Jurkat cells in the presence of LPS (a-d) or in the presence of LPS and NY-ESO-1 (e-h), indicating immunological synapses formation; yellow colour indicates the α-tubulin staining the MTOC complex of moDCs; endogenous KCNE4 is labelled in cyan; magenta shows phalloidin, used as membrane marker. +LPS treatment generated simple contacting cells, lacking the MTOC complex organization and presenting a homogenous distribution of phalloidin; +LPS+NY-ESO-1 treatments gave rise to IS formation, showing both organized-MTOCs closed the immune cluster, and accumulation of phalloidin at the interface between cells. (B, C) Quantification of IS formation; the lower MTOC distance to the IS (B) corresponded to the largest Phalloidin accumulation (C) upon LPS and NY-ESO-1 incubations. (D) Quantification of KCNE4 accumulation considering the cells analysed in B and C; values are mean from two different healthy donors. ** p<0.05, *** p<0.005 (Students t test).

Discussion

The transmembrane regulatory subunit KCNE4 underwent S-acylation at the two C-terminal cysteines and this modification controls the subcellular localization of the protein. KCNE4 interacts with Kv1.3 via the C-terminus of both proteins and, upon association, Kv1.3 currents are drastically reduced. Moreover, the channel surface expression is impaired by a strong ER-retention (33) (44). In this work, we demonstrated that the absence of KCNE4 palmitoylation directly affects the cellular fate of the peptide and, in turn, the downregulation on Kv1.3. In addition to protein's anchoring to the cellular membranes, palmitoylation is known to alter the homodimerization (51) and steric hindrance of peptides (52) (53) (54). Our FRET experiments suggested that the absence of palmitate would expose the structural motifs involved in the oligomerization of KCNE4. On the other hand, the stability of the large, disordered, C-terminal domain would be compromised, promoting the plasma membrane targeting of the subunit. We found that in absence of palmitoylation, the association with Kv1.3 was not altered, concomitant with a notable increment in the channel membrane expression. However, despite showing significant differences with the wild-type protein, KCNE4 ClessS retained Kv1.3 intracellularly leading to a remarkable decrease in the current density. This apparent controversy was clarified by analysing the subcellular trafficking of Kv1.3 / KCNE4 heteroligomers. We demonstrated that no bipartite complexes are formed at the plasma membrane in absence of KCNE4 palmitoylation. Therefore, the fraction of unpalmitoylated KCNE4 that associates with Kv1.3, at initial stages of protein biogenesis, retained the channel intracellularly and the complex did not reach the cell surface. Collecting those data, we suggest a dynamic mechanism controlling the physiology of KCNE4 (Fig.12). In leukocytes, palmitoylated KCNE4 is stable at the ER membrane, thanks to the ER retention motifs (ERRMs) and the palmitate-anchoring (A). In this context, the KCNE4-mediated intracellular retention of Kv1.3 is enhanced (55). In absence of palmitoylation (B), KCNE4 would act in two parallel ways. First (Ba), KCNE4 increases the dimerization rate. Second (Bb), the large COOH-undocking causes the plasma membrane trafficking of unpalmitoylated KCNE4, reducing the ER abundance of the peptide. As a consequence of these modulations, the Kv1.3 ER retention decreases (C). The selective upregulation of Kv1.3 has been under study during several years (56). Considering the wide range of tissues expressing the channel, alteration of its activity may participate in a number of pathological conditions, such as rheumatoid arthritis, systemic lupus erythematosus or multiple sclerosis (57) (58) (59). Kv1.3 is recruited to lipid-rafts in T-lymphocytes and redistributed to these domains during calcium signalling, providing the electrochemical driving force required for a proper cell activation and consequent cytokines production (60) (61). KCNE4, highly expressed in leukocytes, stands out as an inhibitory subunit, altering the lipid-rafts association of Kv1.3 (44). Therefore, understanding the conformational organization of this channelosome during immunological processes is physiologically relevant. Our results, accordingly to previous publications, showed that unlike KCNE4, Kv1.3 increased its expression upon LPS activation in antigen presenting cells, as well as its membrane distribution, both associated or not with KCNE4. We postulate that by elevating the abundance of Kv1.3 tetramers the forward traffic enhances by escaping the ER-retention mediated by KCNE4. After all, the fraction of KCNE4 binding Kv1.3 targets the cell surface in complex with the channel, since the interaction occurs during early secretory pathways, prior to proteins delivery. Despite that, preliminarily cell-conjugates analyses between human dendritic and Jurkat cells expressing endogenous Kv1.3 and KCNE4, suggests that the subunit did not localize at the immunological synapses, which would be consistent with the importance of the Kv1.3 recruitment to lipid-rafts during immune signalling.

In this context, protein acylation is essential for the membrane inclusion of different immunological partners upon activation, such as the Calcium release-activated calcium channel ORAI1 protein 1, and the ER-resident protein stromal interaction STIM1 molecule 1 (62) (63). Here we highlighted the importance of the modification within the Kv1.3's interactome, also crucial for a proper immune response. Based on our data, it is tempting to speculate that in the presence of stimuli requiring the Kv1.3 lipid-rafts targeting, the S-acylation of KCNE4 would decrease. KCNE4 is S-acylated in CY15 cells (Supp. Fig.2) and the mechanism would decrease upon cell maturation. Even if those data need further analyses, we figure out that during leukocytes activation, the metabolism of cells may be dynamically shifted either against or in favour of KCNE4 palmitoylation, since the absence of the modification leads to a more efficient plasma membrane targeting of Kv1.3. Nonetheless, additionally data are necessary to confirm this theory. Overall, this work pointed to the KCNE4 S-acylation as a potential new target for the immunotherapy against Kv1.3, highlighting important effects on the α- and β-subunits association, during immunological pathways.
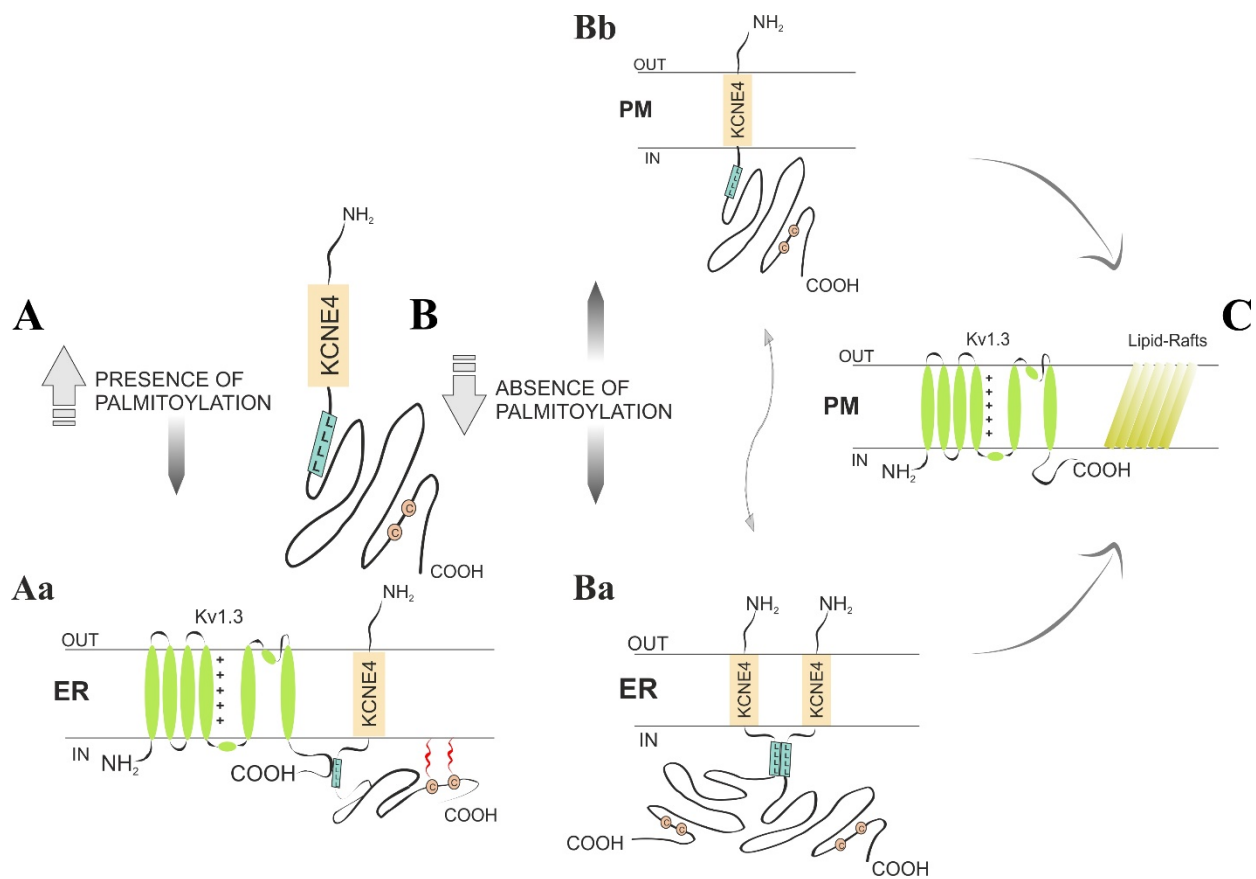
Figure 12. Effects of palmitoylation on KCNE4 subcellular targeting. Cartoon summarizing the KCNE4 modulation by S-acilatyon. (A) Under physiological conditions, KCNE4 subunit is palmitoylated, residing at the Endoplasmic Reticulum (ER) membrane. (Aa) The tight anchoring of the protein's C-terminal disordered (COOH) domain results in the impairment of Kv1.3-forward trafficking. (B) The absence of palmitate molecules to KCNE4 cysteine chains causes conformational changes leading to multiple effects. (Ba) Unpalmitoylated-KCNE4 exposes the structural elements required for dimers formation, enhancing the protein oligomerization. (Bb) When palmitate additions are lacking, the KCNE4 C-terminus anchorage is lost. The relative spatial reorganization induces the plasma membrane targeting of the subunit by hiding the ER-retention motifs of the peptide. (C) The previous modulations resulted in smaller number of KCNE4 monomers available for hetero-oligomerization with Kv1.3 and consequent intracellular retention.

Bibliography

1. L. W. C. Chow, Y. M. Leung, The versatile Kv channels in the nervous system: actions beyond action potentials. *Cell Mol Life Sci* **77**, 2473-2482 (2020).

2. S. Baekkeskov, J. Kanaani, Palmitoylation cycles and regulation of protein function (Review). *Mol Membr Biol* **26**, 42-54 (2009).

3. Z. P. Feng, M. I. Arnot, C. J. Doering, G. W. Zamponi, Calcium channel beta subunits differentially regulate the inhibition of N-type channels by individual Gbeta isoforms. *J Biol Chem* **276**, 45051-45058 (2001).

4. G. Panyi, Z. Varga, R. Gáspár, Ion channels and lymphocyte activation. *Immunol Lett* **92**, 55-66 (2004).

5. A. V. Krishnan, M. C. Kiernan, Sustained-release fampridine and the role of ion channel dysfunction in multiple sclerosis. *Mult Scler* **19**, 385-391 (2013).

6. A. Serrano-Albarrás, S. Cirera-Rocosa, D. Sastre, I. Estadella, A. Felipe, Fighting rheumatoid arthritis: Kv1.3 as a therapeutic target. *Biochem Pharmacol* **165**, 214-220 (2019).

7. P. Bradding, H. Wulff, The K+ channels K(Ca)3.1 and K(v)1.3 as novel targets for asthma therapy. *Br J Pharmacol* **157**, 1330-1339 (2009).

8. G. C. Bett, R. L. Rasmusson, Modification of K+ channel-drug interactions by ancillary subunits. *J Physiol* **586**, 929-950 (2008).

9. J. Capera, C. Serrano-Novillo, M. Navarro-Pérez, S. Cassinelli, A. Felipe, The Potassium Channel

Odyssey: Mechanisms of Traffic and Membrane Arrangement. *Int J Mol Sci* **20**, (2019).

10. L. H. Chamberlain, M. J. Shipston, G. W. Gould, Regulatory effects of protein S-acylation on insulin secretion and insulin action. *Open Biol* **11**, 210017 (2021).

11. J. P. Mitchell, R. J. Carmody, NF-κB and the Transcriptional Control of Inflammation. *Int Rev Cell Mol Biol* **335**, 41-84 (2018).

12. J. Hu, L. Zhang, X. Liu, Role of Post-translational Modifications in Influenza A Virus Life Cycle and Host Innate Immune Response. *Front Microbiol* **11**, 517461 (2020).

13. L. Tian *et al.*, Palmitoylation gates phosphorylation-dependent regulation of BK potassium channels. *Proc Natl Acad Sci U S A* **105**, 21006-21011 (2008).

14. F. Tang *et al.*, Palmitoyl transferases act as potential regulators of tumor-infiltrating immune cells and glioma progression. *Mol Ther Nucleic Acids* **28**, 716-731 (2022).

15. D. A. Mitchell, A. Vasudevan, M. E. Linder, R. J. Deschenes, Protein palmitoylation by a family of DHHC protein S-acyltransferases. *J Lipid Res* **47**, 1118-1127 (2006).

16. C. Gök *et al.*, Dynamic Palmitoylation of the Sodium-Calcium Exchanger Modulates Its Structure, Affinity for Lipid-Ordered Domains, and Inhibition by XIP. *Cell Rep* **31**, 107697 (2020).

17. S. Zeng *et al.*, Inhibition of Fatty Acid Translocase (FAT/CD36) Palmitoylation Enhances Hepatic Fatty Acid β-Oxidation by Increasing Its Localization to Mitochondria and Interaction with Long-Chain Acyl-CoA Synthetase 1. *Antioxid Redox Signal* **36**, 1081-1100 (2022).

18. S. K. Pierce, Lipid rafts and B-cell activation. *Nat Rev Immunol* **2**, 96-105 (2002).

19. A. Carreras-Sureda *et al.*, S-acylation by ZDHHC20 targets ORAI1 channels to lipid rafts for efficient Ca. *Elife* **10**, (2021).

20. M. J. Shipston, Ion channel regulation by protein palmitoylation. *J Biol Chem* **286**, 8709-8716 (2011).

21. G. W. Abbott, Control of Biophysical and Pharmacological Properties of Potassium Channels by Ancillary Subunits. *Handb Exp Pharmacol* **267**, 445-480 (2021).

22. S. Feske, H. Wulff, E. Y. Skolnik, Ion channels in innate and adaptive immunity. *Annu Rev Immunol* **33**, 291-353 (2015).

23. S. Chhabra *et al.*, Kv1.3 channel-blocking immunomodulatory peptides from parasitic worms: implications for autoimmune diseases. *FASEB J* **28**, 3952-3964 (2014).

24. R. Vicente *et al.*, Pattern of Kv beta subunit expression in macrophages depends upon proliferation and the mode of activation. *J Immunol* **174**, 4736-4744 (2005).

25. L. Solé, A. Felipe, Does a physiological role for KCNE subunits exist in the immune system? *Commun Integr Biol* **3**, 166-168 (2010).

26. L. Solé *et al.*, KCNE gene expression is dependent on the proliferation and mode of activation of leukocytes. *Channels (Austin)* **7**, 85-96 (2013).

27. A. Vallejo-Gracia *et al.*, KCNE4-dependent functional consequences of Kv1.3-related leukocyte physiology. *Sci Rep* **11**, 14632 (2021).

28. T. Kammertoens *et al.*, CY15, a malignant histiocytic tumor that is phenotypically similar to immature dendritic cells. *Cancer Res* **65**, 2560-2564 (2005).

29. N. Decher *et al.*, Structural determinants of Kvbeta1.3-induced channel inactivation: a hairpin modulated by PIP2. *EMBO J* **27**, 3164-3174 (2008).

30. J. Greaves, J. A. Carmichael, L. H. Chamberlain, The palmitoyl transferase DHHC2 targets a dynamic membrane cycling pathway: regulation by a C-terminal domain. *Mol Biol Cell* **22**, 1887-1895 (2011).

31. S. Bolte, F. P. Cordelières, A guided tour into subcellular colocalization analysis in light microscopy. *J Microsc* **224**, 213-232 (2006).

32. T. Zimmermann, Photobleaching and Sensitized Emission-Based Methods for the Detection of Förster Resonance Energy Transfer. *Methods Mol Biol* **2040**, 235-274 (2019).

33. M. Grunnet *et al.*, KCNE4 is an inhibitory subunit to Kv1.1 and Kv1.3 potassium channels. *Biophys J* **85**, 1525-1537 (2003).

34. F. Sievers *et al.*, Fast, scalable generation of high-quality protein multiple sequence alignments using Clustal Omega. *Mol Syst Biol* **7**, 539 (2011).

35. L. Solé *et al.*, The C-terminal domain of Kv1.3 regulates functional interactions with the KCNE4 subunit. *J Cell Sci* **129**, 4265-4277 (2016).

36. M. Jansen, B. Beaumelle, How palmitoylation affects trafficking and signaling of membrane receptors. *Biol Cell* **114**, 61-72 (2022).

37. T. Zeppelin, K. B. Pedersen, N. A. Berglund, X. Periole, B. Schiøtt, Effect of palmitoylation on the dimer formation of the human dopamine transporter. *Sci Rep* **11**, 4164 (2021).

38. L. R. Bollu *et al.*, Intracellular activation of EGFR by fatty acid synthase dependent palmitoylation. *Oncotarget* **6**, 34992-35003 (2015).

39. S. R. Roig *et al.*, Calmodulin-dependent KCNE4 dimerization controls membrane targeting. *Sci Rep* **11**, 14046 (2021).

40. H. M. Nguyen *et al.*, Biophysical basis for Kv1.3 regulation of membrane potential changes induced by P2X4-mediated calcium entry in microglia. *Glia* **68**, 2377-2394 (2020).

41. P. Selvakumar *et al.*, Structures of the T cell potassium channel Kv1.3 with immunoglobulin modulators. *Nat Commun* **13**, 3854 (2022).

42. M. P. Matheu *et al.*, Imaging of effector memory T cells during a delayed-type hypersensitivity

reaction and suppression by Kv1.3 channel block. *Immunity* **29**, 602-614 (2008).

43. M. Hiasa *et al.*, GM-CSF and IL-4 induce dendritic cell differentiation and disrupt osteoclastogenesis through M-CSF receptor shedding by up-regulation of TNF-alpha converting enzyme (TACE). *Blood* **114**, 4517-4526 (2009).

44. L. Solé *et al.*, KCNE4 suppresses Kv1.3 currents by modulating trafficking, surface expression and channel gating. *J Cell Sci* **122**, 3738-3748 (2009).

45. D. Li, Z. Liu, X. Ding, Z. Qin, AEBP1 Is One of the Epithelial-Mesenchymal Transition Regulatory Genes in Colon Adenocarcinoma. *Biomed Res Int* **2021**, 3108933 (2021).

46. G. Mondéjar-Parreño, A. Cogolludo, F. Perez-Vizcaino, Potassium (K. *Pharmacol Ther* **225**, 107835 (2021).

47. M. Hundt *et al.*, Palmitoylation-dependent plasma membrane transport but lipid raft-independent signaling by linker for activation of T cells. *J Immunol* **183**, 1685-1694 (2009).

48. A. Ibukić *et al.*, Expression and Prognostic Significance of PD-L1 and NY-ESO1 in Gallbladder Carcinoma. *In Vivo* **37**, 1828-1837 (2023).

49. N. Blas-Rus, E. Bustos-Morán, F. Sánchez-Madrid, N. B. Martín-Cófreces, Analysis of Microtubules and Microtubule-Organizing Center at the Immune Synapse. *Methods Mol Biol* **1584**, 31-49 (2017).

50. E. M. Hiltbold, N. J. Poloso, P. A. Roche, MHC class II-peptide complexes and APC lipid rafts accumulate at the immunological synapse. *J Immunol* **170**, 1329-1338 (2003).

51. Z. Ma *et al.*, Molecular mechanism of CD44 homodimerization modulated by palmitoylation and membrane environments. *Biophys J* **121**, 2671-2683 (2022).

52. P. S. Park *et al.*, Modulation of molecular interactions and function by rhodopsin palmitylation. *Biochemistry* **48**, 4294-4304 (2009).

53. S. Y. Wu, M. D. Pérez, P. Puyol, L. Sawyer, beta-lactoglobulin binds palmitate within its central cavity. *J Biol Chem* **274**, 170-174 (1999).

54. D. Fessas, S. Iametti, A. Schiraldi, F. Bonomi, Thermal unfolding of monomeric and dimeric beta-lactoglobulins. *Eur J Biochem* **268**, 5439-5448 (2001).

55. T. Wada, T. Akagi, Role of the Leucine Zipper Domain of CCAAT/ Enhancer Binding Protein-Epsilon (C/EBPε) in Neutrophil-Specific Granule Deficiency. *Crit Rev Immunol* **36**, 349-358 (2016).

56. T. E. DeCoursey, K. G. Chandy, S. Gupta, M. D. Cahalan, Voltage-gated K+ channels in human T lymphocytes: a role in mitogenesis? *Nature* **307**, 465-468 (1984).

57. Y. Wang *et al.*, A bioengineered probiotic for the oral delivery of a peptide Kv1.3 channel blocker to treat rheumatoid arthritis. *Proc Natl Acad Sci U S A* **120**, e2211977120 (2023).

58. M. Khodoun *et al.*, Targeted knockdown of Kv1.3 channels in T lymphocytes corrects the disease manifestations associated with systemic lupus erythematosus. *Sci Adv* **6**, (2020).

59. H. Rus *et al.*, The voltage-gated potassium channel Kv1.3 is highly expressed on inflammatory infiltrates in multiple sclerosis brain. *Proc Natl Acad Sci U S A* **102**, 11094-11099 (2005).

60. J. Bock, I. Szabó, N. Gamper, C. Adams, E. Gulbins, Ceramide inhibits the potassium channel Kv1.3 by the formation of membrane platforms. *Biochem Biophys Res Commun* **305**, 890-897 (2003).

61. I. Markakis *et al.*, Kv1.3 Channel Up-Regulation in Peripheral Blood T Lymphocytes of Patients With Multiple Sclerosis. *Front Pharmacol* **12**, 714841 (2021).

62. S. J. West *et al.*, S-acylation of Orai1 regulates store-operated Ca2+ entry. *J Cell Sci* **135**, (2022).

63. G. Kodakandla *et al.*, Dynamic S-acylation of the ER-resident protein stromal interaction molecule 1 (STIM1) is required for store-operated Ca. *J Biol Chem* **298**, 102303 (2022).
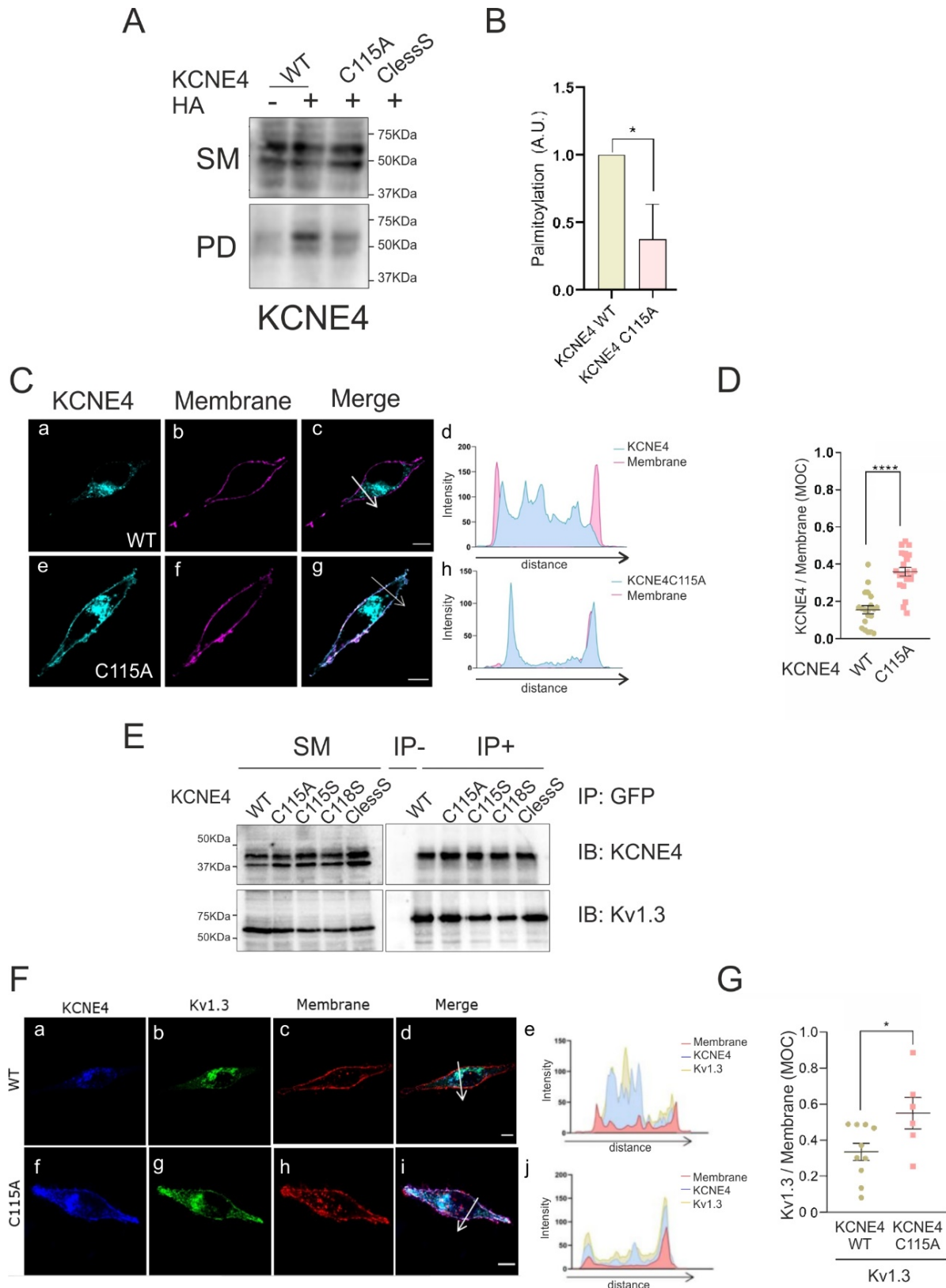
Supplementary figure 1. KCNE4 single cysteine mutants and Kv1.3 association. (A) ABE-palmitoylation assay in HEK293 cells transfected with KCNE4 WT, C115A and ClessS. +/- HA, presence or absence of Hydroxylamine respectively; SM: Starting Material; PD: Pull down of palmitoylated proteins. (B) Quantification of KCNE4 relative palmitoylation; values are means ± S.E. of three different experiments; *p < 0.05; **p < 0.01 (one-way ANOVA-Tukey tests). (C) Confocal images of membrane colocalization analisys in HEK293 cells transfected with KCNE4 WT and C115A mutant. (a-c) CFP-KCNE4 WT is labelled by cyan colour; (e-g) CFP-KCNE4 C115A indicated in cyan; membrane-dsRED is labelled by magenta colour; merge means overlapping channels; scale bars represent 10 µm. (d, h) Pixel-by-pixel analysis of the merged channels, the selected sections are indicated by white arrows. (D) Quantification of MOCs calculating the amount of KCNE4 signals overlapping the membrane-dsRED; values are mean ± S.E.M. of 10-20 cells. KCNE4 alanine-mutant targeted the plasma membrane with a two-fold increase respect to the wild-type protein. (E) Western blot representing immunoprecipitation of KCNE4s-CFP in HEK-293 cells, co-transfected with Kv1.3-HA. SM: starting material collected immunoprecipitation; IP: immunoprecipitation of GFP-tagged proteins; IB: immunoblot against KCNE4 and Kv1.3 antibodies; IP- indicates immunoprecipitation in absence of GFP-antibodies. (F) Membrane colocalization analisys of HEK293 cells transfected with Kv1.3-YFP and KCNE4-CFP. (a, f) Blue colour showing KCNE4 and mutants; (b, g) Green colour indicating the channel; (c, h) plasma membrane is labelled by ds-RED; (d, i) merge means colocalizing channels; (e, j) pixel-by-pixel analysis of the white arrows, showing the distribution of KCNE4 and Kv1.3 along the plasma membrane; scale bars represent 10 µm. (G) MOCs are mean ± S.E.M. of 6-10 cells, indicating the portion of Kv1.3 signals colocalizing with KCNE4; *p<0.05 (Student's t-Test) vs WT.
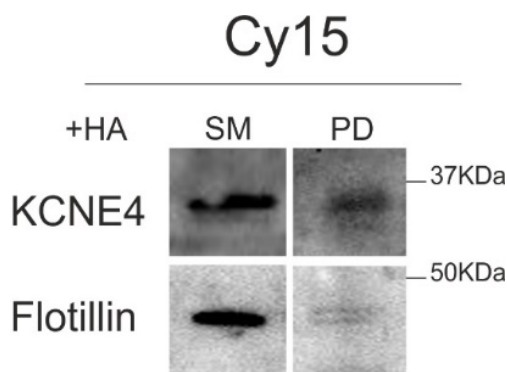
Supplementary Figure 2. KCNE4 is palmitoylated in CY15 dendritic cells. Representative ABE-palmitoylation assay in CY15 dendritic cells expressing KCNE4. HA: hydroxylamine; SM: starting material, collected before the pull-down; PD: pull-down of palmitoylated proteins; flotillin was used as positive control of proteins palmitoylation. KCNE4 is S-acylated in CY15 dendritic cells.

4. Discussion

4. Discussion

The Kv1.3 channelosome represents a dynamic structural complex involved in numerous physiological processes. This work deepened knowledge regarding the intricate regulatory mechanisms that governs this macromolecular system, with a primary focus on protein oligomerization and S-acylation. Both of these processes exert direct influence on distinct modulatory peptides associated with Kv1.3, thus indirectly shaping the functionality of the channel. Protein oligomerization is a ubiquitous phenomenon observed across various biological processes (229). In an immune context, it plays a pivotal role in the activation of numerous transcription factors and chemokines, thereby initiating essential signalling pathways (230). One notable example is the NOD1 and NOD2 proteins, which belong to the innate immune system's category of pathogen recognition receptors. These molecules are responsible for detecting conserved fragments of various bacteria and subsequently initiating pro-inflammatory responses (231). Upon ligand binding, NOD1 and NOD2 undergo conformational changes that enable self-oligomerization, ADP/ATP exchange, and downstream signalling, ultimately activating the NF-kB and MAP kinase pathways (232). Along the NF-kB downstream signalling, higher-order oligomerization events are also critical for the activation of IKKβ, a protein recognized by dimerizing linear poly-ubiquitin (pUb) of NEMO proteins (233). Although NEMO lacks of a catalytic activity, its ability to bind to pUB is indispensable for recruiting IKK and subsequently facilitating NF-kB activation (234). Another key player in this pathway is TRAF6, an E3 ubiquitin ligase whose dimerization is essential for E3 ligase activity and cytokines release. Mutations in TRAF6 that impede dimers formation compromise the assembly of polyubiquitin chains and the phosphorylation of IkB (235). Furthermore, the immune system relies on receptors like RIG-I and MDA5 to detect viral RNAs and trigger IFN1 signalling, establishing an antiviral state within cells. ZAPS, acting as an IFN stimulator, associates with RIG-I to promote its oligomerization and ATPase activity, resulting in robust type I IFN activation (236). In our investigation, we present evidences demonstrating that oligomerization events significantly influence the regulation of both Kvβs and KCNE4, leading to profound consequences for Kv1.3. Specifically, we have found that KCNE4, unlike other KCNE peptides, forms dimers. This dimerization is mediated by a tetraleucine motif within its C-terminal domain, a structural element that simultaneously governs KCNE4's interactions with Kv1.3 and calmodulin (CaM). Dimerization provides redundancy in signalling for the KCNE4 dyad, effectively retaining a pool of peptides within the ER. Consequently, this regulation not only affects the interaction between KCNE4 and Kv1.3 but also influences its association with CaM. When KCNE4 binds either activated-CaM or Kv1.3, it can follow one of two paths: (i) travel to the membrane along with CaM or, (ii) retain the channel intracellularly, by masking forward trafficking motifs of Kv1.3. This dual mechanism allows for precise control over channel expression at the cell membranes, highlighting the critical role of oligomerization in governing Kv1.3-associated cellular responses. In this context, we compared dileucine (LL) clusters to protein trafficking. Notably, several ion channels feature these structural elements. For example, the ClC-2 chloride channel, which plays a pivotal role in the dysfunction of the cystic CFTR in cystic fibrosis, possesses a dileucine motif. Mutations in this signature alter the basolateral targeting of the channel. Similarly, neuronal Kv4 channels evolutionary conserve an LL motif, mediating the channel's axonal and dendritic targeting. Alterations of these moieties lead to incorrect axonal trafficking of the channel (237) (238). In some Kv1 channels, LL motifs allows the oligomerization with COPII machinery (239). The acid-sensing ion channel ASIC2a possesses a double dileucine motif (LLDLL) in the C-terminal juxtamembrane region. Modifying that sequence, either in part or entirely, increases the channel's surface levels. In light of these findings, our data indicates that disrupting or masking the tetraleucine motif impedes dimerization, thereby facilitating the membrane targeting of KCNE4. Consequently, CaM-dependent dimerization of KCNE4 regulates the ER retention of the subunit and its association with Kv1.3. Furthermore, upon interacting with CaM, KCNE4 traffics to the cell surface through the COPII-dependent machinery. These findings hold physiological relevance, as they suggest that KCNE4 dimerization serves as a regulatory mechanism for these interactions, with CaM acting as a key signalling partner. Calcium (Ca^{2+}) and CaM-dependent signalling hold immense significance in T cell activation. Simultaneously, Kvβs soluble peptides, primarily enhancing channel membrane trafficking, are an integral part of this regulatory network. Our

investigations have revealed that in the absence of Kv channels, Kvβ2.1 and Kvβ1.1 form homo- and hetero-oligomers with comparable affinities. Consequently, various stoichiometries are modulated through dynamic regulation of Kvβ peptides. We have observed that Kvβ1.1 formed oligomers with similar affinity and the same holds true for Kvβ1/Kvβ2 heterotetramerization. Interestingly, Kvβ1/Kvβ2 heteroligomers are expressed in coronary arterial myocytes, where they regulate the fine-tuning of Kv1.5's trafficking and membrane localization (240). In this context, macrophages express various Kvβ moieties, influenced by proliferation and distinct activation pathways (241). Consequently, the final hetero-tetrameric structure of Kvβs may dictate the regulation of Kv α-subunits. This phenomenon is not unique, as proteins can alter their oligomeric composition based on the quantity of each partner involved. For instance, differential expression patterns of ZIP1/ZIP2/ZIP3 lead to hetero- and homodimer formations involving Kvβ2 and PKC-ζ (242), similar to how Kv1.3/Kv1.5 complexes may exhibit comparable modulation in macrophages and dendritic cells (243). Since two individual subunits can modulate a single channel, the control of Kvβ expression levels could impact multiple functional channels. It is worth to note that homo- and hetero-oligomers of Kvβ1.1/Kvβ2.1 target the cell membrane surface, although with distinct microdomain localization patterns. The presence of Kvβ1 also alters the functionality of Kvβ2 in a concentration-dependent manner. Moreover, both Kvβ1 and Kvβ1/Kvβ2 heterooligomers can displace Kvβ2 from lipid rafts altering its functionality in these microdomains. Therefore, the interaction between Kvβ1 and Kvβ2 fine-tunes the physiological consequences of Kvβ2 during immune responses. The presence of soluble Kvβ2 at rafts structures introduces the S-acylation as another crucial post-translational mechanism governing the Kv1.3 channelosome. Our results confirm that both KCNE4 and Kvβ peptides undergo S-acylation, a modification that influences the membrane and lipid-rafts targeting of both subunits. Protein palmitoylation plays a pivotal role in immune cell activation and the organization of immunological synapses (244). For instance, palmitoylation of ORAI1 at a specific cysteine residue enhances the channel's affinity for lipid rafts, facilitating its inclusion in the immunological synapse and ensuring the necessary calcium fluxes for T cell activation (245). Additionally, ORAI1 targets lipid rafts through palmitoylation to promote Ca^{2+} entry by forming CRAC channels in conjunction with STIM1. Palmitoylation of STIM1, catalysed by DHHC21, represents a prerequisite for organizing CRACs. Both ORAI1 and STIM1 exhibit similar palmitoylation levels after T cell stimulation, suggesting the involvement of the same plasma membrane DHHC enzyme in their palmitoylation (246). Furthermore, proteins like NOD1 and NOD2, despite lacking transmembrane domains, require inclusion within endosomal and plasma membranes for signal transduction. Palmitoylation by zDHHC5 is indispensable for this process (247). In a pathological context, the DAT transporter plays a pivotal role in dopamine neurotransmission by clearing dopamine from the extracellular space. Dysregulation of DAT is central to the pathophysiology of numerous neuropsychiatric disorders. Palmitoylation on the TM12 region favours the oligomerization of DAT (248). Additionally, ZDHHC18 catalyzes the palmitoylation of the cGAS synthase at residue C474 in the presence of double-stranded DNA. S-palmitoylation of cGAS inhibits the binding of ligand DNA, further impeding cGAS dimerization and dampening the cGAS-STING signaling pathway. Consequently, ZDHHC18 serves as a negative regulator of cGAS-mediated innate immune responses (249) (250). Therefore, a potential crosstalk between protein oligomerization and S-palmitoylation during immunological pathways may exist. Immunological synapses concentrate lipid raft microdomains, and proteins like Flotillin and Caveolin are integral components of these structures (251). Flotillin functions are modulated by S-acylation, facilitating both membrane inclusion and oligomerization of the protein (252). Similarly, Caveolin dimerizes through interactions between NH2-terminal residues, a domain also involved in the interaction with eNOS, a key enzyme during immune cell activation. eNOS is targeted to caveolae through N-myristoylation followed by palmitoylation, which promotes the interaction between the two proteins. Upon binding with Caveolin, eNOS's enzymatic activity is inhibited (253). In alignment with these findings, our research indicates that both Kvβ1.1 and Kvβ2.1 undergo palmitoylation, with only the latter being targeted to lipid rafts. S-acylation thus controls the location of Kvβ2.1 and concentrates the peptide within lipid rafts when immune cell conjugates are activated. Immune cells express several palmitoyl acyltransferases, including DHHC18 and DHHC13 (254) (255), which may be responsible for the palmitoylation of Kvβs. Moreover, the differential

lipid raft targeting of Kvβ2.1 observed during FBS-dependent proliferation or PKC activation suggests that the abundance of Kvβ2.1 in these domains may differentially regulate cell functions. During proliferation, Kvβ2.1 exhibits increased colocalization within lipid rafts. However, PMA-induced PKC activation impairs this targeting, a phenomenon partially counteracted by PSD95. Consequently, controlling Kvβ2.1 distribution through FBS and PKC activation fine-tunes the architecture of the Kv1.3 channelosome. This intricate balance becomes even more complex when considering the influence of other ancillary peptides such as CaM and KCNE4, on the modulation of Kv1.3. Therefore, a delicate equilibrium governs oligomerization and palmitoylation of ancillary subunits, with substantial physiological implications for Kv1.3 activities and leukocyte physiology. Considering KCNE proteins, we demonstrated that KCNE4 member undergoes S-acylation at two terminal cysteines. The protein's stability at the ER membrane is thereby ensured by through ER retention motifs and palmitate anchoring. Our research has revealed that unpalmitoylated KCNE4/Kv1.3 complexes fail to reach the plasma membrane. In the absence of palmitoylation, the lack of palmitate chains would cause the undoking of KCNE4's COOH-terminal region, resulting in structural rearrangements that facilitate the plasma membrane trafficking of the subunit, by masking the ERRMs. As a result, the intracellular abundance of the peptide decreases, along with the availability of Kv1.3-interacting subunits. Our findings align with previous publications, demonstrating that the expression of Kv1.3 increases upon LPS activation in antigen-presenting cells, as does its distribution within the membrane, whether in complex with KCNE4 or as an individual subunit (256). We postulate that the higher abundance of Kv1.3 tetramers enhances forward trafficking by evading the ER retention mediated by KCNE4. After all, the fraction of KCNE4 that binds Kv1.3 targets the cell surface in complex with the channel, as this interaction occurs during early secretory pathways, before protein delivery to the cell membrane. Thus, we propose that unpalmitoylated KCNE4 enhances protein dimerization or calmodulin binding, subsequently promoting plasma membrane trafficking. All these modulations result in reduced downregulation of Kv1.3. The sensitivity to calcium signalling of all the cited proteins further support their importance in an immune environment. In KCNE4 monomers, ERRMs may be counteracted by binding with CaM. This process mirrors the controls mediated by KCNE4 in a Ca^{2+}/CaM-dependent manner for Kv7.1 (257). Signalling pathways dependent on Ca^{2+} and CaM are pivotal for T cell activation. Immunological synapses, rich in lipid rafts, concentrate Ca^{2+}-dependent targets. KCNE4, by retaining Kv1.3 within the ER, impairs its localization within lipid rafts. This aligns with our preliminary results, suggesting that KCNE4 did not localize to the immunological synapse. Kvβs, being part of the AKR protein family, may also play a role in calcium signaling by acting as redox sensors within cells. For example, Kvβ2.1 functions as a redox sensor at immunological synapses during the immune response, with MAGUK proteins stabilizing the architecture of these multimeric domains. Within immunological synapses, ZIP1, ZIP2, and ZIP3 may associate Kvβ2.1 with PKCζ, further supporting its location within these synapses (242) (258). Our research has demonstrated that Kvβ2.1 undergoes palmitoylation in the absence of conducting subunits. This suggests that AKR activity does not necessarily affect Kv channels, and Kvβ2.1 may act independently of Kv channels as a sensor for the redox state of the cell. Meanwhile, Kvβ1.1 does not target lipid rafts but localizes to the plasma membrane through interactions with actin filaments. Additionally, Kvβ1.3 exhibits slower hydride transfer compared to Kvβ2.1 (259). Consequently, the cell may strategically place multiple redox detectors with varying sensing rates at the plasma membrane. Based on the findings discussed so far, we hypothesize the existence of a specific equilibrium governing fate of Kv1.3 during immune pathways. Specific cellular processes, involving protein oligomerization and S-acylation, finely control this balance. Consequently, alterations in these modifications may result in pathological conditions, rendering attractive targets for immunomodulation studies involving the Kv1.3 channel. In summary, the Kv1.3 channelosome is a multifaceted regulatory complex with extensive implications in various physiological processes. Our investigation sheds light on the sophisticated mechanisms of protein oligomerization and S-acylation, revealing their profound impact on Kv1.3 and associated cellular responses. These findings not only deepen our understanding of cellular processes but also open new avenues for potential therapeutic interventions targeting the Kv1.3 channelosome in various pathological conditions, particularly in immune responses.

5. Conclusions

5. Conclusions

1. Kvβ2.1 targets to the cell surface and lipid rafts in the absence of Kvα subunits. The S-acylation concentrates Kvβ2.1 in specific membrane domains upon immune cell activation. Contrary to PKC activation, FBS-dependent proliferation increases the Kvβ2.1 lipid raft targeting and the MAGUK protein PSD-95 stabilizes this location.

2. Kvβ1.1 and Kvβ2.1 form heteromeric complexes with similar affinities. In addition, unlike Kvβ2, neither Kvβ1nor Kvβ1/Kvβ2 heteromers, target lipid raft microdomains. Thus, the Kvβ1 interaction impairs the physiological function of Kvβ2 at these microdomains.

3. Kv1.3, KCNE4 and CaM interact via a tetraleucine cluster of KCNE4. The dimerization of KCNE4 alters such interactions. Therefore, the KCNE4 tetraleucine motif, situated at the C-term of the protein, fine-tunes the cell physiology functioning as a signalling-interaction platform, in which different targets may compete.

4. KCNE4 undergoes S-acylation and the absence of this lipidation enhances peptide dimerization and plasma membrane trafficking. Palmitoylated KCNE4 associates with Kv1.3 at initial stages of biogenesis retaining the channel intracellularly. Kv1.3 increases its expression upon LPS activation in antigen presenting cells, as well as its membrane distribution, both in complex with KCNE4 than individually.

6. Bibliography

1. F. Bezanilla, Voltage-gated ion channels. *IEEE Trans Nanobioscience* **4**, 34-48 (2005).

2. Z. Wu, R. Tan, L. Zhu, P. Yao, Q. Hu, Protein S-Palmitoylation and Lung Diseases. *Adv Exp Med Biol* **1304**, 165-186 (2021).

3. T. Clairfeuille, H. Xu, C. M. Koth, J. Payandeh, Voltage-gated sodium channels viewed through a structural biology lens. *Curr Opin Struct Biol* **45**, 74-84 (2017).

4. M. J. Van Hook, S. Nawy, W. B. Thoreson, Voltage- and calcium-gated ion channels of neurons in the vertebrate retina. *Prog Retin Eye Res* **72**, 100760 (2019).

5. F. Elinder, S. I. Liin, Actions and Mechanisms of Polyunsaturated Fatty Acids on Voltage-Gated Ion Channels. *Front Physiol* **8**, 43 (2017).

6. D. A. Doyle *et al.*, The structure of the potassium channel: molecular basis of K+ conduction and selectivity. *Science* **280**, 69-77 (1998).

7. Y. Jiang *et al.*, The open pore conformation of potassium channels. *Nature* **417**, 523-526 (2002).

8. S. He, L. R. Shao, W. B. Rittase, S. B. Bausch, Increased Kv1 channel expression may contribute to decreased sIPSC frequency following chronic inhibition of NR2B-containing NMDAR. *Neuropsychopharmacology* **37**, 1338-1356 (2012).

9. Q. Zeng *et al.*, The toxin mimic FS48 from the salivary gland of Xenopsylla cheopis functions as a Kv1.3 channel-blocking immunomodulator of T cell activation. *J Biol Chem* **298**, 101497 (2022).

10. P. Cidad *et al.*, Voltage-dependent conformational changes of Kv1.3 channels activate cell proliferation. *J Cell Physiol* **236**, 4330-4347 (2021).

11. A. Grimaldi *et al.*, Kv1.3 activity perturbs the homeostatic properties of astrocytes in glioma. *Sci Rep* **8**, 7654 (2018).

12. M. Bachmann *et al.*, Voltage-Gated Potassium Channels as Regulators of Cell Death. *Front Cell Dev Biol* **8**, 611853 (2020).

13. S. Grissmer *et al.*, Pharmacological characterization of five cloned voltage-gated K+ channels, types Kv1.1, 1.2, 1.3, 1.5, and 3.1, stably expressed in mammalian cell lines. *Mol Pharmacol* **45**, 1227-1234 (1994).

14. R. Ranjan *et al.*, A Kinetic Map of the Homomeric Voltage-Gated Potassium Channel (Kv) Family. *Front Cell Neurosci* **13**, 358 (2019).

15. P. Selvakumar *et al.*, Structures of the T cell potassium channel Kv1.3 with immunoglobulin modulators. *Nat Commun* **13**, 3854 (2022).

16. J. Kupper, A. A. Prinz, P. Fromherz, Recombinant Kv1.3 potassium channels stabilize tonic firing of cultured rat hippocampal neurons. *Pflugers Arch* **443**, 541-547 (2002).

17. J. Xu *et al.*, The voltage-gated potassium channel Kv1.3 regulates energy homeostasis and body weight. *Hum Mol Genet* **12**, 551-559 (2003).

18. J. Xu *et al.*, The voltage-gated potassium channel Kv1.3 regulates peripheral insulin sensitivity. *Proc Natl Acad Sci U S A* **101**, 3112-3117 (2004).

19. Y. Li, P. Wang, J. Xu, G. V. Desir, Voltage-gated potassium channel Kv1.3 regulates GLUT4 trafficking to the plasma membrane via a Ca2+-dependent mechanism. *Am J Physiol Cell Physiol* **290**, C345-351 (2006).

20. M. Pérez-Verdaguer *et al.*, Caveolar targeting links Kv1.3 with the insulin-dependent adipocyte physiology. *Cell Mol Life Sci* **75**, 4059-4075 (2018).

21. J. Capera, M. Navarro-Pérez, A. S. Moen, I. Szabó, A. Felipe, The Mitochondrial Routing of the Kv1.3 Channel. *Front Oncol* **12**, 865686 (2022).

22. E. Gulbins, N. Sassi, H. Grassmè, M. Zoratti, I. Szabò, Role of Kv1.3 mitochondrial potassium channel in apoptotic signalling in lymphocytes. *Biochim Biophys Acta* **1797**, 1251-1259 (2010).

23. R. Swanson *et al.*, Cloning and expression of cDNA and genomic clones encoding three delayed rectifier potassium channels in rat brain. *Neuron* **4**, 929-939 (1990).

24. J. Bielanska *et al.*, Voltage-dependent potassium channels Kv1.3 and Kv1.5 in human fetus. *Cell Physiol Biochem* **26**, 219-226 (2010).

25. R. Vicente *et al.*, Differential voltage-dependent K+ channel responses during proliferation and activation in macrophages. *J Biol Chem* **278**, 46307-46320 (2003).

26. M. Coma *et al.*, Impaired voltage-gated K+ channel expression in brain during experimental cancer cachexia. *FEBS Lett* **536**, 45-50 (2003).

27. N. Villalonga *et al.*, Cell cycle-dependent expression of Kv1.5 is involved in myoblast proliferation. *Biochim Biophys Acta* **1783**, 728-736 (2008).

28. F. Lesage, B. Attali, M. Lazdunski, J. Barhanin, Developmental expression of voltage-sensitive K+ channels in mouse skeletal muscle and C2C12 cells. *FEBS Lett* **310**, 162-166 (1992).

29. H. T. Kurata, G. S. Soon, D. Fedida, Altered State Dependence of C-Type Inactivation in the Long and Short Forms of Human Kv1.5. *J Gen Physiol.* **118**, 315–332 (2001).

30. R. Anton *et al.*, Potassium Channels Kv1.3 and Kir2.1 But Not Kv1.5 Contribute to BV2 Cell Line and Primary Microglial Migration. *Int J Mol Sci* **22**, (2021).

31. N. Comes *et al.*, The voltage-dependent K(+) channels Kv1.3 and Kv1.5 in human cancer. *Front Physiol* **4**, 283 (2013).

32. G. W. Abbott, Control of Biophysical and Pharmacological Properties of Potassium Channels by Ancillary Subunits. *Handb Exp Pharmacol* **267**, 445-480 (2021).

33. J. M. Spear *et al.*, Kv1.3 contains an alternative C-terminal ER exit motif and is recruited into COPII vesicles by Sec24a. *BMC Biochem* **16**, 16 (2015).

34. J. S. Yoo *et al.*, Non-conventional trafficking of the cystic fibrosis transmembrane conductance regulator through the early secretory pathway. *J Biol Chem* **277**, 11401-11409 (2002).

35. A. Oliveras *et al.*, The unconventional biogenesis of Kv7.1-KCNE1 complexes. *Sci Adv* **6**, eaay4472 (2020).

36. A. K. Townley *et al.*, Efficient coupling of Sec23-Sec24 to Sec13-Sec31 drives COPII-dependent collagen secretion and is essential for normal craniofacial development. *J Cell Sci* **121**, 3025-3034 (2008).

37. J. Zhu, B. Gomez, I. Watanabe, W. B. Thornhill, Kv1 potassium channel C-terminus constant HRETE region: arginine substitution affects surface protein level and conductance level of subfamily members differentially. *Mol Membr Biol* **24**, 194-205 (2007).

38. L. Solé *et al.*, The C-terminal domain of Kv1.3 regulates functional interactions with the KCNE4 subunit. *J Cell Sci* **129**, 4265-4277 (2016).

39. G. Henke, G. Maier, S. Wallisch, C. Boehmer, F. Lang, Regulation of the voltage gated K+ channel Kv1.3 by the ubiquitin ligase Nedd4-2 and the serum and glucocorticoid inducible kinase SGK1. *J Cell Physiol* **199**, 194-199 (2004).

40. I. Estadella *et al.*, Endocytosis: A Turnover Mechanism Controlling Ion Channel Function. *Cells* **9**, (2020).

41. R. Martínez-Mármol *et al.*, Ubiquitination mediates Kv1.3 endocytosis as a mechanism for protein kinase C-dependent modulation. *Sci Rep* **7**, 42395 (2017).

42. T. C. Holmes, D. A. Fadool, I. B. Levitan, Tyrosine phosphorylation of the Kv1.3 potassium channel. *J Neurosci* **16**, 1581-1590 (1996).

43. N.-P. M. *et al.*, The Phosphorylation of Kv1.3: A Modulatory Mechanism for a Multifunctional Ion Channel. *Cancers* **15**, 2716.

44. M. R. Bowlby, D. A. Fadool, T. C. Holmes, I. B. Levitan, Modulation of the Kv1.3 potassium channel by receptor tyrosine kinases. *J Gen Physiol* **110**, 601-610 (1997).

45. M. C. Chang, R. Khanna, L. C. Schlichter, Regulation of Kv1.3 channels in activated human T lymphocytes by Ca(2+)-dependent pathways. *Cell Physiol Biochem* **11**, 123-134 (2001).

46. V. E. Scott *et al.*, Primary structure of a beta subunit of alpha-dendrotoxin-sensitive K+ channels from bovine brain. *Proc Natl Acad Sci U S A* **91**, 1637-1641 (1994).

47. O. Pongs *et al.*, Functional and molecular aspects of voltage-gated K+ channel beta subunits. *Ann N Y Acad Sci* **868**, 344-355 (1999).

48. S. H. Heinemann, J. Rettig, F. Wunder, O. Pongs, Molecular and functional characterization of a rat brain Kv beta 3 potassium channel subunit. *FEBS Lett* **377**, 383-389 (1995).

49. Y. Li, S. Y. Um, T. V. McDonald, Voltage-gated potassium channels: regulation by accessory subunits. *Neuroscientist* **12**, 199-210 (2006).

50. S. B. Long, E. B. Campbell, R. Mackinnon, Crystal structure of a mammalian voltage-dependent Shaker family K+ channel. *Science* **309**, 897-903 (2005).

51. J. M. Gulbis, M. Zhou, S. Mann, R. MacKinnon, Structure of the cytoplasmic beta subunit-T1 assembly of voltage-dependent K+ channels. *Science* **289**, 123-127 (2000).

52. Z. Xie, O. A. Barski, J. Cai, A. Bhatnagar, S. M. Tipparaju, Catalytic reduction of carbonyl groups in oxidized PAPC by Kvβ2 (AKR6). *Chem Biol Interact* **191**, 255-260 (2011).

53. O. Pongs, J. R. Schwarz, Ancillary subunits associated with voltage-dependent K+ channels. *Physiol Rev* **90**, 755-796 (2010).

54. J. M. Gulbis, S. Mann, R. MacKinnon, Structure of a voltage-dependent K+ channel beta subunit. *Cell* **97**, 943-952 (1999).

55. S. Q. Liu, H. Jin, A. Zacarias, S. Srivastava, A. Bhatnagar, Binding of pyridine nucleotide coenzymes to the beta-subunit of the voltage-sensitive K+ channel. *J Biol Chem* **276**, 11812-11820 (2001).

56. S. M. Tipparaju, S. Q. Liu, O. A. Barski, A. Bhatnagar, NADPH binding to beta-subunit regulates inactivation of voltage-gated K(+) channels. *Biochem Biophys Res Commun* **359**, 269-276 (2007).

57. P. J. Kilfoil, S. M. Tipparaju, O. A. Barski, A. Bhatnagar, Regulation of ion channels by pyridine nucleotides. *Circ Res* **112**, 721-741 (2013).

58. S. M. Tipparaju, O. A. Barski, S. Srivastava, A. Bhatnagar, Catalytic mechanism and substrate specificity of the beta-subunit of the voltage-gated potassium channel. *Biochemistry* **47**, 8840-8854 (2008).

59. R. Vicente *et al.*, Pattern of Kv beta subunit expression in macrophages depends upon proliferation and the mode of activation. *J Immunol* **174**, 4736-4744 (2005).

60. N. Sahoo *et al.*, Heme impairs the ball-and-chain inactivation of potassium channels. *Proc Natl Acad Sci U S A* **110**, E4036-4044 (2013).

61. K. P. Giese *et al.*, Reduced K+ channel inactivation, spike broadening, and after-hyperpolarization in Kvbeta1.1-deficient mice with impaired learning. *Learn Mem* **5**, 257-273 (1998).

62. G. G. Murphy *et al.*, Increased neuronal excitability, synaptic plasticity, and learning in aged Kvbeta1.1 knockout mice. *Curr Biol* **14**, 1907-1915 (2004).

63. J. Tur *et al.*, Deletion of Kvβ1.1 subunit leads to electrical and haemodynamic changes causing cardiac hypertrophy in female murine hearts. *Exp Physiol* **101**, 494-508 (2016).

64. M. V. Autieri, S. M. Belkowski, C. S. Constantinescu, J. A. Cohen, M. B. Prystowsky, Lymphocyte-specific inducible expression of

potassium channel beta subunits. *J Neuroimmunol* **77**, 8-16 (1997).

65. Y. Pan, J. Weng, E. J. Levin, M. Zhou, Oxidation of NADPH on Kvbeta1 inhibits ball-and-chain type inactivation by restraining the chain. *Proc Natl Acad Sci U S A* **108**, 5885-5890 (2011).

66. R. Bähring *et al.*, Coupling of voltage-dependent potassium channel inactivation and oxidoreductase active site of Kvbeta subunits. *J Biol Chem* **276**, 22923-22929 (2001).

67. P. McIntosh *et al.*, Modification of rat brain Kv1.4 channel gating by association with accessory Kvbeta1.1 and beta2.1 subunits. *Pflugers Arch* **435**, 43-54 (1997).

68. S. M. Lamothe, H. T. Kurata, Slc7a5 alters Kvβ-mediated regulation of Kv1.2. *J Gen Physiol* **152**, (2020).

69. M. T. Pérez-García, J. R. López-López, C. González, Kvbeta1.2 subunit coexpression in HEK293 cells confers O2 sensitivity to kv4.2 but not to Shaker channels. *J Gen Physiol* **113**, 897-907 (1999).

70. S. K. England, V. N. Uebele, J. Kodali, P. B. Bennett, M. M. Tamkun, A Novel K + Channel β-Subunit (hKvβ1.3) Is Produced via Alternative mRNA Splicing. **270**, 28531-28534 (1995).

71. N. Decher *et al.*, Structural determinants of Kvbeta1.3-induced channel inactivation: a hairpin modulated by PIP2. *EMBO J* **27**, 3164-3174 (2008).

72. M. Grande *et al.*, Voltage-dependent K+ channel beta subunits in muscle: differential regulation during postnatal development and myogenesis. *J Cell Physiol* **195**, 187-193 (2003).

73. K. C. Chapalamadugu *et al.*, Physiological role of Kvβ2 (AKR6) in murine skeletal muscle growth and regulation. *Acta Physiol (Oxf)* **224**, e13083 (2018).

74. O. A. Barski, K. H. Gabbay, C. E. Grimshaw, K. M. Bohren, Mechanism of human aldehyde reductase: characterization of the active site pocket. *Biochemistry* **34**, 11264-11275 (1995).

75. S. M. Raph, A. Bhatnagar, M. A. Nystoriak, Biochemical and physiological properties of K. *Chem Biol Interact* **305**, 21-27 (2019).

76. G. Shi *et al.*, Beta subunits promote K+ channel surface expression through effects early in biosynthesis. *Neuron* **16**, 843-852 (1996).

77. J. Kisselbach *et al.*, Enhancement of K2P2.1 (TREK1) background currents expressed in Xenopus oocytes by voltage-gated K+ channel β subunits. *Life Sci* **91**, 377-383 (2012).

78. M. J. Abraham, K. L. Fleming, S. Raymond, A. Y. C. Wong, R. Bergeron, The sigma-1 receptor behaves as an atypical auxiliary subunit to modulate the functional characteristics of Kv1.2 channels expressed in HEK293 cells. *Physiol Rep* **7**, e14147 (2019).

79. E. Suárez-Delgado *et al.*, KV1.2 channels inactivate through a mechanism similar to C-type inactivation. *J Gen Physiol* **152**, (2020).

80. M. Lolicato *et al.*, K. *Nature* **547**, 364-368 (2017).

81. S. Akhtar, O. Shamotienko, M. Papakosta, F. Ali, J. O. Dolly, Characteristics of brain Kv1 channels tailored to mimic native counterparts by tandem linkage of alpha subunits: implications for K+ channelopathies. *J Biol Chem* **277**, 16376-16382 (2002).

82. X. Wang *et al.*, Protein kinase C-mediated phosphorylation of Kv beta 2 in adult rat brain. *Neurochem Res* **29**, 1879-1886 (2004).

83. L. Lewin *et al.*, Molecular and cellular correlates in Kv channel clustering: entropy-based regulation of cluster ion channel density. *Sci Rep* **10**, 11304 (2020).

84. I. Deschênes, G. F. Tomaselli, Modulation of Kv4.3 current by accessory subunits. *FEBS Lett* **528**, 183-188 (2002).

85. A. de Benito-Bueno *et al.*, Modulation of K. *Int J Mol Sci* **23**, (2022).

86. S. Bunse *et al.*, The potassium channel subunit Kvbeta3 interacts with pannexin 1 and attenuates its sensitivity to changes in redox potentials. *FEBS J* **276**, 6258-6270 (2009).

87. K. Nakajo, Gating modulation of the KCNQ1 channel by KCNE proteins studied by voltage-clamp fluorometry. *Biophys Physicobiol* **16**, 121-126 (2019).

88. L. Solé, A. Felipe, Does a physiological role for KCNE subunits exist in the immune system? *Commun Integr Biol* **3**, 166-168 (2010).

89. M. C. Sanguinetti, Maximal function of minimal K+ channel subunits. *Trends Pharmacol Sci* **21**, 199-201 (2000).

90. Y. F. Melman, A. Krumerman, T. V. McDonald, A single transmembrane site in the KCNE-encoded proteins controls the specificity of KvLQT1 channel gating. *J Biol Chem* **277**, 25187-25194 (2002).

91. M. Roura-Ferrer *et al.*, Impact of KCNE subunits on KCNQ1 (Kv7.1) channel membrane surface targeting. *J Cell Physiol* **225**, 692-700 (2010).

92. L. Solé *et al.*, KCNE gene expression is dependent on the proliferation and mode of activation of leukocytes. *Channels (Austin)* **7**, 85-96 (2013).

93. I. Splawski, M. Tristani-Firouzi, M. H. Lehmann, M. C. Sanguinetti, M. T. Keating, Mutations in the hminK gene cause long QT syndrome and suppress IKs function. *Nat Genet* **17**, 338-340 (1997).

94. G. W. Abbott *et al.*, MiRP2 forms potassium channels in skeletal muscle with Kv3.4 and is associated with periodic paralysis. *Cell* **104**, 217-231 (2001).

95. M. C. Sanguinetti, J. S. Mitcheson, Predicting drug-hERG channel interactions that cause acquired long QT syndrome. *Trends Pharmacol Sci* **26**, 119-124 (2005).

96. Z. Mustapha, L. Pang, S. Nattel, Characterization of the cardiac KCNE1 gene promoter. *Cardiovasc Res* **73**, 82-91 (2007).

97. G. Dixit, C. Dabney-Smith, G. A. Lorigan, The membrane protein KCNQ1 potassium ion channel: Functional diversity and current

98. X. Wu, H. P. Larsson, Insights into Cardiac IKs (KCNQ1/KCNE1) Channels Regulation. *Int J Mol Sci* **21**, (2020).

99. M. S. Bohnen *et al.*, Molecular Pathophysiology of Congenital Long QT Syndrome. *Physiol Rev* **97**, 89-134 (2017).

100. J. M. Nerbonne, R. S. Kass, Molecular physiology of cardiac repolarization. *Physiol Rev* **85**, 1205-1253 (2005).

101. M. Varshneya, R. A. Devenyi, E. A. Sobie, Slow Delayed Rectifier Current Protects Ventricular Myocytes From Arrhythmic Dynamics Across Multiple Species: A Computational Study. *Circ Arrhythm Electrophysiol* **11**, e006558 (2018).

102. V. A. Kanda, K. Purtell, G. W. Abbott, Protein kinase C downregulates I(Ks) by stimulating KCNQ1-KCNE1 potassium channel endocytosis. *Heart Rhythm* **8**, 1641-1647 (2011).

103. I. Alesutan *et al.*, Inhibition of the heterotetrameric K+ channel KCNQ1/KCNE1 by the AMP-activated protein kinase. *Mol Membr Biol* **28**, 79-89 (2011).

104. S. Sakata *et al.*, Instability of KCNE1-D85N that causes long QT syndrome: stabilization by verapamil. *Pacing Clin Electrophysiol* **37**, 853-863 (2014).

105. Z. A. McCrossan, T. K. Roepke, A. Lewis, G. Panaghie, G. W. Abbott, Regulation of the Kv2.1 potassium channel by MinK and MiRP1. *J Membr Biol* **228**, 1-14 (2009).

106. A. Lewis, Z. A. McCrossan, G. W. Abbott, MinK, MiRP1, and MiRP2 diversify Kv3.1 and Kv3.2 potassium channel gating. *J Biol Chem* **279**, 7884-7892 (2004).

107. S. Radicke *et al.*, Functional modulation of the transient outward current Ito by KCNE beta-subunits and regional distribution in human non-failing and failing hearts. *Cardiovasc Res* **71**, 695-703 (2006).

108. H. M. Nguyen *et al.*, Intracellular trafficking of the KV1.3 potassium channel is regulated by the prodomain of a matrix metalloprotease. *J Biol Chem* **288**, 6451-6464 (2013).

109. Z. A. McCrossan, G. W. Abbott, The MinK-related peptides. *Neuropharmacology* **47**, 787-821 (2004).

110. M. Lindner *et al.*, Expression and Localization of Kcne2 in the Vertebrate Retina. *Invest Ophthalmol Vis Sci* **61**, 33 (2020).

111. M. Uhlén *et al.*, Proteomics. Tissue-based map of the human proteome. *Science* **347**, 1260419 (2015).

112. W. Liu *et al.*, KCNE2 modulates cardiac L-type Ca(2+) channel. *J Mol Cell Cardiol* **72**, 208-218 (2014).

113. V. A. Kanda, A. Lewis, X. Xu, G. W. Abbott, KCNE1 and KCNE2 inhibit forward trafficking of homomeric N-type voltage-gated potassium channels. *Biophys J* **101**, 1354-1363 (2011).

114. P. Li *et al.*, Differential modulations of KCNQ1 by auxiliary proteins KCNE1 and KCNE2. *Sci Rep* **4**, 4973 (2014).

115. S. M. Lee *et al.*, Kcne2 deletion causes early-onset nonalcoholic fatty liver disease via iron deficiency anemia. *Sci Rep* **6**, 23118 (2016).

116. V. A. Kanda, G. W. Abbott, KCNE Regulation of K(+) Channel Trafficking - a Sisyphean Task? *Front Physiol* **3**, 231 (2012).

117. Z. Hu *et al.*, Kcne2 deletion creates a multisystem syndrome predisposing to sudden cardiac death. *Circ Cardiovasc Genet* **7**, 33-42 (2014).

118. Z. Hu, S. M. Crump, P. Zhang, G. W. Abbott, Kcne2 deletion attenuates acute post-ischaemia/reperfusion myocardial infarction. *Cardiovasc Res* **110**, 227-237 (2016).

119. G. W. Abbott, T. K. Roepke, KCNE2 and gastric cancer: bench to bedside. *Oncotarget* **7**, 17286-17287 (2016).

120. J. D. Roberts *et al.*, Loss-of-Function. *Circ Arrhythm Electrophysiol* **10**, (2017).

121. A. L. Lundquist, C. L. Turner, L. Y. Ballester, A. L. George, Expression and transcriptional control of human KCNE genes. *Genomics* **87**, 119-128 (2006).

122. J. P. David, J. I. Stas, N. Schmitt, E. Bocksteins, Auxiliary KCNE subunits modulate both homotetrameric Kv2.1 and heterotetrameric Kv2.1/Kv6.4 channels. *Sci Rep* **5**, 12813 (2015).

123. A. Lundby, S. P. Olesen, KCNE3 is an inhibitory subunit of the Kv4.3 potassium channel. *Biochem Biophys Res Commun* **346**, 958-967 (2006).

124. G. W. Abbott, KCNE1 and KCNE3: The yin and yang of voltage-gated K(+) channel regulation. *Gene* **576**, 1-13 (2016).

125. U. Lisewski *et al.*, Increased aldosterone-dependent Kv1.5 recycling predisposes to pacing-induced atrial fibrillation in Kcne3-/- mice. *FASEB J* **30**, 2476-2489 (2016).

126. K. Kelemen, I. D. Greener, X. Wan, S. Parajuli, J. K. Donahue, Heterogeneous repolarization creates ventricular tachycardia circuits in healed myocardial infarction scar. *Nat Commun* **13**, 830 (2022).

127. R. Mazhari, H. B. Nuss, A. A. Armoundas, R. L. Winslow, E. Marbán, Ectopic expression of KCNE3 accelerates cardiac repolarization and abbreviates the QT interval. *J Clin Invest* **109**, 1083-1090 (2002).

128. E. C. King *et al.*, Targeted deletion of. *FASEB J* **31**, 2937-2947 (2017).

129. E. Delpón *et al.*, Functional effects of KCNE3 mutation and its role in the development of Brugada syndrome. *Circ Arrhythm Electrophysiol* **1**, 209-218 (2008).

130. A. Al-Hazza, J. Linley, Q. Aziz, M. Hunter, G. Sandle, Upregulation of basolateral small conductance potassium channels (KCNQ1/KCNE3) in ulcerative colitis. *Biochem Biophys Res Commun* **470**, 473-478 (2016).

131. G. W. Abbott, KCNE4 and KCNE5: K(+) channel regulation and cardiac arrhythmogenesis. *Gene* **593**, 249-260 (2016).

132. G. W. Abbott, Novel exon 1 protein-coding regions N-terminally extend human KCNE3 and KCNE4. *FASEB J* **30**, 2959-2969 (2016).

133. D. I. Levy, S. Wanderling, D. Biemesderfer, S. A. Goldstein, MiRP3 acts as an accessory subunit with the BK potassium channel. *Am J Physiol Renal Physiol* **295**, F380-387 (2008).

134. M. Grunnet *et al.*, KCNE4 is an inhibitory subunit to Kv1.1 and Kv1.3 potassium channels. *Biophys J* **85**, 1525-1537 (2003).

135. G. W. Abbott, β Subunits Functionally Differentiate Human Kv4.3 Potassium Channel Splice Variants. *Front Physiol* **8**, 66 (2017).

136. G. W. Abbott, Regulation of human cardiac potassium channels by full-length KCNE3 and KCNE4. *Sci Rep* **6**, 38412 (2016).

137. M. Grunnet, S. P. Olesen, D. A. Klaerke, T. Jespersen, hKCNE4 inhibits the hKCNQ1 potassium current without affecting the activation kinetics. *Biochem Biophys Res Commun* **328**, 1146-1153 (2005).

138. E. J. Ciampa, R. C. Welch, C. G. Vanoye, A. L. George, KCNE4 juxtamembrane region is required for interaction with calmodulin and for functional suppression of KCNQ1. *J Biol Chem* **286**, 4141-4149 (2011).

139. L. Solé *et al.*, KCNE4 suppresses Kv1.3 currents by modulating trafficking, surface expression and channel gating. *J Cell Sci* **122**, 3738-3748 (2009).

140. A. Vallejo-Gracia *et al.*, KCNE4-dependent functional consequences of Kv1.3-related leukocyte physiology. *Sci Rep* **11**, 14632 (2021).

141. H. D. Mistry *et al.*, Novel expression and regulation of voltage-dependent potassium channels in placentas from women with preeclampsia. *Hypertension* **58**, 497-504 (2011).

142. L. S. Ravn *et al.*, Gain of function in IKs secondary to a mutation in KCNE5 associated with atrial fibrillation. *Heart Rhythm* **5**, 427-435 (2008).

143. L. S. Ravn *et al.*, Relation of 97T polymorphism in KCNE5 to risk of atrial fibrillation. *Am J Cardiol* **96**, 405-407 (2005).

144. B. R. Palmer *et al.*, KCNE5 polymorphism rs697829 is associated with QT interval and survival in acute coronary syndromes patients. *J Cardiovasc Electrophysiol* **23**, 319-324 (2012).

145. M. Pérez-Verdaguer *et al.*, The voltage-gated potassium channel Kv1.3 is a promising multitherapeutic target against human pathologies. *Expert Opin Ther Targets* **20**, 577-591 (2016).

146. S. Feske, Calcium signalling in lymphocyte activation and disease. *Nat Rev Immunol* **7**, 690-702 (2007).

147. R. Immler, S. I. Simon, M. Sperandio, Calcium signalling and related ion channels in neutrophil recruitment and function. *Eur J Clin Invest* **48 Suppl 2**, e12964 (2018).

148. S. Feske, H. Wulff, E. Y. Skolnik, Ion channels in innate and adaptive immunity. *Annu Rev Immunol* **33**, 291-353 (2015).

149. J. Lam, H. Wulff, The Lymphocyte Potassium Channels Kv1.3 and KCa3.1 as Targets for Immunosuppression. *Drug Dev Res* **72**, 573-584 (2011).

150. A. Tóth, O. Szilágyi, Z. Krasznai, G. Panyi, P. Hajdú, Functional consequences of Kv1.3 ion channel rearrangement into the immunological synapse. *Immunol Lett* **125**, 15-21 (2009).

151. G. Panyi *et al.*, Kv1.3 potassium channels are localized in the immunological synapse formed between cytotoxic and target cells. *Proc Natl Acad Sci U S A* **101**, 1285-1290 (2004).

152. O. Szilágyi, A. Boratkó, G. Panyi, P. Hajdu, The role of PSD-95 in the rearrangement of Kv1.3 channels to the immunological synapse. *Pflugers Arch* **465**, 1341-1353 (2013).

153. R. Vicente *et al.*, Kv1.5 association modifies Kv1.3 traffic and membrane localization. *J Biol Chem* **283**, 8756-8764 (2008).

154. J. Capera *et al.*, Dynamics and spatial organization of Kv1.3 at the immunological synapse of human CD4+ T cells. *Biophys J*, (2023).

155. I. Kazama, T. Tamada, Lymphocyte Kv1.3-channels in the pathogenesis of chronic obstructive pulmonary disease: novel therapeutic implications of targeting the channels by commonly used drugs. *Allergy Asthma Clin Immunol* **12**, 60 (2016).

156. J. Liu *et al.*, Review on Biological Characteristics of Kv1.3 and Its Role in Liver Diseases. *Front Pharmacol* **12**, 652508 (2021).

157. I. Kazama, Roles of lymphocyte kv1.3-channels in the pathogenesis of renal diseases and novel therapeutic implications of targeting the channels. *Mediators Inflamm* **2015**, 436572 (2015).

158. A. Gilhar, R. Bergman, B. Assay, Y. Ullmann, A. Etzioni, The beneficial effect of blocking Kv1.3 in the psoriasiform SCID mouse model. *J Invest Dermatol* **131**, 118-124 (2011).

159. S. A. Nicolaou *et al.*, Differential calcium signaling and Kv1.3 trafficking to the immunological synapse in systemic lupus erythematosus. *Cell Calcium* **47**, 19-28 (2010).

160. S. Rangaraju, V. Chi, M. W. Pennington, K. G. Chandy, Kv1.3 potassium channels as a therapeutic target in multiple sclerosis. *Expert Opin Ther Targets* **13**, 909-924 (2009).

161. I. Maezawa *et al.*, Kv1.3 inhibition as a potential microglia-targeted therapy for Alzheimer's disease: preclinical proof of concept. *Brain* **141**, 596-612 (2018).

162. A. Teisseyre, A. Palko-Labuz, K. Sroda-Pomianek, K. Michalak, Voltage-Gated Potassium Channel Kv1.3 as a Target in Therapy of Cancer. *Front Oncol* **9**, 933 (2019).

163. U. Schulte *et al.*, The epilepsy-linked Lgi1 protein assembles into presynaptic Kv1 channels and inhibits inactivation by Kvbeta1. *Neuron* **49**, 697-706 (2006).

164. V. Portero *et al.*, Dysfunction of the Voltage-Gated K+ Channel β2 Subunit in a Familial Case of Brugada Syndrome. *J Am Heart Assoc* **5**, (2016).

165. J. J. Perkowski, G. G. Murphy, Deletion of the mouse homolog of KCNAB2, a gene linked to monosomy 1p36, results in associative memory impairments and amygdala hyperexcitability. *J Neurosci* **31**, 46-54 (2011).

166. L. H. Nguyen, A. E. Anderson, mTOR-dependent alterations of Kv1.1 subunit expression in the neuronal subset-specific Pten knockout mouse model of cortical dysplasia with epilepsy. *Sci Rep* **8**, 3568 (2018).

167. P. I. Jukkola, A. E. Lovett-Racke, S. S. Zamvil, C. Gu, K+ channel alterations in the progression of experimental autoimmune encephalomyelitis. *Neurobiol Dis* **47**, 280-293 (2012).

168. S. Akhtar *et al.*, A functional spliced-variant of beta 2 subunit of Kv1 channels in C6 glioma cells and reactive astrocytes from rat lesioned cerebellum. *Biochemistry* **38**, 16984-16992 (1999).

169. K. Tian *et al.*, KCNE4 expression is correlated with the pathological characteristics of colorectal cancer patients and associated with the radioresistance of cancer cells. *Pathol Res Pract* **241**, 154234 (2023).

170. Z. H. Wu, C. Li, Y. J. Zhang, W. Zhou, Identification of a Cancer Stem Cells Signature of Head and Neck Squamous Cell Carcinoma. *Front Genet* **13**, 814777 (2022).

171. R. Mano *et al.*, Induction of potassium channel regulator KCNE4 in a submandibular lymph node metastasis model. *Sci Rep* **12**, 13208 (2022).

172. L. R. Treviño *et al.*, Germline genomic variants associated with childhood acute lymphoblastic leukemia. *Nat Genet* **41**, 1001-1005 (2009).

173. M. B. Freĭdin *et al.*, [Genome-wide association study of allergic diseases in Russians of Western Siberia]. *Mol Biol (Mosk)* **45**, 464-472 (2011).

174. J. E. Smotrys, M. E. Linder, Palmitoylation of intracellular signaling proteins: regulation and function. *Annu Rev Biochem* **73**, 559-587 (2004).

175. E. Yousefi-Salakdeh, J. Johansson, R. Strömberg, A method for S- and O-palmitoylation of peptides: synthesis of pulmonary surfactant protein-C models. *Biochem J* **343 Pt 3**, 557-562 (1999).

176. C. Zou *et al.*, Acyl-CoA:lysophosphatidylcholine acyltransferase I (Lpcat1) catalyzes histone protein O-palmitoylation to regulate mRNA synthesis. *J Biol Chem* **286**, 28019-28025 (2011).

177. J. A. Gutierrez *et al.*, Ghrelin octanoylation mediated by an orphan lipid transferase. *Proc Natl Acad Sci U S A* **105**, 6320-6325 (2008).

178. R. B. Pepinsky *et al.*, Identification of a palmitic acid-modified form of human Sonic hedgehog. *J Biol Chem* **273**, 14037-14045 (1998).

179. Y. Ji, M. M. Bachschmid, C. E. Costello, C. Lin, S- to N-Palmitoyl Transfer During Proteomic Sample Preparation. *J Am Soc Mass Spectrom* **27**, 677-685 (2016).

180. Y. Fukata, M. Fukata, Protein palmitoylation in neuronal development and synaptic plasticity. *Nat Rev Neurosci* **11**, 161-175 (2010).

181. B. R. Martin, B. F. Cravatt, Large-scale profiling of protein palmitoylation in mammalian cells. *Nat Methods* **6**, 135-138 (2009).

182. S. I. Patterson, J. H. Skene, A shift in protein S-palmitoylation, with persistence of growth-associated substrates, marks a critical period for synaptic plasticity in developing brain. *J Neurobiol* **39**, 423-437 (1999).

183. K. Lemonidis, O. A. Gorleku, M. C. Sanchez-Perez, C. Grefen, L. H. Chamberlain, The Golgi S-acylation machinery comprises zDHHC enzymes with major differences in substrate affinity and S-acylation activity. *Mol Biol Cell* **25**, 3870-3883 (2014).

184. A. D. Goddard, A. Watts, Regulation of G protein-coupled receptors by palmitoylation and cholesterol. *BMC Biol* **10**, 27 (2012).

185. Y. Ohno, A. Kihara, T. Sano, Y. Igarashi, Intracellular localization and tissue-specific distribution of human and yeast DHHC cysteine-rich domain-containing proteins. *Biochim Biophys Acta* **1761**, 474-483 (2006).

186. G. Morris, K. Walder, B. K. Puri, M. Berk, M. Maes, The Deleterious Effects of Oxidative and Nitrosative Stress on Palmitoylation, Membrane Lipid Rafts and Lipid-Based Cellular Signalling: New Drug Targets in Neuroimmune Disorders. *Mol Neurobiol* **53**, 4638-4658 (2016).

187. J. Greaves, L. H. Chamberlain, Differential palmitoylation regulates intracellular patterning of SNAP25. *J Cell Sci* **124**, 1351-1360 (2011).

188. J. Greaves, O. A. Gorleku, C. Salaun, L. H. Chamberlain, Palmitoylation of the SNAP25 protein family: specificity and regulation by DHHC palmitoyl transferases. *J Biol Chem* **285**, 24629-24638 (2010).

189. A. J. Laude, I. A. Prior, Palmitoylation and localisation of RAS isoforms are modulated by the hypervariable linker domain. *J Cell Sci* **121**, 421-427 (2008).

190. B. Attali *et al.*, Voltage-gated potassium channels (Kv) *IUPHAR/BPS Guide to Pharmacology CITE* **Vol 2021 No 3**, ISSN 2633-1020 (Online) (2021).

191. S. S. Sanders *et al.*, The palmitoyl acyltransferase ZDHHC14 controls Kv1-family potassium channel clustering at the axon initial segment. *Elife* **9**, (2020).

192. R. A. Gubitosi-Klug, D. J. Mancuso, R. W. Gross, The human Kv1.1 channel is palmitoylated, modulating voltage sensing: Identification of a palmitoylation consensus sequence. *Proc Natl Acad Sci U S A* **102**, 5964-5968 (2005).

193. L. Zhang, K. Foster, Q. Li, J. R. Martens, S-acylation regulates Kv1.5 channel surface expression. *Am J Physiol Cell Physiol* **293**, C152-161 (2007).

194. H. K. Jindal, E. J. Folco, G. X. Liu, G. Koren, Posttranslational modification of voltage-

194. dependent potassium channel Kv1.5: COOH-terminal palmitoylation modulates its biological properties. *Am J Physiol Heart Circ Physiol* **294**, H2012-2021 (2008).

195. G. M. Thomas, T. Hayashi, S. L. Chiu, C. M. Chen, R. L. Huganir, Palmitoylation by DHHC5/8 targets GRIP1 to dendritic endosomes to regulate AMPA-R trafficking. *Neuron* **73**, 482-496 (2012).

196. M. Setou *et al.*, Glutamate-receptor-interacting protein GRIP1 directly steers kinesin to dendrites. *Nature* **417**, 83-87 (2002).

197. G. S. Brigidi, B. Santyr, J. Shimell, B. Jovellar, S. X. Bamji, Activity-regulated trafficking of the palmitoyl-acyl transferase DHHC5. *Nat Commun* **6**, 8200 (2015).

198. D. P. McEwen, L. L. Isom, Heterophilic interactions of sodium channel beta1 subunits with axonal and glial cell adhesion molecules. *J Biol Chem* **279**, 52744-52752 (2004).

199. A. A. Bouza *et al.*, Sodium channel β1 subunits are post-translationally modified by tyrosine phosphorylation,. *J Biol Chem* **295**, 10380-10393 (2020).

200. A. E. El-Husseini *et al.*, Dual palmitoylation of PSD-95 mediates its vesiculotubular sorting, postsynaptic targeting, and ion channel clustering. *J Cell Biol* **148**, 159-172 (2000).

201. R. Vassar, P. C. Kandalepas, The β-secretase enzyme BACE1 as a therapeutic target for Alzheimer's disease. *Alzheimers Res Ther* **3**, 20 (2011).

202. H. S. Wang *et al.*, KCNQ2 and KCNQ3 potassium channel subunits: molecular correlates of the M-channel. *Science* **282**, 1890-1893 (1998).

203. R. W. Manville, M. Papanikolaou, G. W. Abbott, M-Channel Activation Contributes to the Anticonvulsant Action of the Ketone Body. *J Pharmacol Exp Ther* **372**, 148-156 (2020).

204. A. Murthy *et al.*, Dynamic palmitoylation regulates trafficking of K channel interacting protein 2 (KChIP2) across multiple subcellular compartments in cardiac myocytes. *J Mol Cell Cardiol* **135**, 1-9 (2019).

205. S. S. Sanders *et al.*, Curation of the Mammalian Palmitoylome Indicates a Pivotal Role for Palmitoylation in Diseases and Disorders of the Nervous System and Cancers. *PLoS Comput Biol* **11**, e1004405 (2015).

206. F. B. Young, S. L. Butland, S. S. Sanders, L. M. Sutton, M. R. Hayden, Putting proteins in their place: palmitoylation in Huntington disease and other neuropsychiatric diseases. *Prog Neurobiol* **97**, 220-238 (2012).

207. L. R. Bollu *et al.*, Intracellular activation of EGFR by fatty acid synthase dependent palmitoylation. *Oncotarget* **6**, 34992-35003 (2015).

208. B. Chen, Y. Sun, J. Niu, G. K. Jarugumilli, X. Wu, Protein Lipidation in Cell Signaling and Diseases: Function, Regulation, and Therapeutic Opportunities. *Cell Chem Biol* **25**, 817-831 (2018).

209. S. J. West *et al.*, S-acylation of Orai1 regulates store-operated Ca2+ entry. *J Cell Sci* **135**, (2022).

210. Y. Gurfinkel *et al.*, Functional and structural consequences of TBK1 missense variants in frontotemporal lobar degeneration and amyotrophic lateral sclerosis. *Neurobiol Dis* **174**, 105859 (2022).

211. R. Tewari, B. Shayahati, Y. Fan, A. M. Akimzhanov, T cell receptor-dependent S-acylation of ZAP-70 controls activation of T cells. *J Biol Chem* **296**, 100311 (2021).

212. M. P. Matheu *et al.*, Imaging of effector memory T cells during a delayed-type hypersensitivity reaction and suppression by Kv1.3 channel block. *Immunity* **29**, 602-614 (2008).

213. A. S. Kazim, P. Storm, E. Zhang, E. Renström, Palmitoylation of Ca. *Biochem Biophys Res Commun* **491**, 740-746 (2017).

214. L. Ge *et al.*, Big Potassium (BK) ion channels in biology, disease and possible targets for cancer immunotherapy. *Int Immunopharmacol* **22**, 427-443 (2014).

215. N. Hoa *et al.*, Molecular mechanisms of paraptosis induction: implications for a non-genetically modified tumor vaccine. *PLoS One* **4**, e4631 (2009).

216. J. F. Hancock, A. I. Magee, J. E. Childs, C. J. Marshall, All ras proteins are polyisoprenylated but only some are palmitoylated. *Cell* **57**, 1167-1177 (1989).

217. G. Calero *et al.*, The crystal structure of palmitoyl protein thioesterase-2 (PPT2) reveals the basis for divergent substrate specificities of the two lysosomal thioesterases, PPT1 and PPT2. *J Biol Chem* **278**, 37957-37964 (2003).

218. N. J. Marianayagam, M. Sunde, J. M. Matthews, The power of two: protein dimerization in biology. *Trends Biochem Sci* **29**, 618-625 (2004).

219. E. de la Fuente-Ortega *et al.*, Basolateral sorting of chloride channel 2 is mediated by interactions between a dileucine motif and the clathrin adaptor AP-1. *Mol Biol Cell* **26**, 1728-1742 (2015).

220. S. Paris, R. Longhi, P. Santambrogio, I. de Curtis, Leucine-zipper-mediated homo- and hetero-dimerization of GIT family p95-ARF GTPase-activating protein, PIX-, paxillin-interacting proteins 1 and 2. *Biochem J* **372**, 391-398 (2003).

221. M. Durán-Prado, M. M. Malagón, F. Gracia-Navarro, J. P. Castaño, Dimerization of G protein-coupled receptors: new avenues for somatostatin receptor signalling, control and functioning. *Mol Cell Endocrinol* **286**, 63-68 (2008).

222. Z. Wang, ErbB Receptors and Cancer. *Methods Mol Biol* **1652**, 3-35 (2017).

223. A. Patwardhan, N. Cheng, J. Trejo, Post-Translational Modifications of G Protein-Coupled Receptors Control Cellular Signaling Dynamics in Space and Time. *Pharmacol Rev* **73**, 120-151 (2021).

224. T. Zeppelin, K. B. Pedersen, N. A. Berglund, X. Periole, B. Schiøtt, Effect of palmitoylation on the

dimer formation of the human dopamine transporter. *Sci Rep* **11**, 4164 (2021).

225. R. Bhattacharyya, R. H. Fenn, C. Barren, R. E. Tanzi, D. M. Kovacs, Palmitoylated APP Forms Dimers, Cleaved by BACE1. *PLoS One* **11**, e0166400 (2016).

226. L. Abrami *et al.*, Identification and dynamics of the human ZDHHC16-ZDHHC6 palmitoylation cascade. *Elife* **6**, (2017).

227. Z. Ma *et al.*, Molecular mechanism of CD44 homodimerization modulated by palmitoylation and membrane environments. *Biophys J* **121**, 2671-2683 (2022).

228. K. Seno, F. Hayashi, Palmitoylation is a prerequisite for dimerization-dependent raftophilicity of rhodopsin. *J Biol Chem* **292**, 15321-15328 (2017).

229. Y. Gambin *et al.*, Confocal Spectroscopy to Study Dimerization, Oligomerization and Aggregation of Proteins: A Practical Guide. *Int J Mol Sci* **17**, (2016).

230. W. Wang, C. J. Roberts, Protein aggregation - Mechanisms, detection, and control. *Int J Pharm* **550**, 251-268 (2018).

231. R. Caruso, N. Warner, N. Inohara, G. Núñez, NOD1 and NOD2: signaling, host defense, and inflammatory disease. *Immunity* **41**, 898-908 (2014).

232. D. Li, M. Wu, Pattern recognition receptors in health and diseases. *Signal Transduct Target Ther* **6**, 291 (2021).

233. F. J. Ivins *et al.*, NEMO oligomerization and its ubiquitin-binding properties. *Biochem J* **421**, 243-251 (2009).

234. J. Cui, Y. Chen, H. Y. Wang, R. F. Wang, Mechanisms and pathways of innate immune activation and regulation in health and cancer. *Hum Vaccin Immunother* **10**, 3270-3285 (2014).

235. J. Napetschnig, H. Wu, Molecular basis of NF-κB signaling. *Annu Rev Biophys* **42**, 443-468 (2013).

236. J. Zheng *et al.*, RIG-I-like receptors: Molecular mechanism of activation and signaling. *Adv Immunol* **158**, 1-74 (2023).

237. J. S. Yoo *et al.*, Non-conventional trafficking of the cystic fibrosis transmembrane conductance regulator through the early secretory pathway. *J Biol Chem* **277**, 11401-11409 (2002).

238. J. F. Rivera, S. Ahmad, M. W. Quick, E. R. Liman, D. B. Arnold, An evolutionarily conserved dileucine motif in Shal K+ channels mediates dendritic targeting. *Nat Neurosci* **6**, 243-250 (2003).

239. D. F. Steele, J. Eldstrom, D. Fedida, Mechanisms of cardiac potassium channel trafficking. *J Physiol* **582**, 17-26 (2007).

240. M. A. Nystoriak, D. Zhang, G. Jagatheesan, A. Bhatnagar, Heteromeric complexes of aldo-keto reductase auxiliary K. *Chem Biol Interact* **276**, 210-217 (2017).

241. R. Vicente *et al.*, Pattern of Kv beta subunit expression in macrophages depends upon proliferation and the mode of activation. *J Immunol* **174**, 4736-4744 (2005).

242. C. Croci, J. H. Brändstatter, R. Enz, ZIP3, a new splice variant of the PKC-zeta-interacting protein family, binds to GABAC receptors, PKC-zeta, and Kv beta 2. *J Biol Chem* **278**, 6128-6135 (2003).

243. N. Comes *et al.*, The voltage-dependent K(+) channels Kv1.3 and Kv1.5 in human cancer. *Front Physiol* **4**, 283 (2013).

244. H. Lin, Protein cysteine palmitoylation in immunity and inflammation. *FEBS J* **288**, 7043-7059 (2021).

245. A. Carreras-Sureda *et al.*, S-acylation by ZDHHC20 targets ORAI1 channels to lipid rafts for efficient Ca. *Elife* **10**, (2021).

246. G. Kodakandla *et al.*, Dynamic S-acylation of the ER-resident protein stromal interaction molecule 1 (STIM1) is required for store-operated Ca. *J Biol Chem* **298**, 102303 (2022).

247. Y. Lu *et al.*, Palmitoylation of NOD1 and NOD2 is required for bacterial sensing. *Science* **366**, 460-467 (2019).

248. B. Nepal, S. Das, M. E. Reith, S. Kortagere, Overview of the structure and function of the dopamine transporter and its protein interactions. *Front Physiol* **14**, 1150355 (2023).

249. C. Shi *et al.*, ZDHHC18 negatively regulates cGAS-mediated innate immunity through palmitoylation. *EMBO J* **41**, e109272 (2022).

250. J. Cai, J. Cui, L. Wang, S-palmitoylation regulates innate immune signaling pathways: molecular mechanisms and targeted therapies. *Eur J Immunol*, e2350476 (2023).

251. S. B. Taner *et al.*, Control of immune responses by trafficking cell surface proteins, vesicles and lipid rafts to and from the immunological synapse. *Traffic* **5**, 651-661 (2004).

252. K. Kwiatkowska, O. V. Matveichuk, J. Fronk, A. Ciesielska, Flotillins: At the Intersection of Protein. *Int J Mol Sci* **21**, (2020).

253. M. S. Goligorsky, H. Li, S. Brodsky, J. Chen, Relationships between caveolae and eNOS: everything in proximity and the proximity of everything. *Am J Physiol Renal Physiol* **283**, F1-10 (2002).

254. F. Tang *et al.*, Palmitoyl transferases act as potential regulators of tumor-infiltrating immune cells and glioma progression. *Mol Ther Nucleic Acids* **28**, 716-731 (2022).

255. E. Morrison *et al.*, Quantitative analysis of the human T cell palmitome. *Sci Rep* **5**, 11598 (2015).

256. A. Vallejo-Gracia *et al.*, KCNE4-dependent functional consequences of Kv1.3-related leukocyte physiology. *Sci Rep* **11**, 14632 (2021).

257. E. J. Ciampa, R. C. Welch, C. G. Vanoye, A. L. George, KCNE4 juxtamembrane region is required for interaction with calmodulin and for functional suppression of KCNQ1. *J Biol Chem* **286**, 4141-4149 (2011).

258.   K. Bi *et al.*, Antigen-induced translocation of PKC-theta to membrane rafts is required for T cell activation. *Nat Immunol* **2**, 556-563 (2001).

259.   C. R. Campomanes *et al.*, Kv beta subunit oxidoreductase activity and Kv1 potassium channel trafficking. *J Biol Chem* **277**, 8298-8305 (2002).